2009

# Single-Molecule Detection of Unique Genome Signatures: Applications in Molecular Diagnostics and Homeland Security

Jason M. Emory
*Louisiana State University and Agricultural and Mechanical College*

# SINGLE-MOLECULE DETECTION OF UNIQUE GENOME SIGNATURES: APPLICATIONS IN MOLECULAR DIAGNOSTICS AND HOMELAND SECURITY

A Dissertation
Submitted to the Graduate Faculty of the
Louisiana State University and
Agricultural and Mechanical College
in partial fulfillment of the
requirements for the degree of
Doctor of Philosophy

In

The Department of Chemistry

by
Jason M. Emory
B.S., M. S., University of North Carolina at Charlotte
May, 2010

# Dedication

I dedicate this work and accomplishment to my parents, Coy and Cheryl Emory and my loving wife Melanie. Thank you for all the support and encouragement.

“Discovery consists in seeing what everyone else has seen and thinking what no one else has thought.”

Albert Szent-Gyorgyi

## Acknowledgements

The author would like to first acknowledge and thank his collaborators. It's through a multidisciplinary approach that is the foundation for this work and leads to these outstanding developments encompassed in this dissertation. The Soper group members (past and present) have always been willing and eager to lend not only a helping hand but also their time, energy and ideas. Matt Hupert has been a valuable resource with his expert advice on AutoCAD and microchip fabrication. Jason Guy was always helpful processing and machining my designs and mold inserts. Maggie Witek provided valuable insight and knowledge on LDR, PCR, and the CGE (Beckman) which was a valuable asset and a real help so I could focus on my objectives. Additionally, Samuel Njoroge was also helpful with my molecular biology work which was greatly appreciated. Andre Adams and Rondedrick Sinville gave me some great advice and encouragement in the end to help me finish strong. Additionally, the strong friendships developed will be cherished. I would like to acknowledge my research collaborators, Paul Okagbare for his collaborative work on the COC waveguides fabrication and Zhiyong Peng for his work on the pathogenic bacteria detection using the LDR-spFRET that made a much more impactful chapter/paper possible. Technical support for my compact SMD came from Don Patterson with his work on instrumental designing and the fabrication of the electrical boards and Brad Ellison's work with the FPGA that helped minimized the size of the instrument. As for my other group members your contributions were small but meaningful which was greatly appreciated. Collaborators from outside the chemistry department included Arnold Rosslett for the simulations of the fluidic flow show in chapter 4 and Pin-Chuan Chen for the thermal modeling shown in chapter 5. Both of these guys worked hard and generated some nice simulations which helped support my results. The chemistry department staff was always helpful

and friendly taking care of the little everyday things so that I could work on my research and achieve these great results. Additionally, my committee members (Paul Russo, Doug Gilman, and Kermit Murray) have played a big part in mentoring me and working with me on this difficult journey.

Most importantly I would like to thank my advisor Steven A. Soper. But first let me once again thank my master's advisor Brian Cooper. Without your encouragement and support as an undergraduate and master student I doubt I would have gone on to these great accomplishments. It was Brian who first exposed me to research that sparked my interest which has continued to grow. Steven took over my mentoring upon my arrival here at LSU and helped me grow as a professional and scientist. I owe you both a huge debt of gratitude for spending time and working with me so that I may reach the success that I now enjoy. Thank You!

My family needs a big thank you for all your encouragement and support over the years. I know you all will be happy to have me finally done with school.

Lastly, I would like to thank the funding sources agencies; without the money for research none of these accomplishments would be possible. Financial support was provided by the National Institutes of Health (EB-002115), the national Science Foundation (EPS-0346411) and Louisiana Board of Regents.

# Table of Contents

# List of Tables

# List of Figures

## List of Commonly Used Abbreviations and Acronyms

AMPH – amphiphysin

bp – base pair

CCD – charge coupled device

COC – cyclic olfin copolymer

CRC – colorectal cancer

DC – duty cycle

DNA – deoxyribonucleic acid

dNTP – deoxynucleoside triphosphate

dsDNA, ssDNA – double stranded and single stranded DNA

ECU – event counter unit

EOF – electroosmotic flow

FIFO – first in first out

FPGA -- field programmable gate array

HDA – heteroduplex assay

ICU – instrument control unit

*K-ras* – Kirsten rat sarcoma

LDR – ligase detection reaction

LDR-spFRET – ligase detection reaction single-pair fluorescent resonance energy transfer

LIF – laser-induced fluorescence

LOD – limit of detection

MB – molecular beacon

mRNA – messenger RNA

NA – numerical aperture

PBMC – peripheral blood mononuclear cell

PCR – polymerase chain reaction

PDMS – polydimethylsiloxane

PMMA – poly (methylmethacrylate)

PMT – photo multiplier tube

POC – point-of-care

PNA – peptide nucleic acids

QD – quantum dot

RCA – rolling cycle amplification

rMB – reverse molecular beacon

RNA – ribonucleic acid

SE – sampling efficiency

SMD – single-molecule detection

SNP – single nucleotide polymorphism

SNR – signal-to-noise-ratio

SPAD – single photon avalanche diodes

ST – sampling throughput

TDI – time-delayed integration

TIRF – total internal reflection fluorescence

VCSEL – vertical cavity surface emitting laser

μTAS – micro total analysis system

# Abstract

Single-molecule detection (SMD) offers an attractive approach for identifying the presence of certain markers that can be used for *in vitro* molecular diagnostics in a near real-time format. The ability to eliminate sample processing steps afforded by the ultra-high sensitivity associated with SMD yields a sampling pipeline for diagnostics that require fast reporting of biomarkers. When SMD and microfluidics are used in conjunction with nucleic acid-based assays such as the ligase detection reaction coupled with single-pair fluorescent resonance energy transfer (LDR-spFRET), complete molecular profiling and screening of certain cancers, pathogenic bacteria, and other biomarkers becomes possible at remarkable speeds and sensitivities with high specificity. The merging of these technologies and techniques into two different novel instrument formats has been investigated. (1) The use of a charge-coupled device in a time-delayed integration mode as a means for increasing the throughput of any single-molecule measurement by simultaneously tracking and detecting single-molecules in multiple microfluidic channels was demonstrated. This approach allowed increasing the sample throughput by a factor of 8 compared to a single-assay SMD experiment. A sampling throughput of 276 molecules $s^{-1}$ per channel and 2208 molecules $s^{-1}$ for an eight channel microfluidic system was achieved. A cyclic olefin copolymer waveguide was designed and fabricated in a pre-cast poly(dimethylsiloxane) stencil to increase the SNR by controlling the excitation geometry. The waveguide showed an attenuation of 0.67 dB/cm and the launch angle was optimized to increase the depth of penetration. (2) A compact SMD (cSMD) instrument was designed and built for the reporting of molecular signatures. Optical waveguides were poised within the fluidic chip at an orientation angle of 90° with respect to each other for the interrogation of single-molecule events. Molecular beacons (MB) were designed to probe different types of bacteria for the

classification of Gram +. MBs were mixed with bacterial cells and pumped though the cSMD, which allowed *S. aureus* to be classified from 2,000 cells in 1 min. Finally, the integration of the LDR-spFRET assay with the cSMD was explored with the future direction of designing a molecular screening approach for stroke diagnostics, which is currently unavailable.

# 1 Merging Single-Molecule Detection with Genomic-Based Assays

## 1.1 Introduction: Single-Molecule Detection for Genomic Analysis

Single-molecule detection (SMD) is a powerful enabler for expanding the utility of DNA and RNA-based analyses and represents the ultimate limit-of-detection. SMD allows for the observation of individual molecules free from bulk averaging and provides the highest level of certainty when performing quantitative measurements. Over the past decade, there has been an increase in the number of applications that have used SMD as a tool for the analysis of biological molecules. At the same time, the integration of biological reactions into microfluidic devices has been on the rise and can be integrated with single molecule detectors to create systems capable of providing near-real time detection of important biomarkers. In this chapter, I will survey the detection of single molecules and its application in genomic-based assays.

## 1.2 Background of SMD

The first successful detection of single fluorescent molecules in liquids at room temperature was demonstrated by Hirschfield in 1976.[1] This group demonstrated the ability to detect a single antibody molecule tagged with 80-100 fluorophores. Keller and coworkers later used hydrodynamically focused flows of molecules to show the decreasing limit-of-detection in terms of molecule numbers and finally, first reported on the detection of individual fluorescent molecules in 1990.[2-4] SMD in liquids continues to grow rapidly as shown by papers demonstrating the detection of single rhodamine and phycoerythrine molecules in hydrodynamic flow cells[5, 6] and in levitated microdroplets.[7] Soper *et al.* used fluorescence emission spectra to distinguish between single molecules of rhodamine 6G (R6G) and Texas red.[8] Other biological examples of SMD are the observation of individual adenosine 5'-triphosphate (ATP) turnovers by a single myosin molecule,[9] the sliding motion of single kinesin molecules along

microtubules,[10] and sequencing of DNA through the detection and identification of single fluorescently-labeled mononucleotides expelled from intact DNA-strands using an exonuclease enzyme in a cone-shaped microcapillary.[11]

The information encoded in the photon-burst (the rapid and repeated excitation and subsequent emission from a fluorophore) as the fluorophore traverses a laser excitation volume generates a wealth of information. These bursts can be analyzed in terms of their brightness, duration, spectral properties, and fluorescence lifetime, thereby providing important information about the identity, size, diffusion coefficient, concentration, and electrophoretic drift of single molecules.[12] These techniques have been grouped into the area of single-molecule spectroscopy (SMS), which can be used to measure single-molecule properties, such as fluorescence lifetimes,[13-15] fluorescence intensities,[16-18] fluorescence resonance energy transfer (FRET) efficiency,[19-23] spectral distributions,[24, 25] polarization anisotropies,[26-28] and diffusional motions.[29]

### 1.3 Basic Principles of SMD

Mathies *et al.* first outlined the basic principles of optimizing single-molecule fluorescence, defining the expression between two fundamental variables; k, the ratio of the absorption rate ($k_a$) to the observed fluorescence decay rate ($k_f$) and $\tau$, the ratio of the duration of illumination ($\tau_t$) to the intrinsic photodestruction time ($\tau_d$).[30] Furthermore, the fundamental relationship between transit time and irradiance for improving SMD experiments was outlined. Later, Goodwin *et al.* summarized the techniques available for SMD in solution.[31] More recently Zander discussed the optimization for not only SMD, but also single-molecule identification.[32] The basic issues associated with SMD that warrant careful consideration can be broken down into three areas: (i) background noise; (ii) signal; and (iii) single-to-noise ratio (SNR). A brief summary of these fundamental principles of SMD are given below.

### 1.3.1 Background Noise and Its Reduction

The fluorescent emission from a single-molecule must be detected in the presence of a large number of background photons generated from the solvent and fluorescent impurities present in the solvent. The photons detected from single-molecules must exceed the background level to provide a signal large enough to produce high confidence in associating a photon burst with a single fluorophore molecule. A major component of the background emanates from the solvent (*i.e.*, water), which originates from Raman and/or Rayleigh scattering. Background fluorescence also results from impurities in the solvent, substrates, and optical components and can adversely affect the background level. Optical filtering of background fluorescence and Raman scattering is often difficult because their spectra can in many cases, overlap with the emission spectrum of the target fluorophore.[32] Several approaches have been used to minimize these contributions to the background, which includes high-performance optical filters, ultrapure solvents and the reduction of the illuminated sample volume through the use of laser excitation in confocal, near-field or evanescent configurations.[33] Time-gating has also been used to reduce Rayleigh and Raman scattering.[4] Other approaches include the use of two photon-excitation[34] and near-infrared (NIR) excitation.[35, 36] Photon detectors, such as photomultiplier tubes, PMTs, also have intrinsic noise characteristics, such as dark current and shot noise, which needs to be addressed as well and can contribute to the observed background level.

The volume that is illuminated by the excitation source ($1/e^2$ laser beam profile) and is monitored by the detection element is defined as the probe volume. Small probe volumes can help minimize the background level because its intensity is proportional to the size of the probe volume whereas the signal is proportional to the number of molecules within the probe volume. The background intensity ($n_B$) [$s^-$] is directly proportional to the incident excitation light intensity ($I$) [$cm^{-2}s^{-1}$], scattering cross section of the solvent ($\sigma_{sol}$) [$cm^2$], and the number of solvent

molecules in the probe volume ($N_V$). Equation 1.1 shows this relationship with the additional factor of the noise equivalent photon rate ($n_{nep}$), which is the noise in the electronics ($n_{el}$) divided by the noise in the detector ($n_{det}$).[32] The reduction of the probe volume size reduces the background intensity by lowering the number of solvent molecules in the probe volume.

$$n_B = N_V \sigma_{sol} I + n_{nep} \tag{1.1}$$

Small probe volumes can be obtained in several ways, such as levitated microdroplets (1 fL–1 pL),[37] confocal microscopy (~1 fL),[38] and evanescent illumination (0.1 fL).[9] Alternatively, small probe volumes have been achieved using gel pores,[39] microcapillary tubes,[40] microchannels,[41] and two-photon excitation.[34] The drawback of reducing the probe volume is that a decrease in the sampling efficiency (percentage of molecules that are sampled during the experimental run) typically results because only a small proportion of molecules traveling through the experiment are interrogated by the ultra-small probe volume. Because increasing the probe volume is many times undesirable in SMD due to increases in the background level, a common approach is to use hydrodynamic focusing of sample streams in the fluidic channels to increase the sampling efficiency. Hydrodynamic focusing employs an outer liquid stream that operates at a much higher linear flow rate compared to the sample stream causing focusing of this inner stream within the detection zone.[42] The resulting focusing increases the sampling efficiency by forcing more molecules to flow through the small probe volume.

### 1.3.2 Signal and Its Enhancement

The fluorescent signal is proportional to the number of molecules in the probe volume and the incident light intensity. Small probe volumes assist in one of the major requirements for SMD, which is the probability of single molecule occupancy in the detection volume be significantly smaller than unity. This reduces the probability of multiple occupancy and thus, ensures the observed signal results from a single molecular event. The Poisson distribution can

describe the probability of the number of molecules in the probe volume [$f(k,\lambda)$] by the equation given below, where k is the number of molecules and λ is the expected number of molecules.

$$f(k,\lambda) = \frac{\lambda^k e^{-\lambda}}{k!} \tag{1.2}$$

The fluorescent signal from a single-molecule that is repeatedly excited and emits photons during its transit across the probe volume creates what is called a fluorescence photon burst. Fluorescence detection has proven to be the best method for SMD measurements because fluorophores can emit millions of fluorescent photons in these bursts, which can be transduced into measureable signals given sufficient signal-to-noise.[43, 44] Key physical properties that must be considered when choosing a fluorescent dye are a large absorption cross section ($\sigma_{dye}$), high fluorescence quantum yield ($Q_f$), and low photobleaching rates ($k_B$).

The large absorption cross-section is advantageous because it is directly proportional to the rate of absorption ($k_a$), which is given by Equation 1.3, where $\sigma_{dye}$ is the absorption cross section ($cm^2$/molecule), $I$ is the intensity of light (photon $cm^{-2}$ $s^{-1}$) and ε is the molar extinction coefficient ($cm^{-1}$ $M^{-1}$).

$$k_a = \sigma_{dye} I = 3.8 \times 10^{-21} \epsilon I \tag{1.3}$$

The absorption of a photon by the fluorophore in the ground state, $S_0$, promotes an electron into the excited state ($S_1$). A molecule in the excited state, $S_1$, can return to the ground state by emitting a photon with a rate, $k_f$, or nonradiatively ($k_n$), which includes intersystem crossing ($k_{ST}$), internal conversion, and triplet state population decay ($k_T$). When the absorption rate ($k_a$) equals the $S_1$ decay rate ($k_f + k_n$), ground state saturation occurs. Increasing $I$ to ground state saturation results in an increase in the rate of generation of fluorescent photons ($n_{fl}$), but beyond saturation, no increase in $n_{fl}$ is seen due to the fact that a population inversion cannot occur for a two-level system. The rate of fluorescence is given in Equation 1.4 and demonstrates

that the smaller the fluorescent lifetime, the higher $n_{fl}$. In fact, the maximum rate of fluorescence is determined by $(\tau_f+\tau_f k_{ST}/k_T)^{-1}$ where $\tau_f$ is the natural fluorescence lifetime.[32]

$$n_{fl} = \frac{1}{\tau_f\left(1+\frac{k_{ST}}{k_T}\right)+\frac{1}{I\sigma_{sol}Q_f}} \tag{1.4}$$

The ability to collect the fluorescent photons efficiently is the next step toward increasing the signal. High numerical aperture (NA) optics, where NA describes the light-gathering ability of the lens and characterizes the range of angles over which the system can accept light, can provide favorable signal-to-noise due to their ability to gather large percentages of isotropic emission generated by a fluorophore. The NA of an optic is define by Equation 1.5 shown below with *n* being the refractive index of the working medium and θ is the half angle of the maximum cone of light that can enter or exit the lens. In terms of confocal SMD setups, the large acceptance angle of high NA optics leads to not only the collection of more fluorescent photons (increase in signal), but the reduction in the probe volume as well because high NA microscope objectives are typically associated with higher magnification and also, lower confocal depths.

$$NA = n\sin\theta \tag{1.5}$$

Optical transducers, such as photomultiplier tubes (PMTs), single photon avalanche diodes (SPADs) and charge coupled devices (CCDs), for SMD are required to have high quantum efficiency and low dark noise. Microchannel plate photomultipliers (MCPs) found early experimental success in observing single dye molecules due to their ability to operate in a fast response time to allow time-gating for eliminating scattered radiation.[4] Recently, SPADs have been developed that have an integrated package containing on-board amplifiers and cooling stages, and possess higher quantum efficiencies of ~60% across the visible spectrum even approaching 95% in the near-infrared (NIR) compared to PMTs.[45] CCDs have also been used to

observe single molecule emission[46] and offer a platform to image multiple flow-type SMD experiments simultaneously. For example, van Orden *et al.* described a CCD-based single molecule flow cytometer system in which the effluent from a square-bore tube was imaged onto a 1152 x 1240 pixel CCD camera operated in a snap-shot mode.[47] Table 1.1 shows a list of photodetectors for SMD along with their important properties.

**Table 1.1** Common Photon Properties of SMD Photodetectors

| **Transducer** | **PMT[1]** | **SPAD[2]** | **Back illuminated CCD[3]** | **Framer Transfer CCD with on-chip gain[4]** |
|---|---|---|---|---|
| **Quantum Efficiency** | 20% @420 nm | 65% @650 nm | 95% @600 nm | 60% @600 nm |
| **Response Time** | 0.7 ns | 200 ps | 190 ms/frame (readout) | 110 ms/frame (readout) |
| **Dark Noise** | 100 nA | 50 cps | 1 electron/pixel/h | 1800 electrons/pixel/h |
| **Read Noise** | N/A | N/A | 10-20 e-rms | 1 electron (effective) |
| **Active Area** | 2 cm dia. | 180 μm dia. | 26.8 mm x 2 mm (1340 x 100 pixel) 20 μm pixels | 8 mm x 8 mm (1024 x 1002 pixel) 8 μm pixels |

1. Hamamatsu R4998
2. Perkin Elmer SPCM-AQRH-15
3. Princeton Instruments Spec 10:100B
4. Photometrics Cascade:1K

### 1.3.3 Signal-to-Noise-Ratio (SNR)

Now that the factors influencing background and signal intensity have been examined, we can now provide an analytical expression for the signal-to-noise ratio, SNR, in any photon counting experiment, which is defined as the mean of the signal divided by the standard deviation in the background (σ). The limit-of-detection (LOD) is the lowest amount of an analyte that can be detected, which is typically defined at a SNR of 3. Therefore, in SMD the fluorescent photon burst must have an intensity which is 3 times the σ of the blank in order to be considered a single-molecule event with high confidence.

To maximize the SNR, *I* is operated just below ground state saturation because further increases will only result in increases in the number of background photons ($n_B$). To determine the optimal power ($I_{opt}$), Equation 1.6 is used where $\tau_f$ is the fluorescence lifetime. A typical $I_{opt}$ was determined by Zander to be $3x10^{23}$ photons $cm^{-2}$ $s^{-1}$ for rhodamine 6G.[30, 32]

$$\boldsymbol{I_{opt}} = \sqrt{\frac{\boldsymbol{n_{nep}}}{\boldsymbol{\tau_f}\left(\mathbf{1}+\frac{\boldsymbol{k_{ST}}}{\boldsymbol{k_T}}\right)}}\,\boldsymbol{n_{fl}\sigma_{dye}N_V\sigma_{sol}} \qquad \textbf{(1.6)}$$

Mathies *et al.* also points out that the transit time ($\tau_t$) is an important factor due to $n_{fl}$ being a function of $\tau_t$.[30] The SNR can be approximated as the signal ($n_{fl}$) divide by the square root of the background ($n_B$) which is shown in eq 1.7.

$$SNR = \frac{n_{fl}}{\sqrt{n_B}} = \frac{\frac{Q_f}{Q_d}\left[1-e^{\left\{\frac{-k\tau}{(k+1)}\right\}}\right]}{\sqrt{\frac{Q_f}{Q_d}k\tau\alpha}} \qquad \textbf{(1.7)}$$

## 1.4 SMD of Biomarkers

A biomarker is any biological molecule found in blood, urine, other body fluids, or tissues that can serve as an indicator of a particular disease state or any other particular state of

an organism. Biomolecules such as lipids, carbohydrates, proteins, and nucleic acids have key cellular roles, which makes them ideal and important biomarkers for measuring the response to external stimuli. Additionally, biomarkers can signal normal or abnormal processes to tell how well the body responds to a treatment for a disease or condition. Consequently, the discovery and the use of biomarkers as medical diagnostic and/or prognostic indicators have a valuable role in medicine. However, biomarker analyses presents a challenging analytical problem with limited sample size, complex matrices of the sample, and low abundance. SMD offers an attractive approach for identifying the presence of certain biomarkers that can be used for *in vitro* molecular diagnostics in near-real time due to the ability to eliminate sample processing steps.

### 1.5 Genetic Analysis

Analysis of genetic material, such as DNA or RNA, in a clinical laboratory for diagnostics mainly involves a number of critical molecular processing steps such as: 1) sample collection; 2) DNA extraction and purification; 3) target enrichment; 4) scanning or identification of molecular alterations or sequence-specific reporters using biochemical reactions; and 5) detection of the products generated as a result of step 4. First, samples are collected from body tissues, whole blood, urine, sputum, or feces. Targets contained within those samples are then isolated from potential interferents by the selective extraction and purification of the DNA or RNA, which is normally accomplished through procedures such as ultracentrifugation, liquid-liquid extraction, precipitation, or solid-phase extraction. Following the extraction, selected genes of interest are amplified for further molecular analyses. Finally, the target DNA is analyzed/detected by a number of formats, for example fluorescence.

When SMD is coupled to biological analyses, the high sensitivity afforded enables the detection of rare targets in limited biological samples without amplification.[48, 49] Therefore, SMD

holds promise for the analysis of biomolecules and biomarkers by streamlining the steps required in the assays, potentially creating the possibility for near real-time results.

### 1.6 Microfluidics and SMD

The ability to automate sample processing fully and the associated short analysis times has driven the effort toward microfluidic devices for genomic assays. These systems can offer faster analysis times, integration of sample pre-processing steps and cost reductions because less reagents per analysis are consumed. When these platforms are coupled to SMD, novel systems can be generated that can provide exciting new opportunities in molecular diagnostics by providing full process integration, near real-time reporting and exquisite quantitative data. Early microfluidic single-molecule experiments were performed in glass-based devices.[16, 18, 50] For example, DNA fragment sizing by SMD was demonstrated by Craighead and coworkers in an ultrasmall microfluidic system.[17] The devices consisted of micro/nano-structured fluidic channels that provided femtoliter probe volumes appropriate for single-molecule DNA fragment sizing analysis. Both Ramsey's and Mathies's groups demonstrated the use of glass-based microdevices for single-molecule analyses of both organic chromophores and DNA molecules demonstrating that SMD measurements can be performed in these microfluidic devices.[50, 51] The choice of glass in these cases was based upon its ideal optical properties, producing minimal autofluorescence from the substrate material.

Despite the early use of microfluidic devices fabricated in glass for SMD, a number of drawbacks exist; the cost of micromanufacturing the device is high; high temperature thermal bonding of the coverslip to enclose the channels is required; and relatively low aspect ratio microstructures are produced as a result of wet chemical etching.[52] Polymers are viewed as promising alternative substrates for microfluidic devices because they are less expensive, they possess excellent solvent compatibility and biocompatibility, variable surface properties of

different polymers to match the application need, and they offer greater flexibility in fabrication strategies for producing devices at low-cost and in high production rates.[53-56] Several microfabrication techniques, such as laser ablation,[57] injection-molding, imprinting and embossing,[58] and X-ray lithography,[53] have been reported for the fabrication of devices in polymers. An early example of SMD using as elastomer base device was shown by Effenhauser and coworkers for the analysis of DNA fragments in polydimethylsiloxane (PDMS).[58] In their experiments, single molecules of λ-DNA were stained using a bis-intercalator for fluorescence detection.

Polymer-based microfluidic devices have been widely applied in various fields, such as biomedical, chemistry and biochemistry, and systems for fundamental research. These applications have been the subject of several reviews in the literature.[59-61] The increased demand in biological and life sciences research for high-throughput systems that are efficient and cost-effective has fostered the development of polymer-based microfluidic technologies. These devices have been used in areas such as DNA separations,[62] clinical diagnostics,[63] cell culture and cell handling,[64] DNA sequencing[65-68] and PCR amplification.[69-72]

### 1.7 Integration of Processing Steps on Microchips

As the integration of processing steps continues, the concept of a micro-total analysis systems (μ-TAS) is being realized in applications ranging from clinical medicine, genetic disease diagnostics, forensic science, and genetic sequencing and genotyping.[73] Integration of processing steps (cell lysis, target extraction, purification, and biochemical reactions) involved with genetic analyses can reduce processing time and the need for operator intervention significantly reducing the complexity of carrying out these assays. One of the key processes to integrate onto a microfluidic chip is biological modification reactions such as PCR, ligase chain reaction (LCR)

and ligase detection reactions (LDR).[74-76] The limited sample and low abundancy of biomarkers often requires these amplification techniques to enable downstream analysis and/or detection.

### 1.7.1 Polymerase Chain Reaction (PCR)

PCR in many cases is the first step in most genetic analyses and is used to exponentially amplify specific DNA or RNA sequences of interest through repetitive thermal cycling. The basic steps involved in PCR consists of denaturing, annealing and extension steps of a target by repeatedly subjecting it to different temperatures. In the denaturing step, the target DNA is heated to ~94°C to cause the double helix to unwind and the formation of single stranded DNA. During the annealing step (54-65°C), PCR primers (short oligonucleotides ~20 base pairs, bps) designed to be complementary to specific sites bind to the template DNA and define the region to be amplified. The final step is extension (~72°C), where the four deoxyribonucleoside triphosphates (Adenine; dATP, Cytosine; dCTP, Thymine; dTTP, Guanine; dGTP) are polymerized from the primer in a 3' to 5' direction and inserted according to Watson-Crick base pairing from the target DNA. These steps are repeated to create copies of the DNA in an exponential amplification process because the double-stranded complementary DNA can be used as the template in the next cycle.

Even though PCR is the gold standard and a key step for most genomic-based analysis techniques, it does have some drawbacks. The exponential amplification renders the process susceptible to misinterpretation due to contamination, mis-priming and formation of artifacts.[77] Additionally, the long processing time, non-quantitative results and the need for the optimization of primer designs for each unique sequence of the genome interrogated can be problematic. In addition, regions of the genome can be difficult to amplify via PCR, such as highly repetitive regions or those with high GC contents. Therefore, it is advantageous to consider molecular assays that do not require a PCR.

PCR is normally carried out using thermal cyclers with protocols typically requiring 30 cycles of ~2 h total processing time (240 s cycle$^{-1}$). The rate-limiting step of these cyclers is the long heating and cooling times required to reach thermal equilibrium due to the high thermal capacity of the large micro-centrifuge tubes and metal blocks used in these instruments. The reaction kinetics have been shown to occur relatively rapidly, especially with the high primer concentrations typically used. Wittwer *et al.* showed that denaturing and renaturation occur in less than 1 s,[78] while the extension step by *Taq* DNA polymerase has an extension rate of 60-100 nucleotides s$^{-1}$ at 72ºC. In theory, 30 PCR cycles could take as little as 2.5 mins (5 s cycle $^{-1}$; 1 s: 1 s: 3 s: denaturation: annealing: polymerase extension) for a 300 bp amplicon, which indicates that PCR cycle time is instrument-limited.[79]

### 1.8 Genomic Assays Using SMD

Nucleic acid analysis has been shown to play a valuable role in diagnosis of diseases, detection of infectious agents, forensic and paternity testing, veterinary medicine and environmental monitoring.[80] The recent developments in SMD of fluorescent molecules have made possible the implementation of paradigm-shifting approaches for nucleic acid analyses, such as the complete elimination of amplification strategies, such as PCR. The advantages of SMD applied toward the analysis of nucleic acids includes; (i) increased analysis speed offered by the removal of processing steps, such as PCR; (ii) high sensitivity and better data quality, especially quantitative data; and (iii) direct sequencing of DNA. Highly sensitive detection of DNA is critical in detecting genetic mutations, bacterial detection, and DNA sequencing. Single-molecule DNA sequencing is the focus of a number of research efforts to significantly reduce the cost of genome sequencing and increase the throughput.[65-68, 73, 81-89] Therefore, the focus of this review will be on genotyping assays (mutation and bacterial) and the advantages gained by combining them with SMD.

### 1.8.1 Bacterial Detection and Identification

Bacterial detection and identification is a high priority for health and safety reasons within a number of different agencies ranging from Homeland Security, the Food and Drug Administration, and clinical diagnostic laboratories.[90] Gene-specific biomarkers can also be used for the identification of blood borne or environmental pathogenic bacterium.[91-94] Threats from bacteria, such as *Escherichia coli, Bacillus anthracis,* and *Clostridium botulinum,* can be used as biological weapons; hence, fast reliable detection methods are required for health and safety response.[90] The traditional method for bacterial detection is culturing and plating however, alternative techniques are necessary because culturing is excessively time-consuming and lacks adequate sensitivity.[90] PCR techniques can improve the limit-of-detection compared to culturing by amplifying targets, even from a single DNA molecule, to generate millions of copies to aid in detection. The drawback to this approach is the introduction of ambiguities caused by the PCR.[77, 95, 96] Genomic-based assays allow for strain-specific identification to evaluate the threat level. Other methods, such as antibody or MS, have not shown the ability to provide strain specificity.[97] Identification of pathogenic bacteria requires high specificity, low false positives, and robustness to handle complex matrices. SMD of bacteria based on direct genomic processing offers the potential for fast, sensitive analysis free from false positive artifacts.

### 1.8.2 Mutation Detection

Diseases such as cystic fibrosis,[98, 99] Alzheimer's,[100, 101] sickle cell anemia[102] and certain cancers have known alterations in the sequence of particular genes,[103-108] which can be used as biomarkers for the medical diagnoses of these diseases. Early diagnosis of diseases, such as cancer, often leads to dramatically improved survival rates for patients.[109] Genetic diseases are frequently associated with a variety of errors, such as point mutations, insertions, or deletions, within the DNA and many cancers are associated with a collection of mutations throughout a

number of different genes. Colorectal cancer (CRC), for instance, has been associated with a number of mutations located in the *K-ras* oncogene.[110]

A single-nucleotide polymorphism (SNP) change, also called a single base substitution or point mutation, occurs when one base pair in DNA is changed into another base pair. Point mutations are responsible for a large number of sequence variations in the human genome.[111] The methods for SNP detection can be broadly classified into two major schemes: mutation specific interrogation (mutation detection) and mutation scanning.[112] The mutation-specific method detects SNPs that occur at well-characterized sites, whereas mutation scanning detects genetic variations in a given region with the specific location unknown.

When the location of the polymorphism is unknown or the sequence variation occurs sporadically within a certain section of the genome, and therefore, a mutation scanning approach is applied. Common scanning techniques that are used in conjunction with electrophoresis include single-strand conformation polymorphism (SSCP),[113] heteroduplex analysis (HDA),[114] denaturing gradient gel electrophoresis (DGGE)[115, 116] and temperature gradient gel electrophoresis (TGGE).[115, 117] These techniques are based on conformational-induced mobility shifts of Watson-Crick matched or mismatched double-stranded DNA (dsDNA) fragments. Analyses of this sort are typically used for the detection of unknown SNPs within PCR amplified regions. However, vital information with regard to the exact sequence location and characterization of SNPs are not rendered using most mutation scanning techniques.

Unlike the mutation scanning techniques, mutation detection methods are geared toward the identification and detection of particular genomic variations in which the locus is known within a certain gene. Most assays associated with this class of mutations involve nucleotide recognition enzymes including endonucleases, exonucleases, and thermostable ligases, which specifically cleave or bond DNA sites that harbor the mutation being interrogated. Several of the

mutation detection assays that have been utilized for the identification/detection of point mutations or SNPs include allele-specific PCR (AS-PCR)[118], restriction fragment length polymorphism (RFLP)[119], ligase detection reaction (LDR)[120], ligase chain reaction (LCR)[121] and single base extension assays (SBE).[122]

## 1.9 Coincident Detection Assays

Coincident detection-based assays rely on a two-color system to discriminate between target DNA and noise. The use of two recognition probes that associate specifically with the target molecule adds extra specificity by requiring that both probes be associated to the target to be counted as a positive event for the detection of the target. This procedure creates fast analysis of the target DNA because it reduces the need for extensive washing steps and probe hybridization to the target is completed within a few minutes. D'Antoni *et al.* demonstrated this detection technique on sub-picomolar concentrations of a model RNA target even in a complex background of RNA.[123] The drawback to such a system is the additional complexity required for two laser sources and two detectors. Additionally, at low target concentrations, higher probe concentrations are required to drive the equilibrium to form probe-target complexes. The increased concentration of probes creates random correlation events, which results in false positive signals.

### 1.9.1 Peptide Nucleic Acid Probes

Peptide nucleic acids (PNA) are synthetic DNA mimics with the same hydrogen bonding characteristics of nucleobases, but without the charged backbone. Instead of the negatively charged sugar-phosphate backbone in DNA, PNAs have an achiral, neutral polyamide backbone. This change results in a reduction in electrostatic repulsions, which creates faster and stronger hybridization to complementary targets. Additional benefits from PNAs are the ability to hybridize to the complements required in a large range of salt concentrations, shorter probe

lengths, and resistance to degradation by ubiquitous enzymes. PNAs were first synthesized by Egholm *et al.* in the early 1990s.[124] Since then, they have been used in a variety of diagnostic applications including SNP detection and bacteriology.

PNAs were used by Castro *et al.* to demonstrate a coincident detection technique for the rapid detection of specific nucleic acid sequences in unamplified DNA samples, such as *Bacillus anthracis*.[90] Two nucleic acid probes complementary to different sites on a target DNA sequence were labeled with different fluorescent dyes. When mixed with a sample containing the target DNA, the two probes would hybridize to their respective sequence-specific sites on the same target DNA molecule (Figure 1.1).[49]

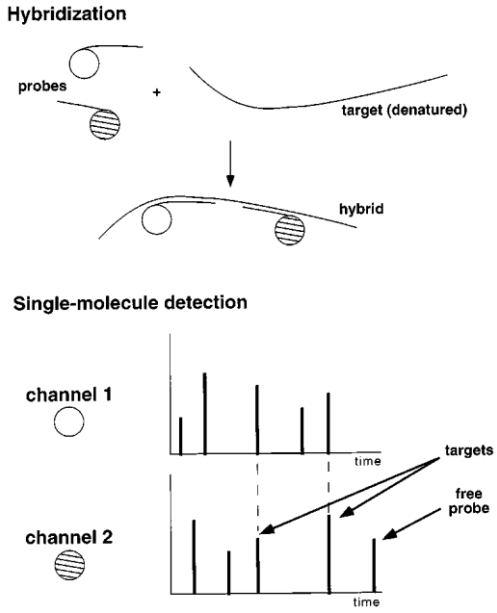


**Figure 1.1** Schematic diagram of the two-probe coincidence DNA homogeneous assay used by Castro. Reprinted with permission.[49]

When the sample was then analyzed by a laser-based ultrasensitive fluorescence system capable of SMD at two different wavelengths, the signals on each color channel appeared simultaneously in time only if the probes hybridized to the same target. Therefore, coincidence detection of both dyes provided the necessary specificity to detect unamplified, single-copy

target DNA molecules in a homogeneous assay. Uncorrelated events originating from free probes observed on either channel indicated that the target was not present. They demonstrated the ability to detect 100 aM of DNA at a SNR of 3 in 200 s and the assay showed good specificity, even in the presence of an excess of *B. globigii*, which did not contain complementary sequences to the PNA probes. The assay allowed for the direct use of genomic DNA allowing for faster analysis time due to the elimination of PCR steps. Limitations of the assay approach included the high cost of PNA probe synthesis compared to DNA-based probes and the system was complex requiring two lasers and two detectors. The other drawbacks included different sized probe volumes created in the confocal setup, the different physical properties of the dyes making identification of single-molecule events more complicated, cross talk between color channels that must be corrected, and finally, the approach was not demonstrated for single base mismatch discrimination.

### 1.9.2 Quantum Dots for Coincidence Detection

Another example of single-molecule coincidence detection was reported by Zhang *et al.* as a homogenous method for the rapid and sensitive detection of NAs using two different colored quantum dots (QDs).[125] Streptavidin-coated QDs were functionalized to act as both a nano-scaffold and as a fluorescence pair for coincidence detection. Two biotinylated oligonucleotide probes were used to recognize and detect specific complementary target DNA through a sandwich hybridization reaction. The DNA hybrids were first assembled on the surface of 605-nm-emitting QDs (605QDs) through specific streptavidin–biotin binding followed by the binding of the 525 nm-emitting QDs (525QDs) to the other end of DNA hybrids. The two QDs created coincidence signals only when in the presence of target DNA, which led to the formation of 605QD/DNA hybrid/525QD complexes (see Figure 1.2). They reported a LOD of $5 \times 10^{-15}$ M, which when compared to one-color QD-based assays, provided an improved LOD. The

coincidence signal in this assay was ~15 copies of the target DNA, which took up to 90 min before complete hybridization was observed. The use of QDs has two major advantages over more traditional organic dyes for coincidence detection. First, reduction of cross talk resulting from the narrow emission profiles of the QDs compared to organic dyes, which allows for better optical filtering of the signal. Secondly, the QDs can be excited by one laser source, which simplifies the detection system and reduces the problems associated with multi-color probe volume overlap, which often reduces the detection efficiency. However, the use of QDs does have drawbacks, such as low diffusion coefficients that increase the time required to hybridize the probes to the target. Also, they tend to aggregate at high concentrations, which may increase the LOD of this assay.

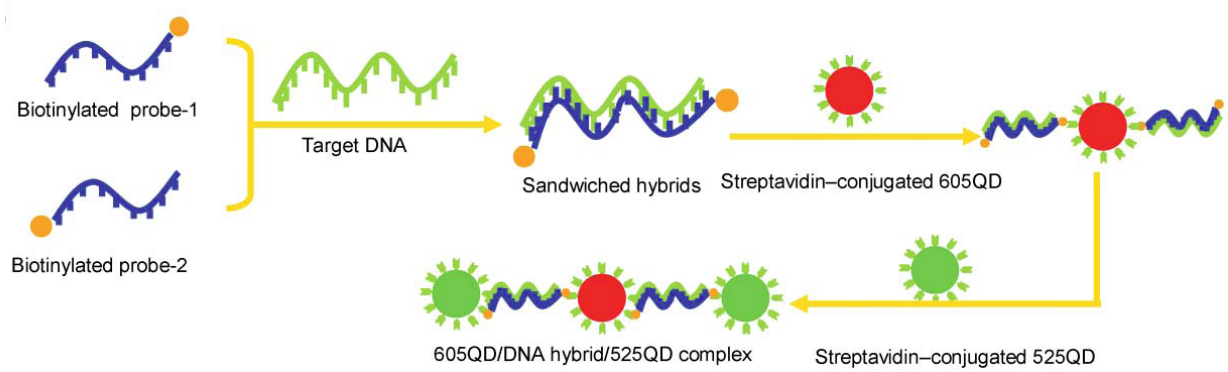


**Figure 1.2** The scheme used by Zhang *et al.* based on quantum dot single-molecule coincidence detection. The 605QD/DNA hybrid/525QD complex was formed by two biotinylated oligonucleotide probes, which created a sandwich hybrid to the specific complementary target DNA. Then, the DNA hybrids were bound to the surface of 605QDs through specific streptavidin–biotin binding, followed by the second 525QDs being bound to the other end of DNA hybrids, which forms the fluorescence complex for coincident detection. Reprinted with permission.[125]

## 1.10 Molecular Probes

Kramer and Tyagi developed novel oligonucleotide probes that could recognize and signal the presence of specific sequences.[126] These probes are called molecular beacons (MB) and are single-stranded oligonucleotides that contain a section complementary to the target DNA

sequence (loop) that is flanked on either side by ~10 bases, which are complementary (stem). The exquisite specificity of MBs results from the thermodynamic balance between the stem and loop, which provides molecular recognition in the presence of a large excess of other DNAs. MBs can be labeled with a fluorescent dye or quencher at the ends of each complementary stem section. Hybridization of the two complementary arms that flank the probe sequence forms the stem as shown in Figure 1.3. Hybridization of the stem section in the absence of the target sequence results in the molecule being closed in a so-called hairpin structure. The hairpin brings the fluorophore and quencher into close proximity, which results in energy transfer to the quencher instead of fluorescence emission from the fluorophore. Hybridization of the probe or loop sequence to the target DNA opens the hairpin loop, which separates the fluorophore and the quencher, consequently restoring the fluorescence.[127]

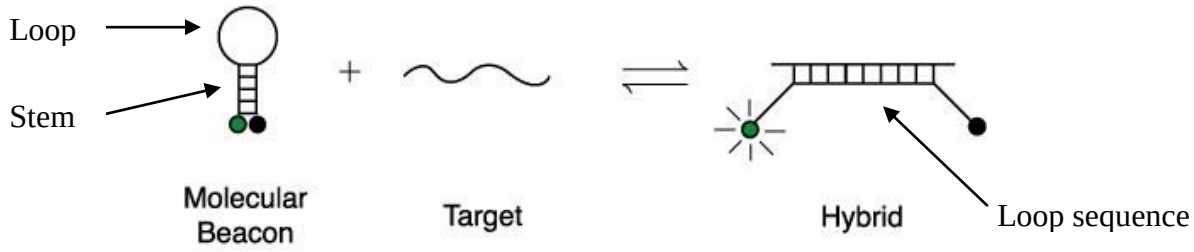


**Figure 1.3** The single-stranded oligonucleotides forms a closed stem and loop structure in the absence of target DNA and opens the stem when hybridized to the target DNA. MBs in the closed form has a quencher next to the fluorophore and emit no signal. In the open form, the quencher and fluorophore are separated due to a conformational change that results in the detection of fluorescence signal. Reprinted with permission.[127]

A number of groups have shown the ability of MBs to detect SNPs.[128-130] MBs are particularly attractive probes because the fluorescence quantum yield increases dynamically due to a conformational change when they bind to their target.[131] This allows for a homogenous assay because the unbound MB is dark and therefore, washing steps are not required for detection. However, MBs have some drawbacks such as the difficulty to attach different constituents to

opposite ends of the probe resulting in high probe cost and low reaction yields. To overcome this, Knemeyer *et al.* developed an interesting MB DNA probe with a 25-mer single-stranded oligonucleotide containing an 18-base recognition sequence.[132] It has a fluorescence energy donor (oxazine dye, JA242) attached to a string of cytosines on one end. The other end has a string of quencher guanosine bases (Smart Probe). In the absence of the DNA target, the cytosines and guanines bind and the DNA probe forms a "hairpin" loop that brings the donor and quenchers, which in this case are the guanosine bases, into close proximity. In the presence of target DNA, the hairpin opens and the probe binds to the target at the complementary sequence, separating the donor from the quenchers leading to a decreased quenching effect and strong emission from the donor. This probe was used to detect target DNA at a concentration of $10^{-12}$ M.

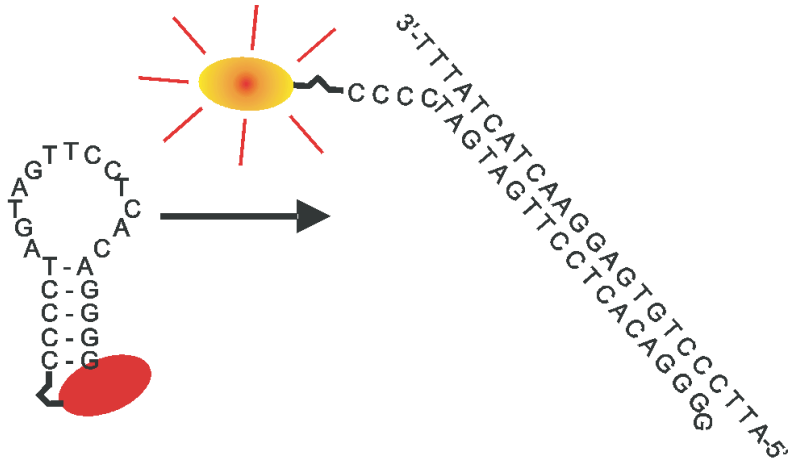


**Figure 1.4** Smart probes use a series of guanosines to quench the fluorophore in the closed DNA hairpin loop conformation instead of a traditional quencher. This makes fabrication of the DNA probe cheaper and easier because only the 5' end is modified. The probe used here was designed to test for a SNP in TB responsible for rifampicin resistance. Reprinted with permission.[133]

Marme *et al.* demonstrated an example of bacterial detection using smart probes with SMD by probing for a single nucleotide polymorphism (SNP) responsible for rifampicin resistance for *Mycobacterium tuberculosis*.[133] By applying fluorescently-labeled DNA-hairpin

structures in combination with single-molecule fluorescence spectroscopy, further discrimination of the bound and unbound probes was achieved by analyzing diffusion rates. Smart probes were hybridized to target sequences inducing a conformational change, which was reflected in a strong increase in fluorescence intensity.

An excess of unlabeled "cold" oligonucleotides were used to prevent the formation of secondary structures in the target sequence and thus facilitated hybridization of smart probes. The authors demonstrated an increase in the detection sensitivity by implementing a confocal fluorescence microscope to observe fluorescence burst sizes, burst duration and fluorescence lifetime to increase specificity of the discrimination between closed and open (hybridized) smart probes. The probe shown in Figure 1.4 was used for the identification of SNPs in $10^{-11}$ M solutions of PCR amplicons from *M. tuberculosis* in only 100 s. Although the hybridization only took 100 s, the PCR step added significant processing time (1-2 h) to this assay. Additionally, the addition of cold probes added complexity to the assay, additional cost, and an excess of these cold probes lead to a decrease in the LOD because they compete with binding to the target sequence.

A two-MB, SMD system for comparative quantification of nucleic acids in a highly sensitive method was demonstrated by Zhang *et al.*[134] This was the first reported use of two different colored MBs to perform a separation-free comparative hybridization assay for simultaneous quantification of both target and control strands. The two-color MB detection strategy provided a more accurate way to quantify target fluorescent signals from background. They demonstrated the use of Oregon green 488 and Cy5 as fluorescent reporter dyes and their results showed a reduction in the probe consumption by 6 orders of magnitude compared to conventional ensemble methods. This two MB system allowed for spectral multiplexing with the potential to screen for multiple SNP's in one assay to facilitate a highly sensitive approach for

mutational analysis. However, the use of two lasers and two APDs made the instrument (see Figure 1.5) more complicated and expensive to setup and run compared to a one-color MB system. Additionally, the broad emission profiles of the organic dyes used limited the ability to increase the multiplexing capability of the system. Other drawbacks for this approach included the obligatory PCR needed to amplify the target molecules prior to detection, which requires time and material. Moreover the requirements for two probes synthesized with two different dyes were a burden as well.

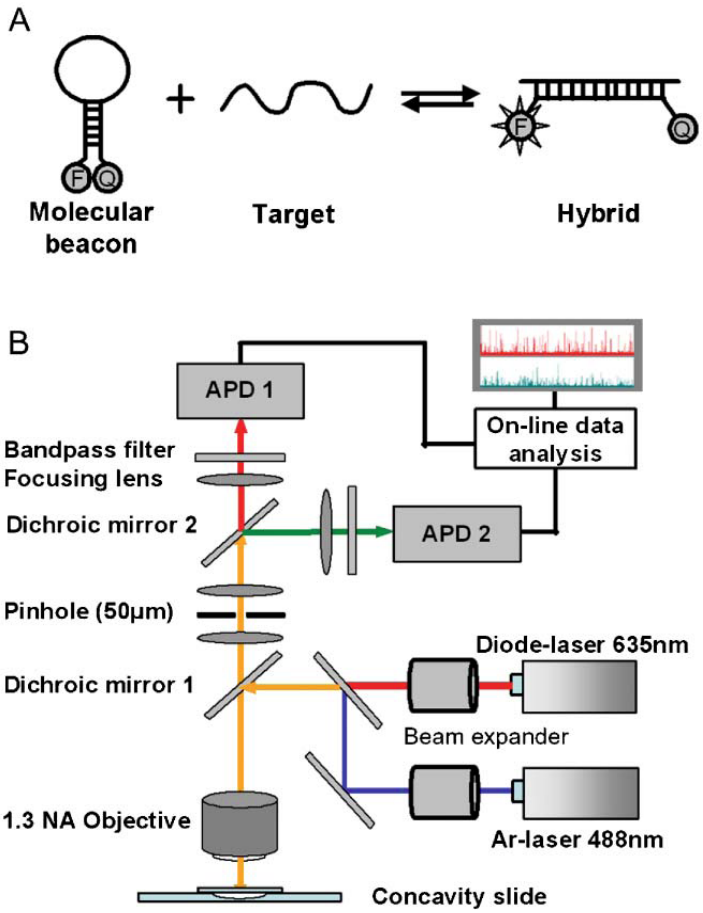


**Figure 1.5** Instrumentation schematic for the detection to two MBs using a dual-color confocal setup. Excitation was provided by a 488 nm argon laser and 635 nm diode laser, which excited Oregon green 488 and Cy5, respectively, on MB1 and MB2. The fluorescent emission of the bound MBs were recorded by APDs after the signal was split with a dichroic mirror and filter with the appropriate bandpass filter. Reprinted with premisson.[134]

MBs have been shown to reach attomolar detection limits when combined with a concentrator, such as Puleo *et al.* demonstrated with inline micro-evaporators.[135] This evaporator allowed for a four-fold decrease in the relative LOD for more complex SMD probe schemes integrated into a microfluidic chip. They used a rotary chamber to transport the target DNA into micro-evaporation chambers with an evaporation membrane, where the concentration was increased to the pM range for detection. Once concentrated, the target could be mixed with the MB and shuttled out of the chamber for SMD. The improved LOD for the MB was impressive with the additional benefit of the possibility of reduced cost if the PCR step was eliminated. The evaporation rates demonstrated were 100's of μL/h, which approached benchtop evaporators, however, this method did add additional processing steps and if large volumes were required to be evaporated the processing time was extended.

## 1.11 Fluorescence Resonance Energy Transfer Molecular Beacons

The MBs described previously utilized the quenching of the fluorophore when the MB was in its closed conformation. This process is broadly defined as resonance energy transfer, where the fluorescent dye is excited and the energy is transferred to a non-fluorescent dye. However, this second molecule or acceptor doesn't have to be a quencher, it can be another fluorescent molecule, which accepts the donor's energy and emits its energy in a fluorescent process at longer wavelengths, which is called fluorescent resonance energy transfer.

### 1.11.1 Fluorescence Resonance Energy Transfer (FRET)

FRET is a non-radiative process that involves the transfer of excited state energy from a donor to an acceptor through a dipole-dipole interaction.[136] The rate of energy transfer depends on several factors; the relative orientation of the donor and acceptor dipole moments ($\kappa^2$); the extent of overlap of the emission spectrum of the donor with the absorption spectrum of the acceptor ($J(\lambda)$, see Figure 1.6); and the distance between the two fluorescent dyes (r).

$$k_T(r) = \frac{Q_D \kappa^2}{\tau_D r^6}\left(\frac{9000(\ln 10)}{128\pi^5 N n^4}\right) J(\lambda) \quad \textbf{(1.8)}$$

$\kappa^2$ describes the relative orientation in space of the transition dipoles of the donor and acceptor and $\tau_D$ is the decay time of the donor. The assumption of dynamic random averaging of the donor and acceptor results in a value of 2/3 for κ. The overlap integral, J(λ), is given by the equation below were $F_D(\lambda)$ is the corrected fluorescence intensity of the donor in the wavelength range λ to λ + Δλ and $\varepsilon_A(\lambda)$ is the extinction coefficient of the acceptor at λ (see Equation 1.9).

$$J(\lambda) = \int_0^\infty F_D\,(\lambda)\varepsilon_A(\lambda)\lambda^4 d\lambda \quad \textbf{(1.9)}$$

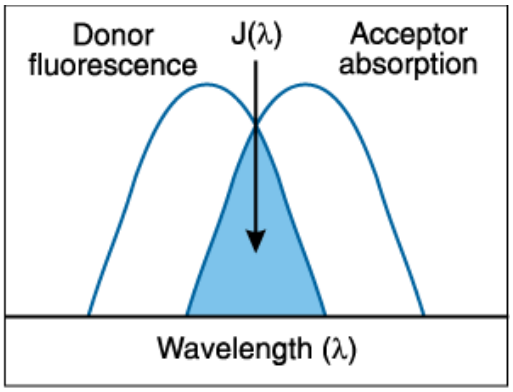


**Figure 1.6** Spectral overlap of the Donor's fluorescence and the Acceptor's absorption is a key factor in creating a FRET pair.

The rate of FRET ($k_T$) in equation 1.8 can be simplified to show the strong dependence on distance, being inversely proportional to $r^6$ as shown in the equation 1.10, where $k_T$ is the rate of energy transfer from a donor to an acceptor, $R_0$ is the distance at which FRET is 50% efficient (Förster distance).

$$k_T = \frac{1}{\tau_D}\left(\frac{R_0}{r}\right)^6 \quad \textbf{(1.10)}$$

The Förster distance can be calculated from the spectral properties of the donor and the acceptor and the donor's quantum yield ($Q_D$) from the equation below.

$$R_0 = 0.211[\kappa^2 n^{-4} Q_D J(\lambda)] \quad \textbf{(1.11)}$$

The overall energy transfer efficiency (E) can then be expressed in the Equation 1.12, which demonstrates the strong distance dependence of the donor-acceptor ($r^6$). The efficiency rapidly increases as r decreases below $R_0$ while the transfer efficiency is nearly zero at r =2$R_0$.

$$E = \frac{R_0^6}{(R_0^6 + r^6)} \quad \textbf{(1.12)}$$

For NIR fluorescence, a common FRET pair is cyanine 5 and cyanine 5.5 dyes, which have been demonstrated by Wabuyele *et al.* using a SMD assay.[48] The structures of the dyes are shown in Figure 1.7. In these experiments, each dye was attached to the stem section of LDR primers and upon ligation, brought into close proximity due to the hybridization of the stem structures of the MBs. The calculated Förster distance ($R_0$) for these dyes was 61.7 Å.

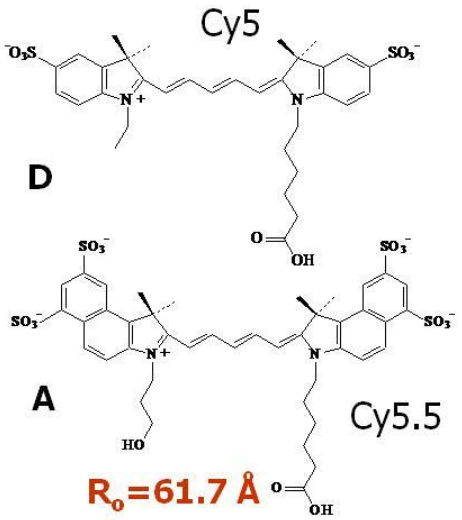


**Figure 1.7** The fluorescent dyes Cy5 and Cy5.5 are a commonly used FRET pair. The Cy5 dye can be excited with either a HeNe laser or a laser diode. The Cy5 dye will transfer its energy to Cy5.5 when they are in close proximity. For this dye pair the $R_0$ distance is 61.7 Å.

## 1.12 FRET Based Assays with Quantum Dots for *K-ras* Point Mutation Detection

Zhang *et al.* reported an ultrasensitive nanosensor based on FRET, which detected low concentrations of DNA in a separation-free format. The system used QDs (605QD) with

streptavidin to bind a biotin capture probe that was complementary to the target DNA. Additionally, a reporter probe labeled with a Cy5 dye was hybridized to the target DNA, which formed a sandwich-hybrid that was bound to the QD through biotin-streptavidin interactions to form the nanosensor (Figure 1.8). The nanonsenor emitted a FRET response due to the bound sandwich-hybrid that was attached to the QD. The QD also functioned as a concentrator that amplified the target signal by confining several targets in the nano-scale domain. Unbound nanosensors produced near-zero background fluorescence, but upon binding to even a small amount of target DNA (~50 copies or less), they generated a very distinct FRET signal.

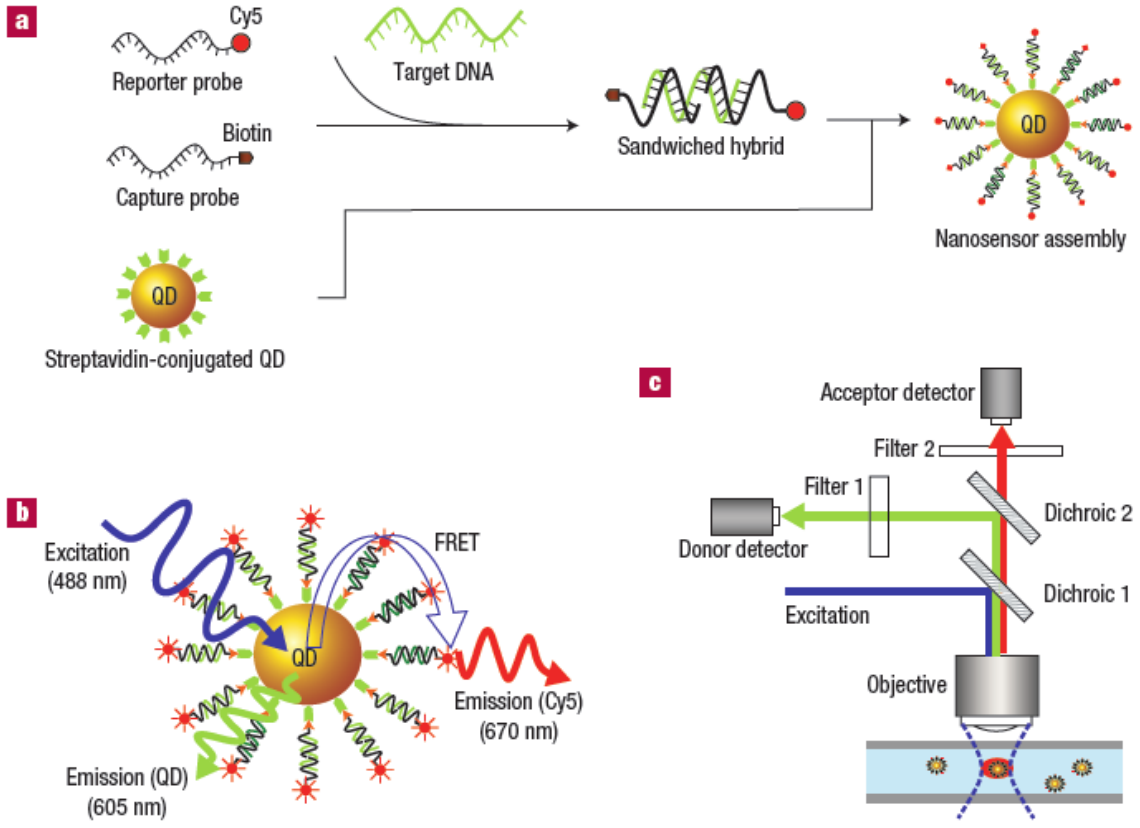


**Figure 1.8** Zhang *et al.* approach involved two probe sequences complementary to the target DNA. These two probes would form a sandwich hybrid with a Cy5 fluorophore and a biotin molecule for capture of the streptavidin conjugated QD, which would form the nanosensor as shown in A. The QD is excited with an argon laser and if the target DNA is present, the sandwich hybrid brings the Cy5 dye into close proximity to the QD to generate the FRET response as shown in B. In C, the detection setup is shown where the authors could monitor not only the FRET response, but also the fluorescence of the donor QD on a second detector. Reprinted with premisson.[137]

The authors validated the method by probing for *K-ras* point mutations (codon 12 GGT to GTT mutation) in clinical samples from patients with ovarian serous borderline tumors. The assays did not require the gel separation and/or washing steps to remove unbound fluorescent probes. They showed discrimination between the homozygous wild-type and the heterozygous targets. The assay provided efficient FRET even at distances approaching $2R_0$. The binding of multiple fluorescent targets yielded a 100-fold increase in the LOD compared to conventional FRET probe-based assays. However, they did not show that a single target DNA could be detected, which indicated that the target DNA would need to undergo PCR before mixing with the nanosensor to insure accurate detection. Additionally, multiple binding makes the quantification difficult.

### 1.13 Ligase Detection Reaction Based Assays

Ligase detection reactions (LDR) are based on a ligase chain reaction (LCR) amplification technique. As opposed to LCR, LDR uses only 2 primers that flank the mutation site and as such, only linearly amplify the target material that contains the desired mutation. Mismatch primers will not be ligated together, therefore a DNA ligase enzyme can be used to discriminate between normal and mutant DNA as required for a SNP assay. Primers can be synthesized to be complementary to the target sequence, which allows for selective amplification of the mutant allele because the wild-type is not complementary to one of the primers used (discriminating primer) and therefore, will not be ligated. LDR has been shown to be capable of screening for sickle cell anemia, ΔF508 mutation in cystic fibrosis and T-cell receptor polymorphisms.[138] Results are easily quantified using an enzyme-linked or direct fluorescent labeling of the LDR products on stem sections just like those used for MBs.

Contrary to the normal MB form, which contains a fluorescent dye and quencher, reverse-molecular beacons (rMBs) use stems that are labeled with two different dyes to form a

FRET pair. In this assay, the $T_m$ (melting temperature of the stem section) of the ligated stem section is higher than the probe section of the LDR primers and the $T_m$ of the unligated stem section. LDR can be performed after an initial PCR amplification of the template DNA or directly on genomic DNA.[48] LDR can be configured in a multiplexing format to quickly identify multiple mutation sites or screening of a large population for monogenic disease polymorphisms.[139]

### 1.14 Ligase Detection Reaction: Single-Pair FRET

An example of the LDR assay for the detection of SNPs in colorectal cancer was shown by Wabuyele *et al.* in which the assay used SMD and could be performed on genomic DNA without PCR leading to fast analyses.[48] A schematic diagram of the assay is shown in Figure 1.9 in which two allele-specific primers are labeled at their 3'- and 5'-ends with fluorescent dyes. These primers flank a single base mutation on the target template. Each primer has a complementary arm sequence. Thermally-stable DNA ligase covalently joins the two adjacent primers only when they perfectly match the template, forming a rMB that can undergo FRET. Conversely, the unligated primers do not show FRET. The detection temperature of the assay was maintained at 75°C to melt the duplex formed between unligated primers, but not the stem of the fully-formed rMB. A rMB is formed by the complementary arm sequences of the ligated primers. The fluorescence emission from the rMB was detected in a polymer microfluidic channel by a confocal optical system. The LDR single-pair fluorescence resonance energy transfer (LDR-spFRET) assay could detect *K-ras* codon 12 (high association with colorectal cancer) in unamplified genomic DNA at a sensitivity of 1:1,000 mutant-to-wild type alleles. An analysis time of less than 5 min was achieved demonstrating the ability of this assay to provide near real-time detection. The LDR allowed for linear amplification of the rMB by increasing the number of thermal cycles. The LDR-spFRET has been shown to be compatible with PCR to

form a continuous flow PCR-LDR.[74, 75] Additionally, the assay has shown great ability to be multiplexed for the analysis of multiple mutations either by product size separation or spatial multiplexing.[140-142]

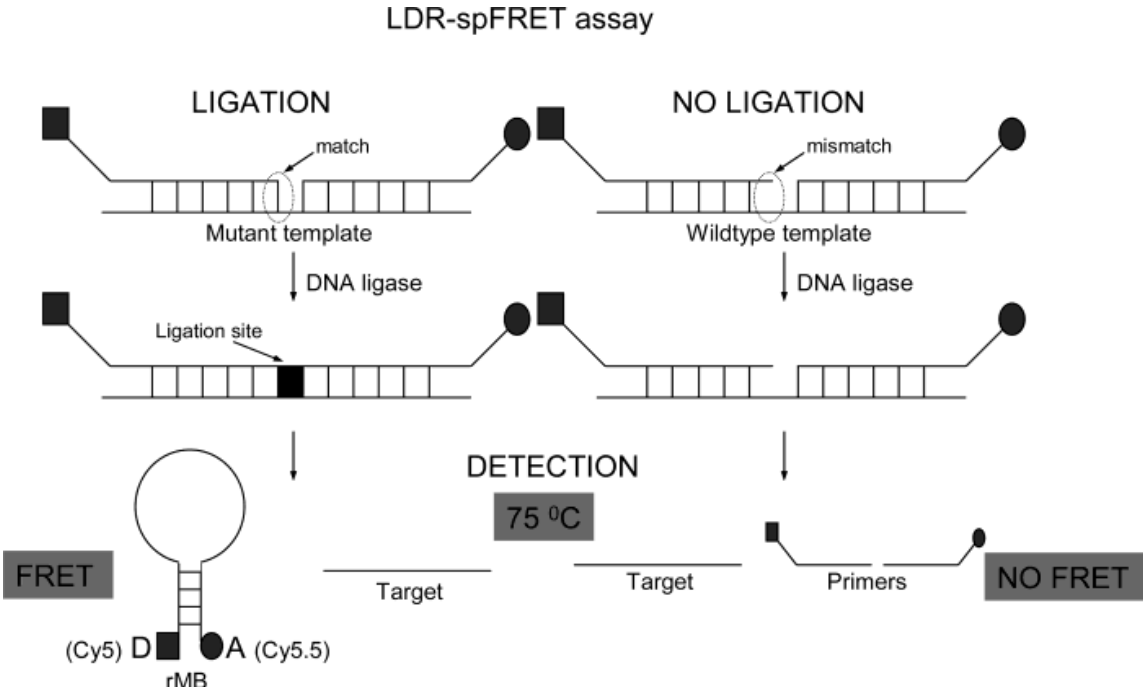


**Figure 1.9** Schematic of the LDR-spFRET assay in which two allele-specific primers are labeled at their 3'- and 5'-ends with fluorescent dyes that flank a SNP on the target template. An enzyme, Taq DNA ligase, covalently joins the two adjacent primers when perfectly matched to the template, forming a MB that can undergo FRET whereas mismatched primers remain unligated and do not show FRET. The detection temperature of the assay was maintained at 75 °C to melt the duplex formed between the target and LDR primers as well as stem sequences of unligated primers but not the stem of the fully formed beacon. Reprinted with premisson.[48]

## 1.15 Rolling-Circle Amplification (RCA)

The ability of small circular oligonucleotides to serve as templates for DNA polymerases has led to the development of rolling-circle amplification (RCA).[143, 144] RCA results in a long single-stranded concatemer DNA molecule (continuous giant DNA molecule) containing the complementary sequence of the circular DNA repeated approximately 500–1,000 times. The use of "padlock" probe-ligation techniques (two target complementary end-sequences hybridizing head-to-tail with a non-complementary segment) keeps the results of the enzymatic amplification

confined in one large molecule instead of many short, freely diffusible copies. This allows for multiple fluorophores per RCA-generated DNA molecule, which makes SMD easier.

Lizardi *et al.* designed an isothermal rolling-circle amplification for mutation detection and single-molecule counting.[145] They devised an assay for ligation-dependent circularization of padlock probes, as well as a method employing preformed circular probes, all of which could be exploited for allele discrimination. They used a novel geometric hyper-branched RCA (HRCA) reaction to detect point mutations in small amounts of human genomic DNA in solution.

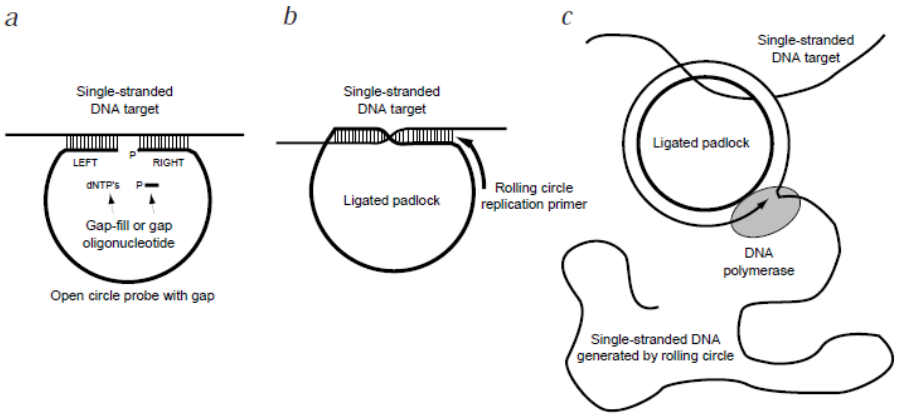


**Figure 1.10** Rolling circle-reaction was used by Lizardi *et al.* to amplify target DNA for SMD. Three types of implementation used were: A) Circularizable probes with a small gap, which was filled by binding a small phosphorylated oligonucleotide target in the gap and then ligation to close the circular probe; B) ligated (padlock) probe, and binding of complementary primer for RCA; and C) Rolling-circle amplification of a padlock probe, catalyzed by a strand displacing DNA polymerase, which yielded a random coil with multiple target sequences. Reprinted with premisson.[145]

The assay had circularizable probes containing two adjacent probe sequences of 20 bases. Specificity was increased by using circularizable probes that could hybridize to the target leaving a small gap of 6-10 nt. This gap could be filled by a DNA polymerase or a short, allele specific oligonucleotide with a 5´ phosphate that fit exactly within the gap, completing a stacked duplex structure that was ligated with DNA ligase to form a closed padlock probe. The gap-ligation reaction was shown to be preferred for allele-specific analysis due to the variable efficiency of

the padlock probes. Although the reaction showed good specificity by requiring two ligation and hybrization events, the reaction time was prolonged and prevented any opportunity for real-time analysis.

Jarvuis *et al.* developed a biomolecule enumeration process by converting nanometer-scale specific molecular recognition events mediated by RCA to fluorescent micrometer-sized DNA molecules amenable to SMD. They used a set of circular DNA molecules to create highly specific molecular probing reactions for DNA using so-called padlock for the detection and quantification of *Vibrio cholera* bacteria. Then, the circular DNA molecules were copied using RCA, which resulted in a collapsed random coil of DNA. When labeled with short fluorescent molecule–tagged hybridization probes, each RCA product was visible in a fluorescence microscope as a bright object with a diameter of approximately 1 mm (see Figure 1.11). This allowed for the hybridization of multiple fluorescent molecules to increase sensitivity with the drawback being increased dye consumption. The key to high sensitivity shown in this paper was the amplification step, which required time consuming and labor-intensive sample preparation.

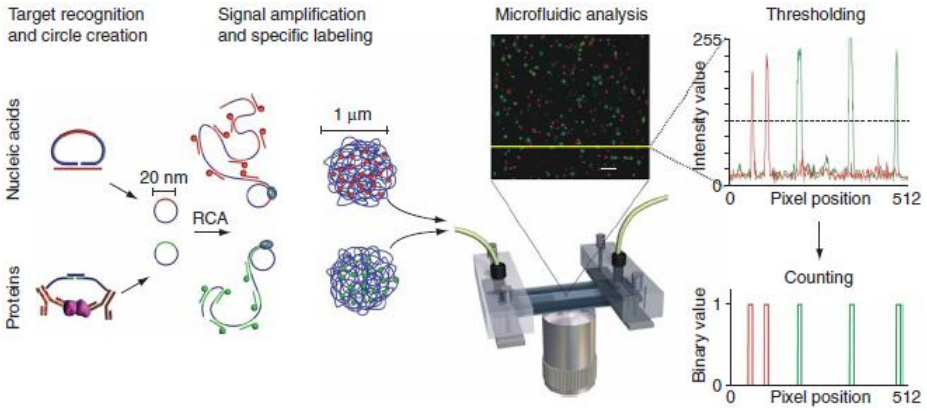


**Figure 1.11** Jarvuis *et al.* RCA for molecular recognition of DNA or protein targets through padlock probe ligation, which resulted in the formation of a unique circular DNA molecule. Fluorescent molecule–tagged probes are hybridized to the repeated sequence, resulting in a significant improvement in sensitivity. The schematic for this assay is shown above with the addition of distinct colors to allow for multiplexed signal readout with each photon burst above the background counted as an event. Reprinted with premisson.[146]

## 1.16 DNA Charge Transfer for SNP

A new method for detection of SNPs at the single-molecule level has recently been shown by Takada *et al.*[147] They demonstrated that DNA charge transfer, which is highly dependent on the electronic interaction between base pairs (π-stack) could be used to scan for DNA mismatches.

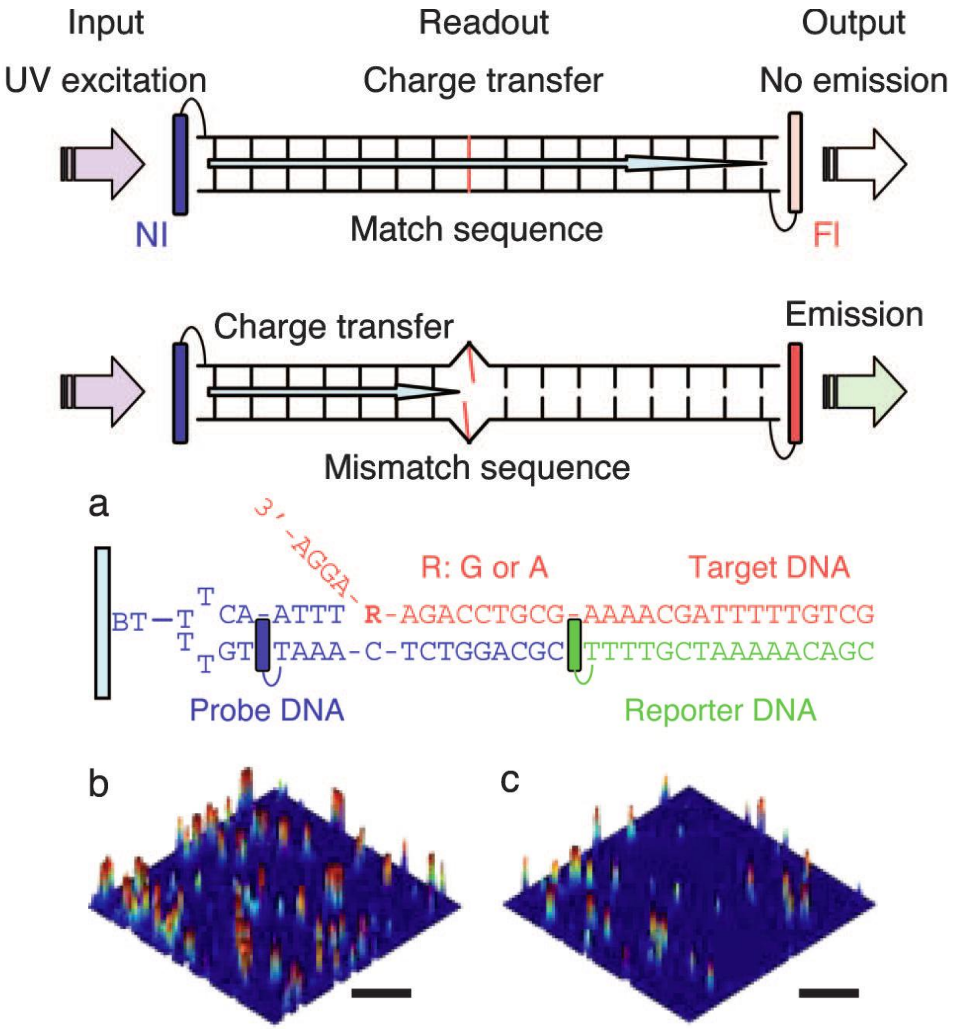


**Figure 1.12** Schematic of a DNA charge transfer detection system where photobleaching of the fluorescent dyes occurs if the dye is oxidized by a freely migrating charge through the DNA. If a point mutation is present, then it disrupts the charge transfer and the dye will emit. As a demonstration of the principle, a single-base mismatch detection experiment was setup. Images of fluorescence before and after the photosensitizer were excited with UV light to cause the oxidation of the fluorescent dye. Adapted and reprinted with permission.[147]

When a photosensitizer (Naphthalimide) is excited it created a charge, which migrates through the π-stack of DNA. If no mismatch was present, then the charge oxidizes the fluorescent dyes resulting in a decrease of fluorescent signal. If there is a mismatch in the sequence, the π-stack is disrupted and the charge migration doesn't reach the fluorophore to oxidize the dye, which means that the fluorescent signal is unchanged. The authors explored this phenomenon by monitoring the on–off signal of the dye after charge injection by the excitation of a photosensitizer. The base sequence affected the bleaching efficiency of the fluorescent dye and single base mismatches strongly suppressed the bleaching efficiency. They used this observation to detect a point mutation in the BRCAI sequence. The authors used total internal reflection fluorescence (TIRF) images to monitor the bleaching efficiency at the single-molecule level (see Figure 1.12). This method provided a SMD system for mutation scanning as opposed to previously described methods, which do mutation detection. Although a novel approach to SNP detection, the method still required PCR and then the hybridization of the target molecule to an immobilized probe sequence with the photosensitizer incorporated into the sequence.

## 1.17 Summary and Prospective

Clinical diagnostics and public health interventions demand rapid and accurate identification of molecular markers/pathogenic bacteria; thus prompt and necessary measures can be undertaken to help minimize health risks. The ability to perform SMD of genomic biomarkers in near-real time will have a number of important applications, such as strain-specific detection of pathogenic bacteria or molecular diagnosis of diseases requiring rapid turn-around-times. The elimination or minimization of front-end processing steps is a major advantage of SMD and will help in realizing real-time analysis. The specificity of the assay is often balanced by the complexity. MB-based assays and coincidence detection have proven to be very rapid and sensitive. Conversely, the RCA padlock and LDR-spFRET provide higher specificity due to the

increased hybridization/ligation steps required. The increased specificity generally requires increased assay time; however, as was demonstrated by Wabuyele *et al.* the products from one LDR-spFRET cycle could be completed and detected in fewer than 5 min.

Growth in this field will be generated from the integration of functionality and the reduction of user interaction steps mirroring the progress made in the overall field of micro total analysis systems. Simplification of user interactions allows for less-trained operators and wider possible applications as commercialized instruments shift to making the detection system a proverbial "black box." Key areas of application are on the front lines of Homeland Security for screening of possible terrorist attacks and food/water safety by directly monitoring samples at remote sites. The other major prospects are in the field of medicine as new molecular targets are identified and personalized treatment becomes the standard of care requiring rapid personalized molecular screening tests. Future prospects for the field continue to grow as SMD moves from a novel laboratory technique to a powerful analysis tool performed by novice users directly in the field.

## 1.18 Research Focus

In the subsequent chapters of this dissertation, research efforts were conducted to advance the development of continuous flow single-molecule detection for LDR-spFRET assays for cancer biomarker and biological weapon detection. Chapter 2 will outline the use of a CCD camera operated in time-delayed integration (TDI) mode for multi-channel detection of point mutations associated with colorectal cancer followed by Chapter 3 showing the design of an orthogonal polymer waveguide for use in a multi-channel SMD application. Chapter 4 will demonstrate the development of a compact, field deployable single-molecule detection instrument, which will be followed by Chapter 5 that focuses on the detection of biological

warfare agents using this compact SMD instrument for gene specific continuous flow LDR-spFRET assays.

## 1.19 References


1. Hirschfeld, T., Optical Microscopic Observation of Single Small Molecules. *Appl Opt* **1976,** *15* (12), 2965-2966.

2. Dovichi, N. J.; Martin, J. C.; Jett, J. H.; Trkula, M.; Keller, R. A., An Approach to Single Molecule Detection by Laser-Induced Fluorescence. *Proc. SPIE Int. Soc. Opt. Eng.* **1983,** *426*, 71-73.

3. Dovichi, N. J.; Martin, J. C.; Jett, J. H.; Trkula, M.; Keller, R. A., Laser-Induced Fluorescence of Flowing Samples as an Approach to Single-Molecule Detection in Liquids. *Anal Chem* **1984,** *56* (3), 348-354.

4. Shera, E. B.; Seitzinger, N. K.; Davis, L. M.; Keller, R. A.; Soper, S. A., Detection of Single Fluorescent Molecules. *Chem Phys Lett* **1990,** *174* (6), 553-557.

5. Nguyen, D. C.; Keller, R. A.; Jett, J. H.; Martin, J. C., Detection of Single Molecules of Phycoerythrin in Hydrodynamically Focused Flows by Laser-Induced Fluorescence. *Anal Chem* **1987,** *59* (17), 2158-2161.

6. Nguyen, D. C.; Keller, R. A.; Trkula, M., Ultrasensitive Laser-Induced Fluorescence Detection in Hydrodynamically Focused Flows. *J. Opt. Soc. Am. B: Opt. Phys.* **1987,** *4* (2), 138-143.

7. Lermer, N.; Barnes, M. D.; Kung, C. Y.; Whitten, W. B.; Ramsey, J. M., High Efficiency Molecular Counting in Solution: Single-Molecule Detection in Electrodynamically Focused Microdroplet Streams. *Anal Chem* **1997,** *69* (11), 2115-2121.

8. Soper, S. A.; Davis, L. M.; Shera, E. B., Detection and Identification of Single Molecules in Solution. *J. Opt. Soc. Am. B: Opt. Phys.* **1992,** *9* (10), 1761-1769.

9. Funatsu, T.; Harada, Y.; Tokunaga, M.; Saito, K.; Yanagida, T., Imaging of Single Fluorescent Molecules and Individual Atp Turnovers by Single Myosin Molecules in Aqueous-Solution. *Nature* **1995,** *374* (6522), 555-559.

10. Vale, R. D.; Funatsu, T.; Pierce, D. W.; Romberg, L.; Harada, Y.; Yanagida, T., Direct Observation of Single Kinesin Molecules Moving Along Microtubules. *Nature* **1996,** *380* (6573), 451-453.

11. Sauer, M.; Angerer, B.; Ankenbauer, W.; Foldes-Papp, Z.; Gobel, F.; Han, K. T.; Rigler, R.; Schulz, A.; Wolfrum, J.; Zander, C., Single Molecule DNA Sequencing in Submicrometer Channels: State of the Art and Future Prospects. *J. Biotechnol.* **2001,** *86* (3), 181-201.

12. Tamarat, P.; Maali, A.; Lounis, B.; Orrit, M., Ten Years of Single-Molecule Spectroscopy. *J Phys Chem A* **2000,** *104* (1), 1-16.

13. Eggeling, C.; Fries, J. R.; Brand, L.; Gunther, R.; Seidel, C. A. M., Monitoring Conformational Dynamics of a Single Molecule by Selective Fluorescence Spectroscopy. *Proc Natl Acad Sci U S A* **1998,** *95* (4), 1556-1561.

14. Moerner, W. E.; Orrit, M., Illuminating Single Molecules in Condensed Matter. *Science* **1999,** *283* (5408), 1670-+.

15. Xie, X. S.; Dunn, R. C., Probing Single-Molecule Dynamics. *Science* **1994,** *265* (5170), 361-364.

16. Chou, H. P.; Spence, C.; Scherer, A.; Quake, S., A Microfabricated Device for Sizing and Sorting DNA Molecules. *Proc Natl Acad Sci U S A* **1999,** *96* (1), 11-13.

17. Foquet, M.; Korlach, J.; Zipfel, W.; Webb, W. W.; Craighead, H. G., DNA Fragment Sizing by Single Molecule Detection in Submicrometer-Sized Closed Fluidic Channels. *Anal Chem* **2002,** *74* (6), 1415-1422.

18. Haab, B. B.; Mathies, R. A., Single-Molecule Detection of DNA Separations in Microfabricated Capillary Electrophoresis Chips Employing Focused Molecular Streams. *Anal Chem* **1999,** *71* (22), 5137-5145.

19. Deniz, A. A.; Dahan, M.; Grunwell, J. R.; Ha, T. J.; Faulhaber, A. E.; Chemla, D. S.; Weiss, S.; Schultz, P. G. In *Single-Pair Fluorescence Resonance Energy Transfer on Freely Diffusing Molecules: Observation of Forster Distance Dependence and Subpopulations*, 1999; pp 3670-3675.

20. Deniz, A. A.; Laurence, T. A.; Beligere, G. S.; Dahan, M.; Martin, A. B.; Chemla, D. S.; Dawson, P. E.; Schultz, P. G.; Weiss, S., Single-Molecule Protein Folding: Diffusion Fluorescence Resonance Energy Transfer Studies of the Denaturation of Chymotrypsin Inhibitor 2. *Proc Natl Acad Sci U S A* **2000,** *97* (10), 5179-5184.

21. Ha, T.; Enderle, T.; Ogletree, D. F.; Chemla, D. S.; Selvin, P. R.; Weiss, S., Probing the Interaction between Two Single Molecules: Fluorescence Resonance Energy Transfer between a Single Donor and a Single Acceptor. *Proc Natl Acad Sci U S A* **1996,** *93* (13), 6264-6268.

22. Jares-Erijman, E. A.; Jovin, T. M., Fret Imaging. *Nat Biotechnol* **2003,** *21* (11), 1387-1395.

23. Schuler, B.; Lipman, E. A.; Eaton, W. A., Probing the Free-Energy Surface for Protein Folding with Single-Molecule Fluorescence Spectroscopy. *Nature* **2002,** *419* (6908), 743-747.

24. Trautman, J. K.; Macklin, J. J.; Brus, L. E.; Betzig, E., Near-Field Spectroscopy of Single Molecules at Room-Temperature. *Nature* **1994,** *369* (6475), 40-42.

25. Zumofen, G.; Klafter, J., Spectral Random-Walk of a Single-Molecule. *Chem Phys Lett* **1994,** *219* (3-4), 303-309.

26. Ha, T.; Glass, J.; Enderle, T.; Chemla, D. S.; Weiss, S., Hindered Rotational Diffusion and Rotational Jumps of Single Molecules. *Phys Rev Lett* **1998,** *80* (10), 2093-2096.

27. Ha, T.; Laurence, T. A.; Chemla, D. S.; Weiss, S., Polarization Spectroscopy of Single Fluorescent Molecules. *J Phys Chem B* **1999,** *103* (33), 6839-6850.

28. Ha, T. J.; Ting, A. Y.; Liang, J.; Caldwell, W. B.; Deniz, A. A.; Chemla, D. S.; Schultz, P. G.; Weiss, S., Single-Molecule Fluorescence Spectroscopy of Enzyme Conformational Dynamics and Cleavage Mechanism. *Proc Natl Acad Sci U S A* **1999,** *96* (3), 893-898.

29. Schmidt, T.; Schutz, G. J.; Baumgartner, W.; Gruber, H. J.; Schindler, H., Imaging of Single Molecule Diffusion. *Proc Natl Acad Sci U S A* **1996,** *93* (7), 2926-2929.

30. Mathies, R. A.; Peck, K., Optimization of High-Sensitivity Fluorescence Detection. *Anal. Chem.* **1990,** *62*, 1786-1791.

31. Goodwin, P. M.; Ambrose, W. P.; Keller, R. A., Single-Molecule Detection in Liquids by Laser-Induced Fluorescence. *Acc Chem Res* **1996,** *29* (12), 607-613.

32. Zander, C., Single-Molecule Detection in Solution: A New Tool for Analytical Chemistry. *Fresenius J. Anal. Chem.* **2000,** *366* (6-7), 745-751.

33. Nie, S. M.; Chiu, D. T.; Zare, R. N., Real-Time Detection of Single-Molecules in Solution by Confocal Fluorescence Microscopy. *Anal Chem* **1995,** *67* (17), 2849-2857.

34. Mertz, J.; Xu, C.; Webb, W. W., Single-Molecule Detection by Two-Photon-Excited Fluorescence. *Opt Lett* **1995,** *20* (24), 2532-2534.

35. Soper, S. A.; Legendre, B. L.; Huang, J. P., Evaluation of Thermodynamic and Photophysical Properties of Tricarbocyanine near-Ir Dyes in Organized Media Using Single-Molecule Monitoring. *Chem Phys Lett* **1995,** *237* (3-4), 339-345.

36. Soper, S. A.; Legendre, B. L.; Williams, D. C., Online Fluorescence Lifetime Determinations in Capillary Electrophoresis. *Anal Chem* **1995,** *67* (23), 4358-4365.

37. Barnes, M. D.; Ng, K. C.; Whitten, W. B.; Ramsey, J. M., Detection of Single Rhodamine-6g Molecules in Levitated Microdroplets. *Anal Chem* **1993,** *65* (17), 2360-2365.

38. Eigen, M.; Rigler, R., Sorting Single Molecules - Application to Diagnostics and Evolutionary Biotechnology. *Proc Natl Acad Sci U S A* **1994,** *91* (13), 5740-5747.

39. Dickson, R. M.; Norris, D. J.; Tzeng, Y. L.; Moerner, W. E., Three-Dimensional Imaging of Single Molecules Solvated in Pores of Poly(Acrylamide) Gels. *Science* **1996,** *274* (5289), 966-969.

40. Lee, Y. H.; Maus, R. G.; Smith, B. W.; Winefordner, J. D., Laser-Induced Fluorescence Detection of a Single-Molecule in a Capillary. *Anal Chem* **1994,** *66* (23), 4142-4149.

41. Fister, J. C.; Jacobson, S. C.; Davis, L. M.; Ramsey, J. M., Counting Single Chromophore Molecules for Ultrasensitive Analysis and Separations on Microchip Devices. *Anal Chem* **1998,** *70* (3), 431-437.

42. Wabuyele, M. B.; Ford, S. M.; Stryjewski, W.; Barrow, J.; Soper, S. A., Single Molecule Detection of Double-Stranded DNA in Poly(Methylmethacrylate) and Polycarbonate Microfluidic Devices. *Electrophoresis* **2001,** *22* (18), 3939-3948.

43. Soper, S. A.; Nutter, H. L.; Keller, R. A.; Davis, L. M.; Shera, E. B., The Photophysical Constants of Several Fluorescent Dyes Pertaining to Ultrasensitive Fluorescence Spectroscopy. *Photochem. Photobiol.* **1993,** *57* (6), 972-977.

44. Soper, S. A.; Mattingly, Q. L.; Vegunta, P., Photon Burst Detection of Single near-Infrared Fluorescent Molecules. *Anal. Chem.* **1993,** *65* (6), 740-747.

45. Li, L. Q.; Davis, L. M., Single-Photon Avalanche-Diode for Single-Molecule Detection. *Rev Sci Instrum* **1993,** *64* (6), 1524-1529.

46. Unger, M.; Kartalov, E.; Chiu, C. S.; Lester, H. A.; Quake, S. R., Single-Molecule Fluorescence Observed with Mercury Lamp Illumination. *BioTechniques* **1999,** *27* (5), 1008-+.

47. Van Orden, A.; Keller, R. A.; Ambrose, W. P., High-Throughput Flow Cytometric DNA Fragment Sizing. *Anal Chem* **2000,** *72* (1), 37-41.

48. Wabuyele, M. B.; Farquar, H.; Stryjewski, W.; Hammer, R. P.; Soper, S. A.; Cheng, Y. W.; Barany, F., Approaching Real-Time Molecular Diagnostics: Single-Pair Fluorescence Resonance Energy Transfer (Spfret) Detection for the Analysis of Low Abundant Point Mutations in K-Ras Oncogenes. *J Am Chem Soc* **2003,** *125* (23), 6937-6945.

49. Castro, A.; Williams, J. G. K., Single-Molecule Detection of Specific Nucleic Acid Sequences in Unamplified Genomic DNA. *Anal Chem* **1997,** *69* (19), 3915-3920.

50. Fister, J. C.; Jacobson, S. C.; Ramsey, J. M., Ultrasensitive Cross Correlation Electrophoresis on Microchip Devices. *Anal Chem* **1999,** *71* (20), 4460-4464.

51. Betzig, E.; Chichester, R. J., Single Molecules Observed by near-Field Scanning Optical Microscopy. *Science* **1993,** *262* (5138), 1422-1425.

52. Fan, Z. H.; Harrison, D. J., Micromachining of Capillary Electrophoresis Injectors and Separators on Glass Chips and Evaluation of Flow at Capillary Intersections. *Anal Chem* **1994,** *66* (1), 177-184.

53. Ford, S. M.; Davies, J.; Kar, B.; Qi, S. D.; McWhorter, S.; Soper, S. A.; Malek, C. K., Micromachining in Plastics Using X-Ray Lithography for the Fabrication of Micro-

Electrophoresis Devices. *Journal Of Biomechanical Engineering-Transactions Of The Asme* **1999,** *121* (1), 13-21.

54. Becker, H.; Gartner, C., Polymer Microfabrication Methods for Microfluidic Analytical Applications. *Electrophoresis* **2000,** *21* (1), 12-26.

55. Becker, H.; Locascio, L. E., Polymer Microfluidic Devices. *Talanta* **2002,** *56* (2), 267-287.

56. McDonald, J. C.; Duffy, D. C.; Anderson, J. R.; Chiu, D. T.; Wu, H. K.; Schueller, O. J. A.; Whitesides, G. M., Fabrication of Microfluidic Systems in Poly(Dimethylsiloxane). *Electrophoresis* **2000,** *21* (1), 27-40.

57. McCormick, R. M.; Nelson, R. J.; AlonsoAmigo, M. G.; Benvegnu, J.; Hooper, H. H. In *Microchannel Electrophoretic Separations of DNA in Injection-Molded Plastic Substrates*, 1997; pp 2626-2630.

58. Effenhauser, C. S.; Bruin, G. J. M.; Paulus, A.; Ehrat, M., Integrated Capillary Electrophoresis on Flexible Silicone Microdevices: Analysis of DNA Restriction Fragments and Detection of Single DNA Molecules on Microchips. *Anal Chem* **1997,** *69* (17), 3451-3457.

59. Soper, S. A.; Ford, S. M.; Qi, S.; McCarley, R. L.; Kelly, K.; Murphy, M. C., Polymeric Microelectromechanical Systems. *Anal Chem* **2000,** *72* (19), 642A-651A.

60. Auroux, P. A.; Iossifidis, D.; Reyes, D. R.; Manz, A., Micro Total Analysis Systems. 2. Analytical Standard Operations and Applications. *Anal Chem* **2002,** *74* (12), 2637-2652.

61. Boone, T.; Fan, Z. H.; Hooper, H.; Ricco, A.; Tan, H. D.; Williams, S., Plastic Advances Microfluidic Devices. *Anal Chem* **2002,** *74* (3), 78A-86A.

62. Liu, Y. J.; Ganser, D.; Schneider, A.; Liu, R.; Grodzinski, P.; Kroutchinina, N., Microfabricated Polycarbonate Ce Devices for DNA Analysis. *Anal Chem* **2001,** *73* (17), 4196-4201.

63. Fanguy, J. C.; Henry, C. S., The Analysis of Uric Acid in Urine Using Microchip Capillary Electrophoresis with Electrochemical Detection. *Electrophoresis* **2002,** *23* (5), 767-773.

64. Lin, Y. C.; Jen, C. M.; Huang, M. Y.; Wu, C. Y.; Lin, X. Z., Electroporation Microchips for Continuous Gene Transfection. *Sens. Actuators, B* **2001,** *79* (2-3), 137-143.

65. Eid, J.; Fehr, A.; Gray, J.; Luong, K.; Lyle, J.; Otto, G.; Peluso, P.; Rank, D.; Baybayan, P.; Bettman, B.; Bibillo, A.; Bjornson, K.; Chaudhuri, B.; Christians, F.; Cicero, R.; Clark, S.; Dalal, R.; Dewinter, A.; Dixon, J.; Foquet, M.; Gaertner, A.; Hardenbol, P.; Heiner, C.; Hester, K.; Holden, D.; Kearns, G.; Kong, X. X.; Kuse, R.; Lacroix, Y.; Lin, S.; Lundquist, P.; Ma, C. C.; Marks, P.; Maxham, M.; Murphy, D.; Park, I.; Pham, T.; Phillips, M.; Roy, J.; Sebra, R.; Shen, G.; Sorenson, J.; Tomaney, A.; Travers, K.; Trulson, M.; Vieceli, J.; Wegener, J.; Wu, D.; Yang, A.; Zaccarin, D.; Zhao, P.; Zhong,

F.; Korlach, J.; Turner, S., Real-Time DNA Sequencing from Single Polymerase Molecules. *Science* **2009,** *323* (5910), 133-138.

66. Clarke, J.; Wu, H. C.; Jayasinghe, L.; Patel, A.; Reid, S.; Bayley, H., Continuous Base Identification for Single-Molecule Nanopore DNA Sequencing. *Nat Biotechnol* **2009,** *4* (4), 265-270.

67. Harris, T. D.; Buzby, P. R.; Babcock, H.; Beer, E.; Bowers, J.; Braslavsky, I.; Causey, M.; Colonell, J.; Dimeo, J.; Efcavitch, J. W.; Giladi, E.; Gill, J.; Healy, J.; Jarosz, M.; Lapen, D.; Moulton, K.; Quake, S. R.; Steinmann, K.; Thayer, E.; Tyurina, A.; Ward, R.; Weiss, H.; Xie, Z., Single-Molecule DNA Sequencing of a Viral Genome. *Science* **2008,** *320* (5872), 106-109.

68. Branton, D.; Deamer, D. W.; Marziali, A.; Bayley, H.; Benner, S. A.; Butler, T.; Di Ventra, M.; Garaj, S.; Hibbs, A.; Huang, X. H.; Jovanovich, S. B.; Krstic, P. S.; Lindsay, S.; Ling, X. S. S.; Mastrangelo, C. H.; Meller, A.; Oliver, J. S.; Pershin, Y. V.; Ramsey, J. M.; Riehn, R.; Soni, G. V.; Tabard-Cossa, V.; Wanunu, M.; Wiggin, M.; Schloss, J. A., The Potential and Challenges of Nanopore Sequencing. *Nat Biotechnol* **2008,** *26* (10), 1146-1153.

69. Beer, N. R.; Hindson, B. J.; Wheeler, E. K.; Hall, S. B.; Rose, K. A.; Kennedy, I. M.; Colston, B. W., On-Chip, Real-Time, Single-Copy Polymerase Chain Reaction in Picoliter Droplets. *Anal Chem* **2007,** *79* (22), 8471-8475.

70. Koh, C. G.; Tan, W.; Zhao, M. Q.; Ricco, A. J.; Fan, Z. H., Integrating Polymerase Chain Reaction, Valving, and Electrophoresis in a Plastic Device for Bacterial Detection. *Anal Chem* **2003,** *75* (17), 4591-4598.

71. Liu, P.; Seo, T. S.; Beyor, N.; Shin, K. J.; Scherer, J. R.; Mathies, R. A., Integrated Portable Polymerase Chain Reaction-Capillary Electrophoresis Microsystem for Rapid Forensic Short Tandem Repeat Typing. *Anal Chem* **2007,** *79* (5), 1881-1889.

72. Ottesen, E. A.; Hong, J. W.; Quake, S. R.; Leadbetter, J. R., Microfluidic Digital Pcr Enables Multigene Analysis of Individual Environmental Bacteria. *Science* **2006,** *314* (5804), 1464-1467.

73. Dittrich, P. S.; Manz, A., Single-Molecule Fluorescence Detection in Microfluidic Channels - the Holy Grail in Mu Tas? *Anal Bioanal Chem* **2005,** *382* (8), 1771-1782.

74. Hashimoto, M.; Barany, F.; Soper, S. A., Polymerase Chain Reaction/Ligase Detection Reaction/Hybridization Assays Using Flow-through Microfluidic Devices for the Detection of Low-Abundant DNA Point Mutations. *Biosen. Bioelectro.* **2006,** *21* (10), 1915-1923.

75. Hashimoto, M.; Barany, F.; Xu, F.; Soper, S. A., Serial Processing of Biological Reactions Using Flow-through Microfluidic Devices: Coupled Pcr/Ldr for the Detection of Low-Abundant DNA Point Mutations. *Analyst* **2007,** *132* (9), 913-921.

76. Hashimoto, M.; Chen, P. C.; Mitchell, M. W.; Nikitopoulos, D. E.; Soper, S. A.; Murphy, M. C., Rapid Pcr in a Continuous Flow Device. *Lab Chip* **2004,** *4* (6), 638-645.

77. Bej, A. K.; Mahbubani, M. H.; Atlas, R. M., Amplification of Nucleic-Acids by Polymerase Chain-Reaction (Pcr) and Other Methods and Their Applications. *Crit Rev Biochem Mol Biol* **1991,** *26* (3-4), 301-334.

78. Wittwer, C. T.; Fillmore, G. C.; Garling, D. J., Minimizing the Time Required for DNA Amplification by Efficient Heat-Transfer to Small Samples. *Ana. Biochem* **1990,** *186* (2), 328-331.

79. Wittwer, C. T.; Garling, D. J., Rapid Cycle DNA Amplification - Time and Temperature Optimization. *Biotechniques* **1991,** *10* (1), 76-&.

80. Asseline, U., Development and Applications of Fluorescent Oligonucleotides. *Curr Org Chem* **2006,** *10* (4), 491-518.

81. Yeh, H. C.; Chao, S. Y.; Ho, Y. P.; Wang, T. H., Single-Molecule Detection and Probe Strategies for Rapid and Ultrasensitive Genomic Detection. *Curr Pharm Biotechnol* **2005,** *6* (6), 453-461.

82. Marziali, A.; Akeson, M., New DNA Sequencing Methods. *Annu Rev Biomed Eng* **2001,** *3*, 195-223.

83. Franca, L. T. C.; Carrilho, E.; Kist, T. B. L., A Review of DNA Sequencing Techniques. *Q Rev Biophys* **2002,** *35* (2), 169-200.

84. Meldrum, D., Automation for Genomics, Part Two: Sequencers, Microarrays, and Future Trends. *Genome Res* **2000,** *10* (9), 1288-1303.

85. Davis, L. M.; Fairfield, F. R.; Harger, C. A.; Jett, J. H.; Keller, R. A.; Hahn, J. H.; Krakowski, L. A.; Marrone, B. L.; Martin, J. C.; Nutter, H. L.; Ratliff, R. L.; Shera, E. B.; Simpson, D. J.; Soper, S. A., Rapid DNA Sequencing Based Upon Single Molecule Detection. *Gene. Ana. - Biomol Eng* **1991,** *8* (1), 1-7.

86. Chan, E. Y., Advances in Sequencing Technology. *Mutation Research-Fundamental and Molecular Mechanisms of Mutagenesis* **2005,** *573* (1-2), 13-40.

87. Bennett, S. T.; Barnes, C.; Cox, A.; Davies, L.; Brown, C., Toward the $1000 Human Genome. *Pharmacogenomics* **2005,** *6* (4), 373-382.

88. Astier, Y.; Braha, O.; Bayley, H., Toward Single Molecule DNA Sequencing: Direct Identification of Ribonucleoside and Deoxyribonucleoside 5 '-Monophosphates by Using an Engineered Protein Nanopore Equipped with a Molecular Adapter. *J Am Chem Soc* **2006,** *128* (5), 1705-1710.

89. Krieg, A.; Ruckstuhl, T.; Seeger, S., Towards Single-Molecule DNA Sequencing: Assays with Low Nonspecific Adsorption. *Anal Biochem* **2006,** *349* (2), 181-185.

90. Castro, A.; Okinaka, R. T., Ultrasensitive, Direct Detection of a Specific DNA Sequence of Bacillus Anthracis in Solution. *Analyst* **2000,** *125* (1), 9-11.

91. Chen, W. J.; Tsai, P. J.; Chen, Y. C., Functional Nanoparticle-Based Proteomic Strategies for Characterization of Pathogenic Bacteria. *Anal Chem* **2008,** *80* (24), 9612-9621.

92. Conway, G. C.; Smole, S. C.; Sarracino, D. A.; Arbeit, R. D.; Leopold, P. E., Phyloproteomics: Species Identification of Enterobacteriaceae Using Matrix-Assisted Laser Desorption/Ionization Time-of-Flight Mass Spectrometry. *J Mol Microbiol Biotechnol* **2001,** *3* (1), 103-112.

93. Hendricker, A. D.; Abbas-Hawks, C.; Basile, F.; Voorhees, K. J.; Hadfield, T. L., Rapid Chemotaxonomy of Pathogenic Bacteria Using in Situ Thermal Hydrolysis and Methylation as a Sample Preparation Step Coupled with a Field-Portable Membrane-Inlet Quadrupole Ion Trap Mass Spectrometer. *Int J Mass Spectrom* **1999,** *191*, 331-342.

94. Hong, B. X.; Jiang, L. F.; Hu, Y. S.; Fang, D. Y.; Guo, H. Y., Application of Oligonucleotide Array Technology for the Rapid Detection of Pathogenic Bacteria of Foodborne Infections. *J. Microbiol. Methods* **2004,** *58* (3), 403-411.

95. Peccoud, J.; Jacob, C., Theoretical Uncertainty of Measurements Using Quantitative Polymerase Chain Reaction. *Biophys J* **1996,** *71* (1), 101-108.

96. Reiss, J.; Krawczak, M.; Schloesser, M.; Wagner, M.; Cooper, D. N., The Effect of Replication Errors on the Mismatch Analysis of Pcr-Amplified DNA. *Nucleic Acids Res* **1990,** *18* (4), 973-978.

97. Dworzanski, J. P.; Snyder, A. P.; Chen, R.; Zhang, H.; Wishart, D.; Li, L., Identification of Bacteria Using Tandem Mass Spectrometry Combined with a Proteome Database and Statistical Scoring. *Anal Chem* **2004,** *76* (8), 2355-2366.

98. Fanen, P.; Ghanem, N.; Vidaud, M.; Besmond, C.; Martin, J.; Costes, B.; Plassa, F.; Goossens, M., Molecular Characterization of Cystic-Fibrosis - 16 Novel Mutations Identified by Analysis of the Whole Cystic-Fibrosis Conductance Transmembrane Regulator (Cftr) Coding Regions and Splice Site Junctions. *Genomics* **1992,** *13* (3), 770-776.

99. Highsmith, W. E.; Burch, L. H.; Zhou, Z. Q.; Olsen, J. C.; Boat, T. E.; Spock, A.; Gorvoy, J. D.; Quittell, L.; Friedman, K. J.; Silverman, L. M.; Boucher, R. C.; Knowles, M. R., A Novel Mutation in the Cystic-Fibrosis Gene in Patients with Pulmonary-Disease but Normal Sweat Chloride Concentrations. *N Engl J Med* **1994,** *331* (15), 974-980.

100. Goate, A.; Chartierharlin, M. C.; Mullan, M.; Brown, J.; Crawford, F.; Fidani, L.; Giuffra, L.; Haynes, A.; Irving, N.; James, L.; Mant, R.; Newton, P.; Rooke, K.; Roques, P.; Talbot, C.; Pericakvance, M.; Roses, A.; Williamson, R.; Rossor, M.; Owen, M.; Hardy, J., Segregation of a Missense Mutation in the Amyloid Precursor Protein Gene with Familial Alzheimers-Disease. *Nature* **1991,** *349* (6311), 704-706.

101. Kim, S. D.; Kim, J., Sequence Analyses of Presenilin Mutations Linked to Familial Alzheimer's Disease. *Cell Stress & Chaperones* **2008,** *13* (4), 401-412.

102. Cheung, M. C.; Goldberg, J. D.; Kan, Y. W., Prenatal Diagnosis of Sickle Cell Anaemia and Thalassaemia by Analysis of Fetal Cells in Maternal Blood. *Nat Genet* **1996,** *14* (3), 264-268.

103. Diamandis, E. P., Point: Epca-2: A Promising New Serum Biomarker for Prostatic Carcinoma? *Clin Biochem* **2007,** *40* (18), 1437-1439.

104. Saranath, D.; Tandle, A. T.; Teni, T. R.; Dedhia, P. M.; Borges, A. M.; Parikh, D.; Sanghavi, V.; Mehta, A. R., P53 Inactivation in Chewing Tobacco-Induced Oral Cancers and Leukoplakias from India. *Oral Oncology* **1999,** *35* (3), 242-250.

105. Anker, P.; Lefort, F.; Vasioukhin, V.; Lyautey, J.; Lederrey, C.; Chen, X. Q.; Stroun, M.; Mulcahy, H. E.; Farthing, M. J. G., K-Ras Mutations Are Found in DNA Extracted from the Plasma of Patients with Colorectal Cancer. *Gastroenterology* **1997,** *112* (4), 1114-1120.

106. Hruban, R. H.; Vanmansfeld, A. D. M.; Offerhaus, G. J. A.; Vanweering, D. H. J.; Allison, D. C.; Goodman, S. N.; Kensler, T. W.; Bose, K. K.; Cameron, J. L.; Bos, J. L., K-Ras Oncogene Activation in Adenocarcinoma of the Human Pancreas - a Study of 82 Carcinomas Using a Combination of Mutant-Enriched Polymerase Chain-Reaction Analysis and Allele-Specific Oligonucleotide Hybridization. *Am J Pathol* **1993,** *143* (2), 545-554.

107. Levi, S.; Urbanoispizua, A.; Gill, R.; Thomas, D. M.; Gilbertson, J.; Foster, C.; Marshall, C. J., Multiple K-Ras Codon-12 Mutations in Cholangiocarcinomas Demonstrated with a Sensitive Polymerase Chain-Reaction Technique. *Cancer Res* **1991,** *51* (13), 3497-3502.

108. Rodenhuis, S.; Slebos, R. J. C., Clinical-Significance of Ras Oncogene Activation in Human Lung-Cancer. *Cancer Res* **1992,** *52* (9), S2665-S2669.

109. Barany, F.; Gerry, N. P.; Witowski, N. E.; Day, J.; Hammer, R. P.; Barany, G., Universal DNA Microarray Method for Multiplex Detection of Low Abundance Point Mutations. *J. Mol. Biol.* **1999,** *00*, 1-12.

110. Samowitz, W. S., Curtin, K., Schaffer, D., Robertson, M., Leppert, M., and Slattery, M.L., Relationship of Ki-Ras Mutationsin Colon Cancers to Tumor Location, Stage, and Survival: A Population-Based Study. *Cancer Epidemiol Biomarkers Prev* **2000,** *9*, 1193-1197.

111. Twist, C. R.; Winson, M. K.; Rowland, J. J.; Kell, D. B., Single-Nucleotide Polymorphism Detection Using Nanomolar Nucleotides and Single-Molecule Fluorescence. *Anal Biochem* **2004,** *327* (1), 35-44.

112. Sinville, R.; Soper, S. A., High Resolution DNA Separations Using Microchip Electrophoresis. *J Sep Sci* **2007,** *30* (11), 1714-1728.

113. Sheffield, V. C.; Beck, J. S.; Kwitek, A. E.; Sandstrom, D. W.; Stone, E. M., The Sensitivity of Single-Strand Conformation Polymorphism Analysis for the Detection of Single Base Substitutions. *Genomics* **1993,** *16* (2), 325-332.

114. Delwart, E. L.; Shpaer, E. G.; Louwagie, J.; McCutchan, F. E.; Grez, M.; Rubsamenwaigmann, H.; Mullins, J. I., Genetic-Relationships Determined by a DNA Heteroduplex Mobility Assay - Analysis of Hiv-1 Env Genes. *Science* **1993,** *262* (5137), 1257-1261.

115. Muyzer, G.; Smalla, K., Application of Denaturing Gradient Gel Electrophoresis (Dgge) and Temperature Gradient Gel Electrophoresis (Tgge) in Microbial Ecology. *Antonie Van Leeuwenhoek International Journal of General and Molecular Microbiology* **1998,** *73* (1), 127-141.

116. Myers, R. M.; Maniatis, T.; Lerman, L. S., Detection and Localization of Single Base Changes by Denaturing Gradient Gel-Electrophoresis. *Methods Enzymol* **1987,** *155*, 501-527.

117. Nubel, U.; Engelen, B.; Felske, A.; Snaidr, J.; Wieshuber, A.; Amann, R. I.; Ludwig, W.; Backhaus, H., Sequence Heterogeneities of Genes Encoding 16s Rrnas in Paenibacillus Polymyxa Detected by Temperature Gradient Gel Electrophoresis. *J Bacteriol* **1996,** *178* (19), 5636-5643.

118. Heim, M.; Meyer, U. A., Genotyping of Poor Metabolizers of Debrisoquine by Allele-Specific Pcr Amplification. *Lancet* **1990,** *336* (8714), 529-532.

119. Chang, C.; Bowman, J. L.; Dejohn, A. W.; Lander, E. S.; Meyerowitz, E. M., Restriction Fragment Length Polymorphism Linkage Map for Arabidopsis-Thaliana. *Proc Natl Acad Sci U S A* **1988,** *85* (18), 6856-6860.

120. Barany, F., Genetic-Disease Detection and DNA Amplification Using Cloned Thermostable Ligase. *Proc Natl Acad Sci U S A* **1991,** *88* (1), 189-193.

121. Lee, H. H.; Chernesky, M. A.; Schachter, J.; Burczak, J. D.; Andrews, W. W.; Muldoon, S.; Leckie, G.; Stamm, W. E., Diagnosis of Chlamydia-Trachomatis Genitourinary Infection in Women by Ligase Chain-Reaction Assay of Urine. *Lancet* **1995,** *345* (8944), 213-216.

122. Di Giusto, D.; King, G. C., Single Base Extension (Sbe) with Proofreading Polymerases and Phosphorothioate Primers: Improved Fidelity in Single-Substrate Assays. *Nucleic Acids Res* **2003,** *31* (3).

123. D'Antoni, C. M.; Fuchs, M.; Harris, J. L.; Ko, H. P.; Meyer, R. E.; Nadel, M. E.; Randall, J. D.; Rooke, J. E.; Nalefski, E. A., Rapid Quantitative Analysis Using a Single Molecule Counting Approach. *Anal Biochem* **2006,** *352* (1), 97-109.

124. Egholm, M.; Buchardt, O.; Nielsen, P. E.; Berg, R. H., Peptide Nucleic-Acids (Pna) - Oligonucleotide Analogs with an Achiral Peptide Backbone. *J Am Chem Soc* **1992,** *114* (5), 1895-1897.

125. Zhang, C. Y.; Johnson, L. W., Homogenous Rapid Detection of Nucleic Acids Using Two-Color Quantum Dots. *Analyst* **2006,** *131* (4), 484-488.

126. Tyagi, S., and Kramer,F.R.,, Molecular Beacons: Probes That Fluoresce Upon Hybridization. *Nat. Biotechnol.,* **1995,** *14*, 303-308.

127. Knemeyer, J. P., Marme, N., and Sauer,M., Probes for Detection of Specific DNA Sequences at the Single-Molecule Level. *Anal. Chem.* **2000,** *72*, 3717-3724.

128. Szemes, M.; Schoen, C. D., Design of Molecular Beacons for Amplidet Rna Assay - Characterization of Binding Stability and Probe Specificity. *Anal Biochem* **2003,** *315* (2), 189-201.

129. Wu, Z. S.; Jiang, J. H.; Shen, G. L.; Yu, R. Q., Highly Sensitive DNA Detection and Point Mutation Identification: An Electrochemical Approach Based on the Combined Use of Ligase and Reverse Molecular Beacon. *Human Mutation* **2007,** *28* (6), 630-637.

130. Yang, L.; Coo, Z. H.; Lin, Y. M.; Wood, W. C.; Staley, C. A., Molecular Beacon Imaging of Tumor Marker Gene Expression in Pancreatic Cancer Cells. *Cancer Biology & Therapy* **2005,** *4* (5), 561-570.

131. Venkatesan, N.; Seo, Y. J.; Kim, B. H., Quencher-Free Molecular Beacons: A New Strategy in Fluorescence Based Nucleic Acid Analysis. *Chem Soc Rev* **2008,** *37* (4), 648-663.

132. Knemeyer, J. P.; Marme, N.; Sauer, M., Probes for Detection of Specific DNA Sequences at the Single-Molecule Level. *Anal Chem* **2000,** *72* (16), 3717-3724.

133. Marme, N.; Friedrich, A.; Muller, M.; Nolte, O.; Wolfrum, J.; Hoheisel, J. D.; Sauer, M.; Knemeyer, J. P., Identification of Single-Point Mutations in Mycobacterial 16s Rrna Sequences by Confocal Single-Molecule Fluorescence Spectroscopy. *Nucleic Acids Res* **2006,** *34* (13).

134. Zhang, C. Y.; Chao, S. Y.; Wang, T. H., Comparative Quantification of Nucleic Acids Using Single-Molecule Detection and Molecular Beacons. *Analyst* **2005,** *130* (4), 483-488.

135. Puleo, C. M.; Wang, T. H., Microfluidic Means of Achieving Attomolar Detection Limits with Molecular Beacon Probes. *Lab Chip* **2009,** *9* (8), 1065-1072.

136. Lakowicz, J. R., *Principles of Fluorescence Spectroscopy*. 2nd Edition ed.; Kluwer Academic/Pelnum Publishers: New York, 1999.

137. Zhang, C. Y.; Yeh, H. C.; Kuroki, M. T.; Wang, T. H., Single-Quantum-Dot-Based DNA Nanosensor. *Nat Mater* **2005,** *4* (11), 826-831.

138. Barany, F.; Widmann, M.; Wilson, W. J.; Czajka, J.; Luo, J.; Batt, C. A., Ligase Chain Reaction (Lcr)-- Overview and Applications. *PCR Methods and Applications* **1994**, S51-S64.

139. Khanna, M., Park, P., Zirvi, M., Cao, W., Picon, A., Day, J., Paty, P. and Barany, F., Multiplex Pcr/Ldr for Detection of K-Ras Mutations in Primary Colon Tumors. *Oncogene* **1999,** *18*, 27-38.

140. Sinville, R.; Coyne, J.; Meayher, R. J.; Cheng, Y. W.; Barany, F.; Barron, A.; Soper, S. A., Ligase Detection Reaction for the Analysis of Point Mutations Using Free-Solution Conjugate Electrophoresis in a Polymer Microfluidic Device. *Electrophoresis* **2008,** *29* (23), 4751-4760.

141. Thomas, G.; Sinville, R.; Sutton, S.; Farquar, H.; Hammer, R. P.; Soper, S. A.; Cheng, Y. W.; Barany, F., Capillary and Microelectrophoretic Separations of Ligase Detection Reaction Products Produced from Low-Abundant Point Mutations in Genomic DNA. *Electrophoresis* **2004,** *25* (10-11), 1668-1677.

142. Emory, J. M.; Soper, S. A., Charge-Coupled Device Operated in a Time-Delayed Integration Mode as an Approach to High-Throughput Flow-Based Single Molecule Analysis. *Anal Chem* **2008,** *80* (10), 3897-3903.

143. Fire, A.; Xu, S. Q., Rolling Replication of Short DNA Circles. *Proc Natl Acad Sci U S A* **1995,** *92* (10), 4641-4645.

144. Liu, D. Y.; Daubendiek, S. L.; Zillman, M. A.; Ryan, K.; Kool, E. T., Rolling Circle DNA Synthesis: Small Circular Oligonucleotides as Efficient Templates for DNA Polymerases. *J Am Chem Soc* **1996,** *118* (7), 1587-1594.

145. Lizardi, P. M.; Huang, X. H.; Zhu, Z. R.; Bray-Ward, P.; Thomas, D. C.; Ward, D. C., Mutation Detection and Single-Molecule Counting Using Isothermal Rolling-Circle Amplification. *Nat Genet* **1998,** *19* (3), 225-232.

146. Jarvius, J.; Melin, J.; Goransson, J.; Stenberg, J.; Fredriksson, S.; Gonzalez-Rey, C.; Bertilsson, S.; Nilsson, M., Digital Quantification Using Amplified Single-Molecule Detection. *Nat Methods* **2006,** *3* (9), 725-727.

147. Takada, T.; Fujitsuka, M.; Majima, T., Single-Molecule Observation of DNA Charge Transfer. *Proc Natl Acad Sci U S A* **2007,** *104* (27), 11179-11183.

# 2 Charge-Coupled Device Operated in a Time-Delayed Integration Mode as an Approach to High-Throughput Flow-Based Single Molecule Analysis*

## 2.1 Introduction

Processing of biochemical/chemical information in high-throughput formats is becoming a necessity in systems targeted for a variety of applications, such as genome sequencing, molecular diagnostics, and drug discovery to name a few. High rates of information throughput can be accomplished by building systems that process many samples in parallel, increase the multiplexing capability of the assay, reduce processing time, or use a combination of the aforementioned approaches. The ability to process large amounts of biochemical/chemical information has been realized through the evolution of several novel technologies, such as capillary array electrophoresis,[1-3] high density plate readers[4] and micro-total analysis systems ($\mu$-TAS).[5, 6] The use of $\mu$-TAS has significantly enhanced throughput capabilities for many applications due to characteristics inherent in this technology, such as decreased analysis times, full automation of the sample processing pipeline, and the ability to configure processing units in a highly parallel fashion.[7]

Single molecule detection (SMD) is another enabler that can assist in realizing high-throughput processing due to its ability to eliminate sample processing steps in multistep assays (reduce assay time) and the short readout times required for each single molecule event. For example, Wabuyele et al. demonstrated the ability to detect single nucleotide polymorphisms (SNPs) from genomic DNA in less than 5 min using single-pair FRET.[8] Reductions in processing times were realized by eliminating the overhead time associated with PCR amplification of the target DNA being interrogated.

*The work reported in this chapter has been published in the Journal of Analytical Chemistry and has been reprinted with permission.

For flow-based SMD experiments in which the single molecule events are transported either hydrodynamically or electrokinetically through a fixed interrogation (sampling) zone, the sample throughput (ST) can be calculated from

$$ST = SE \times DE \times DR \times DC \tag{1}$$

where SE represents the percentage of molecules that are sampled during the experimental run, DR is the delivery rate of molecules into the sampling volume, DC is the readout duty cycle, and DE is the detection efficiency. SE is calculated from

$$SE = \frac{\pi \omega_{\circ}^{2}}{d \times w} \tag{2}$$

where $\omega_o$ is the $1/e^2$ laser beam waist (cm) and $d$ and $w$ are the depth and width (cm) of the flow cell. DR can be calculated using

$$DR = F_v \times C_b \tag{3}$$

where $F_v$ represents the volume flow rate ($cm^3\ s^{-1}$) and $C_b$ is the molecular concentration (molecules $cm^{-3}$). DE is basically the percentage of molecules detected above a threshold value, which is selected to minimize the number of false positives generated during the experiment.

As can be seen from eq 1, increasing the laser spot size, the volume flow rate, or the concentration of the input sample can increase ST. However, these parameters must be balanced by the requirements for achieving high signal-to-noise ratios (SNR) in the single molecule measurement[9] and generating high confidence that the signals monitored during readout are those emanating from single molecule events.[10] For example, in the case of fluorescence single molecule detection with the excitation laser possessing a $1/e^2$ beam waist of 7 $\mu$m (probe volume ~1 pL), a square bore flow tube with a 100 $\mu$m width (SE = 0.015), $F_v = 2 \times 10^{-5}$ $cm^3\ s^{-1}$, and a concentration of $1 \times 10^8$ molecules $cm^{-3}$ (DR = 2000 $s^{-1}$), a ST of only 30 molecules $s^{-1}$ would be realized. The value for $F_v$ was selected based on the condition that the transit time must be

approximately equal to the bleaching lifetime of the fluorophore when excited at optical saturation to produce optimal SNR in the single molecule measurement,[5] and the concentration was chosen to minimize the probability of double occupancy within the sampling (probe) volume.

Confocal setups that are commonly used in many SMD experiments focus the laser beam to a diffraction-limited area within a sampling channel and have a pinhole filter in the secondary image plane of the relay objective to spatially reject light from outside the focal volume, which can improve the SNR in the single molecule measurement. While this setup ensures high DE, it results in low SE. An alternative approach would be to maximize the SE to improve ST by overfilling the sampling channel with the laser excitation beam and removing the pinhole filter.

A format for increasing single molecule ST is to operate the reader in a multichannel configuration, in which samples are dynamically passed through a series of parallel fluidic channels. The resulting fluorescence would be imaged onto a series of detectors with the increase in throughput directly related to the number of channels being interrogated. A charge-coupled device (CCD) provides a platform to image multiple flow-type SMD experiments simultaneously, which can have a profound influence on the SMD ST. For example, van Orden *et al.* described a CCD-based single molecule flow cytometer system in which the effluent from a square-bore tube was imaged onto a 1152 × 1240 pixel CCD camera operated in the snapshot mode.[11] The authors used the system to perform single DNA fragment sizing and were able to demonstrate an increase in ST from 100 fragments $s^{-1}$ using a single element detector to 2000 fragments $s^{-1}$ using the CCD approach. Unfortunately, the camera was operated in the snapshot mode, which significantly reduced the duty cycle of the measurement (duty cycle = $t_{int}/T$, where $t_{int}$ is the signal accumulation time, and $T = t_{int} + t_{rd}$, where $t_{rd}$ is the CCD readout time).

Another operational mode of the CCD is time-delayed integration (TDI), which has been used in astronomy to track weak light emitting objects by adjusting the parallel shift rate of the camera to match the rate of movement of the emitting object. Sweedler and co-workers first applied this CCD mode to an electrophoretic separation in a capillary.[12] They discovered that the advantages of TDI over the snapshot mode were reductions in the amount of data produced, increases in the integration times, better duty cycles, and reduced read noise.[13] Recently, Hesse and co-workers were able to demonstrate the ability to use the TDI mode for the CCD in a single molecule imaging experiment, in which fluorescently labeled lipid molecules embedded in bilayer membranes were interrogated. The scanning speed over the surface to be imaged was matched with the parallel shift rate of the CCD camera. The authors were able to demonstrate the ability to image a 5 mm × 5 mm area in ~11 min.[14]

In normal snapshot readout, the CCD shutter opens and exposes each pixel of the CCD to light. Incident photons promote the formation of a charge that is collected in a potential well. The shutter then closes and the read process begins. The rows of pixels are shifted over one row at a time. The last row finally gets shifted into the parallel shift register. The charges in the parallel shift register are then moved down one pixel at a time into a serial shift register and then to the output node where they are read, amplified and sent to the controller to be recorded.

In TDI mode (see Figure 2.1), the pixel array of the camera is exposed to incident light for the duration of the experiment. The CCD chip in the TDI mode is configured to read out one row at a time instead of a full chip readout as described above. As the light-emitting object enters the field of view, photons are collected by the relay optic and imaged onto the first row of pixels of the CCD camera. As the emitting object traverses the field-of-view, the projection moves down across the rows of the CCD array. The movement of the projection down the CCD rows is

matched with the parallel shift in the TDI mode. In Figure S1 for the mismatched case, the light emitting object is moving slower than the parallel shift rate of the CCD. This mismatch of the net velocity of the emitting object and the parallel shift rate leads to a smeared image in the resulting output. In the matched case shown in Figure S1, the shift rate of charge in CCD pixel rows is matched with the rate of movement of the emitting object through the field-of-view causing all collected charge to be accumulated into a single pixel. The resulting output of the matched rates between parallel shift and the emitting object's rate of travel produces a focused spot in the CCD image producing a much higher SNR than for the mismatched case.[12, 15] The SNR enhancement for the TDI-mode scales with $N^{1/2}$, where $N$ is the number of rows in the CCD camera used in the parallel shift.

In this report, we present for the first time a multichannel system for flow-based single molecule measurements using a CCD camera operated in a TDI mode as a means for increasing the ST of any single molecule measurement. We adapted the CCD to operate in the TDI mode to track single double-stranded DNA molecules ($\lambda$ and pBR322) labeled with an intercalating dye (TOTO-3) in a series of microfluidic channels poised on a PMMA-based microchip. A laser beam was launched into the side of the chip, which irradiated a series of fluidic channels (eight) with the resulting fluorescence imaged onto the CCD.

## 2.2 Experimental Details

### 2.2.1 Optical Setup

The optical system used for the flow-based multichannel single molecule measurements is shown in Figure 2.2a. Excitation was provided by a Sanyo DL5038-21 635 nm laser diode (Thorlabs, Newton, NJ) that was mounted in a temperature control unit (TCLDM9, Thorlabs).

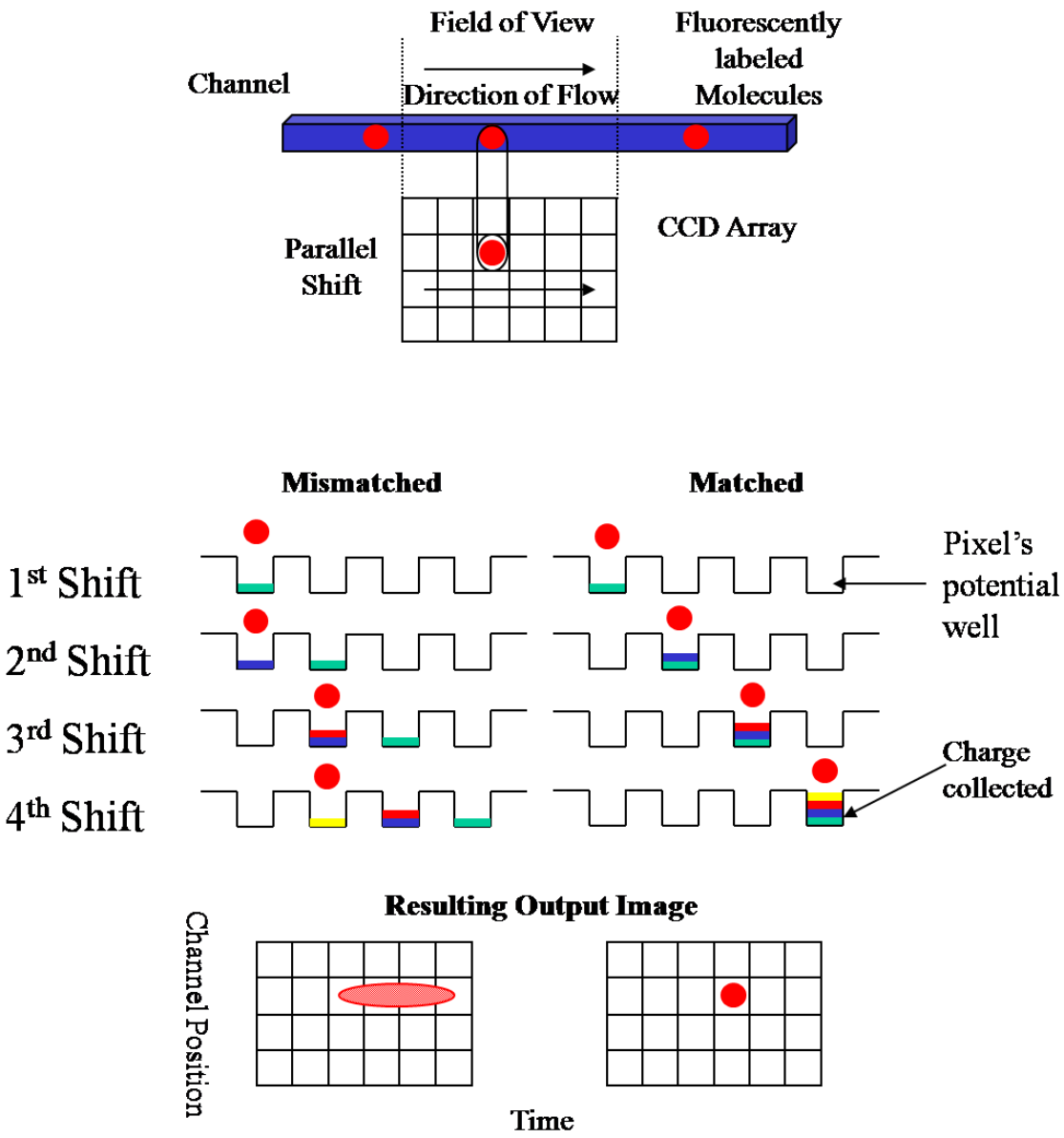


**Figure 2.1** Diagram showing the Time-Delayed Integration (TDI) operational mode of a CCD camera, which occurs when there is a match between the parallel shift rate of the CCD and the rate of travel of emitting objects through the excitation volume. All photons are accumulated into the same potential well of the CCD when these rates are matched. If the timing is mismatched, the fluorescence photons are spread across multiple pixels, resulting in a smeared image.

The laser output was passed through a 635 nm laser line filter (XL37, Omega Optical, Brattleboro, VT) before being collimated with an ashperic lens (C230TMB, Thorlabs). The laser

beam was then directed through a Newport 20×, 0.40 NA objective that focused the laser beam into a single mode fiber optic cable (P1-630A-FC-2, Thorlabs), which was used to produce a circular beam from the elliptical output of the diode laser. The fiber output was launched into an OFR fiber port (PAF-X-11-$\lambda$, OFR, Caldwell, NJ) to produce a collimated beam with a diameter of 2.4 mm. A beam expander was used in the reverse mode to reduce the beam diameter to 200 $\mu$m ($1/e^2$). The beam reducer consisted of a plano-concave lens with a focal length of -6.0 mm and a plano-convex lens with a focal length of 100.0 mm (LC2969-A, AC254-100-A1, Thorlabs). The collimated beam was then launched into the side of a PMMA microchip.

The fluorescence emission was collected with a low magnification, high numerical aperture objective (Fluar 10×, 0.50 NA, Carl Zeiss, Germany) from the bottom side of the PMMA chip and orthogonal to the laser propagation axis. The collected light was directed though an optical tube, which contained a long-pass filter (650 nm long-pass, FEL0650, Thorlabs) and a laser rejection filter (XB23, Omega Optical). A Roper Scientific (Trenton, NJ) Spec- 10 charge-coupled device camera was used to transduce the fluorescence photons and was placed at the secondary image plane of the collection objective. The CCD camera was thermoelectrically cooled to -90 °C and contained a 1 MHz digital converter for fast data acquisition. The CCD possessed 20 $\mu$m pixels and was configured in a 1340 × 100 back-illuminated format. The net velocity of the single molecules through the field-of-view was matched with the parallel shift of the CCD. The strip images of the TDI process were examined after each run to determine if the parallel shift matched the net velocity of the single molecules. If the timing was mismatched, the molecular images appeared as streaks across the strip image whereas if they were matched, the molecules appeared as discrete spots on the TDI image.

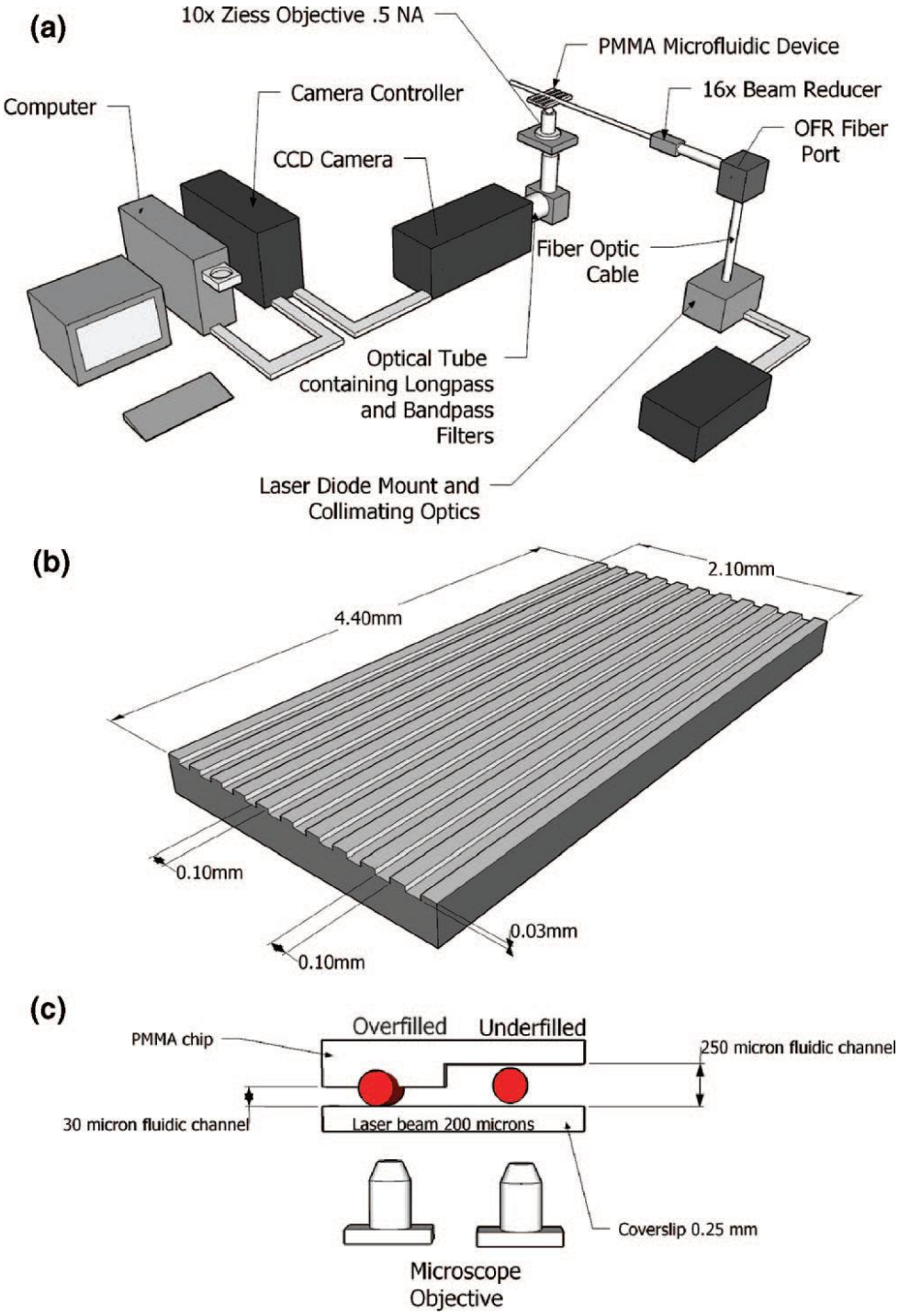


**Figure 2.2** (a) Instrumental arrangement for the high-throughput, multichannel single molecule detection system using a PMMA microfluidic device and a CCD camera operated in a TDI mode. (b) Dimensions of the PMMA chip used for multichannel detection. (c) Horizontal illumination of the PMMA microfluidic device using either an overfilled or underfilled design of the fluidic channels with the laser beam. The overfilled design used 30 $\mu$m deep channels while the underfilled design used 250 $\mu$m deep channels. Both designs were irradiated by a 200 $\mu$m diameter (1/e2) laser beam with 10 mW of average laser power.

### 2.2.2 Microfluidic Chips

The microfluidic devices were fabricated following previously published procedures for producing a mold master and using this master for subsequent hot embossing and coverslip annealing.16 The microfluidic devices were replicated from a brass master (0.25” thick alloy 353 engravers brass, McMaster-Carr, Atlanta, GA) by high precision micromilling. Microstructureswere milled onto the brass plate with a Kern MMP 2522 micromilling machine (KERN Micro-und Feinwerktechnik GmbH & Co., Germany) using procedures previously described.[16] Micromilling was carried out at 40,000 rpm and a typical milling cycle consisted of a pre-cut of the entire brass surface with a 500 µm milling bit to ensure parallelism between both faces of the brass plate and uniform height of the final milled microstructures over the entire pattern, a rough milling of the microstructures using either a 500 or 200 µm milling bit, and a finishing cut with a smaller diameter milling bit. In the final step of mold fabrication, burrs produced at the top of the microstructures were removed by mechanical polishing on a 3 µm grain size polishing paper (Fibrmet Discs - PSA, Buehler, Lake Bluff, IL). The total time required for fabrication of each mold master of the device layout described herein was less than 3 h.

Following lapping to remove any machining burrs, the brass master was used for hot embossing final parts. The mold master was heated to 160°C and pressed into the polymer, PMMA, with a pressure of 1,100 psi for 410 s using a PHI Precision Press (City of Industry, CA). The microfluidic channels were formed by annealing a cover slip (PMMA sheet of 0.25 mm thickness) to the PMMA substrate. The chip was clamped between two glass plates and the assembly placed in a GC oven and the temperature raised to slightly above the $T_g$ (107°C) of PMMA for 20 min.

The microchips consisted of a series of microchannels that were 100 $\mu$m wide with a pitch of 100 $\mu$m and common sample/waste reservoirs situated at the termini of all fluidic channels (see Figure 2.2b). The depth of these channels was designed to be either 250 or 30 $\mu$m. Following assembly, the laser entry side of the PMMA chip was polished on a granite stone (TRU-Stone Technologies, Waite Park, MN) with Bueller-METII silicon carbide of Grit 400/ P800 and then Grit 600/P1200. Finally, the laser input side was polished with a felt disk using a polycrystalline diamond suspension of 9 $\mu$m followed by a 1 $\mu$m suspension to give an optically transparent entry port for the excitation beam.

### 2.2.3 Chemicals and Materials

Borate buffers were prepared by dissolving the desired amount of sodium borate (Sigma Chemical) into nanopure water secured from a Barnstead NANOpure Infinity System (model D8991, Dubuque, IA). The pH was adjusted by the addition of concentrated NaOH or HCl. The buffer was diluted to a final concentration of 50 mM and filtered with a 0.2 $\mu$m filter before use. Fluorescent reagents used in these experiments consisted of AlexaFluor 647, crimson fluorescent FluoSpheres (diameter) 1.0 $\mu$m), and TOTO-3, which were purchased from Molecular Probes (Eugene, OR). An amount of 1 $\mu$g of $\lambda$-DNA (48.5 kbp) and pBR322 (4.3 kbp), obtained from New England Biomedical Research, were diluted in 25 mM borate buffer (pH 9.1). The bis-intercalating dye, TOTO-3, was added at a 5:1 molar ratio (bp/dye). The samples were diluted in borate buffer to yield the desired concentration.

### 2.2.4 TDI Timing

Optimization of TDI timing was performed using crimson fluorescent FluoSpheres diluted in 25 mM borate buffer. The beads were loaded into the common sample reservoir of the PMMA chip and moved through the microfluidic channels by electrokinetic pumping ($E$ = 250

V/cm) using a high-voltage power supply (Canberra Industries, model 3002, Meriden, CT). The shift rate was adjusted by changing the integration time until the shift rate matched the net velocity of the spheres in the fluidic channels. In the case of the single molecule DNA measurements, the shift rate of the CCD was matched to the apparent mobility of the stained DNA through inspection of the CCD images.

A histogram of the photon burst intensity of the individual DNA molecules versus number of events was generated. A Gaussian curve was fit to the distributions to give the average photon burst size per molecule and the standard deviation for each distribution, which could be related to the size of the DNA fragment due to the stoichiometric staining by the bis-intercalating dye.[11, 17]

## 2.3 Results and Discussion

### 2.3.1 Optical Illumination of the Multichannel Architecture

There are basically two strategies in which to illuminate a series of microchannels for multichannel excitation: illumination from the side of the chip using a properly shaped beam or using a laser line generated from a cylindrical lens irradiating the entire array of channels from the top of the chip. As noted by Mathies *et al.*, multichannel illumination with a laser line requires high laser powers to operate near optical saturation to produce optimal SNR in a single molecule measurement, which can produce high background levels due to scattering from the substrate/solution interfaces and generate large probe volumes.[18] Side-illumination using a collinear beam can reduce the high laser power requirements to achieve optimal irradiance and also provides less scattering at the substrate/solution interfaces.[19] Typically, the laser beam would underfill the channel to reduce specularly scattered radiation generated at the substrate/solution interface. Using the laser beam shaping optics in this study, we were able to

produce a collimated beam with a waist ($1/e^2$) of 200 $\mu$m over the imaging area requiring an ~250 $\mu$m deep channel to create such a geometry (see Figure 2.2c). The numerical aperture of the relay objective was determined to give a depth of focus of ~6.6 $\mu$m. Therefore, some molecules would produce "blurred" or weak images in the CCD TDI strip images if a 250 $\mu$m deep channel was used because many of the molecules would be outside the relay objective's depth of focus. This configuration would also produce a low SE, because the width of the beam is less than the channel depth. In order to avoid this, we also investigated the use of an overfilled (see Figure 2.2c) geometry, in which the 200 $\mu$m beam was launched into channels that were only 30 $\mu$m deep to keep most of the single molecule events within the depth of focus of the relay optic and also every molecule traversing through the channel would be sampled (i.e., high SE).

We compared the scattering patterns generated from both the overfilled design (channel depth of 30 $\mu$m) and the underfilled design (channel depth of 250 $\mu$m) with constant laser diameter and power (200 $\mu$m $1/e^2$ waist and 10 mW, respectively). Figure 2.3 shows CCD images collected from these two illumination formats using buffer-filled channels (six channels were evaluated). As can be seen, the absolute scattering intensity from the overfilled geometry was approximately 56% that of the underfilled configuration (mean = 2297 for overfilled; mean = 3887 counts for underfilled geometry) due to attenuation of the beam when launched into the shallower channels. However, the degree of beam attenuation was not directly related to the decrease in channel depth (30 versus 250 $\mu$m, 12%) most likely due to the higher scattering backgrounds generated for the shallower channels. Close inspection of the trace shown for the 30 $\mu$m deep channels (see Figure 2b) indicated that the intensity changed only minimally across the array (RSD = 2% for overfilled and RSD = 3% for underfilled).

The overfilled horizontal illumination format was further evaluated by filling the parallel fluidic channels with AlexaFluor 647 dye and monitoring the emission using the CCD camera operated in the snapshot mode. The average fluorescence emission intensity (background corrected) from eight fluidic channels was found to be 2159 counts with a standard deviation of 38 counts (RSD = 1.7%).

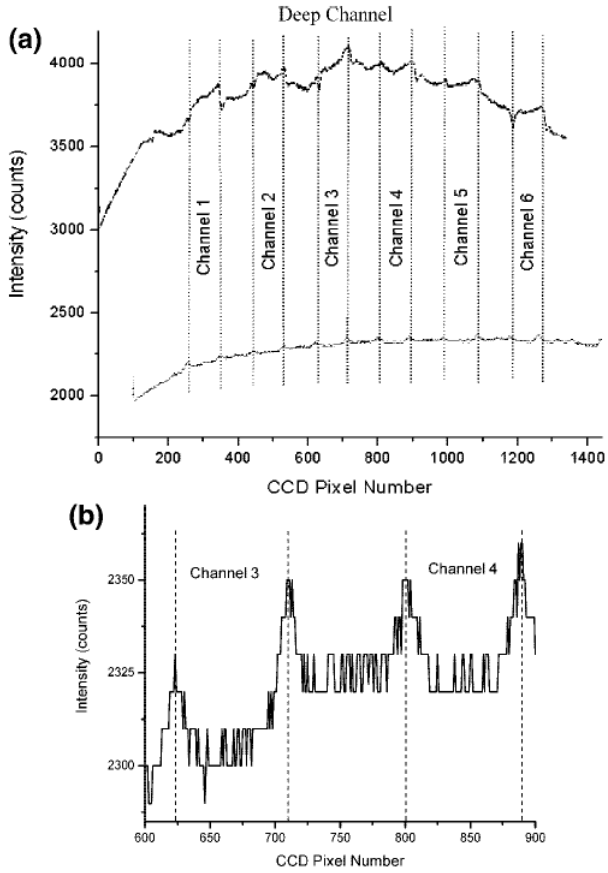


**Figure 2.3** (a) Scattering profiles measured from 250 $\mu$m deep and 30 $\mu$m deep channels. An expanded view of the scattering profile produced from the 30 $\mu$m deep chip is shown in part b. The chips were illuminated with a 10 mW laser (635 nm) and a beam waist ($1/e^2$) of 200 $\mu$m. The channels were filled with borate buffer (pH = 9.1).

With an input beam waist of 200 $\mu$m, a cross sectional area of $4.4 \times 10^{-4}$ cm$^2$ was calculated, which produced an irradiance of 7.3 × 1019 photons cm$^{-2}$ s$^{-1}$ (average laser power = 10 mW) for both the under-filled and overfilled illumination geometries. The fluorescence emission scales linearly with the irradiance until the molecule's excited-state is saturated ($k_{a(sat)}$), which occurs

when $k_{a(sat)} \sim 1/\tau_f$, where $\tau_f$ is the fluorescence lifetime. Zander and co-workers found that for a typical molecular fluorescence lifetime of 10 ns and an absorption cross section of $1.6 \times 10^{-16}$ $cm^2$, optical saturation occurs at an irradiance of approximately $6.2 \times 10^{23}$ photons $cm^{-2}$ $s^{-1}$.[20] Therefore, we are approximately 4 orders of magnitude below optical saturation. Reductions in the beam waist and/or increases in the laser power could further improve the SNR in these single molecule measurements. In the remainder of this work, we adopted a horizontal illumination format with the microchannel depth (30 $\mu$m) close to the depth of field of the objective and overfilled the channels to increase the SE.

### 2.3.2 TDI Timing Optimization

TDI testing was performed by filling the fluidic microchannels with fluorescent microspheres such that the particle density resulted in a single particle occupancy probability of 0.1 in order to reduce the probability of double occupancy. The single particle occupancy probability, $P_v$, can be calculated from the product of the detection volume, $D_v$ (L), and the particle density, $C_p$ (particles $L^{-1}$). In the present case, $D_v$ is not the same as the excitation volume (0.6 nL), which is defined by the $1/e^2$ laser beam waist (200 $\mu$m) and the physical dimensions of the fluidic channel (30 $\mu$m × 100 $\mu$m) but is instead defined by the total magnification of the optical system (10×) and the size of the individual pixels of the CCD camera (20 $\mu$m), producing a $D_v$ of 0.12 pL. Therefore, the particle density for these experiments was selected at $8.3 \times 10^{11}$ particles $L^{-1}$.

The TDI timing was optimized by matching the parallel shift rate of the CCD camera with the linear rate of travel of the fluorescent microspheres (see Figure 2.4) with successful matching determined by observing nonstreaked images of the beads. The image of Figure 2.4a shows long faint streaks, which indicated the timing of the TDI shift rate and bead velocity were

mismatched. The image of Figure 2.4b demonstrated better timing between the bead linear velocity and shift rate due to decreases in the lengths of the streaks shown in the image. As can be seen from the data of Figure 2.4c, nonstreaked images were produced when the CCD parallel shift was set to a rate of 7.5 ms per row, which corresponded to a bead linear velocity of 0.27 cm/s and an apparent mobility of $1.06 \times 10^{-3}$ $cm^2/V$ s. The advantage of electrophoretic pumping as opposed to hydrodynamic pumping is that the flow is plug-like and, as such, the mobility is constant irrespective of the location along the axial direction of the fluidic path. In the case of a mixture of DNA molecules with different sizes, the free solution electrophoretic mobility of DNA is independent of length, and therefore, the same shift rate can be used to interrogate samples comprised of different sized DNAs due to the DNA's free draining behavior.[21]

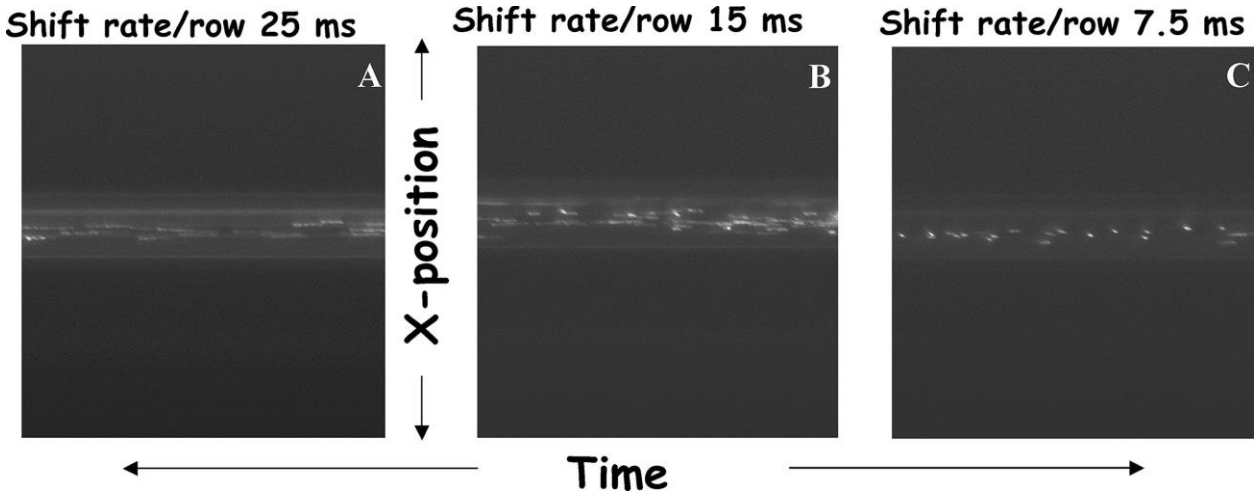


**Figure 2.4** The effects of the parallel shift rate on the TDI images of fluorescent microspheres. The parallel shift rate of the CCD was incrementally changed: (a) 25 ms, (b) 15 ms, and (c) 7.5 ms. The images were accumulated using the fluorescent microspheres excited at 635 nm and electrokinetically pumped using *E* ) 250 V/cm.

### 2.3.3 Comparison of TDI versus Snapshot Modes for CCD Operation

We made a rigorous comparison of the performance metrics of TDI versus snapshot modes of operation for the CCD in single molecule experiments using the fluorescent microbeads. A conventional snap-shot mode of operation of the CCD was compared to the TDI

mode. For these comparisons, fluorescent microbeads were used. The single microbead fluorescence signal, background from the solvent, the net SNR, and the camera duty cycle were rigorously calculated and compared for both modes, the results of which are shown in Table 2.1 for 3 different $t_{int}$ used for the snap-shot mode. Because the laser irradiance, transit time, and bead-type were similar for both modes of CCD operation, only the integration time used for the snap-shot mode should affect the SNR.

For the snap-shot mode, lower background corrected signal levels were observed compared to the TDI mode when $t_{int} < t_T$, because the camera collected and processed photons from the beads for a smaller period of time compared to their transit time through the excitation volume. If $t_{int}$ was set longer or approximately equal to the bead transit time, the background-corrected signals for the TDI and snap-shot modes gave similar net signal intensities. In the snap-shot mode, the pixels along the direction of travel of the beads during their transit through the excitation volume were binned either on or off chip to yield the total fluorescent signal.

The background was found to be higher in all cases of the snap-shot modes compared to TDI because the solvent background was accumulated over all pixels in a single CCD column during $t_{int}$ for snap-shots, while in the case of TDI, only background from a single pixel contributed to the total. Binning of each column (100 x 1) resulted in summing all background counts from each pixel of the CCD. The net effect is the creation of a larger effective probe volume for the snap-shot mode as compared to TDI. Inspection of Table S1 indicated that the TDI mode of operation resulted in a larger single particle SNR compared to all snap-shot modes, with an approximately 10-fold enhancement in the SNR when the integration time was equivalent to the single particle transit time for the snap-shot mode, which agrees with the

predicted √N increase in SNR for the TDI mode, where N is the number of integrated pixels and represents 100 pixels along the particle trajectory path in our experiment.

Comparison of the duty cycles between the snapshot and TDI modes of operation are also shown in Table 2.1. As can be seen, the snapshot modes demonstrated lower duty cycles because the full array of pixels must be read out before another image was captured. For the TDI mode, the CCD shutter remains open during the entire experiment, resulting in a 100% duty cycle. To summarize, the TDI mode produced a single particle SNR of 150 compared to 7 for the snapshot mode when the CCD integration time was less than the particle's transit time. In addition, the duty cycle was 100% for TDI and only 65% for the snapshot mode.

**Table 2.1.** Comparison of the performance metrics for TDI versus snap-shot modes for CCD operation in single molecule measurements using different snap-shot integration times. The exposure time of the CCD ($t_{int}$) was changed for the snap-shot mode with respect to the single particle transit time ($t_T$). In these experiments, fluorescent microspheres were used with laser excitation at 635 nm (10 mW) and the 30 μm deep over-filled channels (beam waist = 200 μm).

| | **Signal + Background Counts** | **Background Counts** | **Net Signal Counts** | **SNR[a]** | **Duty Cycle** |
|---|---|---|---|---|---|
| **TDI** | 8426 | 1890 | 6536 | 150 | 100% |
| $\mathbf{t_{int} \sim t_T}$ | 194591 | 188380 | 6211 | 14 | 86% |
| $\mathbf{t_{int} > t_T}$ | 218554 | 212214 | 6340 | 13 | 96% |
| $\mathbf{t_{int} < t_T}$ | 46938 | 45500 | 1438 | 7 | 65% |

[a]The SNR was calculated from: SNR = (Signal counts – Background counts) / (Background counts)$^{1/2}$.

### 2.3.4 Detection of Single DNA Molecules Using TDI

The TDI optimization for the detection of single DNA molecules labeled with an intercalating dye (TOTO-3) was carried out using horizontal illumination with the CCD camera operated in the TDI mode using λ-DNA and pBR322 as model targets. TOTO-3 binds stoichiometrically to double-stranded DNA, and therefore, the single molecule burst size can be related to the length (in bp) of the DNA molecule being interrogated.[11] The samples were diluted

to ~1 and 10 pM for $\lambda$-DNA and pBR322, respectively. The DNAs were electrokinetically pumped through the microfluidic channels by setting $E$ = 125 V/cm and the fluorescence tracked by adjusting the TDI shift rate to 8 ms per shift. A typical single DNA molecule TDI image for an eight-channel measurement is shown in Figure 2.5a. The peak pixel intensity of each molecular event was identified and recorded from several runs. The data was then plotted as a histogram of molecular events versus burst intensity with the resulting distributions fit to Gaussian functions to secure the mean and standard deviations of the photon bursts (see Figure 2.5b). The mean background (913 units) and standard deviation of the noise (13) was used to plot a Gaussian distribution of the background noise. A threshold level of $3\sigma$ above the average background (952 units) was employed to minimize errors due to false positives and thus, only events exceeding this level were scored as events. The lower amplitude burst distribution was found to possess a mean of 974 units with a standard deviation of 17, which we attributed to the smaller pBR322 DNAs. The second distribution provided a mean of 1268 units with a standard deviation of 23, which was assigned to $\lambda$-DNA due to its larger size compared to pBR322. In addition, because pBR322 DNA was loaded into the device at a 10-fold higher copy number compared to $\lambda$-DNA, the number of events for this distribution was consistent with the higher number concentration of pBR322. The ratio of the mean burst intensity was 5.7, which is in close agreement to the length ratio of the two DNAs ($\lambda$-DNA/pBR322 = 11.3). The background corrected counts for pBR322 was determined to be 61 and with a background noise standard deviation of 13, the SNR for pBR322 in these experiments is 4.7. Because of truncation of the data below 952 CCD units, the pBR322 distribution is skewed and the Gaussian fit should be viewed as provisional in this case.

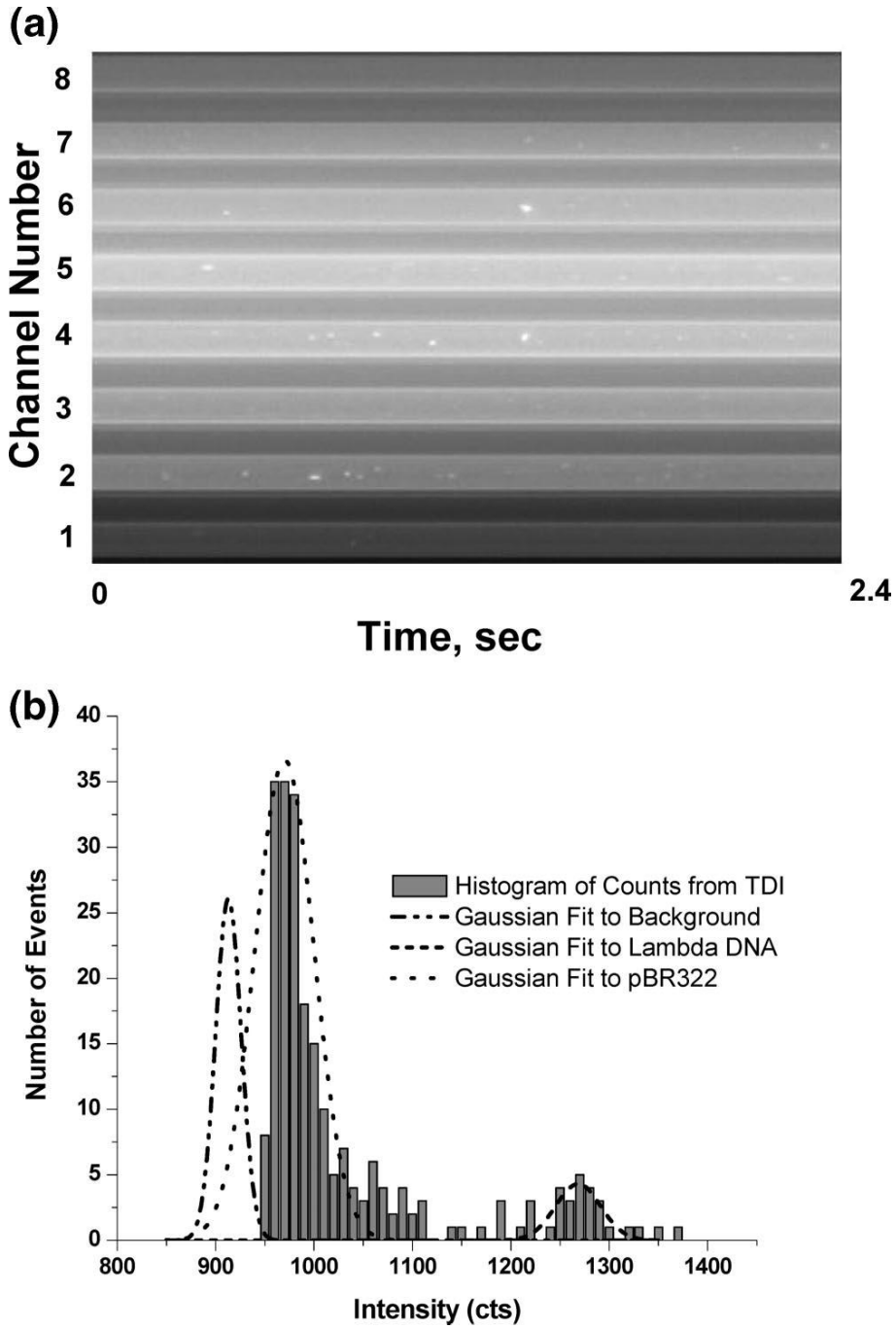


**Figure 2.5** (a) TDI image of $\lambda$-DNA and pBR322 DNAs traveling electrokinetically through eight microfluidic channels with an orthogonally positioned Gaussian laser beam (25 mM borate buffer pH 9.1; shift rate 8 ms; *E* ) 125 V/cm; 10 mW; $\lambda$ex ) 635 nm). (b) Histograms of the peak intensities versus number of events from TDI images shown in part a. The histograms were fit to Gaussian functions from which the mean burst amplitude and standard deviations were derived (mean ) 1268, standard deviation ) 23 for $\lambda$-DNA and mean ) 974, standard deviation ) 17 for pBR322). A Gaussian curve of the noise was also plotted to determine the detection threshold level of 952. The intensity in the images was truncated below the threshold level of ~952 pixel counts.

### 2.3.5 High-Throughput DNA Detection Using TDI

The TDI detection system was then set up to demonstrate the ability to process large numbers of single molecule events by increasing the DNA concentration and also increasing the delivery rate. A solution of $1.0 \times 10^7$ molecules $cm^{-3}$ of $\lambda$-DNA labeled with TOTO-3 was loaded into an eight-channel microfluidic chip. The parallel shift rate in this case was set to the maximum value (1 $ms^{-1}$), and the electrical field was adjusted to give correct timing ($E$= 425 V/cm). The TDI images from a buffer blank and sample from these runs are shown in Figure 2.6a. The average background was subtracted from the images to set a threshold condition to minimize false positive signals and individual events were then counted from enlarged frames (see Figure 2.6b). The ST for this data set was determined to be 276 molecules $s^{-1}$ per channel corresponding to 2208 molecules $s^{-1}$ for imaging the entire eight channel microfluidic chip.

We can further improve both the SNR and the ST for the CCD-based TDI mode of operation for single molecule detection using eq 1 as a guide. For example, reducing the excitation beam waist to ~5 $\mu$m will increase the irradiance by 1600 improving the SNR in the single molecule measurements. Also, reductions in the channel depth from 30 to ~1 $\mu$m will improve the SE and reduce the effective probe volume, hence further reducing background signal. The DR of molecules entering a single channel observation zone in this case depends on the maximum parallel shift rate of the CCD camera, which is hardware limited and sets the maximum volume flow rate (assuming a microchannel crosssectional area of $1 \times 10^{-6}$ $cm^2$) to $1.06 \times 10^{-6}$ $cm^3/s$. If we assume that the probability of single molecule occupancy is set at 0.1 (probability of double occupancy is 0.01), the concentration ($C_b$) that can be used for a probe volume of $4 \times 10^{-12}$ $cm^3$ (probe volume defined by the CCD pixel size, 20 $\mu$m, the total magnification of the optical system, 10×, and a channel depth of 1 $\mu$m), the maximum

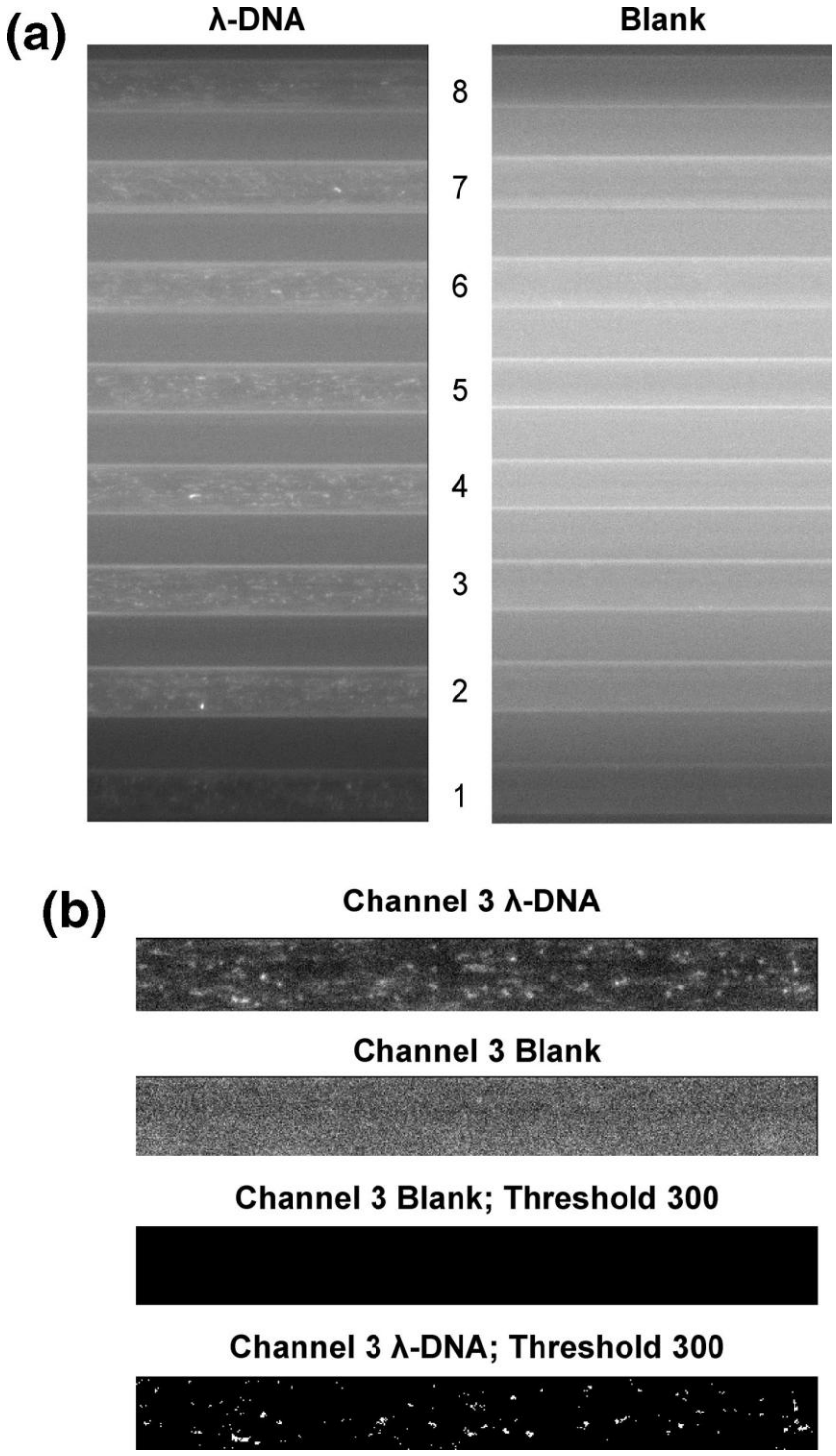


**Figure 2.6** (a) TDI image of $\lambda$-DNA labeled with TOTO-3 and a blank TDI image (25 mM borate buffer, pH 9.1; shift rate of 1 ms-1; $E$ ) 425 V/cm; 10 mW; $\lambda$ex ) 635 nm). (b) Enlarged images of channel 3 from part a after the average background were subtracted at 3$\sigma$ above the mean. At this threshold level of 300, the blank had no counts but the $\lambda$-DNA TDI image produced 138 individual molecular events in the image.

concentration allowed by these conditions would be $2.5 \times 10^{10}$ molecules $cm^{-3}$. Therefore, an acceptable DR would be $2.6 \times 10^{4}$ molecules $s^{-1}$. Assuming a DE of 1.0, the ST for a single channel is calculated to be approximately 26 000 molecules $s^{-1}$ (duty cycle, DC, for our TDI CCD readout mode is 1.0). Because the system in the present case used eight parallel channels, the total system ST is 208 000 molecules $s^{-1}$.In addition, we have not fully utilized the imaging capacity of the CCD camera in the present system in terms of the number of channels that could be interrogated simultaneously. The CCD used in these experiments possessed 1340 pixels for channel imaging. Diffraction limited resolution is approximately $\lambda/2$ indicating that the channel and interchannel spacing could be reduced to ~350 nm in order to optically resolve each experiment, which means our CCD could image 670 channels. This would yield a theoretical ST of $1.7 \times 10^{7}$ molecules $s^{-1}$. Van Orden and co-workers suggested that their snapshot CCD single molecule system could detect ~100,000 fragments $s^{-1}$, which would suggest that our experimental system could provide an ~170-fold higher ST.[11]

## 2.4 Conclusions

The ability to simultaneously track and detect flowing single molecules in multiple microfluidic channels by employing a CCD camera operated in a TDI mode was demonstrated using double-stranded DNA labeled with an intercalating dye as the model. TDI was shown to offer some attractive characteristics in terms of single molecule readout. For example, the TDI mode of operation provided a DC near 100% and favorable SNR for single molecule detection as compared to a snapshot mode of operation where the DC was only 65% and provided a lower single molecule SNR (SNR = 150 for TDI and SNR = 7 for snapshot; see Table 2.1). In addition, the imaging capacity of the CCD can offer some unique opportunities in terms of ST. For

microchannels geometrically configured in a diffraction limited architecture, the system could effectively image ~670 channels, providing a single molecule ST of $>10^7$ molecules $s^{-1}$.

Using the size of the DNA interrogated in this study and the molar ratio of dye-to-DNA base pairs, we calculated that the load of dye per DNA molecule was approximately 9700 for $\lambda$-DNA and 860 for pBR322 DNA. The results depicted in Figure 4b produced a SNR for pBR322 of 4.7, indicating that the present system does not display single fluorophore sensitivity in its current format. Improvements in the SNR for single-fluorophore detection can be realized by increasing the irradiance. Reduction of the laser beam waist and channel depth to more closely match the depth of focus for the optics (1 $\mu$m), the use of a higher laser power (100 mW), and the integration of micro-optics, such as freestanding SU-8 converging lenses for slight focusing of the laser beam in the center of the channels,[22] would provide the necessary increase in the irradiance to approach optical saturation.

## 2.5 References


1. Mathies, R. A.; Huang, X. C., Capillary Array Electrophoresis - an Approach to High-Speed, High-Throughput DNA Sequencing. *Nature* **1992,** *359* (6391), 167-169.

2. Huang, X. H. C.; Quesada, M. A.; Mathies, R. A., Capillary Array Electrophoresis Using Laser-Excited Confocal Fluorescence Detection. *Analytical Chemistry* **1992,** *64* (8), 967-972.

3. Lu, X. D.; Yeung, E. S., Optimization of Excitation and Detection Geometry for Multiplexed Capillary Array Electrophoresis of DNA Fragments. *Applied Spectroscopy* **1995,** *49* (5), 605-609.

4. Huang, K. S.; Mark, D.; Gandenberger, F. U., High-Throughput Measurements of Biochemical Responses Using the Plate: Vision Multimode 96 Minilens Array Reader. In *Measuring Biological Responses with Automated Microscopy*, 2006; Vol. 414, pp 589-600.

5. Blom, N.; Fettinger, J. C.; Koch, J.; Ludi, H.; Manz, A.; Widmer, H. M., Implementing Chemical Sensors in Industry - Novel Approaches. *Sensors and Actuators B-Chemical* **1991,** *5* (1-4), 75-78.

6. Dittrich, P. S.; Manz, A., Single-Molecule Fluorescence Detection in Microfluidic Channels - the Holy Grail in Mu Tas? *Analytical And Bioanalytical Chemistry* **2005,** *382* (8), 1771-1782.

7. Soper, S. A.; Ford, S. M.; Qi, S.; McCarley, R. L.; Kelly, K.; Murphy, M. C., Polymeric Microelectromechanical Systems. *Analytical Chemistry* **2000,** *72* (19), 642A-651A.

8. Wabuyele, M. B.; Farquar, H.; Stryjewski, W.; Hammer, R. P.; Soper, S. A.; Cheng, Y. W.; Barany, F., Approaching Real-Time Molecular Diagnostics: Single-Pair Fluorescence Resonance Energy Transfer (Spfret) Detection for the Analysis of Low Abundant Point Mutations in K-Ras Oncogenes. *Journal Of The American Chemical Society* **2003,** *125* (23), 6937-6945.

9. Mathies, R. A.; Peck, K.; Stryer, L., Optimization of High-Sensitivity Fluorescence Detection. *Analytical Chemistry* **1990,** *62* (17), 1786-1791.

10. Nie, S. M.; Chiu, D. T.; Zare, R. N., Real-Time Detection of Single-Molecules in Solution by Confocal Fluorescence Microscopy. *Analytical Chemistry* **1995,** *67* (17), 2849-2857.

11. Van Orden, A.; Keller, R. A.; Ambrose, W. P., High-Throughput Flow Cytometric DNA Fragment Sizing. *Analytical Chemistry* **2000,** *72* (1), 37-41.

12. Sweedler, J. V.; Shear, J. B.; Fishman, H. A.; Zare, R. N.; Scheller, R. H., Fluorescence Detection in Capillary Zone Electrophoresis Using a Charge-Coupled Device with Time-Delayed Integration. *Analytical Chemistry* **1991,** *63* (5), 496-502.

13. Hanley, Q. S.; Earle, C. W.; Pennebaker, F. M.; Madden, S. P.; Denton, M. B., Charge-Transfer Devices in Analytical Instrumentation. *Analytical Chemistry* **1996,** *68* (21), A661-A667.

14. Hesse, J.; Jacak, J.; Kasper, M.; Regl, G.; Eichberger, T.; Winklmayr, M.; Aberger, F.; Sonnleitner, M.; Schlapak, R.; Howorka, S.; Muresan, L.; Frischauf, A. M.; Schutz, G. J., Rna Expression Profiling at the Single Molecule Level. *Genome Research* **2006,** *16* (8), 1041-1045.

15. Karger, A. E.; Weiss, R.; Gesteland, R. F., Line Scanning System for Direct Digital Chemiluminescence Imaging of DNA-Sequencing Blots. *Analytical Chemistry* **1993,** *65* (13), 1785-1793.

16. Hupert, M. L.; Guy, W. J.; Llopis, S. D.; Shadpour, H.; Rani, S.; Nikitopoulos, D. E.; Soper, S. A., Evaluation of Micromilled Metal Mold Masters for the Replication of Microchip Electrophoresis Devices. *Microfluidics and Nanofluidics* **2007,** *3* (1), 1-11.

17. Wabuyele, M. B.; Ford, S. M.; Stryjewski, W.; Barrow, J.; Soper, S. A., Single Molecule Detection of Double-Stranded DNA in Poly(Methylmethacrylate) and Polycarbonate Microfluidic Devices. *Electrophoresis* **2001,** *22* (18), 3939-3948.

18. Woolley, A. T.; Sensabaugh, G. F.; Mathies, R. A., High-Speed DNA Genotyping Using Microfabricated Capillary Array Electrophoresis Chips. *Analytical Chemistry* **1997,** *69* (11), 2181-2186.

19. Chen, D. H.; Peterson, M. D.; Brumley, R. L.; Giddings, M. C.; Buxton, E. C.; Westphall, M.; Smith, L.; Smith, L. M., Side Excitation of Fluorescence in Ultrathin Slab Gel-Electrophoresis. *Analytical Chemistry* **1995,** *67* (19), 3405-3411.

20. Zander, C., Single-Molecule Detection in Solution: A New Tool for Analytical Chemistry. *Fresenius Journal of Analytical Chemistry* **2000,** *366* (6-7), 745-751.

21. Stellwagen, N. C.; Gelfi, C.; Righetti, P. G., The Free Solution Mobility of DNA. *Biopolymers* **1997,** *42* (6), 687-703.

22. Yang, R.; Wang, W. J.; Soper, S. A., Out-of-Plane Microlens Array Fabricated Using Ultraviolet Lithography. *Applied Physics Letters* **2005,** *86* (16).

# 3 Fabrication of a Cyclic Olefin Copolymer Planar Waveguide Embedded in a Multi-Channel Poly(methyl methacrylate) Fluidic Chip for Evanescence Excitation

The fabrication of the waveguide and characterization of the surface properties were performed by Dr. Paul Okagbare.

## 3.1 Introduction

Lab-on-a-chip (LOC) systems offer a number of compelling advantages compared to their conventional bench-top counterparts, including the ability to process large amounts of chemical/biochemical information due to the ability to build chips in a highly parallel format and the high processing speed they offer.[1-6] A major challenge associated with these miniaturized, multi-channel systems is the associated ultra-small sampling volumes, which places a high demand on the detection system to provide the required limit-of-detection for interrogating a few molecules present in these small detection volumes. While several detection modalities exist for microfluidic systems,[7, 8] laser-induced fluorescence (LIF) has been widely adopted due to the high sensitivity, selectivity and extremely low limits-of-detection obtainable.[9, 10]

Classical optical configurations for LIF are often based on epi-illumination formats,[11, 12] in which both excitation and fluorescence light propagate in the same optical path with spectral sorting accomplished using dichroic filters. Another optical configuration, which has found applications in LIF detection, is total internal reflection (TIR) fluorescence,[13-15] in which fluorescent samples are excited using a surface-confined excitation field. Several reports have documented the use of TIR optics, which use prisms,[16-18] microscope objectives,[19, 20] or optical fibers.[21, 22] In all cases, fluorescence excitation utilized the evanescent field generated by TIR at a high refractive index to a low refractive index boundary.

The penetration depth of the evanescent field is usually fairly small (<750 nm) with the absolute value dependent upon the excitation wavelength, the refractive indices of the waveguiding material and substrate and the launch angle of the incident light. The intensity of the evanescent field, which is proportional to the square of the electric field amplitude,[23] normally drops off exponentially into the lower index medium, thus enabling the realization of small excitation volumes.

A common class of materials used for TIR fluorescence is optical waveguides,[24, 25] which offer advantages such as the realization of compact sensing elements suitable for LOC applications and the potential for fabricating multiple sensors on a single chip.[26] Planar waveguides for biosensing have been made using a variety of materials, such as metal films,[27] metal oxide films,[28] photonic crystals,[29, 30] or silicon oxynitride.[31] While glass remains the most commonly used material for waveguide applications,[15, 32] its incorporation into other sample processing units required for LOC sensing is a challenge due to its limited and sometimes costly fabrication modalities. As a result, polymer-based waveguides[33, 34] have attracted much interest because of their simple fabrication characteristics and in some cases, their favorable optical properties.[35] Also, the ease of integrating these materials into instruments suitable for point-of-care (POC) applications is of great value.

Several polymer materials have been employed for waveguiding including poly(dimethylsiloxane), PDMS,[36, 37] SU-8,[26, 38-40] and poly(methyl methacrylate), PMMA.[41] As an example, Xu *et al*.[41] recently demonstrated the use of a PMMA-based air-embedded planar waveguide for reading DNA microarrays. This waveguide was fabricated in a single step using double-sided hot embossing from two metal mold masters. Another polymeric material, which

holds promise as a potential waveguide material, is cyclic olefin copolymer (COC). COC has properties that can be tailored within a wide range of physicochemical characteristics during polymerization.[42] COC possesses high optical transparency, excellent electrical properties, high rigidity, good biocompatibility, high chemical resistance to acids and alkalis and good thermal properties.[42, 43] Several works have reported on the microfabrication of COC devices,[44-49] which have created avenues for expanding the utility of this polymer, especially as a waveguide material due to its exquisite optical properties and the fact that the optical properties, such as the refractive index, can be tuned by adjusting the percent composition of the monomer comprising the copolymer.[50]

Although progress has been made toward integrating waveguides into microfluidic systems,[14, 51-53] the effective propagation of light through a single planar waveguide for evanescent excitation of multiple fluidic channels suitable for high throughput fluorescence analyses has not been reported to-date. In this paper, we present for the first time the fabrication of a polymer waveguide embedded in a lower refractive index polymer serving as a cover plate for a substrate that contained a series of fluidic channels. The waveguide was situated orthogonal to the microfluidic channels to provide evanescent excitation of the material moving through the fluidic channels. The fluidic channels were hot embossed from a metal master into a PMMA sheet, which was thermally fusion bonded to a PMMA cover plate containing the orthogonal COC waveguide. To carefully control the laser launch angle into the waveguide near the critical angle, which was defined by the refractive index of COC (n = 1.53) and PMMA (n = 1.48), a monolithic prism was integrated to the COC waveguide in a single fabrication step eliminating the need for an external prism and index matching oil.

## 3.2 Experimental

### 3.2.1 Materials and Reagents

COC sheets (grade: 5010L; $T_g$ = 110$^o$C; n = 1.53) were obtained from Topas (Topas Advanced Polymer, USA); the molecular structure of Topas COC is shown in Figure 3.1a with the monomer units represented as x and y. Toluene was obtained from Fisher Scientific (Fisher Chemicals, USA) and used as supplied to make a polymer solution of COC, which was obtained by dissolving pieces of COC in toluene, which made a clear solution of the polymer. A PDMS base and curing agents were obtained from Dow Corning (Dow Corning Corporation, Midland, USA.). AlexaFluor 647 was obtained from Molecular Probes (Eugene, Oregon, USA) with the stock and sample solutions made in 1X Tris-Taps-EDTA (TTE) buffer (pH = 8.7).

### 3.2.2 Image Acquisition

All fluorescence images were acquired using a Roper Scientific (Trenton, NJ) Spec-10 charge-coupled (CCD) camera that was thermally cooled to -90$^o$C and contained a 1 MHz digital converter. The CCD camera had 20 µm pixels that were configured in a 1340 x 100 back-illuminated format. Scanning electron micrograph (SEM) images were acquired using a Cambridge S-260 SEM (Cambridge instruments Ltd. Cambridge, UK) interfaced to Video Wave 5 (Real Networks Inc. Washington, USA). Atomic force microscopy (AFM) images were acquired using a Nanoscope III instrument (Digital Instruments, CA).

### 3.2.3 Layout of the Integrated System

Figure 3.1b shows a schematic diagram of the multi-channel fluidic device with an embedded COC waveguide and monolithic prism. The device consisted of two layers; a PMMA cover plate (refractive index, n, = 1.48, $T_g$ = 107$^o$C) into which the COC waveguide (refractive index, n = 1.53) was embedded and a PMMA substrate, which contained the fluidic channels

(100 µm x 30 µm) that were replicated/embossed from a metal mold master (see Figure 3.1c). The waveguide (200 µm x 200 µm) was situated orthogonal to the longitudinal axis of the fluidic channels along the width of the PMMA cover plate, the size of which defined the excitation volume in each fluidic channel along with the penetration depth of the evanescent field. The monolithic prism (see Figure 3.1b) facilitated coupling the excitation light into the waveguide without the need for an external prism or index matching oil.

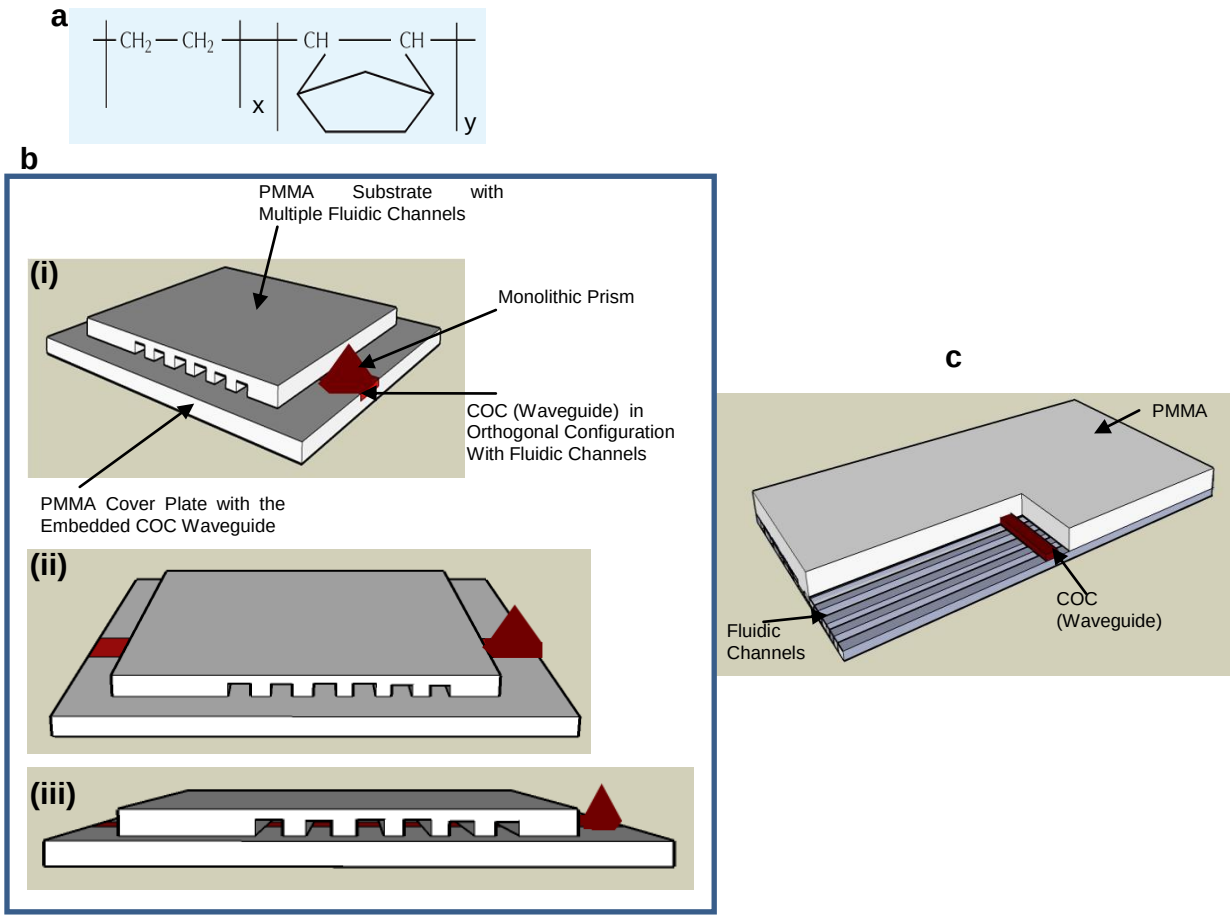


**Figure 3.1** (a) Molecular structure of Topas COC; x and y represent the monomer units, which are polymerized by metallocene catalyzed polymerization. The $T_g$ and the refractive index, n, can be modified by increasing or decreasing the amount of norbornene (y) units in the monomer mixture during polymerization. (b) Schematic representation of the fluidic device with embedded COC planar waveguide with a monolithic coupling prism: (i) diagonal view, (ii) frontal view, (iii) cross sectional view. (c) Schematic of a portion of the device showing the multi-channel fluidic architecture and interconnected waveguide.

### 3.2.4 Fabrication of the Embedded Waveguide

The stepwise fabrication process for creating the embedded COC orthogonal planar waveguide and monolithic prism is shown in Figure 3.2a. The first step involved the generation of a PDMS stencil, which was used to define the waveguide and coupling prism and was produced by casting the PDMS against a relief. The relief contained a prism-shaped structure that was aligned to a 1 mm diameter pole structure (height of structure = 2.0 mm) used to create an access reservoir. The plastic relief was replicated from a brass mold master fabricated by high precision micromilling (Kern MMP micromilling machine).[54, 55] A PDMS pre-polymer solution was obtained by mixing the PDMS base and the curing agent at a ratio of 10:1 by mass. This solution was degassed and loaded through the injection port of a molding frame containing the relief to completely fill the mold cavity (see (i) in Figure 3.2a). Curing of the PDMS pre-polymer solution was achieved in 1.5 h using a vacuum oven set at 70$^{o}$C. The resulting PDMS stencil containing the prism-shaped recess and a 1 mm diameter reservoir (created by the 1 mm diameter pole) was peeled from the relief (see (ii) in Figure 3.2a).

The PDMS stencil was then placed onto a sheet of PMMA containing a pre-fabricated waveguide channel (200 µm x 200 µm) (see (iii) in Figure 3.2a). The waveguide channel was replicated onto a sheet of PMMA from a brass mold master that was fabricated by high precision micromilling. The prism-shaped recess on the PDMS stencil and the access reservoir were carefully aligned with the waveguide channel under a microscope. A COC solution (melt) was then introduced into the waveguide channel through the access reservoir in the PDMS stencil to fill the channel and the prism-shaped recess (see (iv) in Figure 3.2a). This assembly was allowed

to cure in a vacuum oven for 24 h at room temperature. Following curing of the COC, the PDMS stencil was carefully peeled from the PMMA sheet, which formed the embedded COC waveguide and the monolithic coupling prism (see (v) in Figure 3.2a). Figure 3.2b shows an image of the embedded COC waveguide with monolithic prism.

### 3.2.5 Integration of the Embedded Waveguide with the Multi-Channel Substrate

The fluidic channels were replicated into a PMMA substrate (thickness = 250 µm) via hot embossing from a brass mold master, which was fabricated by high precision micromilling.[54, 55] This PMMA wafer contained channels with dimensions of 100 µm width x 30 µm depth and was thermally fusion bonded to the waveguide-bearing PMMA cover plate in an orthogonal configuration with the waveguide spanning the length of the entire array of fluidic channels (see (vi) in Figure 3.2a). In this case, the embedded waveguide defined the illumination cross sectional area for each fluidic channel. Figure 3.2c shows an optical micrograph of the waveguide and the fluidic channel when thermally assembled.

### 3.2.6 Water Absorption Measurements

The COC polymer was prepared for water absorption measurements by coating a portion of the COC melt onto a glass slide to a thickness of 200 µm. The COC coated glass slide was then placed into a vacuum oven for 24 h at room temperature. Following curing, the polymer film was extracted for water absorption measurements. The polymer films were heated to 95$^{o}$C for 50 min, allowed to cool to room temperature, and subsequently weighed. The sample was then immersed into water for 24 h at room temperature and re-weighed following drying under a constant flow of $N_2$ to remove surface moisture. The difference in weight was calculated in order to establish the percentage of water absorption.[50]

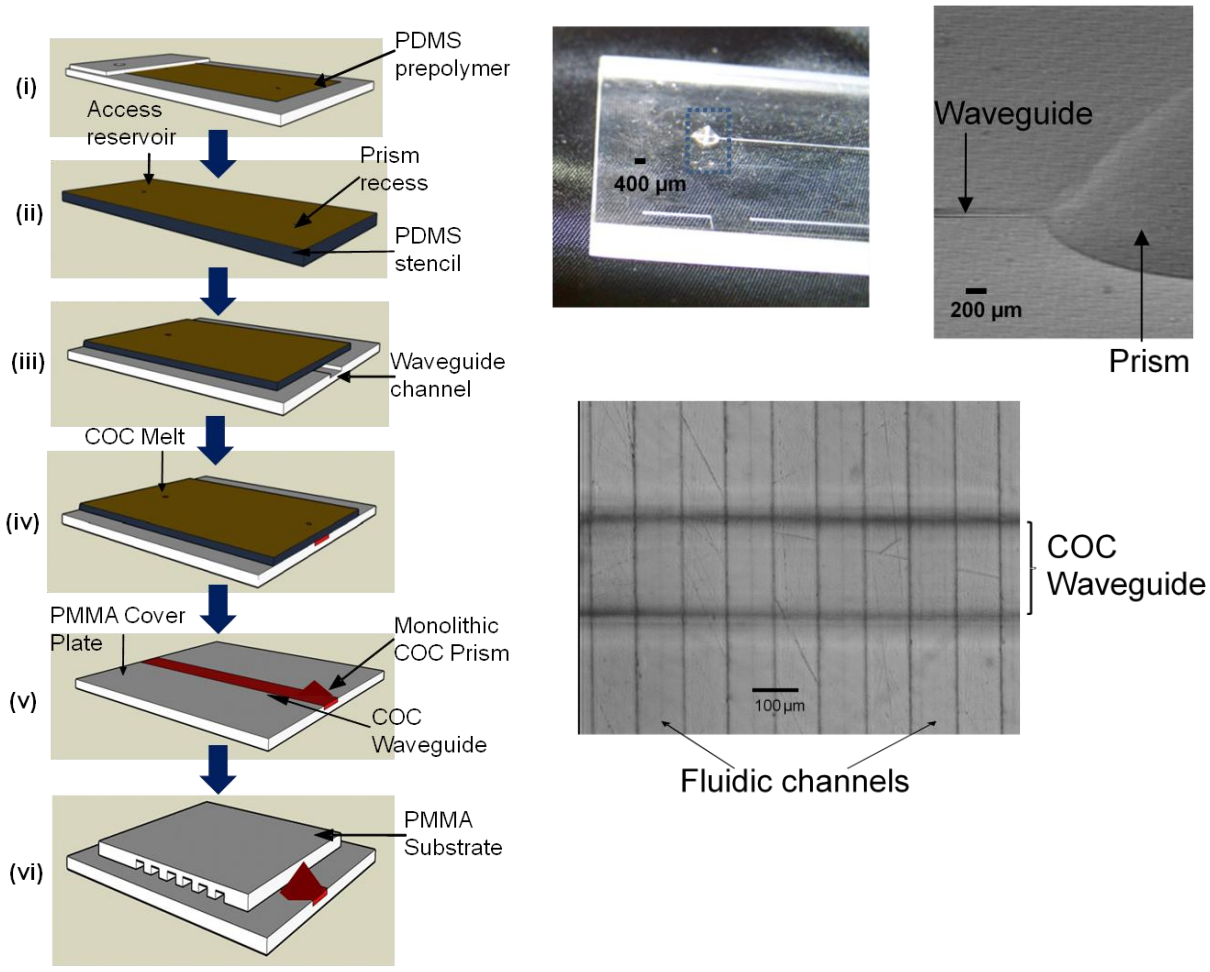


**Figure 3.2** (a) Schematic representation of the stepwise process for the fabrication of the embedded COC orthogonal waveguide in a PMMA chip. A relief was used for casting a PDMS pre-polymer against (PDMS + Curing agent at 10:1 ratio) to form the stencil, which contained the recess for molding the COC prism and an access reservoir to allow filling of the COC melt (i). The PDMS stencil was peeled from the relief after curing at 70$^{o}$C for 90 min (ii) and placed on the surface of a PMMA sheet, which would serve as the device cover plate, containing a pre-fabricated waveguide channel (waveguide channel was embossed from a mold master fabricated using high precision micromilling) and a COC melt (prepared using toluene as the solvent) was introduced into the assembly to form the waveguide and coupling prism (iv). The PDMS stencil was then peeled off from the PMMA cover plate, which created the embedded waveguide with the monolithic coupling prism (v). Finally, the PMMA cover plate with waveguide assembly was thermal fusion bonded to a PMMA substrate containing multiple fluidic channels (vi) that were prepared using hot embossing. The fluidic substrate and the PMMA cover plate were thermally fusion bonded at ~105$^{o}$C, near the $T_g$ of both polymeric materials. (b) Photographs of the PMMA sheet showing the embedded waveguide with the integrated monolithic prism (to the right is the SEM of a section of the prism). (c) Optical micrograph of the embedded waveguide integrated to the fluidic channels.

### 3.2.7 Coupling of Light into the Waveguide

The excitation laser (635 nm) was generated from a laser diode (HL6322G Hitachi Laser Diode, Thorlabs) and coupled into a fiber optic cable (AFS50/125Y, Thorlabs), which at its distal end was coupled to an OFR fiber port (PAF-X-2-B) equipped with a collimation lens to generate a collimated laser beam. To minimize light loss at the entrance to the waveguide, the collimated laser beam was passed through a beam expander that was used in the reverse mode to reduce the beam diameter from 2 mm to ~200 µm. The resulting beam (4.4 mW) was launched through the monolithic prism into the waveguide with a launch angle adjusted to ~76$^{o}$ (critical angle $\theta_c = 75^{o}$) using a goniometer, which allowed the light to propagate through the waveguide via total internal reflection. The critical angle ($\theta_c = \sin^{-1} n_{clad}/n_{core}$) was defined by the refractive indices of the PMMA cladding (n = 1.48) and the COC core (n = 1.53).

## 3.3 Results and Discussion

### 3.3.1 Evaluation and Characterization of the Embedded COC Waveguide

To confirm that loading of the waveguide channel with the COC melt generated an optically homogeneous interface between the COC core and PMMA after curing the COC, a SEM of the empty waveguide channel and the COC filled channel were obtained (data not shown). In addition, we also inspected via optical microscopy the COC core for any in-homogeneities resulting from air bubbles that may create speckle patterns in the waveguide due to refractive index changes. Close examination of the SEMs revealed a highly uniform interface between the COC/PMMA with no observable imperfections in the COC core. These results were further supported by AFM images (see Figure 3.3a) of the surface of the embedded waveguide, which generated a RMS value (surface roughness) of 61.2 ±0.1 nm. As can be seen from this image, the COC core surface was smooth and showed no evidence of large pits arising from air

bubbles or other materials during its production, which could generate light loss. We also noticed no speckles in the waveguide when light was coupled into it.

Among the properties of waveguides that define their suitability for efficient operation is their optical transparency at different wavelengths. This is particularly important for fluorescence applications because light loss due to optical absorption by the waveguide can give rise to autofluorescence that can degrade the signal-to-noise ratio in any sensitive fluorescence measurement.[35] Therefore, transmission spectra were collected between 600 and 900 nm for both the native COC sheet material and the cured COC core waveguide. A comparison of the transmission properties of COC were made to other potential polymeric waveguiding materials as well. The results of these measurements can be seen in Figure 3.3b. COC showed high optical transparency (~91%) across the entire wavelength range interrogated. In addition, there was no significant difference in the transmission spectrum obtained for native COC and the cured COC waveguide. This indicated that the fabrication procedure did not impact the optical properties of COC preserving its high optical transparency, making it suitable for sensitive fluorescence applications.

Water absorption is also a critical issue in selecting proper waveguide materials because water absorption can change the refractive index of the material inducing light loss or specularly scattered radiation increasing the background in any optical measurement. Therefore, an investigation of the moisture resistance of the embedded COC waveguide was carried out. A COC melt was spin-coated onto a glass slide, dried, weighed, soaked in water and then re-weighed as described in the Experimental section. Films of other polymers were also processed in a similar fashion, but using a solvent in which each particular polymer showed high solubility. Figure 3.3c shows the water absorption characteristics of COC and other polymer films with

COC providing the highest moisture resistance. This result could be explained based on COC's more hydrophobic nature compared to the other investigated materials. The high moisture resistance of COC indicates that it will maintain stable optical properties, especially its refractive index, during the fluorescence measurements even though the waveguide is in contact with the interrogating solution (see Figure 3.1b).

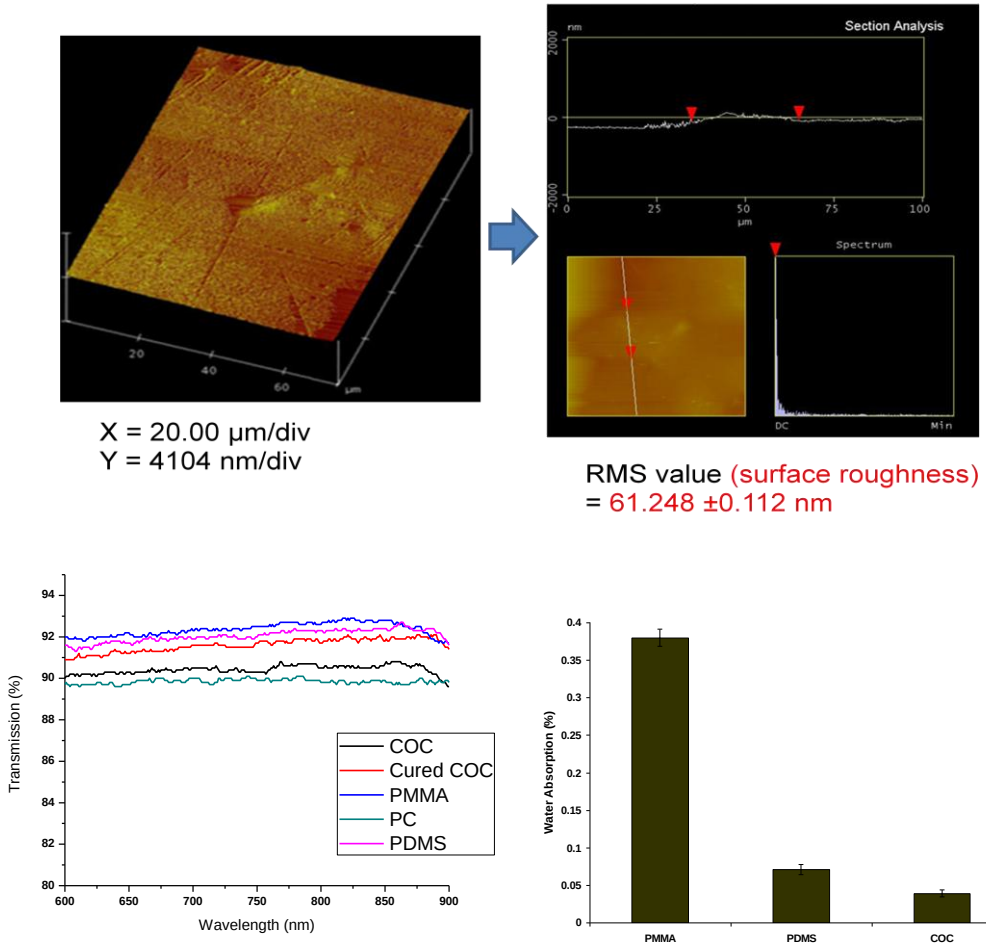


**Figure 3.3** (a) Left; AFM image of the surface of the cured COC planar polymer waveguide embedded in sheet PMMA; z-scale is 4104 nm/div., x-scale is 20 µm/div. Right; section analysis of the waveguide surface; top panel shows the surface roughness with RMS = 61.284 ±0.112 nm. (b) Optical transmission spectra (600 nm – 900 nm) of COC (black), cured COC waveguide (red), PMMA (blue), PC (green) and PDMS (purple). (c) Moisture resistance of COC compared to other polymers.

Another important optical characteristic of waveguides is their transmission efficiency. We measured light attenuation in decibels (dB) per unit length (cm) using the equation;

$$A = -10\log (P_{out}/P_{in}) \times 1/L \qquad (1)$$

where A is the attenuation in dB, $P_{in}$ is the input laser power (mW), $P_{out}$ is the output power (mW) and L is the length of the waveguide (cm). Light was launched into the waveguide (launch angle = $76^{o}$) near the critical angle (to maximize the penetration depth) when a PMMA sheet (n = 1.48) was thermally fusion bonded to the COC/PMMA waveguide/cover plate. Using an input laser power of 4.4 mW, an output power of 2.76 mW was measured resulting in an attenuation of 0.67 dB/cm. However, from our observations most of the light loss occurred from scattering of the beam entering the prism coupler due to the fact that the beam diameter was comparable to the size of the coupling prism. Increasing the size of the coupling prism or reducing the input beam size will improve this figure-of-merit.

As mentioned earlier, propagation of light through a planar waveguide generates an evanescent electromagnetic field, which penetrates into the surrounding medium with an amplitude that decays exponentially with distance from the interface. The penetration depth (at the 1/e intensity) of the evanescent field can be estimated with respect to the launch angle from the expression;[56]

$$d_{\mathrm{p}} = \frac{\lambda}{2\pi(n_1^2 \sin^2\theta - n_2^2)^{1/2}} \qquad (2)$$

where $\theta$ is the launch angle, $n_1$ is the refractive index of the waveguide and $n_2$ is the refractive index of the cladding. For example, if the laser light ($\lambda$ = 635 nm) is launched at $76^{o}$, which is

near the critical angle of the waveguide (n for COC = 1.53, n for PMMA = 1.48), the corresponding penetration depth is ~870 nm, whereas if the launch angle is increased by $1^{o}$, the corresponding penetration depth is 564 nm. Therefore, the appropriate launch angle must be carefully controlled to obtain the maximum penetration depth of the evanescent field into the adjacent solution layer to maximize the amount of sample excited by the evanescent field.

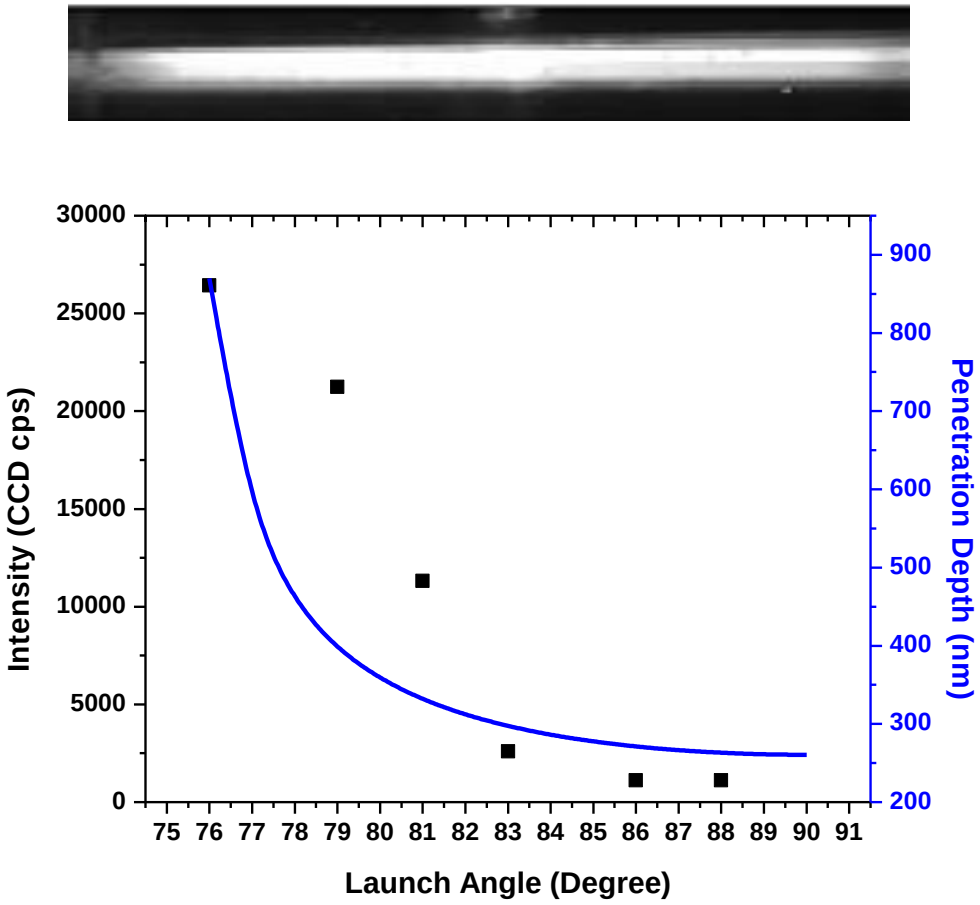


**Figure 3.4** The top panel shows a typical fluorescence image acquired with the CCD when light was launched into the waveguide with a fluorescent solution sandwiched between a cover slip and the COC waveguide surface. The bottom panel shows the resultant fluorescence intensity at different launch angles. The solid blue line represents the penetration depth plotted as a function of the launch angle using equation (2).

We evaluated the ability of our embedded polymer waveguide for efficient fluorescence excitation into the adjacent solution by depositing 20 µL of a 1 µM solution of AlexaFluor 647 onto the waveguide and placing a thin cover slip on the surface with a spacer to provide a uniform thickness of fluid above the waveguide. Laser light ($\lambda$ = 635 nm) was launched into the embedded waveguide through the prism and fluorescent signals were collected at different launch angles using a 2x microscope objective to image the entire length (see top panel of Figure 3.4) of the waveguide onto a CCD camera (exposure time = 1 s). Figure 3.4 shows a plot of the fluorescence intensity as a function of launch angle. As can be seen, the highest fluorescence intensity was obtained at a launch angle of 76$^o$, which is close to the critical angle of this waveguide. We also plotted equation 2 (see solid blue line in Figure 3.4) to show the decay in $d_p$ as a function of launch angle. As can be seen from this plot, the results from equation 2 agreed with the observed trend in the fluorescence yield, indicating that the decrease in fluorescence intensity was most likely due to the effective decrease in the sampling zone defined by the evanescent field thickness. The modest agreement at launch angles below 82$^o$ most likely resulted in errors associated with adjusting the launch angle in this region because abrupt changes in $d_p$ occur with slight changes in $\theta$. Measurements carried out below 75$^o$ showed negligible levels of fluorescence (data not shown). This is expected because the laser light did not undergo total internal reflection when launched at angles below the critical angle.

### 3.3.2 Multi-Channel Fluorescence Measurements from a Microchip

The ability to utilize the waveguide and fluidic architecture after assembly for fluorescence measurements in a multi-channel format was demonstrated by hydrodynamically pumping fluorescent solutions through the fluidic channels (see Figure 3.2c) using a 100 nM solution of AlexaFluor 647 and reading the fluorescence signal from each fluidic channel with

the CCD (relay optic was a 10x objective, NA = 0.5). The results of these measurements are shown in Figure 3.5.

In Figure 3.5a, a fluorescence image from 11 microchannels (100 μm wide x 30 μm deep with a 100 μm pitch) is shown with a clear demarcation between the dye-filled channels and the inter-channel space, which showed negligible fluorescence signal. The fluorescence generated using a 100 nM dye solution produced a SNR of 25. It is important to note that the background signal registered in this image is primarily due to camera bias and electronic offset. This bias is stable and can be subtracted from the image using a zero exposure time as background.[57] We determined that the SNR was ~48 after this bias was removed. With the volume interrogated in this fluorescence measurement, which is defined by the dimensions of the waveguide and the fluidic channel and the depth of the evanescent field (100 μm x 200 μm x 0.87 μm at a launch angle of $76^{o}$; ~17 pL sampling volume), the optical system could detect $4.6 \times 10^{-20}$ mol at a SNR = 2 or ~42,000 molecules occupying the sampling volume. We should note that we are using a relatively low NA objective in this case, which provides low light gathering ability. The use of higher NA relay objective would significantly increase the signal-to-noise in these measurements, but also reduce the field-of-view of the optical system.

Artifacts and imperfections in the wall of the fluidic channels generated some speckles along the fluidic channel walls, which was partially responsible for the high levels of apparent fluorescence along the edges of the channel/solution interface. We can potentially reduce this artifact by improving the fabrication process of the fluidic channels by reducing surface roughness of the channel walls. For example, employing UV-lithography in conjunction with LiGA for generating the mold master would produce side walls with significantly less surface roughness compared to micromilling.[58] We also note that slight variations in the measured

fluorescence intensity across the effective field-of-view comprised of the multiple fluidic channels is partially a result of the non-flatness of the collection field by the relay microscope objective, which in this case does not have a high 'flatness of field' value. Implementation of an improved optical system with a wide field-of-view with a high flatness factor would improve intensity uniformity.

To clearly visualize the waveguide geometry for collecting fluorescence from the fluidic channels using evanescent excitation of the intervening solution contained in the channels, a lower magnification objective (2x, NA = 0.1) was used to acquire a second image. Figure 3.5b shows this fluorescence image from each fluidic channel with the region outside the waveguide area showing a relatively dark background. This indicated that fluorescence excitation was confined only to the area corresponding to the waveguide, which generated the evanescent field.

## 3.4 Conclusion

We have fabricated and evaluated a novel COC planar waveguide embedded into a PMMA cover plate that was situated orthogonal to multiple fluidic channels and sampled the resulting fluorescence in the channels via evanescent excitation. The geometry employed for this COC waveguide and the fluidic network can be configured to allow matching the excitation area with the dimensions of the collection optics and array detector. The design reported herein allowed for fluorescence detection from the multiple fluidic channels using evanescent excitation and a CCD camera for parallel readout. The use of a monolithic prism allowed for precise control of the laser launch angle into the waveguide to provide sampling via the evanescent field. The launch angle was found to play a critical role in achieving high sampling efficiency by maximizing the penetration depth of the evanescent field into the adjoining solution. While the sampling efficiency is rather modest in the present case (100% x 0.56 / 30 ~ 2%), this can be

improved by matching the fluidic channel depth to the depth of penetration of the evanescent field.

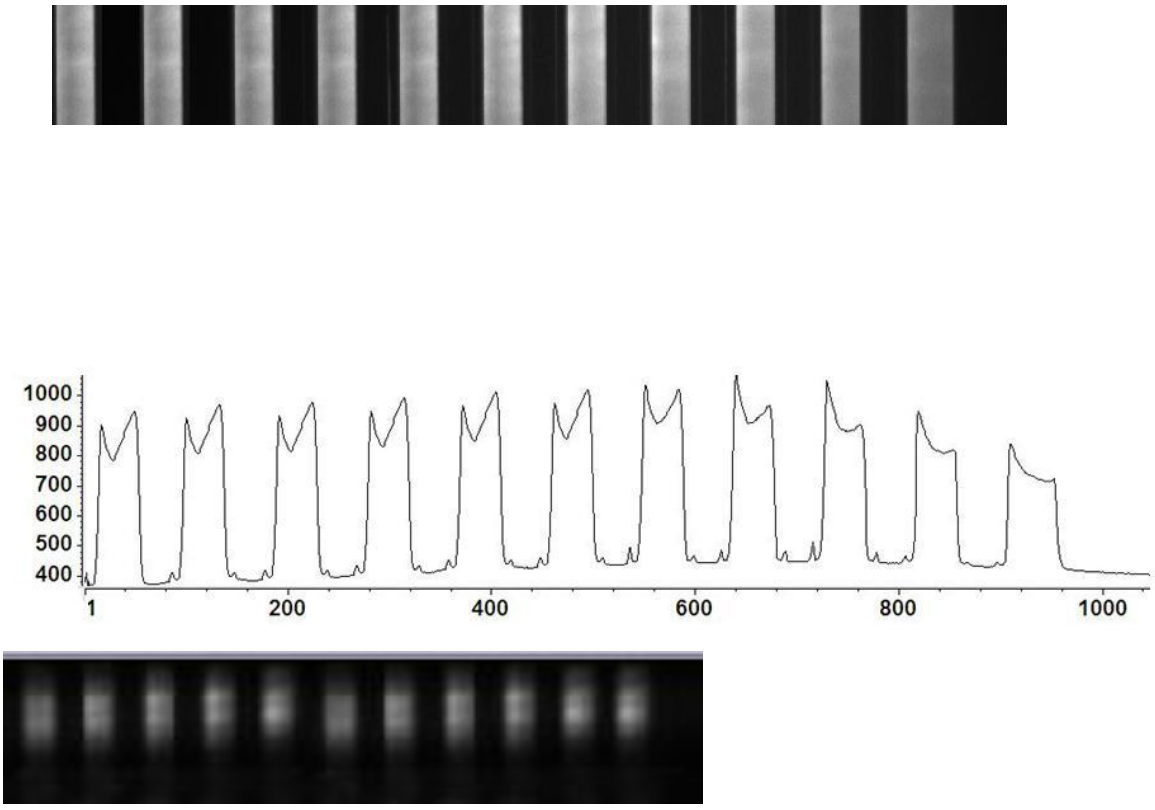


**Figure 3.5** (a) Fluorescence image acquired from multiple fluidic channels (11 micro-channels shown) filled with 100 nM AlexaFluor 647 when light was launched into the COC planar waveguide through the monolithic prism; there was a clear distinction between channels (with sample) showing fluorescence signal with fairly uniform intensity (bottom panel) and the inter-channel area showing dark background. The image was acquired with a 10x microscope objective (NA = 0.5). (b) Fluorescence image from the same device acquired with a 2x microscope objective (NA = 0.1) to clearly show the waveguide geometry.

This design generated an evanescent field for the wide field excitation of fluorescent solutions traveling above the waveguide in fluidic channels, which enabled reading fluorescence signals from multiple fluidic channels in a parallel format using a CCD camera. This technology may be particularly attractive for high throughput or multiplexed sample analyses and point-of-care applications due to the simplicity in design and fabrication. In the present studies, we

monitored fluorescence produced from 11 fluidic channels. However, this throughput could be dramatically improved by reducing the channel width and also the channel pitch. For example, if we match the channel width to the CCD pixel size as well as the channel pitch, we could monitor ~670 fluidic channels for an optical system with 1X magnification.

In future studies, the waveguide described herein will be integrated to a high density fluidic network possessing multiple channels for high throughput screening of biochemical reactions for drug discovery applications. While the present design provides for the ability to build inexpensive microfluidic devices with integrated optics, future work will also investigate alternative steps to further reduce fabrication complexity. For example, the use of double injection molding can produce the embedded waveguide within the cover plate in a single step.[59] Other future design implementations will include lenses into the integrated device to facilitate coupling of the fluorescence signal to array detectors.

## 3.5 References


1. Reyes, D. R.; Iossifidis, D.; Auroux, P. A.; Manz, A., Micro Total Analysis Systems. 1. Introduction, Theory, and Technology. *Anal. Chem.* **2002,** *74* (12), 2623-2636.

2. Auroux, P. A.; Iossifidis, D.; Reyes, D. R.; Manz, A., Micro Total Analysis Systems. 2. Analytical Standard Operations and Applications. *Anal. Chem.* **2002,** *74* (12), 2637-2652.

3. Vilkner, T.; Janasek, D.; Manz, A., Micro Total Analysis Systems. Recent Developments. *Anal. Chem.* **2004,** *76* (12), 3373-3385.

4. Whitesides, M. G., *Nature* **2006,** *442*, 368-373.

5. Dittrich, S. P.; Tachikawa, K.; Manz, A., *Anal. Chem.* **2006,** *78*, 3887-3907.

6. West, J.; Becker, M.; Tombrink, S.; Manz, A., *Anal. Chem.* **2008,** *80*, 4403-4419.

7. Vandaveer, W. R.; Pasas-Farmer, S. A.; Fischer, D. J.; Frankenfeld, C. N.; Lunte, S. M., Recent Developments in Electrochemical Detection for Microchip Capillary Electrophoresis. *Electrophoresis* **2004,** *25* (21-22), 3528-3549.

8. Mogensen, K. B.; Klank, H.; Kutter, J. P., Recent Developments in Detection for Microfluidic Systems. *Electrophoresis* **2004,** *25* (21-22), 3498-3512.

9. Tao, L.; Kennedy, T. R., Laser-Induced Fluorescence Detection in Microcolumn Separations. *Trends Anal. Chem.* **1998,** *17* (8+9), 484-491.

10. Gooijer, C.; Kok, S. J.; Ariese, F., Capillary Electrophoresis with Laser-Induced Fluorescence Detection for Natively Fluorescent Analytes. *ANALUSIS* **2000,** *28* (8), 679-685.

11. Duveneck, L. G.; Abel, P. A.; Bopp, A. M.; Kresbach, M. G.; Ehrat, M., Planar Waveguides for Ultra-High Sensitivity of the Analysis of Nucleic Acids. *Anal. Chimica Acta* **2002,** *469*, 49-61.

12. Bermini, R.; Cennamo, N.; Minardo, A.; Zeni, L., Planar Waveguides for Fluorescence-Based Biosensing: Optimization and Analysis. *IEEE Sens. J.* **2006,** *6* (5), 1218-1226.

13. Kronick, M. N.; Little, W. A., A New Immunoassay Based on Fluorescence Excitation by Internal Reflection Spectroscoy. *J. Immunol. Methods* **1975,** *8* (3), 235-240.

14. Sapdford, K. E.; Shubin, Y. S.; Delehanty, J. B.; Golden, J. P.; Taitt, C. R.; Shriver-Lake, L. C.; Ligler, F. S., Fluorescent-Based Array Biosensors for Detection of Biohazards. *J. Appl. Microbiol.* **2004,** *96* (1), 47-58.

15. Taitt, C. R.; Anderson, G. P.; Ligler, F. S., Evanescent Wave Fluorescence Biosensors. *Biosens. Bioelectron.* **2005,** *20* (12), 2470-2487.

16. Moerner, W. E.; Peterman, E. J. G.; Brasselet, S.; Kummer, S.; Dickson, R. M., Optical Methods for Exploring Dynamics of Single Copies of Green Fluorescent Protein. *Cytometry* **1999,** *36* (3), 232-238.

17. Xu, N. X.-H.; Edward, S. Y., Long-Range Electrostatic Trapping of Single-Protein Molecules at a Liquid-Solid Interface. *Science* **1998,** *281*, 1650-1653.

18. Xu, X.-H.; Edward, S. Y., Direct Measurement of Single-Molecule Diffusion and Photodecomposition in Free Solution. *Science* **1997,** *275*, 1106 - 1109.

19. Paige, M. F.; Bjerneld, E. J.; Moerner, W. E., A Comparison of through-the-Objective Total Internal Reflection Microscopy and Epifluorescence Microscopy for Single-Molecule Fluorescence Imaging. *Single Mol.* **2001,** *2* (3), 191-201.

20. Ambrose, W. P.; Goodwin, P. M.; Nolan, J. P., Single-Molecule Detection with Total Internal Reflection Excitation: Comparing Signal-to-Background and Total Signals in Different Geometries. *Cytometry* **1999,** *36* (3), 224-231.

21. Mehrvar, M.; Bis, C.; Scharer, J. M.; Moo-Young, M.; Luong, J. H., Fiber-Optic Biosensors - Trends and Advances. *Anal. Sci.* **2000,** *16*, 677-692.

22. Fang, X.; Tan, W., Imaging Single Fluorescent Molecules at the Interface of an Optical Fiber Probe by Evanescent Wave Excitation. *Anal. Chem.* **1999,** *71* (15), 3101 - 3105.

23. Moerner, W. E.; Fromm, D. P., Methods of Single-Molecule Fluorescence Spectroscopy and Microscopy. *Rev. Sci. Instrum.* **2003,** *74* (8), 3597-3619.

24. Potyrailo, A. R.; Hobbs, E. S.; Hieftje, M. G., Optical Waveguide Sensor in Analytical Chemistry: Today's Instrumentation, Applications and Trends for Future Development. *Fresenius J. Anal. Chem.* **1998,** *362*, 349-373.

25. Grandin, H. M.; Stadler, B.; Textor, M.; Voros, J., Waveguide Excitation Fluorescence Microscopy: A New Tools for Sensing and Imaging the Biointerface. *Biosens. Bioelectron.* **2006,** *21*, 1476-1482.

26. Ong, B. H.; Yuan, X.; Tan, Y. Y.; Irawan, R.; Fang, X.; Zhang, L.; Tjin, S. C., Two-Layered Film-Induced Surface Plasmon Polariton for Fluorescence Eission Enhancement in on-Chip Waveguide. *Lab Chip* **2007,** *7*, 506-512.

27. Barnes, W. L.; Dereux, A.; Ebbesen, T. W., Surface Plasmon Subwavelength Optics. *Nature* **2003,** *424* (6950), 824-830.

28. Budach, W.; Abel, P. A.; Bruno, E. A.; Neuschafer, D., Planar Waveguides as High-Perfomance Sensing Platforms for Fluorescence-Based Multiplexed Oligonucleotide Hybridization Assays. *Anal. Chem.* **1999,** *71*, 3347-3355.

29. Pawlak, M.; Schick, E.; Bopp, M. A.; Schneider, M. J.; Oroszlan, P.; Ehrat, M., Zeptosens' Protein Microarrays: A Novel High Performance Microarray Platform for Low Abundance Protein Analysis. *Proteomics* **2002,** *2* (4), 383-393.

30. Arentoft, J.; Sondergaard, T.; Kristensen, M.; Boltasseva, A.; Thorhauge, M.; Frandsen, L., Low-Loss Silicon-on-Insulator Photonic Crystal Waveguides. *Electron. Lett.* **2002,** *38* (6), 274-275.

31. Plowman, T. E.; Durstchi, J. D.; Wang, H. K.; Christensen, D. A.; Herron, J. N.; Reichert, W. M., Multiple-Analyte Fluoroimmunoassay Using an Integrated Optical Waveguide Sensor. *Anal. Chem.* **1999,** *71* (19), 4344-4352.

32. Rowe, C. A.; Tender, L. M.; Feldstein, M. J.; Golden, J. P.; Scruggs, S. B.; MacCraith, B. D.; Cras, J. J.; Ligler, F. S., Array Biosensor for Simultaneous Identification of Bacteria, Viral, and Protein Analysis. *Anal. Chem.* **1999,** *71*, 3846-3852.

33. Ives, J. T.; Reichert, W. M., Protein Adsorption on the Surface of a Thin-Film Polymer Integrated Optical Wave-Guide. *Appl. Spect.* **1988,** *42* (1), 68-72.

34. Reichert, W. M.; Ives, J. T.; Suci, P. A.; Hlady, V., Excitation of Fluorescent Emission from Solutions at the Surface of Polymer Thin-Film Wave-Guides - an Integrated-Optics

Technique for the Sensing of Fluorescence at the Polymer-Solution Interface. *Appl. Spect.* **1987,** *41* (4), 636-640.

35. Shadpour, H.; Musyimi, H.; Chen, J. F.; Soper, S. A., Physiochemical Properties of Various Polymer Substrates and Their Effects on Microchip Electrophoresis Performance. *J. Chrom.* **2006,** *1111* (2), 238-251.

36. Bliss, C. L.; McMullin, J. N.; Backhouse, C. J., Rapid Fabrication of a Microfluidic Device with Integrated Optical Waveguides for DNA Fragment Analysis. *Lab Chip* **2007,** *7*, 1280-1287.

37. Chang-Yen, A. D.; Eich, K. R.; Gale, K. B., A Monolithic Pdms Waveguide System Fabricated Using Soft-Lithography Techniques. *J. Lightwave Technol.* **2005,** *23* (6), 2088-2093.

38. Powers, M. A.; Koev, S. T.; Schleunitz, A.; Yi, H. M.; Hodzic, V.; Bentley, W. E.; Payne, G. F.; Rubloff, G. W.; Ghodssi, R., A Fabrication Platform for Electrically Mediated Optically Active Biofunctionalized Sites in Biomems. *Lab Chip* **2005,** *5* (6), 583-586.

39. Huang, S. H.; Tseng, F. G., Development of a Monolithic Total Internal Reflection-Based Biochip Utilizing a Microprism Array for Fluorescence Sensing. *J. Micromech. Microeng.* **2005,** *15* (12), 2235-2242.

40. Balslev, S.; Jorgensen, A. M.; Bilenberg, B.; Mogensen, K. B.; Snakenborg, D.; Geschke, O.; Kutter, J. P.; Kristensen, A., Lab-on-a-Chip with Integrated Optical Transducers. *Lab Chip* **2006,** *6* (2), 213-217.

41. Xu, F.; Datta, P.; Wang, H.; Gurung, S.; Hashimoto, M.; Wei, S.; Goettert, J.; McCarley, R. L.; Soper, S. A., Polymer Microfluidic Chips with Integrated Waveguides for Reading Microarrays. *Anal. Chem.* **2007,** *79* (23), 9007-9013.

42. Huang, W. J.; Chang, F. C.; Chu, P. P. J., Functionalization and Chemical Modification of Cyclo Olefin Copolymers (Coc). *Polymer* **2000,** *41* (16), 6095-6101.

43. Khanarian, G.; Celanese, H., Optical Properties of Cyclic Olefin Copolymer. *Opt. Eng.* **2001,** *40* (6), 1024-1029.

44. Fredrickson, K. C., Effects of Fabrication Process Parameters on the Properties of Cyclic Olefin Copolymer Microfluidic Devices. *J. Microelectro. Sys.* **2006,** *15* (5), 1060-1068.

45. Esch, B. M.; Kapur, S.; Irizarry, G.; Genova, V., Influence of Master Fabrication Techniques on the Characteristics of Embossed Microfluidic Channels. *Lab Chip* **2003,** *3*, 121-127.

46. Mela, P.; Berg van den, A.; Cummings, B. E.; Simmons, A. B.; Kirby, J. B., The Zeta Potential of Cyclo-Olefin Polymer Microchannels and Its Effects on Insulative

(Electrodeless) Dielectrophoresis Particle Trapping Devices. *Electrophoresis* **2005,** *26*, 1792-1799.

47. Koh, G. C.; Tan, W.; Zhao, M.-q.; Ricco, J. A.; Hugh, F. Z., Integrating Polymerase Chain Reaction, Valving, and Electrophoresis in a Plastic Device for Bacteria Detection. *Anal. Chem.* **2003,** *75*, 4591-4598.

48. Pu, Q.; Oyesanya, O.; Thompson, B.; Liu, S.; Alvarez, C. J., On-Chip Micropatterning of Plastic (Cyclic Olefin Copolymer, Coc) Microfluidic Channels for the Fabrication of Biomolecule Microarrays Using Photografting Methods. *Langmuir* **2007,** *23*, 1577-1583.

49. Stachowiak, B. T.; Mair, A. D.; Holden, G. T.; Lee, J. L.; Svec, F.; Frechet, M. J. J., Hydrophilic Surface Modification of Cyclic Olefin Copolymer Microfluidic Chips Using Sequential Photografting. *J. Sep. Sci.* **2007,** *30*, 1088 - 1093.

50. Hwang, S. J.; Yu, H. H., Novel Cyclo Olefin Copolymer Used as Waveguide Film. *Japanese J. Appl. Phys. part 1* **2005,** *44* (4B), 2541-2545.

51. Schmidt, H.; Hawkins, A. R., Optofluidic Waveguides: I. Concepts and Implementations. *Microfluid. Nanofluid.* **2008,** *4*, 3 - 16.

52. Mogensen, K. B.; Petersen, N. J.; Hubner, J.; Kutter, J. P., Monolithic Integration of Optical Waveguides for Absorbance Detection in Microfabricated Electrophoresis Devices. *Electrophoresis* **2001,** *22* (18), 3930-3938.

53. Mogensen, K. B.; El-Ali, J.; Wolff, A.; Kutter, J. P., Integration of Polymer Waveguides for Optical Detection in Microfabricated Chemical Analysis Systems. *Appl. Optics* **2003,** *42* (19), 4072-4079.

54. Hupert, M. L.; Guy, J. W.; Llopis, S. D.; Situma, C.; Rani, S.; Nikitopoulos, D. E.; Soper, S. A., High-Precision Micromilling for Low-Cost Fabrication of Metal Mold Masters. *Proc. SPIE* **2006,** *6112*, 61120B-1 - 61120B-12.

55. Hupert, M. L.; Guy, J. W.; Llopis, S. D.; Shadpour, H.; Rani, S.; Nikitopoulos, D. E.; Soper, S. A., Evaluation of Micromilled Metal Mold Masters for the Replication of Microchip Electrophoresis Devices. *Microfluid. Nanofluid* **2007,** *3*, 1-11.

56. Ahmad, M.; Hench, L. L., Effect of Taper Geometries and Launch Angle on Evanescent Wave Penetration Depth in Optical Fibers. *Biosens. Bioelectron.* **2005,** *20*, 1312-1319.

57. Karl, G., Quantitative Fluorescence Microscopy: Considerations and Controls. *Springer Ser Fluoresc* **2008,** *6*, 55-68.

58. Hupert, M. L.; Guy, W. J.; Llopis, S. D.; Shadpour, H.; Rani, S.; Nikitopoulos, D. E.; Soper, S. A., Evaluation of Micromilled Metal Mold Masters for the Replication of Microchip Electrophoresis Devices. *Microfluidics and Nanofluidics* **2007,** *3* (1), 1-11.

59. Vaz, C. M.; van Doeveren, P. F. N. M.; Reis, R. L.; Cunha, A. M., Development and Design of Double-Layer Co-Injection Moulded Soy Protein Based Drug Delivery Devices. *Polymer* **2003,** *44*, 5983-5992.

# 4 A Compact, Portable/Field-Deployable Single-Molecule Detection Platform for Universal Analysis of Molecular Markers

The fluidic modeling included in this work was performed by Arnold Rousselet in the Mechanical Engineering department at LSU.

## 4.1 Introduction

Miniaturization of fluidic systems has a number of advantages such as reduced analysis time, reagent usage, and better control of process parameters involving chemical and biochemical reactions. There are a number of applications where microfluidics have provided some compelling advantages compared to their benchtop counterparts, including high resolution separations of DNA, RNA and proteins, development of cell-based assays, and drug discovery.[1] Micro total analysis systems (μTAS) offer the possibility of generating systems appropriate for point-of-use analyses that can provide some far-reaching advantages such as personalized health-care where the measurements are performed using autonomously operating system that possess a small footprint.

Unfortunately, many existing microfluidic-based systems often lack in their ability to fully realize this goal. The required peripheral equipment associated with the microfluidic used for signal acquisition and processing, such as the electronics and optics, typically over-shadow the footprint of the microfluidic chip and prevent its use for field monitoring applications. Thus, continued miniaturization of not only the microfluidic chip but also the peripheral equipment is paramount to realize the delivery of true point-of-use μTAS.

A number of groups have reported on portable microfluidic devices that contain the support peripherals possessing a small footprint, such as the miniature thermal cycling instrument developed by Northrup *et al.*[2] or the portable, disc-based, and fully automated

enzyme-linked immuno-sorbent assay (ELISA) system demonstrated by Lee and coworkers.[3] While these are good examples of integrating the support peripherals into a single compact unit, the readout phases of the assay continue to be problematic due to the fact that the generation of microsystems typically demands the analysis of minute quantities of material. For example, the analysis volume of many microfluidic systems can be on the order of 1 nL, and thus, the analysis of 1 nM of material would require the detector to transduce the presence of 1 amol of material. If this sampling volume is reduced to 1 pL, the mass limit-of-detection must be 1 zmol or ~600 molecules for this same concentration. Clearly, efforts in reducing the footprint of the readout hardware must take into account the required low mass detection limits often associated with microfluidics.

Single-molecule detection (SMD) using laser-induced fluorescence (LIF) would appear to be an ideal approach for creating the necessary signal-to-noise ratio and mass detection limits for microfluidics. However, the large-scale and complex support peripherals required for SMD normally used to create the necessary high optical irradiance and efficient collection of fluorescent photons are prohibitive in terms of creating a truly portable system. Some operational components required for SMD systems have been reported, for example the miniature power supply developed by Erickson;[4] Giudice *et al.* also reported on recent progress in the development of a compact photon counting module using Si avalanche photodiodes;[5] and several groups have also reported SMD for lab-on-a-chip (LOC) devices with potential field-use applications.[6-10] However, the literature is currently devoid of reports detailing the development of a fully autonomous field-deployable SMD instrument that can provide processing of input samples and the subsequent detection of single molecules using LIF.

### 4.1.1 Miniaturization of Optics

Integration of optical components into LOC devices that can replace the bulky off-chip optical components is an important developmental area for the realization of a compact, portable SMD system. The recent development of equipment such as light emitting diodes, laser diodes, optical fibers, and gradient refractive index lenses has important applications to LOC.[11] These allow for the control and shaping of the excitation source to create the necessary photon density to provide optical saturation of the fluorescent dye molecule for SMD generating high signal-to-noise ratios. The integration of a silicon based p-i-n photodiode and an organic light emitting diode with a LOC system was demonstrated by Kim and coworkers.[12] Krogmeier *et al.* built an integrated optical system for the detection of single λ DNA molecules using an illumination and collection lens that were bonded onto the microfluidic device and coupled the light into fiber optics.[13] The system allowed for the controlled excitation of the fluidic channel and effective collection of the fluorescent signal; however, it still relied on macro-sized external optics, which required proper alignment with respect to the microfluidic device of the vision lens, illuminator, and the collector lens to detect the fluorescent signals. On-chip lenses were also demonstrated by a number of groups to increase the sensitivity of detection.[14-16] The small size of these 3D lenses makes them ideal for integration into microfluidic devices.

Waveguides are another important optical component that can be integrated into microfluidic devices for both illumination and detection using fluorescence. Recently, Yin and coworkers demonstrated an anti-resonant reflecting optical waveguides (ARROW) for single-molecule fluorescence correlation spectroscopy (FCS) in a microfluidic format.[7] The compact planar opto-fluidic device showed that intergraded waveguides could be used to define small excitation volumes (~fL) and signals coupled to external optical fibers for both excitation and

detection. The ARROWs were fabricated by a sacrificial layer process on a silicon nitride substrate with silicon dioxide layers serving as the core.

The drawback to the aforementioned approaches that discussed the integration of pin photodiodes, organic leds, 3D lenses and ARROW waveguides to the fluidic chip is the increased cost associated with the fluidic chip, making it difficult to realize low-cost disposable platforms appropriate for diagnostic applications. Therefore, simple optical components incorporated into a microfluidic chip body and fabricated in the same step as that used for the generation of the microfluidic network or with just a few additional steps would be advantageous. Seo *et al.* demonstrated a 2D planar lens in PDMS to focus light from a LED into a fluidic channel. They designed single and multiple element lenses to effectively shape the excitation beam to increase the resulting fluorescence intensity from fluorescent nanospheres. The lenses were fabricated in the same step used to fabricate the microfluidic channels and required no additional processing steps. However, 2D lenses only focused the light in one dimension.

The direct integration of off-the-shelf fiber optics into micro-capillary electrophoresis devices has been demonstrated by a number of groups.[14, 17-26] Fiber optics guide the incident light through a series of total internal reflections created by the difference in refractive indices (*n*) between the core and the cladding. When the fibers are integrated into polymer-based microfluidic devices, they have the ability to deliver excitation light to a defined location of the device in a well controlled volume, producing high photon irradiances. The illumination volume is controlled by the core diameter of the fiber optics as well as the acceptance angle of the fiber with typical diameters ranging from 4 μm to 1 mm. Additionally, fiber optics can act as collection optics in the same way as off-chip optics such as microscope objectives. In a method

called “butt-end fiber coupling” the fiber is placed against a diffuse light source (i.e. fluorophore) and collects the light from an area of radius r and solid angle defined by the numerical aperture (NA) of the fiber. This is the maximum collection efficiency of the fiber because focusing light from a larger area would lead to a reduction of the solid angle of the same factor, which reduces the coupling efficiency.[27] However, a lens system allows the optical system to be moved away from the source while maintaining high collection efficiency. Therefore, overall collection efficiency of a fiber optic cable is dependent on the core diameter and the NA.

The NA of the fiber defines a collection cone that along with the core diameter defines the light gathering ability of the fiber. Typical SMD experiments are performed with high NA objectives to increase the collection efficiency. The NAs of a typical optical fiber (NA 0.12 to 0.22) are generally lower than that of a microscope objective typically used in SMD experiments, however, high NA fibers are also available with a NA as high as 0.48. The equation below demonstrates the light gathering ability of a fiber optic integrated into a polymer chip. In this equation, $\theta_{MAX}$ is the half-angle, $n_{air}$ the refractive index outside the fiber end (air =1.0).

$$NA = n_{air} \times \sin\theta_{max} \quad (1)$$

### 4.1.2 Electronics

The requirements for a compact SMD instrument not only include the reduction in the size of the required optics, but also miniaturizing the data processing electronics. Field programmable gate arrays (FPGA) offer a number of advantages compared to standard printed circuit boards for the electronic processing of data (see Table 4.1).[28] FPGA is a semiconductor device containing programmable logic components and programmable interconnects with functionality of basic logic gates such as AND, OR, XOR, NOT. Programmable interconnects allow the logic blocks of the FPGA to be connected by the customer/designer to implement any

logic function. The reduction of electronic component sizes helps reduce the footprint of the instrumentation. The integration of FPGA into portable devices have been shown in several clinical applications.[29] Additionally, the use of an FPGA allows for prototyping by easily allowing the function and connections to be changed as improvements to the experiential systems are made.

**Table 4.1** Comparison of conventional printed circuit board to an FPGA.

| | **Conventional Board** | **FPGA** |
|---|---|---|
| **Size (inches)** | 8 x 11 | 1 ½ x 1 ½ |
| **Speed (MHz)** | 20-50 | 200-500 |
| **Power Consumption** | High | Low |
| **Cost** | High | Low ~$50 |

## 4.2 Genomic Based Assays

Genomic-based assays can be used for the identification of pathogenic species, such as bacteria, and provide the ability for strain specific identification to evaluate possible threat levels imposed by that bacterium.[30] Polymerase chain reactions (PCR) are typically employed in genome assays because they can improve the sensitivity by creating millions of targets to detect from a few starting copies of the genomic DNA. PCR-based schemes have demonstrated advancements over culturing and plating methods with results usually provided in several

hours.[30] Examples of different PCR methods developed for bacterial detection are: (i) real-time PCR[31] (ii) multiplex PCR[32] and (iii) reverse transcriptase PCR (RT-PCR).[33] Real-time PCR involves the detection of a specific dye that attaches itself to the targeted amplicon, which allows for quick results without much sample manipulation. Multiplex PCR simultaneously detects several organisms by introducing different primers to amplify DNA regions coding for specific genes of each bacterial strain targeted. Reverse-transcriptase PCR (RT-PCR) targets mRNA, which due to its rapid turnover and short half-lives in viable cells can be used to determine if a bacterial cell is viable.[34] These relatively fast PCR techniques have a turnaround time of 5-24 hours due to the indispensable thermal cycling required in addition to other enrichment steps; PCR schemes cannot meet the requirements demanded for near real-time reporting applications. Furthermore, these approaches can introduce ambiguities caused by the PCR process.[35-37]

### 4.2.1 Bacterial Detection

SMD of bacteria based on the use of genomic probes offers the potential for fast, sensitive analysis without false positives. Castro *et al.* demonstrated a technique for the rapid detection of specific nucleic acid sequences in unamplified DNA samples for the detection of *Bacillus anthracis*.[38] Two nucleic acid probes complementary to different sites on a target DNA were labeled with different fluorescent dyes. When mixed with a sample containing the target DNA, the two probes would hybridize to their respective sequence-specific sites on the same target DNA molecule.[39] When the samples were then analyzed by a laser-based ultrasensitive fluorescence system capable of SMD at two different wavelengths, the signals on each color channel appear simultaneously. Therefore, coincidence detection of both dyes provided the necessary specificity to detect unamplified, single-copy target DNA molecules in a homogeneous assay. Uncorrelated events originating from free probes observed on either color-channel

indicated the target was not present. They demonstrated the ability to detect 100 amol of target DNA at a SNR of 3 in 200 s and the assay showed good specificity, even in the presence of an excess of *B. globigii.*

### 4.2.2 Molecular Beacon (MB) Probes

MB probes consist of single-stranded oligonucleotides that contain a section complementary to the target DNA sequence (loop). MBs can be labeled with a fluorescent dye or quencher at either end, which are flanked on either side by ~10 bases that are complementary (stem). Hybridization of the two complementary arms that flank the probe loop sequence forms the stem, which in the absence of the target sequence results in the molecule being closed in a so-called hairpin structure. The hairpin brings the fluorophore and quencher into close proximity, which results in energy transfer to the quencher instead of fluorescence emission from the fluorophore. Hybridization of the probe to the target DNA opens the hairpin loop, which separates the fluorophore and the quencher consequently restoring the fluorescence.[40] MB are particularly attractive probes because the fluorescence quantum yield increases dramatically when they bind to their target.[41] This allows for a homogenous assay because the unbound MB is dark and therefore, washing steps are not required for detection.

An example of bacterial strand-specific detection using MBs at SMD limits was shown by Marme *et al.,* who demonstrated the specific identification of a single nucleotide polymorphism (SNP) responsible for rifampicin resistance of *Mycobacterium tuberculosis*.[42] The probe was used for the identification of SNPs in $10^{-11}$ M solutions of PCR amplicons from *M. tuberculosis* in only 100 s.

### 4.2.3 Gram Positive vs. Gram Negative Bacteria

Traditionally, Gram stain classification has been used to determine patient treatment plans and initial antibiotic therapy. Kalin *et al.* found Gram-stained smears to be a valuable aid in the diagnosis of bacterial pneumonia; the results were in agreement with those of the culture for about 75% of the purulent samples.[43] Gram stain classification has been successfully demonstrated by Gram stain-specific PCR,[44] and nested PCR.[45] In design of a POC assay for personalized treatment the assay should be rapid, therefore the elimination of the culturing and staining and/or PCR steps are required. SMD of MBs specific to gram classification would provide a rapid, sensitive analysis tool for physicians.

### 4.2.4 Research Goals

In this chapter, we describe the hardware and fluidic components necessary for an optical reader that was configured in a compact, portable/field-deployable instrument capable of performing a SMD-MB assay for the determination of Gram positive bacteria. The use of microfluidics coupled to SMD generates sample processing pipelines that can provide near real-time readout through the elimination of many of the sample processing steps, enhancing the rate of molecular processing and automation to eliminate the need for operator intervention making the approach appropriate for field tests. The ability to monitor biomarkers using a portable microfluidic/single-molecule instrument in near-real time will have a number of important applications, such as strain-specific detection of pathogenic bacteria or molecular diagnosis of diseases requiring rapid turn-around-times. This polymeric chip used for the molecular/sample processing could be connected to other microfluidic chips/modules to create a simple LOC for other processing steps to provide an autonomous system.

## 4.3 Experimental

### 4.3.1 Microfluidic Chip Design and Fabrication

Figure 4.1a presents the design of the microfluidic chip, which consisted of a single channel that had a width of 50 µm and a depth of 120 µm. The excitation fiber conduit, which was molded into the fluidic chip, was 120 µm wide with a depth of 120 µm. The collection conduit was 220 µm wide and 220 µm deep. The excitation and detection geometry is shown in 4.1b, which is a four way intersection with the fluidic channel.

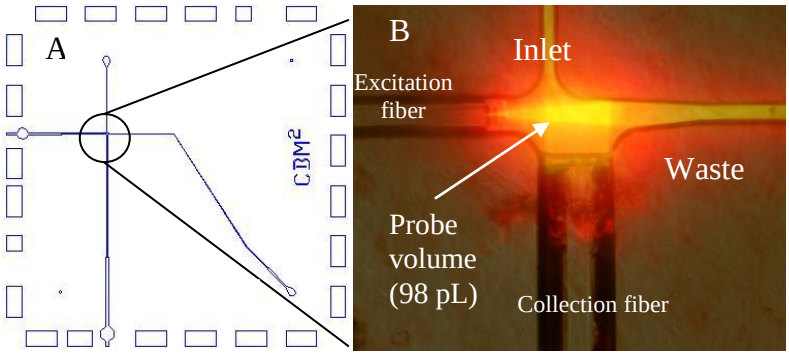


**Figure 4.1** (a) Design of a polymer microfluidic chip with an integrated waveguides, which are placed in guide channels embossed into the chip. (b) Fluorescence image showing the intersection of the optical paths, which defines the on-chip probe volume (98 pL).

A detailed description of the polymer microfluidic chip fabrication is described elsewhere.[46] Briefly, microfluidic channels were hot embossed into a poly(methyl methacrylate) (PMMA) substrate (3/16" thickness, Lucite CP, SABIC Polymershapes, New Orleans, LA) using a high-precision micromilled brass master and a hydraulic press (PHI Precision, City of Industry, CA) supplied with a home-made vacuum chamber. Micromilling of the master was performed with 50 to 500 µm diameter solid-carbide milling bits (McMaster-Carr or Quality Tools, Hammond, LA) at 40,000 rpm using a KERN MMP 2522 CNC milling machine (KERN Micro- und Feinwerktechnik GmbH & Co., Germany). Hot embossing was achieved by pressing the heated (160ºC) metal master into the polymer substrate for 210 s at 62 psi pressure. The polymer

substrate was then cooled below the Tg of the polymer and separated from the molding master. The chip was cut to a final size of 4.5 cm x 4.5 cm and the holes for the fluidic reservoirs were drilled into the substrate. Fiber optics were manually placed in the corresponding conduits in the polymer chip to create the integrated optical waveguides. The microfluidic channels were formed by thermal fusion bonding of a thin (0.25 mm) PMMA coverslip (PMMA film, GoodFellow, Oakdale, PA) to the embossed PMMA substrate. For thermal fusion bonding, the microfluidic chip assembly was clamped between two glass plates and placed in a convection oven at 107°C for 20 min.

### 4.3.2 Instrument Design

The microfluidic chip control electronics consisted of five major sections: (1) photon detection, (2) laser diode control, (3) high voltage, (4) microfluidic channel temperature control, and (5) computer interface. The components and layout of the compact SMD system are presented in Figure 4.2.

The photon counting system used a PCDMini SPAD by SensL that was fiber coupled to the fluidic chip and was used to count the fluorescence photons. The PCDMini was compact in size measuring only 1½’ x 1½’ and had an integrated Peltier cooler. The PCDMini delivers high quantum efficiency at 650-700 nm (> 23%) and low dark counts (10 cps). Collection of the fluorescence photons was achieved by using a high NA (0.48) multimode fiber (200/230 µm BFH48-200, Thorlabs) poised within the fluidic chip and was oriented at 90° with respect to the illumination fiber. The placement of the optics in the microfluidic chip eliminated the need for operator alignment of the optical system and therefore, simplified operation. The bare fibers were spliced into OFR fiber ports (PAF-X-5, Thorlabs) for free beam to fiber coupling that allowed placement of the appropriate filters for excitation and emission and then coupling back

into a fiber optic cable. To minimize dead time and conserve board space, the photon counting was performed by a custom programmed field programmable gate array (FPGA).

The FPGA (XCR3256XL-12TQ44I, Xilinx Inc., San Jose, CA) was a surface mount 144-pin device and was programmed using the ISE Webpack software, version 7.1. The design used a JTAG interface for in-circuit programming so that the FPGA code could be loaded or modified on the target board without the need to remove the FPGA chip for updating the code. The SPAD outputs a TTL pulse to the FPGA, which was used for processing the photon events from the SPAD. A diagram of the electronic components including the FPGA operation is shown in Figure 4.2d.

An Opnext HL6385DG laser diode was used as the excitation source with a lasing wavelength of 642 nm. To minimize output power fluctuations, a highly stable constant current source was designed to provide up to 280 mA drive current to the laser. The laser diode was contained in an SMA connectorized housing and had a built-in pin diode for laser power monitoring. At 250 mA current, the laser output from the fiber optic was approximately 24 mW. Conditioning electronics were designed to convert the pin diode output to a 0 to +5 V signal that was linearly proportional to the laser diode output power. Optical coupling of the diode to the chip used 10/125 μm (SMF-28-10, Thorlabs) single-mode fibers.

Finally, communication between the microcontroller and the analog systems used 12-bit A/D and D/A converters via an I2C serial bus. Data transmission between the control board and the computer was via the standard USB port. Custom software was written in-house using LabView and installed on a mini computer (OQO, Marlton, NJ) for end user control.

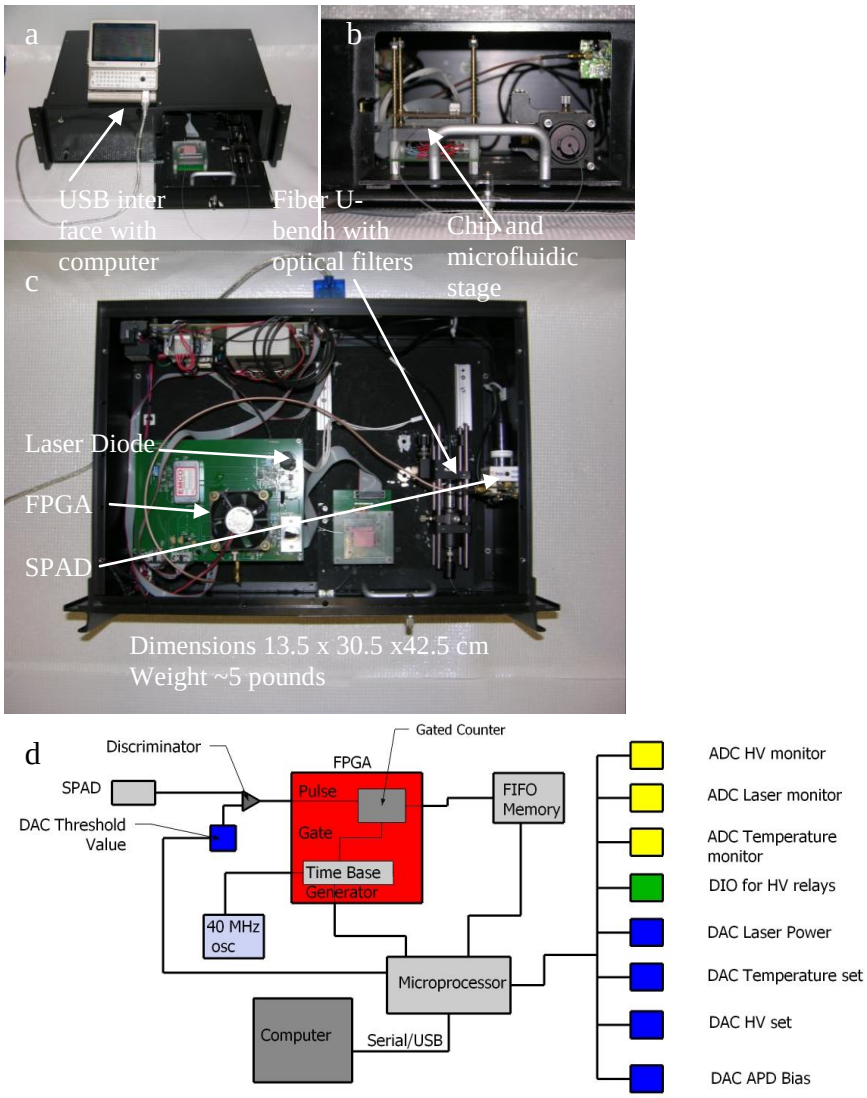


**Figure 4.2** (a) Picture of the outside of the compact, field deployable instrument connected to a mini-computer for data collection and instrument control. (b) Access panel for loading sample onto the microfluidic device and connecting the fiber optics integrated onto the chip to the Fiber U-benches for placement of the optical filters. (c) Inside the compact SMD showing the arrangement of the integrated laser diode, SPAD, and the FPGA. (d) Diagram of FPGA integrated into the electronics of the compact SMD instrument. The FPGA counts the single photon bursts from the SPAD and outputs the information to first in first out (FIFO) memory

### 4.3.3 Chemicals and Materials

Borate buffer was prepared by dissolving the desired amount of sodium borate (Sigma Chemical) into nanopure water secured from a Barnstead NANOpure Infinity System (Model D8991, Dubuque IA). The pH (pH 8.5) was adjusted by the addition of concentrated HCl. The buffer was diluted to a final concentration of 50 mM and filtered with a 0.2 μm filter before use.

Bovine serum albumin from Sigma was added to the buffer (0.1 mg/mL) to reduce surface non-specific interactions. Alexa Fluor 660 and Dark red fluorescent FluoSpheres (diameter = 0.2 μm) were both purchased from Invitrogen (Eugene, Oregon). The fluorescent spheres were sonicated and diluted in the borate buffer to yield a final concentration of $1.9 \times 10^8$ particles /mL. The fluorescent dye was diluted in buffer to yield a final concentration of 2 fM.

MBs were purchased from Integrated DNA Technologies (Coralville, Iowa) with a custom sequence where the underline section was the complementary stem section (5'-GCACGAAAGCCTGACGGAGCAACGCCGCGTGAGTGATGACGTGC-3'). The 5' end was modified with TYE 665 fluorescent dye and the 3' was modified with Iowa Black RQ-Sp. The MB sequence was designed to probe for the presence of ribosomal DNA (rDNA), which codes for the ribosomal RNA(rRNA) related to the Gram + gene.[47] Two bacterial strains; *Staphylococcus aureus* subsp. Aureus (ATCC 700699) and *Escherichia coli* (ATCC 700926) were investigated in this study and the genomic DNA for each strain was acquired from ATCC (Manassas, VA).

### 4.3.4 Flow Velocity Modeling

A computational fluid dynamic (CFD) simulation was run using Ansys Fluent 12.0 software. The general-purpose preprocessor for CFD analysis was done with Gambit 2.0, which created quad elements meshing with 80,000 nodes. The input volume flow rate was 0.05 mL/h.

## 4.4 Results and Discussion

The diameter of the optical fibers in the microfluidic device had an important role in determining the irradiance and the probe volume size. The reduction in the core diameter of the excitation fiber lead to a decrease in the excitation cross section, consequently increasing the irradiance producing better signal-to-noise ratio in the SMD measurement. The effective field-of-

view of the collection fiber overlaid with the excitation fiber's field-of-view defined the probe volume. Ideally, this volume should be minimized to reduce noise generated from scattering photons produced from the buffer, however, larger collection fibers allow for more efficient collection of the fluorescence photons. To visualize the cross section of the excitation fiber and the collection fiber to define the probe volume, we filled the microfluidic device with Alexa Fluor 647. We then collected three images using a Nikon microscope equipped with a CCD camera, which included a bright field image, fluorescence generated from the excitation fiber and fluorescence generated from the collection fiber when the excitation light was launched in each fiber (see Figure 4.1B). By overlaying the three images, the probe volume could be easily calculated by measuring the overlap of the two fluorescence images. The cross section of the excitation fiber fluorescence gave a diameter of 10 μm or a cross sectional area of $7.85 \times 10^{-7}$ $cm^2$. With this cross section, the 24 mW output power from the optical fiber generated an irradiance of $\sim 10^{23}$ photon $cm^{-2}$ $s^{-1}$ (laser power/(hc/λ) divided by the cross section). The probe volume was defined as the overlap of the two fluorescence images from the excitation fiber ($1/e^2$ diameter, 12.5 μm) and the collection fiber (observation length = 200 μm) and was determined to be $9.8 \times 10^{-11}$ L or 98 pL. This probe volume was used to determine the correct concentration so that the occupancy (molecules/probe volume) was 0.1% and the probability of double occupancy was 0.01%.

The detection zone was at a right angle with respect to the sample input with two fiber optics meeting at a four-way junction. Due to the irregular shape of this detection geometry, we decided to simulate the flow velocities and flow vectors as the fluid moved from the inlet channel into the detection zone and then subsequently to waste (see Figure 4.1). The simulation was run using Fluent software with quad elements meshing done in Gambit with 80,000 nodes.

The simulation showed the drop in linear velocity as the solution entered the wider detection zone. The velocity through the probe volume showed minor linear velocity changes, however, the paths through the probe volume were distinct. We categorized these different paths into three types; perpendicular to the excitation axis, diagonal to the excitation axis, and parallel to the excitation axis. We overlaid the CFD with the trapezoid shaped (black outline) probe volume (Figure 4.3a). The corresponding path lengths across the probe volume for these were 50, 75, and 200 μm.

The distribution of the irradiance as a function of channel position was plotted versus the irradiance (photon $cm^{-2}$ $s^{-1}$) in Figure 4.3b with 8 cross sections taken (shown as red lines) from Figure 4.3a. This shows that as the laser beam expand its irradiance decreases. Therefore the flow paths that are perpendicular to the laser beam will have the optimal irradiance since other flow path encounter a reduced irradiance. This perpendicular flow path will result in the best SNR of the various flow paths due to the higher irradiance resulting from the smaller cross sectional area. Other paths through the probe volume have lower irradiance since they occur further from the excitation fiber core. Additionally, the perpendicular region was closer and centered over the collection fiber, which resulted in a higher collection efficiency of the fluorescent photons. The flow paths that were traveling parallel to the excitation beam showed longer transit times (>75 ms).

The compact field-deployable SMD instrument was first tested using fluorescent spheres due to the high signal-to-noise-ratio (SNR) generated by these spheres due to the high load of dye. A diluted solution of spheres ($3.1 \times 10^6$ particles/mL) had an occupancy of 0.3%. The spheres were pumped through the microfluidic channel using a syringe pump, which allowed for

a reproducible transit time in the detection zone. The flow rate was set to 0.05 mL/h (linear flow rate 0.096 cm/s); however the transit time is dependent of which flow path was taken. The

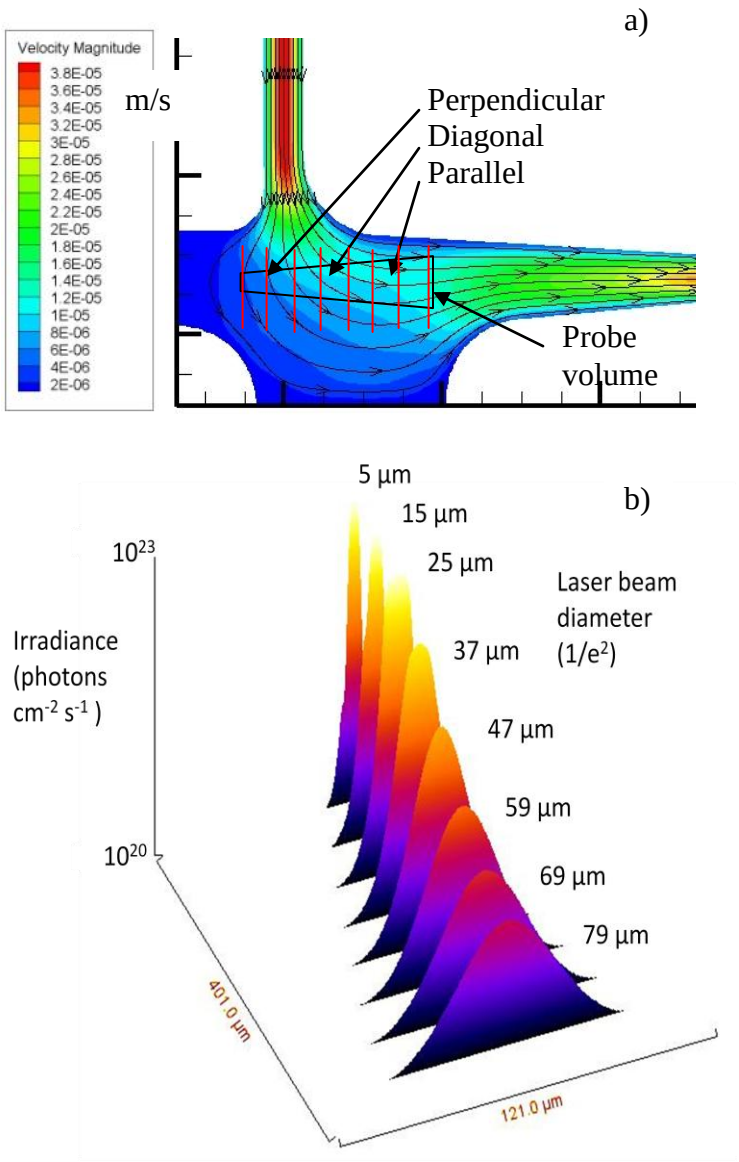


**Figure 4.3** (a) Simulation of the flow velocities and vectors as the fluid moves from the input channel into the detection zone (units are m/s). The simulation was run using fluent software with quad elements meshing and 80000 nodes done in Gambit. An outline of the probe volume was layered into visualize the flow path and the path length of single molecules as they traverse the probe volume. (b) 3D surface plot of the detection zone versus the irradiance experienced by the fluorophore. The intensity drops as the beam expands and fluorophores on the edge of the Gaussian show significantly less irradiance.

perpendicular path the beam expands to 47 - 59 μm at $1/e^2$ ( at 200 - 250 μm from the end of the excitation fiber) diameter where the molecule will transverse the probe volume, the corresponding theoretical transit time of 49-61 ms should be observed. The other paths (75-200 μm) would yield transit time of 78-208 ms. Figure 4.4a presents a plot of the photon burst (rapid cycling of the fluorophore) or peaks versus time along with the blank at a collection time of 10 ms. The counts were converted into counts per second and plotted as a function of time. A Savitzky-Golay smoothing function was applied to the data.

The next test for the compact system was the detection of a single-fluorophore molecules (see Figure 4.4b). In this case, we chose Alexa Flour 660 due to its high quantum yield and favorable photostablity.[48] The dye was diluted to a concentration of 2 fM, which corresponded to an occupancy of 0.12% (Avogadro's number x concentration x probe volume x 100%). The solution was then pumped through the microfluidic chip at the same rate as the spheres (0.05mL/h). The free fluorescent dye showed a drop in SNR compared to the spheres, which was anticipated due the high load ($1.1e^5$ fluorescein equivalents per microsphere) of the polystyrene spheres with fluorescent dyes. A threshold level was set by using a blank sample with no fluorescent molecules. A level was set such that no signal from the blank exceeds the threshold but when applied to the fluorescent sample the photon burst were above this level. The single-molecule data showed photon burst signals above the background counts (25,315 cps) and a threshold level of 32,000 cps was chosen for the Alexa Fluor dye which represents 48 photon bursts and zero background events (See Figure 4.4d). A lower threshold could have been set to allow more photon burst to be counted but this would allow false hits from the blank to be counted as events.

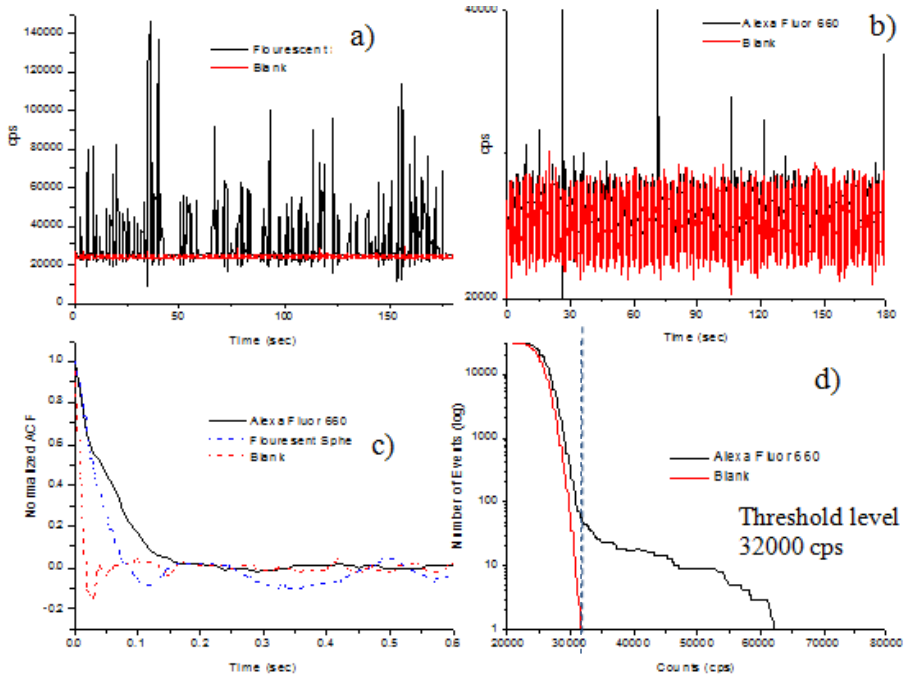


**Figure 4.4** Data collected on the compact, field deployable single-molecule instrument. The red line is the blank and the black line is the fluorescent signal (a) Plot of the fluorescent spheres photon bursts which are well above the background counts of the blank (b) Free Alexa Fluor 660 dye showing single-molecule photon burst above the background of the blank. (c) Autocorrelation was performed on the Blank, Fluorescent spheres, and Alexa Fluor 660. The fluorescent spheres and the free Alexa Fluor dye showed similar transit time (49 msec and 53 msec respectively) under the same flow rate which supports the conclusion that Figure 4.4b contains single-molecule photon bursts. (d) Histogram of the number of photon burst from Alexa Fluor 660 at different threshold levels. At 32000 cps the Alexa Fluor dye showed 48 events while the background had zero events.

The normalized autocorrelation function was derived for the samples (blank, fluorescent spheres and the Alexa Fluor dye), which are shown in Figure 4.4c. The differences in the autocorrelation function (ACF) from the blank and the fluorescent sample indicated that single molecular events were being detected. Further analysis of the transit times for the fluorescent spheres and Alexa Fluor dye was performed by using the full width at half height of the autocorrelation function (ACF), which yielded results of 49 ms for the spheres and 53 ms for the fluorescent dye. The ACF does not show the longer transit time (78-208 ms) associated with other flow path but the ACF is a weighted average by intensity therefore the lower intensity

bursts would minimized by the more intense burst related to the short transit times( 49-61 ms). The transit time shows close agreement with the theoretical transit times of single molecules traversing the single-mode fiber's excitation cross section. Additionally, both the fluorescent spheres and the free Alexa Fluor dyes have approximately the same transit times, which were expected for samples flowing through the probe volume at the same linear velocity.

### 4.4.1 Molecular Beacons

The molecular beacons from Integrated DNA Technologies were diluted in 50 mM borate buffer with BSA to a concentration of 0.5 nM. The calibration curve had concentrations ranging from 0.5 to 10 fM and was prepared by adding different concentrations of target DNA sequences (synthetic complementary DNA sequence to the loop section of the MB) to aliquots of the 0.5 nM MB solution. The MB and targets were incubated for 5 min prior to the mixtures being loaded into a 1 ml syringe and pumped through the optical fiber chip at 0.01 mL/h (see Figure 4.5). Peaks above the threshold level were counted as events and then, divided by the time of the experimental run (1 min). Three runs with each sample concentration were made and the average events/min was used for further calculations.

Table 4.2 shows the percent occupancy for each sample along with the delivery rate (DR), theoretical results in events/min, experimental events/min, and the calculated sampling efficiency (SE). DR was calculated by multiplying the concentration by the flow rate (0.01 mL/h) and Avogadro's number. Based on the average illumination diameter (25 μm and the channel cross section (120μm x 120 μm), a sampling efficiency (SE) of 13.6% was predicted. The theoretical results were obtained by multiplying the DR and the theoretical SE. The detection efficiency (DE) was arrived at by dividing the experimental results by theoretical results. The averaged experimental DE was 22.6%. This deviation is an indication that sample

was passing through the probe volume but was not counted as events. Wang *et al* reported on the inefficiency of hybridization of MB at low concentrations which would decrease the number of expected events.

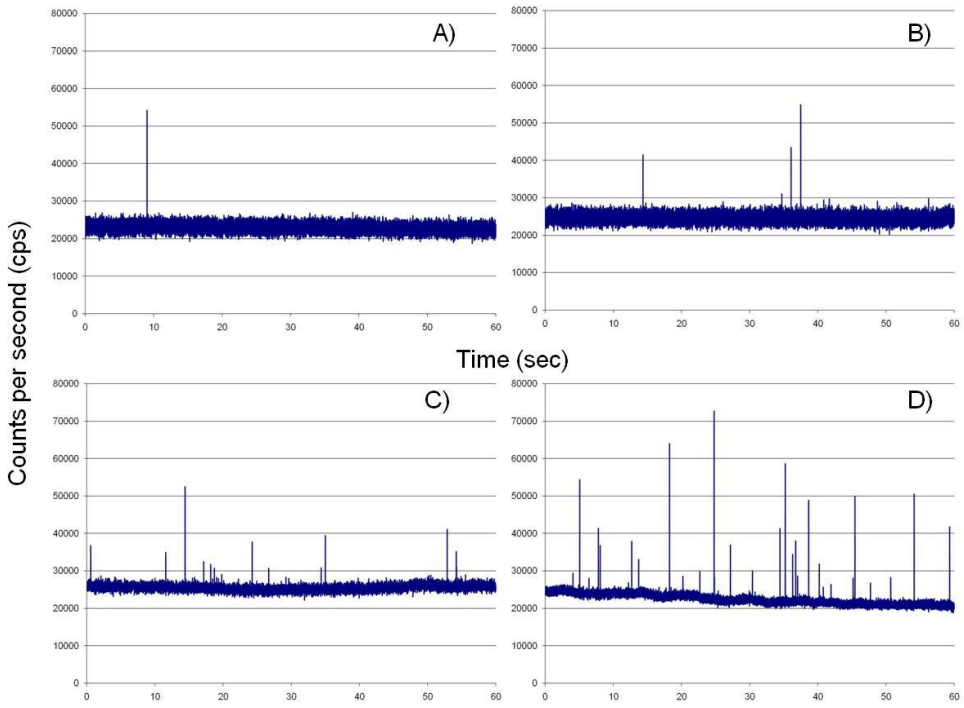


**Figure 4.5** The target DNA was mixed with 0.5 nM of the MB and pumped through the microfluidic device at 0.01 mL/h. Peaks above the threshold level were counted as events and divided by the time. Target concentration; a) 5.0 x $10^{-16}$ M; b) 1.0 x $10^{-15}$ M; c) 5.0 x $10^{-15}$ M; d) 1.0 x $10^{-14}$ M.

**Table 4.2** Summary of the run parameters and run conditions extracted from the calibration plot shown in Figure 4.5.

| Sample | Concentration of DNA Target | Occupancy | Delivery Rate (events/min) | Theoretical Results* (events/min) | Actual Results (events/min) | Detection Efficiency |
|---|---|---|---|---|---|---|
| a) | 5.00E-16 | 0.03 | 50 | 6.8 | 1.33 | 19.6 |
| b) | 1.00E-15 | 0.06 | 100 | 13.6 | 3.67 | 27.0 |
| c) | 5.00E-15 | 0.29 | 500 | 68 | 12.67 | 18.6 |
| d) | 1.00E-14 | 0.59 | 1000 | 136 | 34.33 | 25.2 |
| *Based on a SE of 13.6% times the DR | | | | | | |

The number of single molecule events above the threshold level were counted and plotted in Figure 4.6 as the number of events per min. The points were fit to a linear function ($y = 3 \times 10^{-15} x - .9291$). The $R^2$ value was 0.97 demonstrating a good fit to the data.

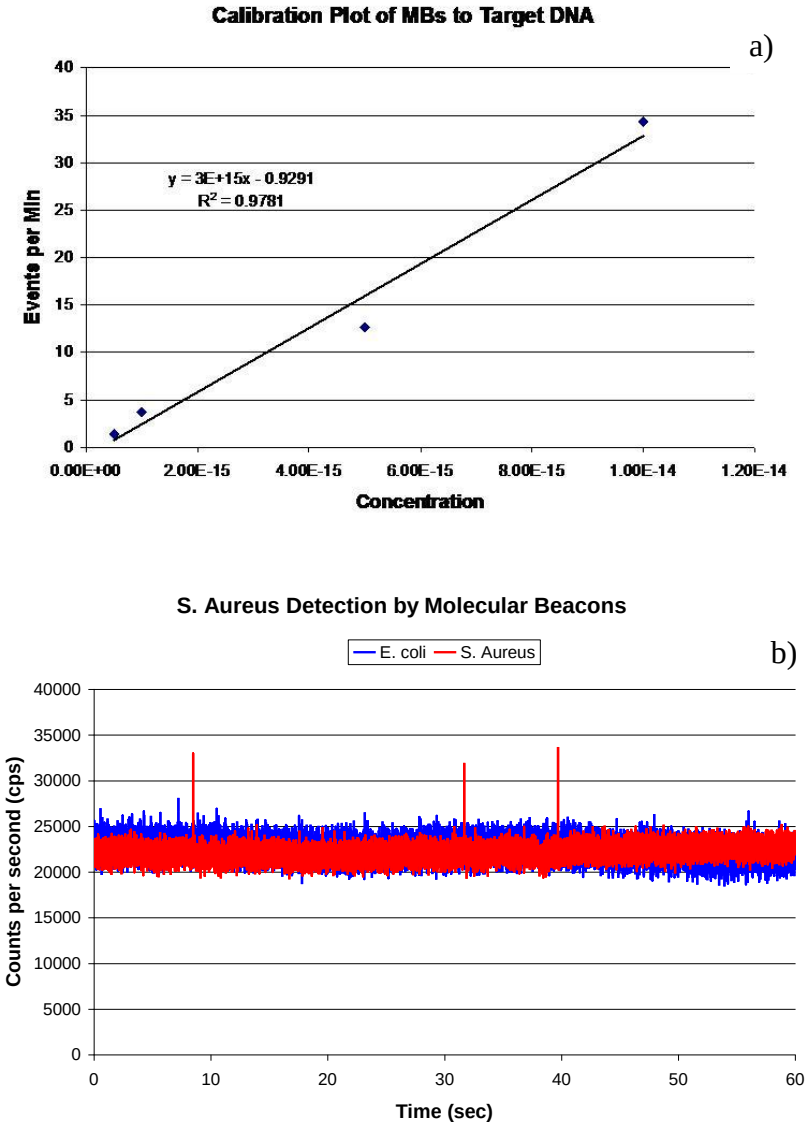


**Figure 4.6** a) Concentration gradient created for the DNA target shown in Figure 4.5. The data points were fit to a linear curve. The equation was $y= 3e^{15} x – 0.9291$ with the $R^2$ value of 0.97, which demonstrated good correlation of the data. b) The rDNA from 2,000 *S. aureus* cells was extracted and mixed with the 0.5 nM MB solution. As a control, DNA from *E. coli* was extracted and mixed with the MB solution. The *S. aureus* showed 3 events above the threshold level whereas the *E. coli* showed no events above the threshold.

The determination of *S. aureus* was performed using DNA extracted from 2,000 cells and suspended into a 0.5 nM solution of MB and 50 mM borate buffer (pH 8.5) to a final volume of 50 μL. The mixture was then loaded into a Hamilton 100 μL glass syringe and pumped through the fiber optic detection chip at 10 μL/h. As a control, DNA from *E. coli* was extracted and mixed with the MB solution. The *S. aureus* showed 3 events above the threshold level (28,000 cps) whereas the *E. coli* showed no events above this threshold. The three events from the *S. aureus* predicts a concentration (derived from the calibration curve) of $1.3 \times 10^{-15}$ M. This indicates that more than one copy of the gene is present in each cell since 2,000 cells would only yield a concentration of $6.6 \times 10^{-17}$ M. If 20 copies of the gene are present in each cell then the data would be in good agreement. Kim *et al* demonstrated that the copy number of 16S ribosomal DNA varied considerable from 1 to 15 *in Candidatus Liberibacter asiaticus*.[49] Lower copy or cell number could be achieved by extending the collection time to longer data run times and/or increasing the delivery rate as well as increasing the sampling efficiency.

## 4.5 Conclusions

We have shown for the first time, the ability to detect single-molecule events using a compact field-deployable instrument with minimal end user optical alignment by incorporating the fiber optics into the microfluidic device, which opens the possibility for less technically qualified operators to manage this device. The integration of fiber optics into the microfluidic chip as waveguides serving as excitation and collection optics removed the normally bulky optics of traditional SMD setups. The implementation of a FPGA allowed for the reduction of the footprint of the control electronics compared to circuit boards, which created a reduction in the overall size of the instrument as well. The transit times for the fluorescent spheres and Alexa Fluor dye were determined to be 49 ms for the spheres and 53 ms, which showed close

agreement with the theoretical transit times. As a demonstration of the possible application of this instrument for rapid analysis, molecular beacons were designed to probe bacterial cells for the gene encoding Gram +. The MB's were shown to be detectable for as little as 2,000 cells in a 1 min date collection run.

This current article focused on the detection of SMD in a compact instrument, which would offer decreased analysis time by eliminating processing steps such as PCR, which makes it ideal for monitoring biomarkers in near-real time. This system will have a number of important applications, such as strain-specific detection of pathogenic bacteria or molecular diagnosis of diseases requiring rapid turn-around-times at the point-of-use.

## 4.6 References


1. Blow, N., Microfluidics: In Search of a Killer Application. *Nat Methods* **2007,** *4* (8), 665-668.

2. Northrup, M. A.; Benett, B.; Hadley, D.; Landre, P.; Lehew, S.; Richards, J.; Stratton, P., A Miniature Analytical Instrument for Nucleic Acids Based on Micromachined Silicon Reaction Chambers. *Anal Chem* **1998,** *70* (5), 918-922.

3. Lee, B. S.; Lee, J. N.; Park, J. M.; Lee, J. G.; Kim, S.; Cho, Y. K.; Ko, C., A Fully Automated Immunoassay from Whole Blood on a Disc. *Lab Chip* **2009,** *9* (11), 1548-1555.

4. Erickson, D.; Sinton, D.; Li, D. Q., A Miniaturized High-Voltage Integrated Power Supply for Portable Microfluidic Applications. *Lab Chip* **2004,** *4* (2), 87-90.

5. Giudice, A.; Ghioni, M.; Biasi, R.; Zappa, F.; Cova, S.; Maccagnani, P.; Gulinatti, A., High-Rate Photon Counting and Picosecond Timing with Silicon-Spad Based Compact Detector Modules. *J Mod Opt* **2007,** *54* (2-3), 225-237.

6. Agrawal, A.; Zhang, C. Y.; Byassee, T.; Tripp, R. A.; Nie, S. M., Counting Single Native Biomolecules and Intact Viruses with Color-Coded Nanoparticles. *Anal Chem* **2006,** *78* (4), 1061-1070.

7. Yin, D. L.; Deamer, D. W.; Schmidt, H.; Barber, J. P.; Hawkins, A. R., Single-Molecule Detection Sensitivity Using Planar Integrated Optics on a Chip. *Opt Lett* **2006,** *31* (14), 2136-2138.

8. Dittrich, P. S.; Manz, A., Single-Molecule Fluorescence Detection in Microfluidic Channels - the Holy Grail in Mu Tas? *Anal Bioanal Chem* **2005,** *382* (8), 1771-1782.

9. Yan, F.; Vo-Dinh, T., Surface-Enhanced Raman Scattering Detection of Chemical and Biological Agents Using a Portable Raman Integrated Tunable Sensor. *Sensors and Actuators B-Chemical* **2007,** *121* (1), 61-66.

10. Mechery, S. J.; Zhao, X. J. J.; Wang, L.; Hilliard, L. R.; Munteanu, A.; Tan, W. H., Using Bioconjugated Nanoparticles to Monitor E-Coli in a Flow Channel. *Chemistry-an Asian Journal* **2006,** *1* (3), 384-390.

11. Verpoorte, E., Chip Vision - Optics for Microchips. *Lab Chip* **2003,** *3* (3), 42N-52N.

12. Kim, Y. H.; Shin, K. S.; Kang, J. Y.; Yang, E. G.; Paek, K. K.; Seo, D. S.; Ju, B. K., Poly(Dimethylsiloxane)-Based Packaging Technique for Microchip Fluorescence Detection System Applications. *Journal of Microelectromechanical Systems* **2006,** *15* (5), 1152-1158.

13. Krogmeier, J. R.; Schaefer, I.; Seward, G.; Yantz, G. R.; Larson, J. W., An Integrated Optics Microfluidic Device for Detecting Single DNA Molecules. *Lab Chip* **2007,** *7* (12), 1767-1774.

14. Camou, S.; Fujita, H.; Fujii, T., Pdms 2d Optical Lens Integrated with Microfluidic Channels: Principle and Characterization. *Lab Chip* **2003,** *3* (1), 40-45.

15. Seo, J.; Lee, L. P., Disposable Integrated Microfluidics with Self-Aligned Planar Microlenses. *Sensors and Actuators B-Chemical* **2004,** *99* (2-3), 615-622.

16. Roulet, J. C.; Volkel, R.; Herzig, H. P.; Verpoorte, E.; de Rooij, N. F.; Dandliker, R., Performance of an Integrated Microoptical System for Fluorescence Detection in Microfluidic Systems. *Anal Chem* **2002,** *74* (14), 3400-3407.

17. Chabinyc, M. L.; Chiu, D. T.; McDonald, J. C.; Stroock, A. D.; Christian, J. F.; Karger, A. M.; Whitesides, G. M., An Integrated Fluorescence Detection System in Poly(Dimethylsiloxane) for Microfluidic Applications. *Anal Chem* **2001,** *73* (18), 4491-4498.

18. Bruno, A. E.; Maystre, F.; Krattiger, B.; Nussbaum, P.; Gassmann, E., The Pigtailing Approach to Optical-Detection in Capillary Electrophoresis. *Trac-Trends in Analytical Chemistry* **1994,** *13* (5), 190-198.

19. Deng, J. J.; Huang, Y. T., A Novel Hybrid Coupler Based on Antiresonant Reflecting Optical Waveguides. *J Lightwave Technol* **1998,** *16* (6), 1062-1069.

20. Galarza, M.; De Mesel, K.; Baets, R.; Martinez, A.; Aramburu, C.; Lopez-Amo, M., Compact Spot-Size Converters with Fiber-Matched Antiresonant Reflecting Optical Waveguides. *Appl Opt* **2003,** *42* (24), 4841-4846.

21. Galarza, M.; De Mesel, K.; Verstuyft, S.; Aramburu, U.; Lopez-Amo, M.; Moerman, I.; Van Daele, P.; Baets, R., A New Spot-Size Converter Concept Using Fiber-Matched Antiresonant Reflecting Optical Waveguides. *J Lightwave Technol* **2003,** *21* (1), 269-274.

22. Hubner, J.; Mogensen, K. B.; Jorgensen, A. M.; Friis, P.; Telleman, P.; Kutter, J. P., Integrated Optical Measurement System for Fluorescence Spectroscopy in Microfluidic Channels. *Rev Sci Instrum* **2001,** *72* (1), 229-233.

23. Litchinitser, N. M.; Abeeluck, A. K.; Headley, C.; Eggleton, B. J., Antiresonant Reflecting Photonic Crystal Optical Waveguides. *Opt Lett* **2002,** *27* (18), 1592-1594.

24. Ren, K. N.; Liang, Q. L.; Yao, B.; Luo, G. O.; Wang, L. D.; Gao, Y.; Wang, Y. M.; Qiu, Y., Whole Column Fluorescence Imaging on a Microchip by Using a Programmed Organic Light Emitting Diode Array as a Spatial-Scanning Light Source and a Single Photomultiplier Tube as Detector. *Lab Chip* **2007,** *7* (11), 1574-1580.

25. Xiang, Q.; Hu, G. Q.; Gao, Y. L.; Li, D. Q., Miniaturized Immunoassay Microfluidic System with Electrokinetic Control. *Biosens Bioelectron* **2006,** *21* (10), 2006-2009.

26. Soper, S. A.; Ford, S. M.; Xu, Y. C.; Qi, S. Z.; McWhorter, S.; Lassiter, S.; Patterson, D.; Bruch, R. C., Nanoliter-Scale Sample Preparation Methods Directly Coupled to Polymethylmethacrylate-Based Microchips and Gel-Filled Capillaries for the Analysis of Oligonucleotides. *Journal of Chromatography A* **1999,** *853* (1-2), 107-120.

27. Astier, Y.; Braha, O.; Bayley, H., Toward Single Molecule DNA Sequencing: Direct Identification of Ribonucleoside and Deoxyribonucleoside 5 '-Monophosphates by Using an Engineered Protein Nanopore Equipped with a Molecular Adapter. *J Am Chem Soc* **2006,** *128* (5), 1705-1710.

28. Lorenz, M. G.; Mengibar, L.; Entrena, L.; Sanchez-Reillo, R., Data Processing System with Self-Reconfigurable Architecture, for Low Cost, Low Power Applications. In *Field-Programmable Logic and Applications, Proceedings*, Cheung, P. Y. K.; Constantinides, G. A.; DeSousa, J. T., Eds. 2003; Vol. 2778, pp 220-229.

29. Chowdhury, S. R.; Chakrabarti, D.; Saha, H., Fpga Realization of a Smart Processing System for Clinical Diagnostic Applications Using Pipelined Datapath Architectures. *Microprocessors and Microsystems* **2008,** *32* (2), 107-120.

30. Zhang, T.; Fang, H. H. P., Applications of Real-Time Polymerase Chain Reaction for Quantification of Microorganisms in Environmental Samples. *Appl Microbiol Biotechnol* **2006,** *70* (3), 281-289.

31. Fortin, N. Y.; Mulchandani, A.; Chen, W., Use of Real-Time Polymerase Chain Reaction and Molecular Beacons for the Detection of Escherichia Coli O157 : H7. *Anal Biochem* **2001,** *289* (2), 281-288.

32. Shi, M. M., Enabling Large-Scale Pharmacogenetic Studies by High-Throughput Mutation Detection and Genotyping Technologies. *Clinical Chemistry* **2001,** *47* (2), 164-172.

33. Kaigala, G. V.; Hoang, V. N.; Stickel, A.; Lauzon, J.; Manage, D.; Pilarski, L. M.; Backhouse, C. J., An Inexpensive and Portable Microchip-Based Platform for Integrated Rt-Pcr and Capillary Electrophoresis. *Analyst* **2008,** *133* (3), 331-338.

34. Sheridan, G. E. C.; Masters, C. I.; Shallcross, J. A.; Mackey, B. M., Detection of Mrna by Reverse Transcription Pcr as an Indicator of Viability in Escherichia Coli Cells. *Appl Environ Microbiol* **1998,** *64* (4), 1313-1318.

35. Peccoud, J.; Jacob, C., Theoretical Uncertainty of Measurements Using Quantitative Polymerase Chain Reaction. *Biophys J* **1996,** *71* (1), 101-108.

36. Bej, A. K.; Mahbubani, M. H.; Atlas, R. M., Amplification of Nucleic-Acids by Polymerase Chain-Reaction (Pcr) and Other Methods and Their Applications. *Crit Rev Biochem Mol Biol* **1991,** *26* (3-4), 301-334.

37. Reiss, J.; Krawczak, M.; Schloesser, M.; Wagner, M.; Cooper, D. N., The Effect of Replication Errors on the Mismatch Analysis of Pcr-Amplified DNA. *Nucleic Acids Res* **1990,** *18* (4), 973-978.

38. Castro, A.; Okinaka, R. T., Ultrasensitive, Direct Detection of a Specific DNA Sequence of Bacillus Anthracis in Solution. *Analyst* **2000,** *125* (1), 9-11.

39. Castro, A.; Williams, J. G. K., Single-Molecule Detection of Specific Nucleic Acid Sequences in Unamplified Genomic DNA. *Anal Chem* **1997,** *69* (19), 3915-3920.

40. Knemeyer, J. P., Marme, N., and Sauer,M., Probes for Detection of Specific DNA Sequences at the Single-Molecule Level. *Anal Chem* **2000,** *72,* 3717-3724.

41. Venkatesan, N.; Seo, Y. J.; Kim, B. H., Quencher-Free Molecular Beacons: A New Strategy in Fluorescence Based Nucleic Acid Analysis. *Chem Soc Rev* **2008,** *37* (4), 648-663.

42. Marme, N.; Friedrich, A.; Muller, M.; Nolte, O.; Wolfrum, J.; Hoheisel, J. D.; Sauer, M.; Knemeyer, J. P., Identification of Single-Point Mutations in Mycobacterial 16s Rrna Sequences by Confocal Single-Molecule Fluorescence Spectroscopy. *Nucleic Acids Res* **2006,** *34* (13).

43. Kalin, M.; Lindberg, A. A., Diagnosis of Pneumococcal Pneumonia - a Comparison between Microscopic Examination of Expectorate, Antigen-Detection and Cultural Procedures. *Scandinavian Journal of Infectious Diseases* **1983,** *15* (3), 247-255.

44. Klausegger, A.; Hell, M.; Berger, A.; Zinober, K.; Baier, S.; Jones, N.; Sperl, W.; Kofler, B., Gram Type-Specific Broad-Range Pcr Amplification for Rapid Detection of 62 Pathogenic Bacteria. *J Clin Microbiol* **1999,** *37* (2), 464-466.

45. Carroll, N. M.; Jaeger, E. E. M.; Choudhury, S.; Dunlop, A. A. S.; Matheson, M. M.; Adamson, P.; Okhravi, N.; Lightman, S., Detection of and Discrimination between Gram-Positive and Gram-Negative Bacteria in Intraocular Samples by Using Nested Pcr. *J Clin Microbiol* **2000,** *38* (5), 1753-1757.

46. Hupert, M. L.; Guy, W. J.; Llopis, S. D.; Shadpour, H.; Rani, S.; Nikitopoulos, D. E.; Soper, S. A., Evaluation of Micromilled Metal Mold Masters for the Replication of Microchip Electrophoresis Devices. *Microfluidics and Nanofluidics* **2007,** *3* (1), 1-11.

47. Ojo, K. K.; Tung, D.; Luis, H.; Bernardo, M.; Leitao, J.; Roberts, M. C., Gram-Positive Mera Gene in Gram-Negative Oral and Urine Bacteria. *FEMS Microbiology Letters* **2004,** *238* (2), 411-416.

48. Panchuk–Voloshina, N.; Haugland, R. P.; Bishop–Stewart, J.; Bhalgat, M. K.; Millard, P. J.; Mao, F.; Leung, W.-Y.; Haugland, R. P., Alexa Dyes, a Series of New Fluorescent Dyes That Yield Exceptionally Bright, Photostable Conjugates. *J. Histochem. Cytochem.* **1999,** *47* (9), 1179-1188.

49. Kim, J.-s.; Wang, N., Characterization of Copy Numbers of 16s Rdna and 16s Rrna of Candidatus Liberibacter Asiaticus and the Implication in Detection in Planta Using Quantitative Pcr. *BMC Research Notes* **2009,** *2* (1), 37.

# 5 Detection of Pathogenic Bacterium Using a Continuous Flow Ligase Detection Reaction on a Compact, Field Deployable Single-Molecule Instrument

The Ansys5.5 thermal molding work was performed by Pin-Chuan Chen and the pathogenic bacteria work on the confocal system was performed by Zhiyong Peng.

## 5.1 Introduction and Background

Bacteria detection and identification is a high priority for health and safety reasons within a number of different areas ranging from Homeland Security, the Food and Drug Administration, and Clinical diagnostic laboratories.[1] The traditional method for bacterial detection is culturing and plating,[2] however, other techniques are necessary because culturing methods are excessively time-consuming and lack adequate sensitivity.[1] Clinical diagnostics and public health interventions demand rapid and accurate identification of pathogenic bacteria thus prompt and necessary measures can be taken to help minimize health risks. Identification of pathogenic bacteria requires high specificity, low false positives, and robustness to handle the different complex matrices. Genomic-based assays allow for strain-specific identification to evaluate the threat level. Other methods such as antibody or mass spectrometry have not shown the ability to identify strain specific bacteria.[3]

### 5.1.1 Conventional Methods

Conventional detection methods mainly rely on characterizing the phenotypic features of high purity species obtained by culturing the microorganisms in target specific growth media followed by isolation of the colony. It is time-consuming with a minimum of two days required for identification of the bacteria and interpretation of the diagnostic results is usually subjective and prone to human errors.[4]

The high selectivity of antigen-antibody binding interactions makes immunoassay a good alternative for bacteria detection and it can be directly applied to complex biological matrixes such as plasma, blood, or urine with little sample preparation.[5, 6] In addition it can perform parallel analysis of various analytes when microarray techniques are coupled.[7, 8] Advances in DNA sequencing technology allow researchers to obtain the complete genetic information of pathogens after capture.

### 5.1.2 Nucleic Acid Assays

Since the nucleic acid sequence is unique to each bacterium, these microorganisms can be identified more specifically than other techniques at the molecular level. Usually a set of primers are designed based on the DNA sequence of the target pathogens to amplify the region of interest, but the process is still time consuming.

Due to the high sensitivity and specificity of polymerase chain reactions (PCR), it is widely used to detect trace amounts of microorganisms in many scenarios like monitoring water quality,[9] food contamination,[10] and infectious biological agents.[11] Genomic based assays allow for strain specific identification to evaluate the threat level. PCR techniques improved the sensitivity by amplifying millions of targets to hybridize to detection probes, thereby making the target visible to a downstream detector. Then the PCR amplicons are subjected to a separation procedure like gel electrophoresis [12] or liquid chromatography [13] to obtain the specific band of interest. The final products can then be interrogated by using ultraviolet spectrometer, mass spectrometer [13] or laser-induced fluorescence instrument [10] for further confirmation or quantitative analysis. PCR based schemes have demonstrated advancements over culturing and plating methods with results usually in several hours.[14] Examples of different PCR methods developed for

bacterial detection are: (i) real-time PCR[15] (ii) multiplex PCR[16] and (iii) reverse transcriptase PCR (RT-PCR).[17] Real-time PCR involves the detection of a specific dye that attaches itself to the targeted amplicon, which allows for quick results without too much manipulation. Multiplex PCR simultaneously detects several organisms by introducing different primers to amplify DNA regions coding for specific genes of each bacterial strain targeted in the same reaction chamber capable of as many as 10 different pathogens simultaneously can be achieved.[13, 18, 19] Reverse-transcriptase PCR (RT-PCR) targets mRNA, which due to its rapid turnover and short half-lives in viable cells can be used to determine if a bacterial cell is viable.[20] These relatively fast PCR techniques have a turnaround time of 5-24 hours due to the required thermal cycling in addition to other enrichment steps. Therefore, PCR schemes cannot meet the requirements demanded for real-time applications. An additional drawback to PCR based assays is the introduction of ambiguities caused by the PCR that can lead to false negatives/positives.[21-23]

### 5.2 Alterative Methods

Zourob *et al.* demonstrated an evanescent waveguide with metal clad for bacteria detection and the detection limit of Bacillus subtilis var. niger bacterial spores was $10^4$ spores/mL.[24] By combining an ultrasound wave to drive and preconcentrate the bacteria to the waveguide surface, this sensor was able to detect as low as $10^3$ spores/mL of the same bacteria.[25] Surface-enhanced Raman scattering (SERS) sensors were also reported to be able to interrogate bacterial pathogens with species or even strain specificity.[26, 27] The innovation of nanotechnology enables researchers to fabricate biological nanosensors to capture and detect tiny amount of pathogenic bacteria with a better sensitivity since at the nano-scale the DNA hybridization and antigen capturing kinetics are greatly favored

over the conventional microarray formats.[28] Tok *et al.* reported the development of a novel multistriped metallic nanowire and feasibility of multiplex immunoassays for biowarfare agent stimulants.[28] The atomic-force microscope (AFM) can be employed as a versatile biosensor with adsorption of biological materials. By watching either the static (deflection of the cantilever) or dynamic (resonance frequency shift) behavior of the cantilever, the target molecules bound to the cantilever surface can be quantified. Microcantilever [29, 30] and Nanocantilever [31] were recently reported to detect a variety of bacterial ranging with amounts from femtogram to zeptogram. These alternative methods while novel lack the ability of near real-time analysis due to sample preparation requirements.

Recently, Pingle *et al*. demonstrated a multiplexed identification of blood-borne bacterial pathogens using a PCR-ligase detection reaction on a capillary electrophoresis (PCR-LDR-CE) array.[32] They demonstrated the ability to identify 20 blood-borne pathogens using a novel 16S rRNA gene in a clinical/microbiology laboratory. They used the conserved sequences on the ribosome RNA (rRNA) of pathogenic bacterium to identify gene specific bacteria. The LDR results are easily quantified by using an enzyme-linked or direct fluorescent labeling of the LDR products. The products in Pingle *et al.* had not only different sizes but also different fluorescents dyes to help discriminate between the various products.

### 5.3 SMD Nucleic Acid Assays

SMD of bacteria based on direct genomic probe offers the potential for fast, sensitive analysis without false positives. Castro *et al.* demonstrate a technique for the rapid detection of specific nucleic acid sequences in unamplified DNA samples for the

detection of *Bacillus anthracis*.[1] Two nucleic acid probes complementary to different sites on a target DNA sequence are each labeled with different fluorescent dyes. When mixed with a sample containing the target DNA, the two probes hybridize to their respective binding sites on the same target DNA molecule.[33] When the sample was analyzed by a laser-based ultrasensitive fluorescence system capable of SMD at two different wavelength channels the signals appear simultaneously. Therefore, coincident detection of both dyes provides the necessary specificity to detect an unamplified, single-copy target DNA molecule in a homogeneous assay. Uncorrelated events originating from free probes observed at either channel indicates the target is not present. They demonstrated the ability to detect 100 attomolar at a SNR of 3 in 200s and the assay showed good specificity even in the presences of an excess of *B. globigii.*

Another example of SMD for bacterial strand-specific detection was shown by Marme *et al.*; who demonstrated the specific identification of a single nucleotide polymorphism (SNP) responsible for rifampicin resistance of Mycobacterium tuberculosis using molecular beacons (MB).[34] The probe was used for the identification of SNPs in $10^{-11}$ M solutions of PCR amplicons from M.tuberculosis in only 100 s.

Jarvuis *et al.* developed a biomolecule enumeration by converting nanometer scale specific molecular recognition events mediated by rolling cycle amplification (RCA) to fluorescent micrometer size DNA molecules amenable to SMD. They used a set of circular DNA molecules to create highly specific molecular probing reactions for DNA, using so-called “padlock” for the detection and quantification of *Vibrio cholera* bacteria.

### 5.3.1 LDR-spFRET

In general LDR can be done after an initial PCR amplification of the template DNA or directly on genomic DNA.[35] The combination of LDR with reverse molecular beacons (rMB) has lead to the development of LDR-spFRET assays for the rapid and efficient molecular analysis of rare point mutations in genomic DNA.[36] The assay's strategy involves the use of two primers that can form a molecular beacon following successful ligation of the primers and melting from the target DNA. The LDR primers possess a stem section, each labeled with a fluorescent dye that when brought into close proximity can undergo fluorescence resonance energy transfer (FRET). Once the primers are ligated, the solution temperature is elevated above the melting temperature ($T_m$) of the DNA duplex to separate the template from the LDR product. The stem of the beacon was designed to have a higher $T_m$ than that of the ligated primers to the template at the concentrations used for the molecular assay. The formation of the hairpin loop brings the fluorescent dyes into close proximity for efficient FRET. If the target was not completely complementary to the primers, the primers are not ligated and therefore do not form a rMB (see Figure 5.1). Wabuyele *et al.* demonstrated that LDR-spFRET could provide mutation detection in less than 5 min with no PCR amplification.[35] This eliminated not only the need for PCR, but also the need for a subsequent clean up step following PCR, which can be time consuming and costly. Only one thermal cycle for LDR is needed to form the rMB, however, multiple cycles can be used to linearly increase the number of rMBs to aid in detection. Single-pair FRET coupled with LDR offers superior specificity, which can provide pathogenic information at the strain level using a microfluidic device. The resulting rMB products can be directly interrogated by a laser-induced fluorescence

(LIF) system at the single-molecule level to rapidly report the presence of certain bacterial pathogens with high sensitivity and reliability.

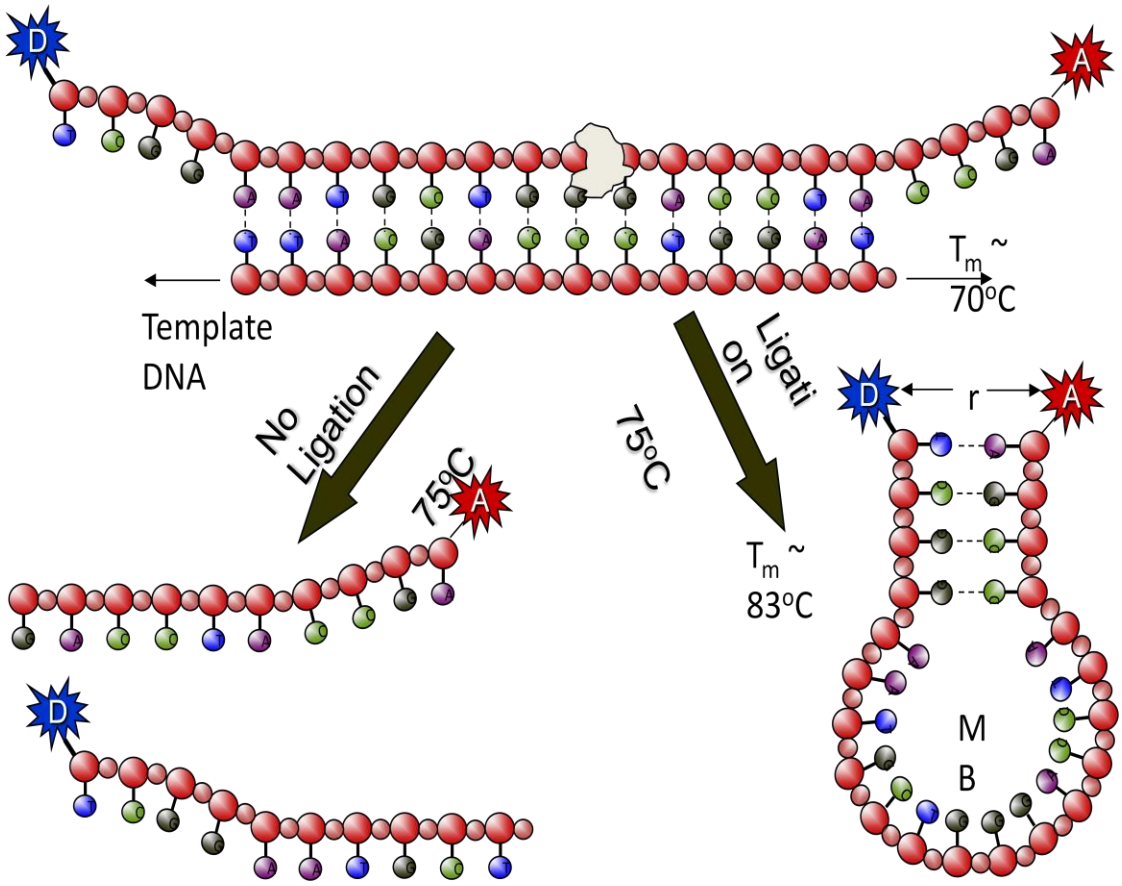


**Figure 5.1** Molecular assay for identifying unique nucleic acid structures using allele-specific ligation (LDR). The LDR involves the use of two primers that recognize a reporter sequence of the target, which in this case is a DNA, and ligates the two primers only if there is complete complementary between the primers and the DNA. If this condition is met, the primers are successfully ligated, forming a molecular beacon bringing the donor/acceptor dyes into close proximity to allow for spFRET to occur. If the primers are not perfectly matched to the reporter sequence of the DNA, no ligation occurs and consequently, no spFRET results.

## 5.4 Point-of-Care (POC)

While many have demonstrated the utility of SMD for several molecular assays,[35, 37-45] there has been no demonstration of the use of SMD for routine clinical measurements by novice users in a field-deployable instrument. The major bottleneck has been limitations imposed by the equipment required to make these measurements,

typically using continuous or pulsed lasers, an extensive array of opto-mechanical components and expensive photon transducers, such as CCDs or channel plates.[46, 47] The ability to monitor biomarkers onsite using a portable microfluidic/single-molecule instrument in near-real time will have a number of important applications, such as strain-specific detection of pathogenic bacteria or molecular diagnosis of diseases requiring rapid turn-around-times at the point-of-care (POC).

We report here a compact, field deployable instrument for the near real-time reporting of molecular signatures using microfluidics for a continuous flow thermal processing of genomic DNA with integrated optics for single-molecule readout. The assay/system is designed to require minimal molecular processing steps with each step optimized for processing speed, proper fluid handling and thermal management. Interfacing the fluidic microchip to the optical readout hardware is provided by optical fibers that are sealed into the fluidic chip to provide for excitation and collection of fluorescent photons. The fiber optic setup offered reproducible alignment of the excitation and emission relay optics as well as a platform for SMD for routine clinical measurements by novice users in a field-deployable instrument. The microfluidic chip was integrated into the instrument peripherals by connecting the bare fibers to optical fibers interfaced to the hardware components (i.e., laser, filters and SPAD). We will show the LDR-spFRET assay to target strain-specific bacteria on the cSMD instrument.

## 5.5 Experimental

### 5.5.1 Microfluidic Chip Design and Fabrication

Figure 5.2a presents an overview of the design of the microfluidic device, which consisted of a series of ten serpentine channels for LDR thermal cycling using a

continuous flow format that had a width of 50 µm and a depth of 80 µm. The chip possessed guide channels to accommodate an excitation fiber (120 µm wide with a depth of 120 µm) and a fluorescence collection fiber (220 µm wide and 220 µm deep).

A detailed description of the polymer microfluidic chip fabrication is described elsewhere.[48] Briefly, microfluidic channels were hot embossed into a poly(methyl methacrylate), PMMA, substrate (3/16" thickness, Lucite CP, SABIC Polymershapes, New Orleans, LA) using a high-precision micromilled brass mold master and hydraulic press (PHI Precision, City of Industry, CA) supplied with a home-built vacuum chamber. Micromilling of the master was performed with 50 to 500 µm diameter solid-carbide milling bits (McMaster-Carr or Quality Tools, Hammond, LA) at 40,000 rpm using a KERN MMP 2522 CNC milling machine (KERN Micro-und Feinwerktechnik GmbH & Co., Germany). Hot embossing was achieved by pressing a heated (160ºC) metal master into a polymer substrate for 210 s at 62 psi. The polymer substrate was then cooled below $T_g$ of the polymer and separated from the mold master. The chip was cut to a final size of 4.5 cm x 4.5 cm and the holes for fluidic reservoirs were drilled. Fiber optics were manually placed in the corresponding conduits in the PMMA chip to create the integrated optical waveguides, which were used for both excitation of fluorescent dyes and collection of the resulting fluorescence. The microfluidic channels were formed by thermal fusion bonding of a thin (0.25 mm) PMMA cover slip (PMMA film, GoodFellow, Oakdale, PA) to the embossed PMMA substrate. For bonding, the microfluidic chip assembly was clamped between two glass plates and placed in a convection oven at 107°C for 20 min.

### 5.5.2 Instrument Design

The microfluidic chip control electronics are divided into five major sections: (1) photon detection, (2) laser diode control, (3) high voltage, (4) microfluidic channel temperature control, and (5) computer interface. The photon counting system used a PCDMini SPAD by SensL that was coupled to a fiber optic and was used to count single fluorescent photons. The PCDMini is compact in size measuring only 1½' x 1½' and has an integrated peltier cooler. To minimize dead time and conserve board space; the photon counting was performed by a custom field programmable gate array (FPGA). The FPGA offered not only a smaller electronic footprint compared to conventional processing electronics, but also additional advantages of fast processing speed and lower power consumption to better accommodate field-deployment. The FPGA (XCR3256XL-12TQ44I, Xilinx Inc., San Jose, CA) was surface mounted on a 144-pin device and was programmed using the ISE Webpack software, version 7.1. The SPAD output was a TTL pulse to the FPGA, which was used for processing the photon events.

An Opnext HL6385DG laser diode was used as the excitation source with a lasing wavelength of 642 nm. To minimize output power fluctuations, a highly stable constant current source was designed to provide up to 280 mA drive current to the laser. The diode comes in a SMA connected housing and has a built-in pin diode for laser power monitoring. At 250 mA current, the laser output from the coupled fiber optic was approximately 24 mW. Optical coupling of the diode to the chip used a 10/125 μm multimode fibers.

The instrument was designed to interrogate single fluorescent molecules and quantify the results detected with a compact SPAD coupled to optical waveguides poised within

the fluidic chip, which were oriented at 90° with respect to each other (see Figure 5.2B). The bare fibers were spliced into OFR fiber ports that contained the appropriate filters for excitation and emission. Finally, the communications between the microcontroller and the analog systems used 12 bit A/D and D/A converters via an I2C serial bus. Data transmission between the control board and the computer was via the standard USB port.

### 5.5.3 Thermal Management

Temperature control of the chips heated zones was provided by a Flextek CLDZ010 digital PID motor speed controller ICs used to regulate the zone temperatures of the thermal reactors microchannels. The IC's were adapted to use temperature feedback via miniature K-type thermocouples instead of motor tachometer voltage. Temperature zones created a continuous flow thermal cycling for the ligation of the primers to the target DNA by thin film heaters integrated onto the chip's stage. Thermal cycling for the LDR was performed in a continuous flow format by electrokinetically transporting (E = 100 V/cm) targets, enzymes and primers through isothermal zones poised at 65°C for annealing/ligation and 94°C for denaturing (see Figure 5.1A). The LDR generates rMBs formed by complementary DNA stem structures, which are labeled with a donor/acceptor pair.[35] The appealing nature of this format is its excellent thermal management capabilities, allowing bio-enzyme kinetic-controlled rates of reaction.[49] Reductions in processing time were affected by simply increasing the linear rate of travel of sample/reagents through the isothermal zones.

### 5.5.4 Electrokinetic Pumping

High voltages for electrokinetic pumping were produced by four EMCO CA -10, DC-DC converters. These converters, along with HV reed relays (model SE051A2O,

SPST from American Relays, Inc), were used to control the magnitude and direction of the electric field for sample and fluorophore movement within the microfluidic channels. To monitor the micro-ampere output of the converters, a unique HV floating current sense circuit was developed, which could measure currents of either polarity down to 1 μA with an accuracy of better than 2%. Currents greater than 50 μA were considered a fault condition causing the computer to shut down the high voltage and alert the user.

### 5.5.5 Bacterial

Two bacterial strains; Staphylococcus aureus subsp. Aureus (ATCC 700699) and Escherichia Coli (ATCC 700926) were investigated in this study and the genomic DNA was acquired from ATCC. A series of dilutions were made in 1X TE buffer. The concentration of the DNA was examined with a UV spectrophotometer (Ultrospec 4000, Amersham Bioscience) using the 260/280 nm absorption ratio. The DNA was stored at -20ºC until being used.

### 5.5.6 Polymerase Chain Reaction

The genomic DNA from these bacterial strains was in some cases pre-amplified by the polymerase chain reaction (PCR). The reaction mixture contained 1X PCR buffer II (Applied Biosystems), 2.5 mM $MgCl_2$, 200 μM dNTPs, 1 μM forward and reverse primers, 1.25 units of DNA polymerase (AmpliTaq Gold Polymerase, Applied Biosystems), 10 ng to 100 ng of template DNA and enough nuclease-free $H_2O$ to make a total reaction volume of 50 μL. The PCR was run in a commercial thermal cycling machine (Eppendorf MasterCycler, Germany). In PCR, the reaction cocktail was first heated to 94ºC for 10 min to activate the Amplitaq gold enzyme. Then, it was subjected to 35 thermal cycles, each of which was composed of a denaturing step at 94ºC for 15 s,

annealing step at 60ºC for 1 min, and extension step at 72ºC for 1 min. Following the thermal cycling, it was further maintained at 72ºC for an additional 7 min to allow complete extension of all PCR products. The PCR products were stored at 4ºC for a subsequent LDR.

### 5.5.7 Ligase Detection Reaction

Ten thermal cycles were performed by electrokinetically transporting (E = 100 V/cm) targets (*S. aureus* or *E. coli*, 0.1 pM) and primers (100 pM) through isothermal zones poised at 65°C for annealing/ligation and 94°C for denaturing (see Figure 5.2A). The reaction cocktail consisted of 2 units/µL of thermostable DNA ligase, 20 mM Tris-HCl (pH 7.6), 25 mM potassium acetate, 10mM magnesium acetate, 1 mM $NAD^+$ cofactor, and 10 mM Dithiothreitol.

### 5.5.8 Primer and Molecular Beacon Design

The primers for the LDR reaction were based on the use of 16S rRNA gene as the target molecule to aid in identification. The 16S rRNA gene is highly conserved, [4, 50, 51] and has been shown to be a viable biomarker for a number of pathogenic bacteria.[32, 52-63] The LDR primer's sequence are shown in Table 5.1. The *S. aureus* target was designed based on the 16S rRNA gene, which were used to differentiate it from *E. coli* bacteria.

The design of rMB was assisted by the DNA folding program from IDT, which uses minimal free energy of formation to predict the melting temperature ($T_m$) of the rMB. The discriminating primer was composed of a 20-base loop and a 10 base stem with the 10 base arm 5'-end labeled with Cy5.5. The 33 base common primer, which contained a 23 base loop and a 10 base stem, was phosphorylated at its 5'- end and at the 3'-end was labeled with Cy5.

**Table 5.1** Sequence of PCR and LDR Primers

| **PCR Primers** | Sequence (5'-3') |
|---|---|
| AMP 2 | CAAACAGGATTAGATACCCTGGTAGTC |
| AMP 2 | GAAGGTGGGGATGACGTCAAAT |
| **LDR Primers** | |
| *S. aureus* common | Cy5.5- AGGCGGCGCGTTACCAAATCTTGACATCCTTTGACA |
| *S. aureus* discrimination | pACTCTAGAGATAGAGCCTTCCCCTTCGGCGCGCCGCCT-Cy5 |

The loop sequence of the beacon was designed based on the known sequence of *S. aureus*. The two stem sequences were designed to be complementary to each other but not to the target and possessed a high GC content resulting in a higher $T_m$. Therefore, the formation of the stem-hairpin loop of the rMB was thermodynamically favored over the loop-target hybridization at a temperature of 75ºC, which resulted in a FRET response from the rMB and no FRET from unligated primers (*E coli*.).

### 5.5.9 Operation of the Microchip

The LDR reaction mixture was first loaded into a 1 ml Becton Dickinson syringe (Franklin Lakes, NJ) equipped with a syringe-to-capillary adapter (InnovaQuartz, Phoenix, AZ). The sample solution was driven by a syringe pump through the microchannels via a capillary tube. The syringe pump was run with a flow rate of 0.05 mL/h to provide the corresponding ligation time.

## 5.6 Results and Discussion

The basis of this continuous flow microfluidic chip is the thermal cycling for the LDR to generate the rMB with the spFRET dyes to determine the presence or absence of Gram + bacteria. The two temperature zones are created by thin film heaters with copper block on the microfluidic stage. The thermal zones were imaged with an IR camera and an overlay of the microfluidic channel design is shown in Figure 5.1B. The denaturing zone was set at 94ºC and the ligation/hybridization was set at 65ºC.

To further understand how the flow rate would affect the residence time in the thermal zones, we modeled the temperature distribution along a single microchannel for flow velocities from 1 mm/s, 3 mm/s, 5 mm/s, and 10 mm/s using the thermofluidic finite element model simulation**.** The result of the Ansys5.5 simulation is shown in Figure 5.1C for the thermal control in a continuous flow thermal reactor. Minimal changes were noted for flow rates ranging from 1 mm/s to 10 mm/s, which indicated that for a 10 mm denaturation zone and a 30 mm ligation/hybridization zone with a flow rate of 10 mm/s a 20 cycle amplification would require as little as 80 s (resident time 1s:3s per cycle). However, the reaction kinetics of the ligase enzyme are slow $k_{cat}$=0.02 $s^{-1}$. This indicates that the highest yields will be obtained with 50 s resident time in the ligation/hybridization zone. Hashimoto *et al.* showed that at a resident time of 60 s the measuring peak intensity versus ligation time platuead.[64] This indicates a linear flow rate of 0.5 mm/s (13.3 min assay time) would yield the most product. Therefore the need for a fast assay and the amount of product must be balanced.

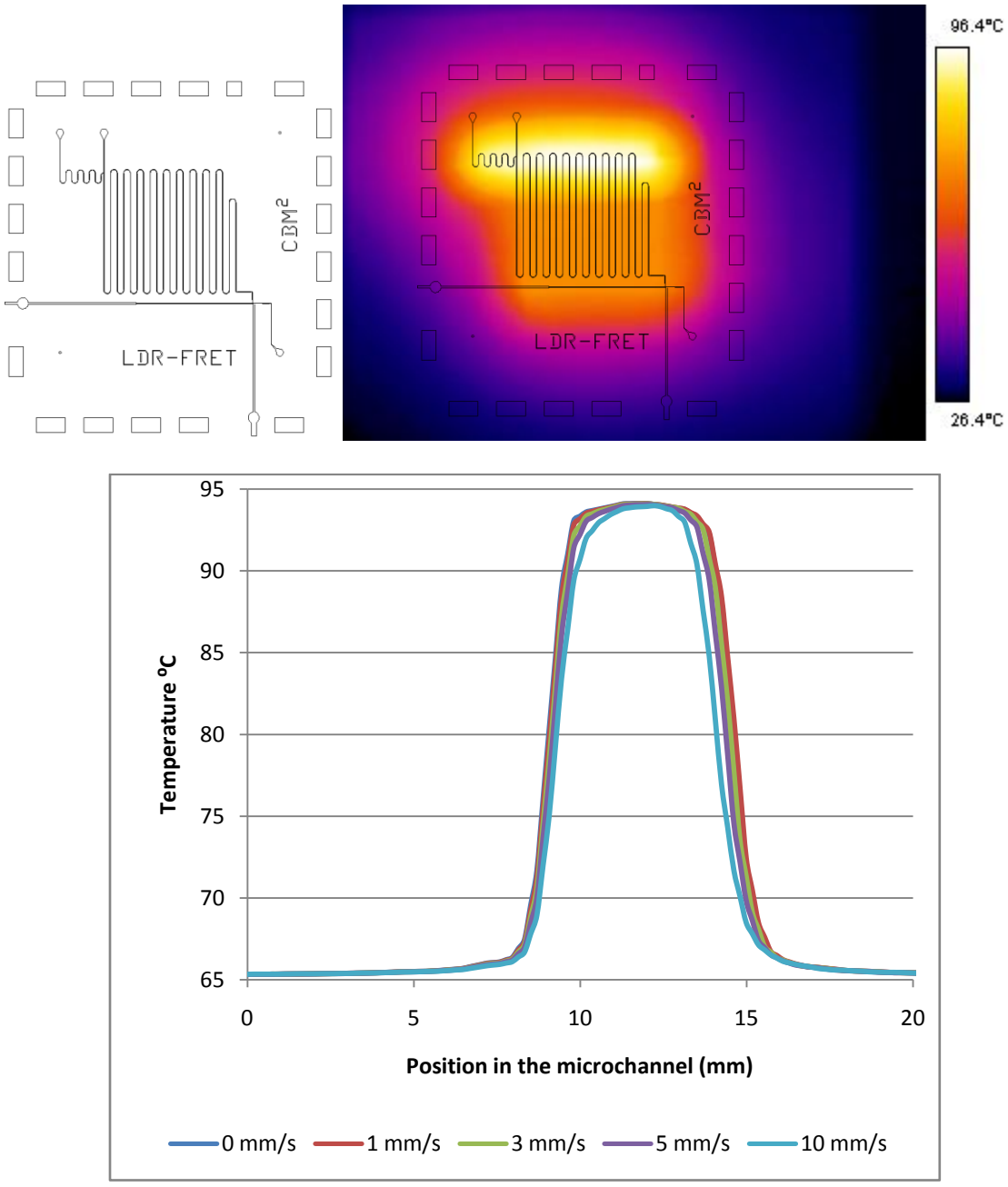


**Figure 5.2** A) Chip layout with a series of ten serpentine channels for LDR thermal cycling (50 µm wide and a depth of 80 µm) Excitation fiber (120 µm wide with a depth of 120 µm) and a fluorescence collection fiber (220 µm wide and 220 µm deep) B) IR thermal camera image of the thin film heaters on the microfluidic stage for continuous flow thermal cycling with a outline of the microfluidic chip laid over top. C) Temperature distribution along a single microchannel for flow velocities from 1 mm/s, 3mm/s, 5 mm/s, and 10mm/s using the thermofluidic finite element model simulation**.** Ansys5.5 simulation of thermal control in a continuous flow thermal reactor. In this simulation, a 2-step temperature reaction was performed with set points of 94°C and 65°C. The reactor has a total length of 20 mm.

The continuous flow LDR-spFRET was validated on a traditional confocal setup described elsewhere.[35] In this experiment, *S. aureus* and *E. coli* underwent the LDR/spFRET assay for Gram staining followed by single molecule measurements. The photons were counted every 1 ms for a duration of 30 s.

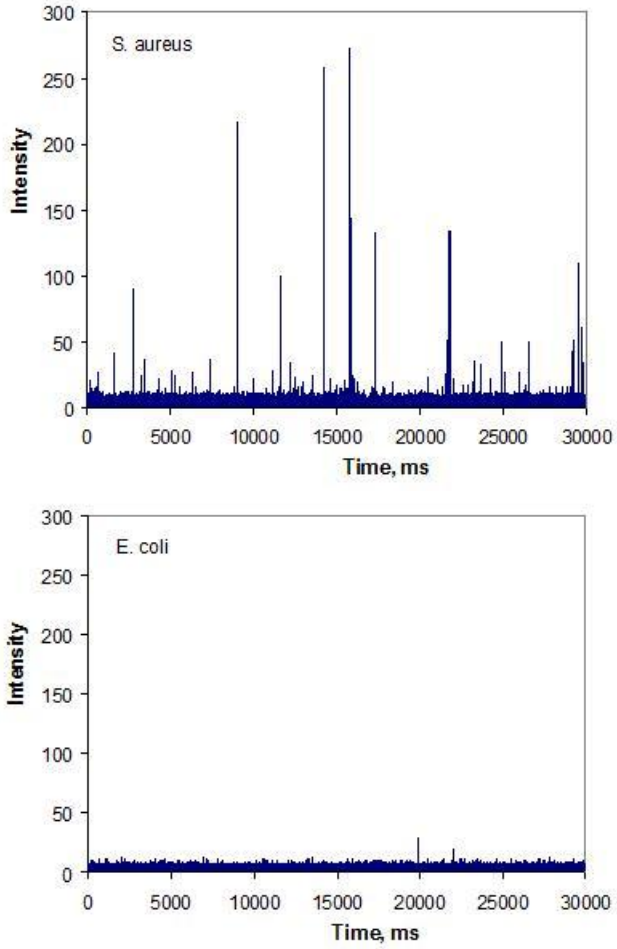


**Figure 5.3** Microfluidic setup for a confocal SMD of rMBs formed from *S. aureus* and *E. coli* using LDR-spFRET. LDR products of 100 pM of common and discriminating primers are loaded in the presence of 0.1 pM of genomic DNA from *S. aureus* (A) and *E. coli* (B). S. aureus is Gram + and the primers ligated together to form a rMB and create a FRET response whereas E. coli is Gram - and the primers are not matched thus no ligation product and no FRET signal.

Figure 5.3 shows the single molecule detection results of a 20-cycle LDR of 100 pM of common and discriminating primers in the presence of 0.1 pM of genomic DNA

from *S. aureus*, and *E. coli*. *S. aureus* is Gram + and the primers are supposed to be ligated together to give a spFRET response, whereas *E. coli* is Gram - and the primers are not matched, thus no ligation product and no spFRET signal. From Figure 5.3A, *S. aureus* demonstrated single photon bursts above the background and *E. coli* (Figure 5.3B) showed no photon burst events. This experiment demonstrated that SMD of LDR-spFRET products can be used to identify Gram + bacteria.

Finally, the LDR product was tested on the compact, field deployable SMD. The samples were diluted to 20 fM of *S. aureus* or *E. coli* LDR-spFRET product and loaded in a 1 ml syringe and placed on a syringe pump. The flow rate was set to 0.05 ml/h and the detection temperature was set to 75ºC. The single molecule photon bursts were collected on the SPAD (Figure 5.4A) and analysis of the data was performed by an autocorrelation function (Figure 5.4B). The half intensity of the function represents the transit time which was 8 ms. The rMB had excellent SNR and photon burst could easily be discriminated. Figure 5.4C shows a histogram of photon events versus burst intensity.

## 5.7 Current Assessment of the Project

The detection of the free dye shown in Chapter 4 and the detection of the LDR-spFRET products on the cSMD demonstrated that the instrument's LOD was in the range for SMD. Therefore, the current road blocks involve the continuous flow reaction on the microchip. Bulk LDR was demonstrated by Hashimoto *et al.* and infer that optimization of the reaction condition is the major obstacle. A more systematic approach would decrease experiential time and lead to positive results. Absorption of dilute concentration of the primer and/or target to the channel wall is a prime suspect for the decreased reaction efficiency. A typical strategy is to add bovine serum albumin to the reaction

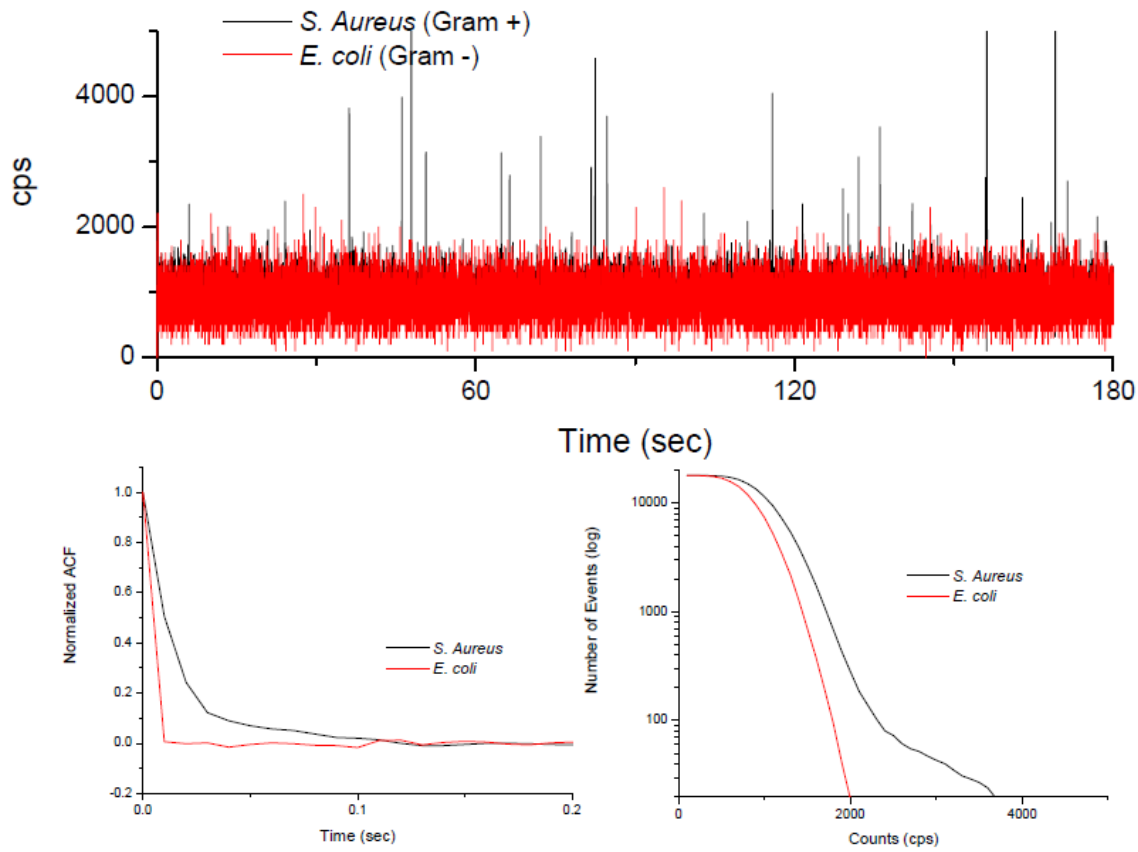


**Figure 5.4** A) Data collected as the photon burst from the LDR-spFRET products are collected on the compact, field deployable SMD. Red is the S. Aureus and Blue is the E. coli. B) Autocorrelation function from A) the blank shows no measurable transit time indicating just noise is present whereas the FRET product had a transit time of 8 msec which corresponds to 10 µm. C) Histogram of photon events versus burst intensity. A discrimination level of 2700 can selected which yields 4 false positives and 103 events. But if no false positives are required a discrimination level of 5200 can be selected which yields 23 photon events.

buffer to prevent the nonspecific absorption to the channel walls. Furthermore, to minimize absorption effects and drive the reaction to higher efficiencies for the formation and detection of rMB the optimal primer to target mixture should be determined. The higher the primer concentration the more efficient the reaction should progress. However, at high primer concentration the fluorophore on the primers can leak past the filter set and increase the background. It's therefore advised that a FRET pair that is further spectrally separated be used such as Cy5-Cy7. This would only see a small drop in FRET

efficiencies but should allow for higher primer concentration due to better optical filtering. The ideal goal is to find the highest primer concentration that the rMB can still be detected with a SNR of 3. With this concentration a series of different target concentration can be run to determine the rMB yield. Furthermore experiments can be run at different number of thermal cycle to optimized speed or input concentration.

## 5.8 Conclusions

The ability to detect gene specific pathogenic bacterium was demonstrated on a compact field deployable single-molecule instrument using the LDR-spFRET assay. The instrument was end user friendly by incorporating the fiber optics into the microfluidic device end user alignment was eliminated opening the possibility for less technically qualified operators to manage this device. Current methods are time consuming such as cell culturing which take 1-2 days,[4] PCR based techniques require 4-24 hours due to the thermal cycling,[14] and nucleic acid based hybridization techniques such as MB, RCA, and coincident detection general require amplification techniques prior to the rapid detection that makes the total analysis time 1-2 h.[33, 34] The rapid analysis time that are achieved here by optimizing thermal cycling by manipulation of the flow rates to precisely controlling the resonance time. Ten cycles of LDR could be performed in 13.3 min followed by a flowing SMD for near real-time detection of strain specific bacteria.

## 5.9 References


1. Castro, A.; Okinaka, R. T., Ultrasensitive, Direct Detection of a Specific DNA Sequence of Bacillus Anthracis in Solution. *Analyst* **2000,** *125* (1), 9-11.

2. Bertke, E. E., Composite Analysis for Escherichia Coli at Coastal Beaches. *Journal of Great Lakes Research* **2007,** *33* (2), 335-341.

3. Dworzanski, J. P.; Snyder, A. P.; Chen, R.; Zhang, H.; Wishart, D.; Li, L., Identification of Bacteria Using Tandem Mass Spectrometry Combined with a Proteome Database and Statistical Scoring. *Anal Chem* **2004,** *76* (8), 2355-2366.

4. Tang, Y. W.; Ellis, N. M.; Hopkins, M. K.; Smith, D. H.; Dodge, D. E.; Persing, D. H., Comparison of Phenotypic and Genotypic Techniques for Identification of Unusual Aerobic Pathogenic Gram-Negative Bacilli. *Journal of Clinical Microbiology* **1998,** *36* (12), 3674-3679.

5. Rowe, C. A.; Scruggs, S. B.; Feldstein, M. J.; Golden, J. P.; Ligler, F. S., An Array Immunosensor for Simultaneous Detection of Clinical Analytes. *Anal Chem* **1999,** *71* (2), 433-439.

6. Rowe, C. A.; Tender, L. M.; Feldstein, M. J.; Golden, J. P.; Scruggs, S. B.; MacCraith, B. D.; Cras, J. J.; Ligler, F. S., Array Biosensor for Simultaneous Identification of Bacterial, Viral, and Protein Analytes. *Anal Chem* **1999,** *71* (17), 3846-3852.

7. Duburcq, X.; Olivier, C.; Malingue, F.; Desmet, R.; Bouzidi, A.; Zhou, F. L.; Auriault, C.; Gras-Masse, H.; Melnyk, O., Peptide-Protein Microarrays for the Simultaneous Detection of Pathogen Infections. *Bioconjugate Chemistry* **2004,** *15* (2), 307-316.

8. Delehanty, J. B.; Ligler, F. S., A Microarray Immunoassay for Simultaneous Detection of Proteins and Bacteria. *Anal Chem* **2002,** *74* (21), 5681-5687.

9. Loge, F. N.; Thompson, D. E.; Call, D. R., Pcr Detection of Specific Pathogens in Water: A Risk-Based Analysis. *Environmental Science & Technology* **2002,** *36* (12), 2754-2759.

10. Alarcon, B.; Garcia-Canas, V.; Cifuentes, A.; Gonzalez, R.; Aznar, R., Simultaneous and Sensitive Detection of Three Foodborne Pathogens by Multiplex Pcr, Capillary Gel Electrophoresis, and Laser-Induced Fluorescence. *Journal of Agricultural and Food Chemistry* **2004,** *52* (23), 7180-7186.

11. Belgrader, P.; Elkin, C. J.; Brown, S. B.; Nasarabadi, S. N.; Langlois, R. G.; Milanovich, F. P.; Colston, B. W.; Marshall, G. D., A Reusable Flow-through Polymerase Chain Reaction Instrument for the Continuous Monitoring of Infectious Biological Agents. *Analytical Chemistry* **2003,** *75* (14), 3446-3450.

12. Lagally, E. T.; Scherer, J. R.; Blazej, R. G.; Toriello, N. M.; Diep, B. A.; Ramchandani, M.; Sensabaugh, G. F.; Riley, L. W.; Mathies, R. A., Integrated Portable Genetic Analysis Microsystem for Pathogen/Infectious Disease Detection. *Analytical Chemistry* **2004,** *76* (11), 3162-3170.

13. Mayr, B. M.; Kobold, U.; Moczko, M.; Nyeki, A.; Koch, T.; Huber, C. G., Identification of Bacteria by Polymerase Chain Reaction Followed by Liquid Chromatography-Mass Spectrometry. *Analytical Chemistry* **2005,** *77* (14), 4563-4570.

14. Zhang, Y. X.; Bahns, J. T.; Jin, Q. L.; Divan, R.; Chen, L. H., Toward the Detection of Single Virus Particle in Serum. *Analytical Biochemistry* **2006,** *356* (2), 161-170.

15. Fortin, N. Y.; Mulchandani, A.; Chen, W., Use of Real-Time Polymerase Chain Reaction and Molecular Beacons for the Detection of Escherichia Coli O157 : H7. *Anal Biochem* **2001,** *289* (2), 281-288.

16. Shi, M. M., Enabling Large-Scale Pharmacogenetic Studies by High-Throughput Mutation Detection and Genotyping Technologies. *Clinical Chemistry* **2001,** *47* (2), 164-172.

17. Kaigala, G. V.; Hoang, V. N.; Stickel, A.; Lauzon, J.; Manage, D.; Pilarski, L. M.; Backhouse, C. J., An Inexpensive and Portable Microchip-Based Platform for Integrated Rt-Pcr and Capillary Electrophoresis. *Analyst* **2008,** *133* (3), 331-338.

18. Brasher, C. W.; DePaola, A.; Jones, D. D.; Bej, A. K., Detection of Microbial Pathogens in Shellfish with Multiplex Pcr. *Current Microbiology* **1998,** *37* (2), 101-107.

19. Kong, R. Y. C.; Lee, S. K. Y.; Law, T. W. F.; Law, S. H. W.; Wu, R. S. S., Rapid Detection of Six Types of Bacterial Pathogens in Marine Waters by Multiplex Pcr. *Water Research* **2002,** *36* (11), 2802-2812.

20. Sheridan, G. E. C.; Masters, C. I.; Shallcross, J. A.; Mackey, B. M., Detection of Mrna by Reverse Transcription Pcr as an Indicator of Viability in Escherichia Coli Cells. *Appl Environ Microbiol* **1998,** *64* (4), 1313-1318.

21. Peccoud, J.; Jacob, C., Theoretical Uncertainty of Measurements Using Quantitative Polymerase Chain Reaction. *Biophys J* **1996,** *71* (1), 101-108.

22. Bej, A. K.; Mahbubani, M. H.; Atlas, R. M., Amplification of Nucleic-Acids by Polymerase Chain-Reaction (Pcr) and Other Methods and Their Applications. *Crit Rev Biochem Mol Biol* **1991,** *26* (3-4), 301-334.

23. Reiss, J.; Krawczak, M.; Schloesser, M.; Wagner, M.; Cooper, D. N., The Effect of Replication Errors on the Mismatch Analysis of Pcr-Amplified DNA. *Nucleic Acids Res* **1990,** *18* (4), 973-978.

24. Zourob, M.; Mohr, S.; Brown, B. J. T.; Fielden, P. R.; McDonnell, M. B.; Goddard, N. J., An Integrated Metal Clad Leaky Waveguide Sensor for Detection of Bacteria. *Analytical Chemistry* **2005,** *77* (1), 232-242.

25. Zourob, M.; Hawkes, J. J.; Coakley, W. T.; Brown, B. J. T.; Fielden, P. R.; McDonnell, M. B.; Goddard, N. J., Optical Leaky Waveguide Sensor for Detection of Bacteria with Ultrasound Attractor Force. *Analytical Chemistry* **2005,** *77* (19), 6163-6168.

26. Premasiri, W. R.; Moir, D. T.; Klempner, M. S.; Krieger, N.; Jones, G.; Ziegler, L. D., Characterization of the Surface Enhanced Raman Scattering (Sers) of Bacteria. *Journal of Physical Chemistry B* **2005,** *109* (1), 312-320.

27. Jarvis, R. M.; Goodacre, R., Discrimination of Bacteria Using Surface-Enhanced Raman Spectroscopy. *Analytical Chemistry* **2004,** *76* (1), 40-47.

28. Tok, J. B. H.; Chuang, F. Y. S.; Kao, M. C.; Rose, K. A.; Pannu, S. S.; Sha, M. Y.; Chakarova, G.; Penn, S. G.; Dougherty, G. M., Metallic Striped Nanowires as Multiplexed Immunoassay Platforms for Pathogen Detection. *Angewandte Chemie-International Edition* **2006,** *45* (41), 6900-6904.

29. Weeks, B. L.; Camarero, J.; Noy, A.; Miller, A. E.; Stanker, L.; De Yoreo, J. J., A Microcantilever-Based Pathogen Detector. *Scanning* **2003,** *25* (6), 297-299.

30. Campbell, G. A.; Mutharasan, R., Detection of Pathogen Escherichia Coli O157 : H7 Using Self-Excited Pzt-Glass Microcantilevers. *Biosensors & Bioelectronics* **2005,** *21* (3), 462-473.

31. Gupta, A. K.; Nair, P. R.; Akin, D.; Ladisch, M. R.; Broyles, S.; Alam, M. A.; Bashir, R., Anomalous Resonance in a Nanomechanical Biosensor. *Proceedings of the National Academy of Sciences of the United States of America* **2006,** *103* (36), 13362-13367.

32. Pingle, M. R.; Granger, K.; Feinberg, P.; Shatsky, R.; Sterling, B.; Rundell, M.; Spitzer, E.; Larone, D.; Golightly, L.; Barany, F., Multiplexed Identification of Blood-Borne Bacterial Pathogens by Use of a Novel 16s Rrna Gene Pcr-Ligase Detection Reaction-Capillary Electrophoresis Assay. *J Clin Microbiol* **2007,** *45* (6), 1927-1935.

33. Castro, A.; Williams, J. G. K., Single-Molecule Detection of Specific Nucleic Acid Sequences in Unamplified Genomic DNA. *Anal Chem* **1997,** *69* (19), 3915-3920.

34. Marme, N.; Friedrich, A.; Muller, M.; Nolte, O.; Wolfrum, J.; Hoheisel, J. D.; Sauer, M.; Knemeyer, J. P., Identification of Single-Point Mutations in Mycobacterial 16s Rrna Sequences by Confocal Single-Molecule Fluorescence Spectroscopy. *Nucleic Acids Res* **2006,** *34* (13).

35. Wabuyele, M. B.; Farquar, H.; Stryjewski, W.; Hammer, R. P.; Soper, S. A.; Cheng, Y. W.; Barany, F., Approaching Real-Time Molecular Diagnostics: Single-Pair Fluorescence Resonance Energy Transfer (Spfret) Detection for the Analysis of Low Abundant Point Mutations in K-Ras Oncogenes. *J Am Chem Soc* **2003,** *125* (23), 6937-6945.

36. Soper, S. A.; Wabuyele, M. B.; Farquar, H.; Stryjewski, W.; Hammer, R. P.; Cheng, Y.-W.; Barany, F., Approaching Real-Time Molecular Diagnostics: Single-Pair Fluorescence Resonance Energy Transfer (Spfret) Detection for the

Analysis of Low Abundant Point Mutations in K-Ras Oncongenes. *J. AM. CHEM. SOC.* **2003,** *125*, 6937-6945.

37. Gell, C.; Sabir, T.; Westwood, J.; Rashid, A.; Smith, D. A. M.; Harris, S. A.; Stockley, P. G., Single-Molecule Fluorescence Resonance Energy Transfer Assays Reveal Heterogeneous Folding Ensembles in a Simple Rna Stem-Loop. *J Mol Biol* **2008,** *384* (1), 264-278.

38. Haupts, U.; Rudiger, M.; Ashman, S.; Turconi, S.; Bingham, R.; Wharton, C.; Hutchinson, J.; Carey, C.; Moore, K. J.; Pope, A. J., Single-Molecule Detection Technologies in Miniaturized High-Throughput Screening: Fluorescence Intensity Distribution Analysis. *Journal of Biomolecular Screening* **2003,** *8* (1), 19-33.

39. Hintersteiner, M.; Auer, M., Single-Bead, Single-Molecule, Single-Cell Fluorescence - Technologies for Drug Screening and Target Validation. In *Fluorescence Methods and Applications: Spectroscopy, Imaging, and Probes*, Wolfbeis, O. S., Ed. 2008; Vol. 1130, pp 1-11.

40. Kang, S. H.; Kim, Y. J.; Yeung, E. S., Detection of Single-Molecule DNA Hybridization by Using Dual-Color Total Internal Reflection Fluorescence Microscopy. *Anal Bioanal Chem* **2007,** *387* (8), 2663-2671.

41. Moore, K. J.; Turconi, S.; Ashman, S.; Ruediger, M.; Haupts, U.; Emerick, V.; Pope, A. J., Single Molecule Detection Technologies in Miniaturized High Throughput Screening: Fluorescence Correlation Spectroscopy. *Journal of Biomolecular Screening* **1999,** *4* (6), 335-353.

42. Neely, L. A.; Patel, S.; Garver, J.; Gallo, M.; Hackett, M.; McLaughlin, S.; Nadel, M.; Harris, J.; Gullans, S.; Rooke, J., A Single-Molecule Method for the Quantitation of Microrna Gene Expression. *Nat Methods* **2006,** *3* (1), 41-46.

43. Qiu, H.; Ferrell, E. P.; Nolan, N.; Phelps, B. H.; Tabibiazar, R.; Whitney, D. H.; Nalefski, E. A., Fluorescence Single-Molecule Counting Assays for High-Sensitivity Detection of Cytokines and Chemokines. *Clinical Chemistry* **2007,** *53* (11), 2010-2012.

44. Wang, L.; Xu, G.; Shia, Z. K.; Jiang, W.; Jin, W. R., Quantification of Protein Based on Single-Molecule Counting by Total Internal Reflection Fluorescence Microscopy with Adsorption Equilibrium. *Anal Chim Acta* **2007,** *590* (1), 104-109.

45. Wu, A. H. B.; Fukushima, N.; Puskas, R.; Todd, J.; Goix, P., Development and Preliminary Clinical Validation of a High Sensitivity Assay for Cardiac Troponin Using a Capillary Flow (Single Molecule) Fluorescence Detector. *Clinical Chemistry* **2006,** *52* (11), 2157-2159.

46. Shera, E. B.; Seitzinger, N. K.; Davis, L. M.; Keller, R. A.; Soper, S. A., Detection of Single Fluorescent Molecules. *Chem Phys Lett* **1990,** *174* (6), 553-557.

47. Soper, S. A.; Shera, E. B.; Martin, J. C.; Jett, J. H.; Hahn, J. H.; Nutter, H. L.; Keller, R. A., Single-Molecule Detection of Rhodamine-6g in Ethanolic Solutions Using Continuous Wave Laser Excitation. *Anal Chem* **1991,** *63* (5), 432-437.

48. Hupert, M. L.; Guy, W. J.; Llopis, S. D.; Shadpour, H.; Rani, S.; Nikitopoulos, D. E.; Soper, S. A., Evaluation of Micromilled Metal Mold Masters for the Replication of Microchip Electrophoresis Devices. *Microfluidics and Nanofluidics* **2007,** *3* (1), 1-11.

49. Hashimoto, M.; Hupert, M. L.; Murphy, M. C.; Soper, S. A.; Cheng, Y. W.; Barany, F., Ligase Detection Reaction/Hybridization Assays Using Three-Dimensional Microfluidic Networks for the Detection of Low-Abundant DNA Point Mutations. *Anal Chem* **2005,** *77* (10), 3243-3255.

50. Krimmer, V.; Merkert, H.; von Eiff, C.; Frosch, M.; Eulert, J.; Lohr, J. F.; Hacker, J.; Ziebuhr, W., Detection of Staphylococcus Aureus and Staphylococcus Epidermidis in Clinical Samples by 16s Rrna-Directed in Situ Hybridization. *Journal of Clinical Microbiology* **1999,** *37* (8), 2667-2673.

51. Clarridge, J. E., Impact of 16s Rrna Gene Sequence Analysis for Identification of Bacteria on Clinical Microbiology and Infectious Diseases. *Clinical Microbiology Reviews* **2004,** *17* (4), 840-+.

52. Beller, H. R.; Kane, S. R.; Legler, T. C.; Alvarez, P. J. J., A Real-Time Polymerase Chain Reaction Method for Monitoring Anaerobic, Hydrotarbon-Degrading Bacteria Based on a Catabolic Gene. *Environ Sci Technol* **2002,** *36* (18), 3977-3984.

53. Cenciarini-Borde, C.; Courtois, S.; La Scola, B., Nucleic Acids as Viability Markers for Bacteria Detection Using Molecular Tools. *Future Microbiology* **2009,** *4* (1), 45-64.

54. Klaschik, S.; Lehmann, L. E.; Raadts, A.; Book, M.; Hoeft, A.; Stuber, F., Real-Time Pcr for Detection and Differentiation of Gram-Positive and Gram-Negative Bacteria. *J Clin Microbiol* **2002,** *40* (11), 4304-4307.

55. Maeda, H.; Fujimoto, C.; Haruki, Y.; Maeda, T.; Kokeguchi, S.; Petelin, M.; Arai, H.; Tanimoto, I.; Nishimura, F.; Takashiba, S., Quantitative Real-Time Pcr Using Taqman and Sybr Green for Actinobacillus Actinomycetemcomitans, Porphyromonas Gingivalis, Prevotella Intermedia, Tetq Gene and Total Bacteria. *FEMS Immunol Med Microbiol* **2003,** *39* (1), 81-86.

56. Malinen, E.; Kassinen, A.; Rinttila, T.; Palva, A., Comparison of Real-Time Pcr with Sybr Green I or 5 '-Nuclease Assays and Dot-Blot Hybridization with Rdna-

Targeted Oligonucleotide Probes in Quantification of Selected Faecal Bacteria. *Microbiology-Sgm* **2003,** *149*, 269-277.

57. Matsuki, T.; Watanabe, K.; Fujimoto, J.; Miyamoto, Y.; Takada, T.; Matsumoto, K.; Oyaizu, H.; Tanaka, R., Development of 16s Rrna-Gene-Targeted Group-Specific Primers for the Detection and Identification of Predominant Bacteria in Human Feces. *Appl Environ Microbiol* **2002,** *68* (11), 5445-5451.

58. Matsuki, T.; Watanabe, K.; Fujimoto, J.; Takada, T.; Tanaka, R., Use of 16s Rrna Gene-Targeted Group-Specific Primers for Real-Time Pcr Analysis of Predominant Bacteria in Human Feces. *Appl Environ Microbiol* **2004,** *70* (12), 7220-7228.

59. Mohammadi, T.; Pietersz, R. N. I.; Vandenbroucke-Grauls, C.; Savelkoul, P. H. M.; Reesink, H. W., Detection of Bacteria in Platelet Concentrates: Comparison of Broad-Range Real-Time 16s Rdna Polymerase Chain Reaction and Automated Culturing. *Transfusion* **2005,** *45* (5), 731-736.

60. Nadkarni, M. A.; Martin, F. E.; Jacques, N. A.; Hunter, N., Determination of Bacterial Load by Real-Time Pcr Using a Broad-Range (Universal) Probe and Primers Set. *Microbiology-Sgm* **2002,** *148*, 257-266.

61. Rinttila, T.; Kassinen, A.; Malinen, E.; Krogius, L.; Palva, A., Development of an Extensive Set of 16s Rdna-Targeted Primers for Quantification of Pathogenic and Indigenous Bacteria in Faecal Samples by Real-Time Pcr. *Journal of Applied Microbiology* **2004,** *97* (6), 1166-1177.

62. Rousselon, N.; Delgenes, J. P.; Godon, J. J., A New Real Time Pcr (Taqman (R) Pcr) System for Detection of the 16s Rdna Gene Associated with Fecal Bacteria. *Journal of Microbiological Methods* **2004,** *59* (1), 15-22.

63. Schuurman, T.; de Boer, R. F.; Kooistra-Smid, A. M. D.; van Zwet, A. A., Prospective Study of Use of Pcr Amplification and Sequencing of 16s Ribosomal DNA from Cerebrospinal Fluid for Diagnosis of Bacterial Meningitis in a Clinical Setting. *J Clin Microbiol* **2004,** *42* (2), 734-740.

64. Hashimoto, M.; Barany, F.; Soper, S. A., Polymerase Chain Reaction/Ligase Detection Reaction/Hybridization Assays Using Flow-through Microfluidic Devices for the Detection of Low-Abundant DNA Point Mutations. *Biosensors & Bioelectronics* **2006,** *21* (10), 1915-1923.

# 6 Conclusions and Future Work: Ischemic and/or Hemorrhagic Stroke Detection in a Point-of-Care (POC) Diagnostic Instrument

## 6.1 Stroke Diagnosis

Currently, no molecular diagnostic test exists for stroke, but fortunately proper therapeutic treatments do exist if the disease is diagnosed within 3 h. Stroke results from the occlusion or rupture of a blood vessel in or around the brain leading to this tissue being deprived of its blood supply. Stroke is a leading cause of death and disability in the United States.[1] There are two types of stroke (see Figure 6.1) - ischemic stroke (80-85%) resulting from vessel occlusion, and hemorrhagic stroke (15-20%) resulting from vessel rupture. But, both cannot be differentiated on clinical grounds and furthermore, 30% of patients presenting stroke-like symptoms do not have stroke at all.[2]

Current stroke diagnoses require the patient to be transported to a hospital and undergo a brain scan, usually with computed tomography (CT), which are very sensitive for the detection of hemorrhagic stroke but less so for ischemic stroke in the first hours of a stroke event; this typically delays therapy from starting for >60 min upon arrival to the hospital. It is imperative that stroke diagnosis be made quickly and accurately because ischemic and hemorrhagic strokes have different treatments and there is only a short time window for effective treatment; 3–6 h.[3-6] The current intravenous treatment for ischemic stroke (recombinant tissue plasminogen activator, rt-(PA)), reaches only 2% of patients and is absolutely contraindicated in hemorrhagic stroke. Delay in diagnosis is a major reason that this treatment reaches so few patients. Furthermore, the earlier treatment starts, the better the outcome.[5, 7] New approaches for speeding up and

improving the accuracy of ischemic and hemorrhagic stroke diagnoses are therefore much needed to accommodate therapy.[8-10]

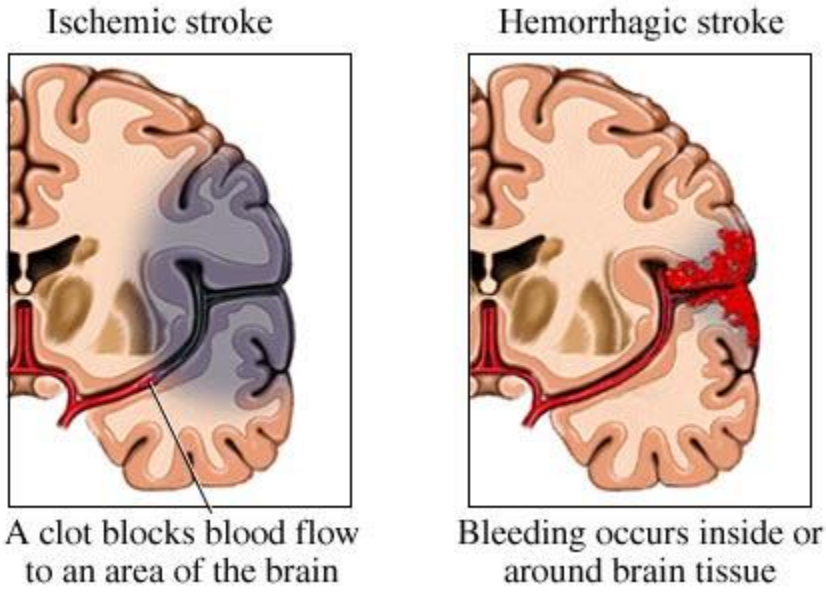


**Figure 6.1** The two types of stroke are ischemic stroke (80-85%) resulting from vessel occlusion, and hemorrhagic stroke (15-20%) resulting from vessel rupture http://myhealth.ucsd.edu/library/healthguide/en-us/images/media/medical/hw/h5551195.jpg

## 6.2 Development of a Molecular Diagnostic Assay and the Associated Hardware Technology

The purpose of this future work is to develop a novel platform for the rapid and point-of-care (POC) molecular diagnosis of stroke using mRNA biomarkers. The accomplishments reported in this dissertation have two major impacts on the development of a POC platform for the molecular diagnosis of stroke using an LDR-spFRET assay: 1) The principles of multi-channel detection for LDR-spFRET (Chapter 2) and an embedded planar waveguide (Chapter 3) to support this development; 2) the development of a compact, field deployable SMD apparatus (Chapter 4) and the optimization of continuous flow LDR-spFRET on this compact SMD instrument (Chapter 5). For the long term goals presented here, we will combine aspects of these projects to create a multi-channel field deployable SMD instrument for fast, real-time diagnosis

of specific biomarkers for stroke. The preceding chapters laid the ground work for the development of the molecular diagnostic strategy and the necessary hardware, for the POC diagnosis of ischemic and/or hemorrhagic stroke. Additionally, the instrument that can be envisioned for this particularly application combines other technologies and techniques developed in our lab. For example, Witek *et al.* recently demonstrated the ability to isolate total RNA using a simple platform, which consisted of PC replicated from a metal master and UV activated to create a solid-phase with high specificity for total RNA.[11] Wang and Chen have developed an integrated modular system for detecting SNPs in certain gene fragments using a PCR/LDR/universal array assay format. The system was used for the detection of SNPs in the rpoB gene of Mycobacterium Tuberculosis (Mtb) toward identifying drug resistant strains.

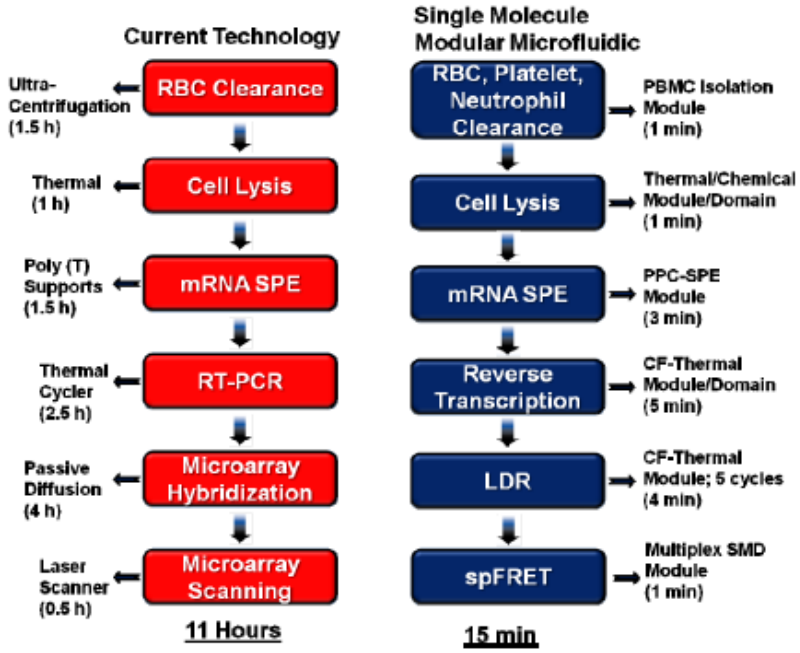


**Figure 6.2** Processing pipelines using a conventional bench-top strategy for processing mRNAs specifically for obtaining expression data and the processing pipeline that will be employed in this POC system for the rapid reporting of mRNA signatures associated with stroke. In addition, the associated processing times for each step of the conventional and proposed methods for mRNA analysis is provided. The sample input for this system is whole blood, which is first subjected to a clearance step to isolate PBMCs (1 min) and then, thermal/chemical cell lysis (1 min), isolation of the RNAs using solid-phase extraction (3 min), reverse transcription (5 min), ligase detection reaction (4 min) and spFRET readout (1 min), producing a turn-around-time of ~15 min.

A fluidic bio-processor fabricated in polymers via micro-replication technology will provide autonomous sample processing and will be comprised of a fluidic motherboard possessing task-specific modules. The sample processing pipeline will be streamlined to generate a rapid assay turn-around-time realized by using microfluidics and single-molecule detection (see Figure 6.2). The output of the clinical sample processing will be molecular beacons undergoing single pair Fluorescence Resonance Energy Transfer (spFRET) that are digitally counted to provide exquisite analytical sensitivity.

## 6.3 Current Research

While no molecular diagnostic test for ischemic or hemorrhagic stroke is currently available, the potential for finding one is being increasingly appreciated. The challenges for realizing this potential were recently reviewed by Whiteley.[12] For neurological disorders, such as stroke, brain tissue is rarely available, but there is a strong rationale for using the peripheral blood for molecular profiling. Blood borne white blood cells, specifically peripheral blood mononuclear cells (PBMCs), are involved in the pathophysiology of many brain disorders.[13] Furthermore, changes in functional gene expression in PBMCs in brain disorders may occur in response to exposure to brain antigens as a result of sensitization of peripheral lymphocytes.[14-16] Early gene expression profiling studies of the blood for stroke has produced promising results in rodents.[17] Additional reports have begun to appear delineating the utility of panels of serum protein and of gene expression transcripts for the molecular diagnosis of stroke. For example (Clark et al. 2002), Biosite has reported a 5-protein marker panel for ischemic stroke, in which conventional CT scans are ineffective in diagnosing (33% clinical sensitivity). The general hypothesis is that endothelial cell death emanating from a stroke can cause proliferation of

cytosolic contents across the blood-brain-barrier into the systemic circulatory system. Therefore, a simple blood test of the serum could uncover over-expressed proteins responding to stroke. The 5 serum protein markers employed included S-100B, B-type neurotrophic growth factor, von Willebrand factor, monocyte chemotactic protein-1 and matrix metalloproteinase-9.[18] The assay consisted of removal of the cellular fraction of whole blood using filters and then, a sandwich-based ELISA in which the primary antibody was linked via biotin/neutravidin to a solid support. A secondary antibody labeled with alkaline phosphatase generated a fluorometric response for the panel of markers and could diagnose hemorrhagic stroke within 6 h of disease onset with a sensitivity and specificity of 92% and 93%, respectively. However, subsequent validation testing revealed only modest discriminative abilities.[19]

### 6.4 Single-Molecule Detection

Single-molecule detection (SMD) was discussed in detail in Chapter 1, but briefly discussed here as another pertinent technology to realize the goals established for this future project. In addition, the SMD must be employed using a field-deployable system. While many have demonstrated the utility of SMD for several molecular assays,[20-28] there has been no demonstration of the use of SMD for routine clinical measurements by novice users in a field-deployable instrument. The major bottleneck has been limitations imposed by the equipment required to make these measurements, typically using continuous or pulsed lasers, an extensive array of opto-mechanical components and expensive photon transducers, such as CCDs or channel plates.[29, 30] In fact, most single molecule measurements are made using confocal microscopes due to the ultra-small probe volume they generate, providing high signal-to-noise ratios (SNR) for the individual molecules. Indeed, many commercial vendors of SMD equipment use high resolution confocal microscopes.

## 6.5 Compact System for SMD

We have recently packaged and assembled optical components into a unit that measures 5" x 7" and is capable of detecting single fluorophore molecules (Chapters 4 & 5). Interfacing the fluidic microchip to the optical readout hardware is provided by optical fibers that are sealed into the fluidic chip and connected to the laser (vertical cavity surface emitting laser, VCSEL) and a single photon avalanche diode (SPAD). The optical breadboard and supporting electronics for performing single photon counting with limited dead time have been assembled. Processing of high frequency electrical signals produced from the SPAD is accomplished using a field programmable gate array. The fluidic system also possesses integrated fiber optics for excitation and collection of fluorescent photons. The fiber optic setup offered reproducible alignment of the excitation and emission optics. A microfluidic chip could be integrated into the instrument peripherals by connecting the bare fibers to optical fibers interfaced to the hardware components (*i.e.*, laser, filters and SPAD).

One of the goals of this future project will be to produce a small footprint multichannel SMD instrument that can be easily interfaced to an integrated fluidic bio-processor for field use. Most examples of SMD configured in a flow-based format have employed a single channel reader with no multiplexing capabilities. It will be necessary in our application to simultaneously analyze multiple markers to provide viable clinical results. The preliminary design of this POC system will utilize a 5-plex assay with the ability to accommodate scale up for additional biomarkers if needed. We have recently demonstrated the ability to perform multi-channel SMD using imaging CCDs operated in a frame-transfer or time-delayed integration mode.[31, 32] In this application, we will employ spatial multiplexing, in which 5 different fluidic vias will be used (actually 7 with two vias used for references) with each fluidic via monitoring a single

biomarker. The advantage of this approach as opposed to color multiplexing is that a single excitation source can be used to assist in reducing instrument footprint and also, it is scalable to higher multiplexing power by simply adding more fluidic vias to the bio-processor readout module as well as more photon transducers.

In collaboration with Dr. Baird at SUNY Downstate Medical Center, we will determine appropriate mRNAs as the marker panel for diagnosing stroke. Previous work in Dr. Baird's Clinical Stroke Research Laboratory has produce two pilot studies where panels of markers for both ischemic stroke and hemorrhagic stroke were developed. Genes of interest for hemorrhagic stroke included amphiphysin and IL1R2. We were also able to show differential expression between ischemic and hemorrhagic stroke, although a small number of genes were common to both types of stroke. These gene panels have been validated using real-time PCR in independent cohorts of subjects. In subsequent studies, pilot data (using real-time PCR) has now been obtained to show proof-of-concept for the adaptation of these panels to the microfluidic technology realized through this application. To be applied to the proposed POC system, the individual mRNAs need to be fully characterized – primers need to be selected, the normal levels of gene expression, the degree of alteration seen in stroke relative to the normal and the time course of expression need to be evaluated as well. Pilot data are shown in Figure 6.3. Real-time PCR data (differential expression with respect to controls for three genes, SPTAN1, IL1R2 and AMPH) are presented from patients with hemorrhagic stroke (red) or ischemic stroke (blue); amphiphysin (AMPH) was highly expressed in all of the hemorrhagic stroke patients but not in the ischemic stroke patients. It appears that this gene becomes "switched on" during acute ICH. In addition, IL1R2 was over-expressed for ICH patients but not for ischemic patients. However,

SPTAN1 showed higher expression levels for ischemic stroked compared to those with ICH stroke.

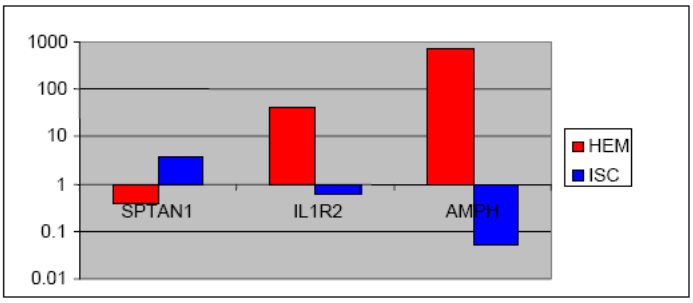


**Figure 6.3** Real-time PCR expression profiling of various genes including Amphiphysin (PMPH), IL1R2, and SPTAN1. Differentially expressed genes between ischemic (blue) and hemorrhagic stroke (red) are shown. Real time PCR was carried out on blood samples from patients clinically diagnosed with the respective stroke condition.

We have recently shown that this assay can be used for the identification and quantitation of mRNAs using primers that recognize unique reporter sequences within the target. As an example, the matrixmetalloproteinase 7 (MMP-7) gene transcript was used (1,147 bp gene that transcribes a linear mRNA molecule) and analyzed in two different cell lines; HT29 (shows high expression of MMP-7) and SW620 (no expression of the MMP-7 gene). The cells were thermally lysed and the whole cell lysate subjected to a solid phase extraction of the mRNAs using a microchip fabricated in polycarbonate (Witek et al. 2008). The purified mRNA was subjected to RT and on-chip LDR using a continuous flow thermal reactor (Chen et al. 2008; Hashimoto et al. 2006; Hashimoto et al. 2004). As can be seen, no photon bursts were evident for the SW620 cell line consistent with this particular cell line not expressing the MMP-7 gene, while the HT29 cell line showed signals consistent with its expression level of the MMP-7 gene. The mRNAs will be converted to their respective cDNAs and then subjected to a LDR to form molecular beacons undergoing spFRET. While SMD of mRNA and miRNA have been reported using a pair of sequence-specific probes labeled with two different dyes and detection

accomplished via coincidence detection,[24, 33] no SMD work has been reported for field molecular diagnostics. We have been working toward developing SMD capabilities for providing readout of a variety of nucleic acid biomarkers. In our first example, spFRET was used to detect point mutations in unamplified genomic DNA.[26] The detection process was required to discriminate between normal and mutant DNAs and was carried out using allele-specific primers and LDR. LDR-spFRET provided the necessary specificity and sensitivity to detect single point mutations in as little as ~600 copies of human genomic DNA without PCR at a level of 1 mutant per 1,000 wild-type sequences in less than 5 min. The major advantages of SMD in molecular analyses include; (1) the ability to alleviate the need for amplifying the target material via PCR, which produces potential difficulties in obtaining quantitative information; (2) reduces the number of processing steps and; (3) significantly reduces processing time and assay cost.

### 6.6 Proposed Research Design

We will develop a simple flow-through modular fluidic bio-processor made from polymeric materials via replication micro-technologies to analyze the molecular content of PBMCs for the expression level analysis of mRNAs that provide diagnostic information for ischemic and/or hemorrhagic stroke in a turn-around-time (TAT) less than 20 min. The fluidic bio-processor (see Figure 6.4) accepts the input sample (whole blood), clears the blood of RBCs, neutrophils and platelets to produce the PBMC fraction, thermally and/or chemically lysis the PBMCs, isolates the total RNA using SPE, reverse transcribes the mRNAs into cDNAs, performs an LDR on the cDNAs using primers that carry reporter sequences for the target and readout of successful ligation events using spFRET. The use of spFRET obviates the need for a PCR step, which not only reduces processing time, but also produces exquisite analytical sensitivity. The proposed fluidic bio-processor shown schematically in Figure 6.4 consists of 3

modules with 1 made in PMMA and another in the appropriate waveguiding material (blue, see Figure 6.4) and the third made from PC (light gray). The fluidic motherboard in which the modules are inserted using the appropriate interconnect technology is made from PC. For this application, the cell sorting module will be fabricated in PMMA due to its tendency to display minimal cell non-specific adsorption artifacts.[34] The RNA SPE module and fluidic motherboard are made from PC due to its relatively high glass transition temperature to allow it to withstand the temperatures required for the thermal reactions and also its unique characteristic to allow the SPE of nucleic acids.[11, 35, 36] The spFRET readout module must be made of a polymeric material that has favorable optical properties and also, supports waveguiding.

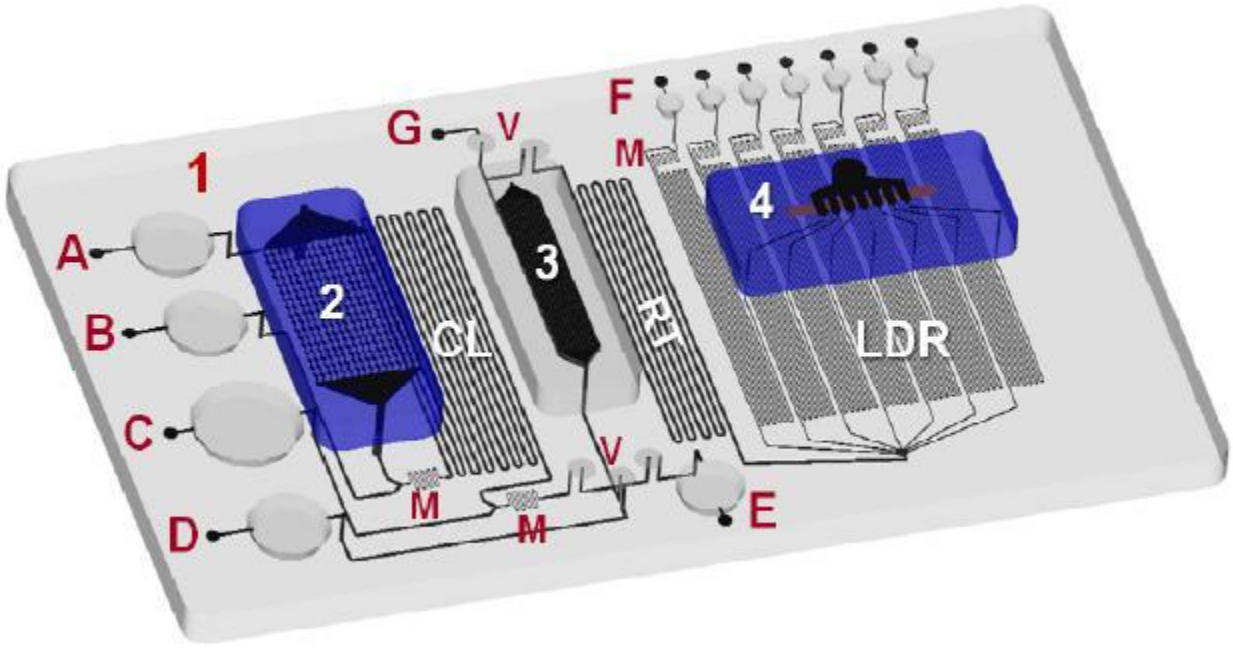


**Figure 6.4** Fluidic bio-processor for the analysis of mRNAs in PBMCs. The fluidic bio-processor has 3 modules that are used for cell selection (depletion of RBCs, neutrophils and platelets), (2) SPE isolation/purification of RNA (3) and spFRET readout (4). These modules are "plugged" into a fluidic motherboard (1) that also contains thermal domains for performing cell lysis (CL), reverse-transcription (RT) and LDR (LDR). Heating of the thermal reaction domains are carried out by placing the fluidic bio-processor on Cu blocks set at the necessary temperatures. Also shown are locations of on-chip valves (V) pumps (A-F) and high-aspect ratio mixers (M). A – sample input; B – lysing buffer; C – SPE buffer; D – ethanol; E – RT cocktail; F – LDR cocktail; G – connection to off-chip vacuum pump.

## 6.7 Thermal Management

Three thermal domains are required for this instrument, which are used for cell lysing, RT, and LDR. All of these domains will be positioned directly on the fluidic motherboard. All thermal energy will be provided by a heating stage located directly on the processor holder frame. After insertion into the instrument, the bio-processor will be gently pressed against the heater surface to provide good thermal contact. The heating stage will consist of commercial Kapton film heaters attached to Cu blocks of the required thickness to provide a uniform heat flux and temperature distribution. Temperatures of the zones are spatially localized over the fluidic motherboard and sensed by type K thermocouples positioned inside the Cu blocks close to the heater-processor interface. A standard PID loop control will be used to maintain the temperatures to within ±1$^{o}$C.

## 6.8 Optical Control and Signal Processing

Circuitry for temperature control of each SPAD along with active quenching will be included in an optical control subsystem. Rapid data acquisition and front end processing will take place using an instrument control unit (ICU) and event counter unit (ECU). Post processing of this data for the end user will be under computer control. The ECU will consist of seven high speed counters for reading out the individual signal channel SPADs. Each counter will be 31-bits wide, permitting a count maximum of more than two billion per channel. The 32$^{nd}$ bit will be used as an overflow indicator. The counter maximum input frequency will be at least 20 MHz, allowing better than 50 ns pulse-to-pulse resolution. The system architecture will allow for expansion to include additional markers if required for the stroke diagnosis. The counters will be individually enabled/disabled, read or cleared by sequence logic under control by the host

computer. The count values from each counter will be temporarily stored in its associated first-in-first-out memory (FIFO). The FIFO will be necessary for short sample intervals because the host computer will not be able to keep up with the counter data stream without losing data or having long dead times between samples.

## 6.9 Microprocessor and Software Control

The operation of all microfluidic peripherals will be achieved by the ICU. The ICU will have an onboard electronic microprocessor that communicates with all electronic subsystems (digital-to-analog and analog-to-digital converters, stepper motor drivers, temperature monitors, ECU, etc.) and coordinates their operation (see Figure 6.5). It also communicates with the personal computer via a USB interface and can be programmed by the user through control software. The ICU and ECU will be designed to generate internal timing signals for the control and synchronization of time sensitive events without requiring intervention. The host computer software will include a GUI that can be customized for a particular operating environment. For normal use, a turn-key interface will be used that leads the user through the required setup and operating steps with robust bound checking and error detection. Figure 6.5. Block diagram of the electronics required for the POC system.

The design complexity of the electronic controlling hardware could require >100 individual discrete function integrated circuits (IC) on a half dozen or more printed circuit boards. For an instrument designed for field deployment, this classical approach is not practical. A better alternative is the use of high density programmable logic devices. These devices are ICs that contain large arrays of basic logic building blocks and programmable interconnection pathways, which can be selectively programmed to implement most logic functions. These devices are called field programmable gate arrays (FPGA) and are readily available at relatively

low-cost from a number of manufacturers. Modern FPGAs contain the equivalence of hundreds to millions of individual logic gates all within a single integrated circuit package. Besides making a complex design possible in a small physical form factor, FPGAs consume much less power than their discrete IC equivalent designs. Because most of the interconnections are done internally to the FPGA, signal propagation times are much smaller than in conventional approaches. We have previously demonstrated the implementation of an FPGA as a photon burst counter (see Figure 4.3) in a compact SMD in Chapter 4. Because FPGAs make possible physically small, low power and high speed complex systems, the ICU and ECU will contain FPGAs whenever possible.

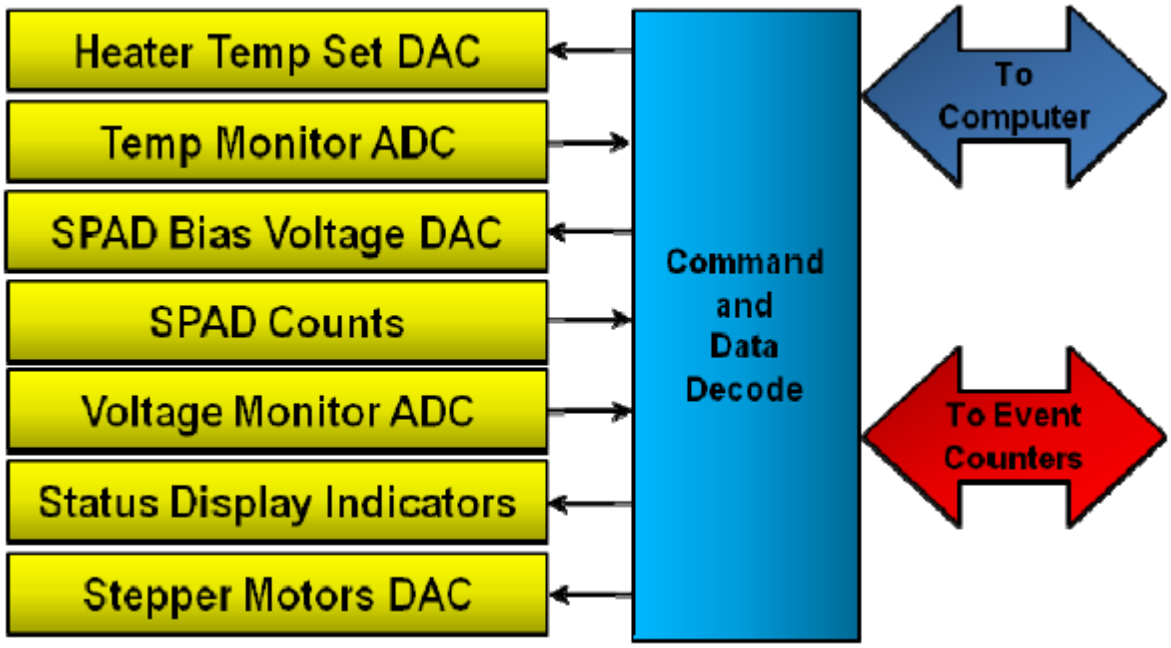


**Figure 6.5** Block diagram of the electronics required for the POC system

The physical dimensions of this POC prototype instrument is projected to be 12” (width) x 9” (depth) x 8” (height) and includes the ICU and ECU boards, solenoids, actuators, laser, fiber optics, filters, SPADs and the fluidic bio-processor. In addition, the POC system will provide full process integration with the user required to load the sample and seal it within the containment

reservoir. Reagents can be loaded at the factory or by the operator. The fluidic bio-processor, once loaded with the sample, requires the operator to insert the chip into the instrument and start the processing through a user-friendly GUI.

### 6.10 Microfluidic Design

On the backside of the fluidic substrate is an array of hemispherical microlenses used to collect the fluorescence radiation from single-molecules. These lenses are situated directly above the waveguide and serve to focus the fluorescence from the single molecules onto a series of multi-mode optical fibers used to direct the fluorescence to single photon avalanche diodes (SPADs), one for each of the 7 fluidic channels. These lenses are embossed into the substrate when the fluidic vias are produced using double-sided embossing.[37] The f/# (i.e., light gathering efficiency) can be increased by increasing the radius of curvature of the lens as well as reducing their distance to the emitting point source. These lenses can be made via a modified X-ray LiGA process with the processing steps outlined here: [38-40] (1) Spin coat a positive tone resist, in this case PMMA, onto a stainless steel plating base. (2) Expose the PMMA resist to x-ray radiation using the required mask.[41] In the present application, we will use 500 μm diameter lenses because these tend to produce lenses with maximum heights giving large radii of curvature.[40] (3) Develop and remove the exposed resist. (4) Expose the remaining PMMA resist, defining the lens array, to X-ray radiation of the required dose to create a top layer of the resist that has a different Tg (i.e., glass transition temperature) compared to the bulk. (5) Heat the PMMA resist to a temperature of ~120º to form the lenses' radius of curvature.[40] (6) Following deposition of a thin conductive layer of Au over the PMMA resist and stainless steel plate, electroplate Ni from a Ni sulfamate bath to create the molding tool containing the lens array. (7) Emboss the desired lens array into the appropriate polymer using double-sided embossing to create the fluidic

network on the opposite side (see Figure 7.5 A). While there are several processing steps required as well as two X-ray exposures to make this molding tool, most of these processing steps are performed only once to generate the desired molding tool with the necessary parts produced via micro-replication. We have found that Ni molding tools can be used to replicate thousands of parts without producing defects in the tool.[41-43]

The linear lens array will not lead to higher coupling efficiency of the fluorescent signal into the fiber optics compared to butt end coupling but raises a few very beneficial possibilities. The lens allow the collection fiber to be move away from the microfluidic channel without losing collection efficiency. By creating this space a single filter for all channels maybe inserted between the lens and the fiber ends. This will have a dramatic reduction in instrumentation since this would eliminate all the OFR fiber ports which currently house the filter sets. The fiber could then be directly coupled to the SPADs.

The second possibility that takes advantage of the mircolens array is the direct coupling to a SPAD array. This would require an insertion of a filter between the microfluidic channel and the microlens which are focusing the fluorescent photon directly on the array. Hofmann *et al.* fabricated a high quality monlithically integrated optical long-pass filter for deposable diagnostic microchips. They dissolved Sudan dyes in toluene and mixed with the PDMS monomer and hardener. The doped PDMS was then poured into molds to fabricate coverslip filters which had < 0.01% transmittance below 500 nm and >80% above 570 nm. We could tailor the dye added to the PDMS for our near-IR application. The filter layer could be sandwiched between the microfluidic channels and the coverslip microlens array. The use of a SPAD array would again reduce the instrumentation size by reducing the number of SPAD modules form seven in the designed prototype to one with the additional removal of the seven OFR filter blocks.

Although these design are optimistic for the stroke panel markers detection the fundamental butt end coupling may be the easiest and straight forward way to progress at first. The fibers can be inserted in to the channel from above the waveguide by either drilling 250μm hole or milling a mold with the preposition post and then fly-cutting to open the holes and insert the fibers. From there the fibers can be glued in place to prevent leakage.

### 6.11 Waveguide

Discussed previously was our approach to build multi-channel orthogonal waveguides and this was found in Chapter 3, but a brief summary is given here. The appropriate waveguiding properties of this module requires minimal losses into the substrate (cover plate) and a critical angle similar to that of the water/polymer interface to generate a maximum penetration depth of the evanescent field into the adjoining solution layer. Polymer selection will be based not only on the refractive indices, but also their autofluorescence properties, wettability and moldability. While a large difference in refractive indices are attractive for creating a deep evanescent field, we can use COC (n = 1.53) as the waveguide and PMMA (n = 1.48) as the substrate as we have already demonstrated (see Figure 3.4). For this example, the evanescent field had a depth of penetration of ~350 nm. The waveguide is made by embossing a channel into the cover plate, which defines the dimensions and location of the waveguide, and reversibly sealing a PDMS stencil onto the cover plate that contains an access port for filling the waveguide channel with a polymer melt and a recess for forming the coupling prism directly onto the waveguide. Following filling the channel and recess with a polymer melt, it is allowed to fill this via and the solvent allowed to evaporate to form the solid polymer waveguide. Following solvent evaporation, the PDMS stencil is peeled from the surface. The waveguide is surrounded by the cover plate substrate on 3 sides and on the top side by the fluidic substrate and the aqueous

solution filling the vias. The results depicted in Figure 3.5 were secured using a waveguide made in this fashion. The integration of the waveguide into the compact SMD system for Stroke detection is shown in Figure 6.6 with the multiple channel being excited by the waveguide and the resulting fluorescents collect by fiber optics position out of the plane.

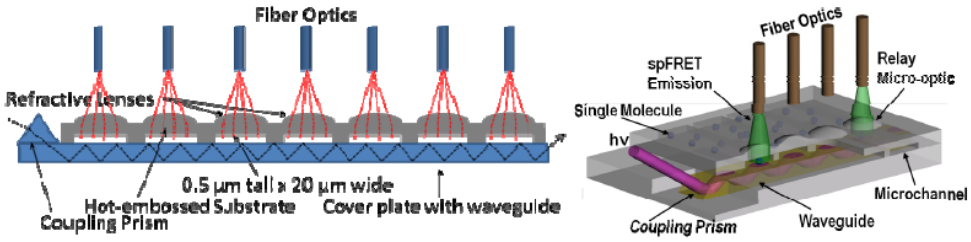


**Figure 6.6** (A) Schematic diagram of the integrated module for reading single-molecule events. This module contains the fluidic vias, hemispherical lenses on the back side of the substrate to collect the resulting fluorescence and image it onto an array of fiber optics. The cover plate contains an embedded waveguide with coupling prism to provide excitation of the microchannel array via an evanescent wave. (B) Diagram of the assembled module showing in the coupling prism and waveguide integrated into the cover plate. The microchannel depth was selected to allow for high sampling efficiency using the evanescent field.

Although the waveguide have been design and built they have not been tested for SMD yet. The key properties of the waveguide should provide a reduced background due to the total internal reflection at the waveguide/channel interface and the reduced probe volume. However, if the excitation is below optical saturation or the channel to channel efficiency is low the alternative will need to be employed. Which would involve the use of horizontal excitation as discussed in Chapter 2 due to the collection optics on-top of the chip and heater on the underside. The best alternative approach would be colliminate the output of the fiber either a custom fiber with a ball end or the integration of micro ball lens. These would allow for a uniform excitation of multiple channels with high irradiance, but the larger probe volume reacted by this method increase the noise above the SMD limits.

## 6.12 Optical Setup

We will build a readout module with the architecture delineated in Figure 6.6B. It consists of a polymer substrate, which contains fluidic channels and microlenses molded onto the backside of this module. A cover plate, made from the same material, contains a monolithic coupling prism and an embedded polymer waveguide to direct the excitation light orthogonal to the array of channels to permit monitoring the entire biomarker panel simultaneously. The waveguide, once the cover plate has been thermally fusion bonded to the substrate, will make intimate contact to the solution contained within the fluidic channels. Excitation of single molecules resident in the solution is therefore accomplished via the evanescent field generated from the waveguide. The advantages of this strategy are that the excitation light can be easily coupled into the system and it provides a uniform field for excitation of all fluidic vias.

The optical components of the system will consist of a 120 mW 642 nm laser diode utilizing constant current control along with laser temperature regulation. Placed in front of this laser will be a line filter to isolate the 642 nm light from erroneous laser diode emission. The laser will be hard-mounted into the instrument at the appropriate launch angle to give maximum penetration depth of the evanescent field. The fluorescence collected by the microlens array will be coupled into a series of multi-mode fiber optics (core diameter ~125 μm) with their terminal end sealed directly to a series of SPADs used to transduce fluorescence photons generated from each fluidic via. The fluorescence is isolated from scattering and other background sources using interference band pass and long pass filters that are in-line with respect to the off-module fiber optics. The fluidic bio-processor will be situated within a mounting frame so that insertion of the bio-processor into the instrument will align the laser and fiber optics to this module. To test this module as a stand-alone unit once fabricated, we can monitor molecular beacons formed from

off-chip LDRs of mRNAs that have been reverse transcribed into cDNAs. The dyes that can be used are Alexa Fluor 647 as the donor and Alexa Fluor 680 as the acceptor due to their similarities in excitation and emission profiles compared to Cy5 and Cy5.5, which we have shown to work favorably for spFRET.[26] However, these dyes tend to be more photostable providing higher photon yields per molecule.[44] Another consideration for dye selection is the absorption spectrum. If we change our dye selection to the Cy5-Cy7 FRET pair then the greater spectral distance between the two dyes could lower the background noise. This is due to the fact that currently the Cy5.5 is minimally excited at the laser wavelength. Increasing the primer concentration to drive low target concentration reaction could lead to increase in the noise and false positive counts. The FRET pair Cy5-Cy7 would have a lower spectral overlap and reduced FRET efficiency ($R_0$), however the $J(\lambda)$ depends on the sixth-root. Lakowicz gave the example of a "120 fold change in the overlap integral results in a 2.2 fold change in the Foster distance." This would indicate that minimal change in the Foster distance would result from the Cy5-Cy7 FRET pair change.

## 6.13 Final Conclusions

The ability to simultaneously track and detect flowing single molecules in multiple microfluidic channels by employing a CCD camera operated in a TDI mode was a major advancement in high sample throughput analysis. The TDI mode was shown to offer some attractive characteristics in terms of single molecule readout which included a DC near 100% and favorable SNR for single molecule detection. In addition, the imaging capacity of the CCD can offer some unique opportunities in terms of ST. For microchannels geometrically configured in a diffraction limited architecture, the system could effectively image ~670 channels, providing a single molecule ST of $>10^7$ molecules $s^{-1}$.

To realize improvements in our multichannel SMD format, we fabricated and evaluated a novel COC planar waveguide embedded into a PMMA cover plate that was situated orthogonal to multiple fluidic channels. The resulting fluorescence in the channels via evanescent excitation was important in the goal of providing improvements in the SNR for single-fluorophore detection. The geometry employed for this COC waveguide and the fluidic network was configured to allow matching the excitation area with the dimensions of the collection optics and array detector. The design allowed for fluorescence detection from the multiple fluidic channels using evanescent excitation and a CCD camera for parallel readout. The use of a monolithic prism allowed for precise control of the laser launch angle into the waveguide providing sampling via the evanescent field. The launch angle was found to play a critical role in achieving high sampling efficiency by maximizing the penetration depth of the evanescent field into the adjoining solution. While the sampling efficiency is rather modest in the present case (100% x 0.87 / 30 ~ 3%), this can be improved further by matching the fluidic channel depth to the depth of penetration of the evanescent field. The current format allowed the monitoring of fluorescence produces from 11 fluidic channels with future work designed to achieve higher channel density for increased ST.

To enhance the applications and usefulness of SMD, we designed, built and demonstrated the ability to detect single-molecule events using a compact field-deployable instrument with minimal end user alignment. This goal was accomplished by incorporating the fiber optics into the microfluidic device, which opens the possibility for less technically qualified operators to manage such a device. The integration of fiber optics into the microfluidic chip as waveguides/excitation and collection optics removes the normally bulky optics of traditional SMD setups. The implementation of FPGA allowed the reduction of size of the operational

circuit boards, which created a reduction in the overall size of the instrument. The initial work focused on the detection of SMD in a compact instrument, which would offer decreased analysis time by eliminating processing steps such as PCR, which makes it ideal for to monitor biomarkers in near-real time. The transit times for the fluorescent spheres and Alexa Fluor dye were determined to be 49 ms for the spheres and 53 ms which show close agreement with the theoretical transit times. As a demonstration of the possible application of this instrument for rapid analysis; molecular beacons were designed to probe bacterial cells for the gene encoding Gram +. The MB's were shown to be detectable for as little as 2,000 cells in a 1 min data collection run.

The follow up work to the compact SMD is the implementation of the ligase detection reaction with single-pair FRET. This system combined with this assay will have a number of important applications, such as strain-specific detection of pathogenic bacteria or molecular diagnosis of diseases requiring rapid turn-around-times at the point-of-care. The current road blocks involve the continuous flow reaction on the microchip. Bulk LDR was demonstrated by Hashimoto *et al.* and infer that optimization of the reaction condition is the major obstacle. A more systematic approach would decrease experiential time and lead to positive results. Absorption of dilute concentration of the primer and/or target to the channel wall is a prime suspect for the decreased reaction efficiency. A typical strategy is to add bovine serum albumin to the reaction buffer to prevent the nonspecific absorption to the channel walls. Furthermore, to minimize absorption effects and drive the reaction to higher efficiencies for the formation and detection of rMB the optimal primer to target mixture should be determined. The higher the primer concentration the more efficient the reaction should progress. However, at high primer concentration the fluorophore on the primers can leak past the filter set and increase the

background. It's therefore advised that a FRET pair that is further spectrally separated be used such as Cy5-Cy7. This would only see a small drop in FRET efficiencies but should allow for higher primer concentration due to better optical filtering. The ideal goal is to find the highest primer concentration that the rMB can still be detected with a SNR of 3. With this concentration a series of different target concentration can be run to determine the rMB yield. Furthermore experiments can be run at different number of thermal cycle to optimized speed or input concentration.

The work of combining the compact SMD instrument with the knowledge and insight gained by the multichannel SMD and waveguide fabrication to detect a biomarkers panel for Strokes is the future direction of this work. Great strides have been accomplished to realize the goal of delivering a viable molecular diagnostic test for stroke directly in the field. Realization of many of the ideas conveyed in the preceding chapter will assist in delivering the first molecular diagnostic for stroke with POC capabilities. Testing of the modular microfluidic system needs to focus on streamlining the chemical processing steps to provide rapid, but yet, accurate results. To shorten the development time and reduce the fabrication iterations, one could employ system-level simulations (in collaboration with the Mechanical Engineering Department; Dr. Dimitris E. Nikitopoulos) to guide the design of the modular biofluidic processor. These simulations should provide the ability to optimize heat/mass transfer, fluid flow, material mismatches, and alignment issues between and within modules as well as assembly. The different molecular processing steps: (1) red blood cell clearance; (2) white blood cell lysis; (3) mRNA purification; (4) reverse transcription; and (5) thermally cycled ligase detection reaction (LDR) should be first tested in bulk with off chip detection to insure proper operation and then, transitioned into a single channel, single-molecule readout mode using microfluidics. At the same time, the optical

elements (waveguide and multiple SPADs or a SPAD array) need to be tested to ensure high response to the rMBs formed by LDR. Once the multichannel SMD and the modular biofluidic processor have been optimized, they can be combined in order to evaluate the expression levels of stroke-related genes.

## 6.14 References


1. Rosamond, W.; Flegal, K.; Furie, K.; Go, A.; Greenlund, K.; Haase, N.; Hailpern, S. M.; Ho, M.; Howard, V.; Kissela, B.; Kittner, S.; Lloyd-Jones, D.; McDermott, M.; Meigs, J.; Moy, C.; Nichol, G.; O'Donnell, C.; Roger, V.; Sorlie, P.; Steinberger, J.; Thom, T.; Wilson, M.; Hong, Y.; Amer Heart Assoc Stat Comm, S., Heart Disease and Stroke Statistics - 2008 Update - a Report from the American Heart Association Statistics Committee and Stroke Statistics Subcommittee. *Circulation* **2008,** *117* (4), E25-E146.

2. Hand, P. J.; Kwan, J.; Lindley, R. I.; Dennis, M. S.; Wardlaw, J. M., Distinguishing between Stroke and Mimic at the Bedside - the Brain Attack Study. *Stroke* **2006,** *37* (3), 769-775.

3. Furlan, A.; Higashida, R.; Wechsler, L.; Gent, M.; Rowley, H.; Kase, C.; Pessin, M.; Ahuja, A.; Callahan, F.; Clark, W. M.; Silver, F.; Rivera, F.; Investigators, P., Intra-Arterial Prourokinase for Acute Ischemic Stroke - the Proact Ii Study: A Randomized Controlled Trial. *Jama-Journal of the American Medical Association* **1999,** *282* (21), 2003-2011.

4. Hacke, W.; Kaste, M.; Toni, D., Thrombolysis 3 to 4.5 Hours after Acute Ischemic Stroke Reply. *N Engl J Med* **2008,** *359* (26), 2841-2841.

5. Marler, J. R.; Brott, T.; Broderick, J.; Kothari, R.; Odonoghue, M.; Barsan, W.; Tomsick, T.; Spilker, J.; Miller, R.; Sauerbeck, L.; Jarrell, J.; Kelly, J.; Perkins, T.; McDonald, T.; Rorick, M.; Hickey, C.; Armitage, J.; Perry, C.; Thalinger, K.; Rhude, R.; Schill, J.; Becker, P. S.; Heath, R. S.; Adams, D.; Reed, R.; Klei, M.; Hughes, S.; Anthony, J.; Baudendistel, D.; Zadicoff, C.; Rymer, M.; Bettinger, I.; Laubinger, P.; Schmerler, M.; Meirose, G.; Lyden, P.; Rapp, K.; Babcock, T.; Daum, P.; Persona, D.; Brody, M.; Jackson, C.; Lewis, S.; Liss, J.; Mahdavi, Z.; Rothrock, J.; Tom, T.; Zweifler, R.; Dunford, J.; Zivin, J.; Kobayashi, R.; Kunin, J.; Licht, J.; Rowen, R.; Stein, D.; Grisolia, J.; Martin, F.; Chaplin, E.; Kaplitz, N.; Nelson, J.; Neuren, A.; Silver, D.; Chippendale, T.; Diamond, E.; Lobatz, M.; Murphy, D.; Rosenberg, D.; Ruel, T.; Sadoff, M.; Schim, J.; Schleimer, J.; Atkinson, R.; Wentworth, D.; Cummings, R.; Frink, R.; Heublein, P.; Grotta, J. C.; Degraba, T.; Fisher, M.; Ramirez, A.; Hanson, S.; Morgenstern, L.; Sills, C.; Pasteur, W.; Yatsu, F.; Andrews, K.; Villarcordova, C.; Pepe, P.; Bratina, P.; Greenberg, L.; Rozek, S.; Simmons, K.; Kwiatkowski, T. G.; Horowitz, S. H.; Libman, R.; Kanner, R.; Silverman, R.; Lamantia, J.; Mealie, C.; Duarte, R.; Donnarumma, R.; Okola, M.; Cullin, V.; Mitchell, E.; Levine, S. R.; Lewandowski, C. A.; Tokarski, G.; Ramadan, N. M.; Mitsias, P.; Gorman, M.; Zarowitz, B.; Kokkinos, J.; Dayno, J.; Verro,

P.; Gymnopoulos, C.; Dafer, R.; Dolhaberriague, L.; Sawaya, K.; Daley, S.; Mitchell, M.; Frankel, M.; Mackay, B.; Barch, C.; Braimah, J.; Faherty, B.; Macdonald, J.; Sailor, S.; Cook, A.; Karp, H.; Nguyen, B.; Washington, J.; Weissman, J.; Williams, M.; Williamson, T.; Kozinn, M.; Hellwick, L.; Haley, E. C.; Bleck, T. P.; Cail, W. S.; Lindbeck, G. H.; Granner, M. A.; Wolf, S. S.; Gwynn, M. W.; Mettetal, R. W.; Chang, C. W. J.; Solenski, N. J.; Brock, D. G.; Ford, G. F.; Kongable, G. L.; Parks, K. N.; Wilkinson, S. S.; Davis, M. K.; Sheppard, G. L.; Zontine, D. W.; Gustin, K. H.; Crowe, N. M.; Massey, S. L.; Meyer, M.; Gaines, K.; Payne, A.; Bales, C.; Malcolm, J.; Barlow, R.; Wilson, M.; Cape, C.; Bertorini, T.; Misulis, K.; Paulsen, W.; Shepard, D.; Tilley, B. C.; Welch, K. M. A.; Fagan, S. C.; Lu, M.; Patel, S.; Masha, E.; Verter, J.; Boura, J.; Main, J.; Gordon, L.; Maddy, N.; Chociemski, T.; Windham, J.; Zadeh, H. S.; Alves, W.; Keller, M. F.; Wenzel, J. R.; Raman, N.; Cantwell, L.; Warren, A.; Smith, K.; Bailey, E.; Froehlich, J.; Breed, J.; Easton, J. D.; Hallenbeck, J. F.; Lan, G.; Marsh, J. D.; Walker, M. D., Tissue-Plasminogen Activator for Acute Ischemic Stroke. *N Engl J Med* **1995,** *333* (24), 1581-1587.

6. Wahlgren, N.; Ahmed, N.; Davalos, A.; Hacke, W.; Millan, M.; Muir, K.; Roine, R. O.; Toni, D.; Lees, K. R.; Investigators, S., Thrombolysis with Alteplase 3-4 Center Dot 5 H after Acute Ischaemic Stroke (Sits-Istr): An Observational Study. *Lancet* **2008,** *372* (9646), 1303-1309.

7. Marler, J. R.; Tilley, B. C.; Lu, M.; Brott, T. G.; Lyden, P. C.; Grotta, J. C.; Broderick, J. P.; Levine, S. R.; Frankel, M. P.; Horowitz, S. H.; Haley, E. C.; Lewandowski, C. A.; Kwiatkowski, T. P.; Grp, N. r.-P. S. S., Early Stroke Treatment Associated with Better Outcome - the Ninds Rt-Pa Stroke Study. *Neurology* **2000,** *55* (11), 1649-1655.

8. Goldstein, L. B., Improving the Clinical Diagnosis of Stroke. *Stroke* **2006,** *37* (3), 754-755.

9. Goldstein, L. B.; Simel, D. L., Is This Patient Having a Stroke? *Jama-Journal of the American Medical Association* **2005,** *293* (19), 2391-2402.

10. Norris, J. W.; Hachinski, V. C., Mis-Diagnosis of Stroke. *Lancet* **1982,** *1* (8267), 328-331.

11. Witek, M. A.; Hupert, M. L.; Park, D. S. W.; Fears, K.; Murphy, M. C.; Soper, S. A., 96-Well Polycarbonate-Based Microfluidic Titer Plate for High-Throughput Purification of DNA and Rna. *Anal Chem* **2008,** *80* (9), 3483-3491.

12. Whiteley, W.; Tseng, M. C.; Sandercock, P., Biomarkers in the Diagnosis of Ischemic Stroke - a Systematic Review. *Stroke* **2008,** *39* (10), 2902-2909.

13. Schroeter, M.; Jander, S.; Witte, O. W.; Stoll, G., Local Immune-Responses in the Rat Cerebral-Cortex after Middle Cerebral-Artery Occlusion. *J Neuroimmunol* **1994,** *55* (2), 195-203.

14. Alvord, E. C.; Hsu, P. C.; Thron, R., Leukocyte Sensitivity to Brain Fractions in Neurological Diseases. *Archives of Neurology* **1974,** *30* (4), 296-299.

15. Becker, K.; Kindrick, D.; McCarron, R.; Hallenbeck, J.; Winn, R., Adoptive Transfer of Myelin Basic Protein-Tolerized Splenocytes to Naive Animals Reduces Infarct Size - a Role for Lymphocytes in Ischemic Brain Injury? *Stroke* **2003,** *34* (7), 1809-1815.

16. Youngchaiyud, U.; Coates, A. S.; Whittingham, S.; Mackay, I. R., Cellular Immune Response to Myelin Protein - Absence in Multiple-Sclerosis and Presence in Cerebrovascular Accidents. *Australian and New Zealand Journal of Medicine* **1974,** *4* (6), 535-538.

17. Tang, Y.; Lu, A. G.; Aronow, B. J.; Sharp, F. R., Blood Genomic Responses Differ after Stroke, Seizures, Hypoglycemia, and Hypoxia: Blood Genomic Fingerprints of Disease. *Annals of Neurology* **2001,** *50* (6), 699-707.

18. Reynolds, M. A.; Kirchick, H. J.; Dahlen, J. R.; Anderberg, J. M.; McPherson, P. H.; Nakamura, K. K.; Laskowitz, D. T.; Valkirs, G. E.; Buechler, K. F., Early Biomarkers of Stroke. *Clinical Chemistry* **2003,** *49* (10), 1733-1739.

19. Laskowitz, D. T.; Kasner, S. E.; Saver, J.; Remmel, K. S.; Jauch, E. C.; Grp, B. S., Clinical Usefulness of a Biomarker-Based Diagnostic Test for Acute Stroke the Biomarker Rapid Assessment in Ischemic Injury (Brain) Study. *Stroke* **2009,** *40* (1), 77-85.

20. Gell, C.; Sabir, T.; Westwood, J.; Rashid, A.; Smith, D. A. M.; Harris, S. A.; Stockley, P. G., Single-Molecule Fluorescence Resonance Energy Transfer Assays Reveal Heterogeneous Folding Ensembles in a Simple Rna Stem-Loop. *J Mol Biol* **2008,** *384* (1), 264-278.

21. Haupts, U.; Rudiger, M.; Ashman, S.; Turconi, S.; Bingham, R.; Wharton, C.; Hutchinson, J.; Carey, C.; Moore, K. J.; Pope, A. J., Single-Molecule Detection Technologies in Miniaturized High-Throughput Screening: Fluorescence Intensity Distribution Analysis. *Journal of Biomolecular Screening* **2003,** *8* (1), 19-33.

22. Hintersteiner, M.; Auer, M., Single-Bead, Single-Molecule, Single-Cell Fluorescence - Technologies for Drug Screening and Target Validation. In *Fluorescence Methods and Applications: Spectroscopy, Imaging, and Probes*, Wolfbeis, O. S., Ed. 2008; Vol. 1130, pp 1-11.

23. Kang, S. H.; Kim, Y. J.; Yeung, E. S., Detection of Single-Molecule DNA Hybridization by Using Dual-Color Total Internal Reflection Fluorescence Microscopy. *Anal Bioanal Chem* **2007,** *387* (8), 2663-2671.

24. Neely, L. A.; Patel, S.; Garver, J.; Gallo, M.; Hackett, M.; McLaughlin, S.; Nadel, M.; Harris, J.; Gullans, S.; Rooke, J., A Single-Molecule Method for the Quantitation of Microrna Gene Expression. *Nat Methods* **2006,** *3* (1), 41-46.

25. Qiu, H.; Ferrell, E. P.; Nolan, N.; Phelps, B. H.; Tabibiazar, R.; Whitney, D. H.; Nalefski, E. A., Fluorescence Single-Molecule Counting Assays for High-Sensitivity Detection of Cytokines and Chemokines. *Clinical Chemistry* **2007,** *53* (11), 2010-2012.

26. Wabuyele, M. B.; Farquar, H.; Stryjewski, W.; Hammer, R. P.; Soper, S. A.; Cheng, Y. W.; Barany, F., Approaching Real-Time Molecular Diagnostics: Single-Pair Fluorescence Resonance Energy Transfer (Spfret) Detection for the Analysis of Low Abundant Point Mutations in K-Ras Oncogenes. *J Am Chem Soc* **2003,** *125* (23), 6937-6945.

27. Wang, L.; Xu, G.; Shia, Z. K.; Jiang, W.; Jin, W. R., Quantification of Protein Based on Single-Molecule Counting by Total Internal Reflection Fluorescence Microscopy with Adsorption Equilibrium. *Anal Chim Acta* **2007,** *590* (1), 104-109.

28. Wu, A. H. B.; Fukushima, N.; Puskas, R.; Todd, J.; Goix, P., Development and Preliminary Clinical Validation of a High Sensitivity Assay for Cardiac Troponin Using a Capillary Flow (Single Molecule) Fluorescence Detector. *Clinical Chemistry* **2006,** *52* (11), 2157-2159.

29. Shera, E. B.; Seitzinger, N. K.; Davis, L. M.; Keller, R. A.; Soper, S. A., Detection of Single Fluorescent Molecules. *Chem Phys Lett* **1990,** *174* (6), 553-557.

30. Soper, S. A.; Shera, E. B.; Martin, J. C.; Jett, J. H.; Hahn, J. H.; Nutter, H. L.; Keller, R. A., Single-Molecule Detection of Rhodamine-6g in Ethanolic Solutions Using Continuous Wave Laser Excitation. *Anal Chem* **1991,** *63* (5), 432-437.

31. Emory, J. M.; Soper, S. A., Charge-Coupled Device Operated in a Time-Delayed Integration Mode as an Approach to High-Throughput Flow-Based Single Molecule Analysis. *Anal Chem* **2008,** *80* (10), 3897-3903.

32. Okagbare, P. I.; Soper, S. A., High Throughput Single Molecule Detection for Monitoring Biochemical Reactions. *Analyst* **2009,** *134* (1), 97-106.

33. Camacho, A.; Korn, K.; Damond, M.; Cajot, J. F.; Litborn, E.; Liao, B. H.; Thyberg, P.; Winter, H.; Honegger, A.; Gardellin, P.; Rigler, R., Direct Quantification of Mrna Expression Levels Using Single Molecule Detection. *J Biotechnol* **2004,** *107* (2), 107-114.

34. Adams, A. A.; Okagbare, P. I.; Feng, J.; Hupert, M. L.; Patterson, D.; Gottert, J.; McCarley, R. L.; Nikitopoulos, D.; Murphy, M. C.; Soper, S. A., Highly Efficient Circulating Tumor Cell Isolation from Whole Blood and Label-Free Enumeration Using Polymer-Based Microfluidics with an Integrated Conductivity Sensor. *J Am Chem Soc* **2008,** *130* (27), 8633-8641.

35. Hashimoto, M.; Hupert, M. L.; Murphy, M. C.; Soper, S. A.; Cheng, Y. W.; Barany, F., Ligase Detection Reaction/Hybridization Assays Using Three-Dimensional Microfluidic Networks for the Detection of Low-Abundant DNA Point Mutations. *Anal Chem* **2005,** *77* (10), 3243-3255.

36. Witek, M. A.; Llopis, S. D.; Wheatley, A.; McCarley, R. L.; Soper, S. A., Purification and Preconcentration of Genomic DNA from Whole Cell Lysates Using Photoactivated Polycarbonate (Ppc) Microfluidic Chips. *Nucleic Acids Res* **2006,** *34* (10).

37. Xu, F.; Datta, P.; Wang, H.; Gurung, S.; Hashimoto, M.; Wei, S.; Goettert, J.; McCarley, R. L.; Soper, S. A., Polymer Microfluidic Chips with Integrated Waveguides for Reading Microarrays. *Anal Chem* **2007,** *79* (23), 9007-9013.

38. Kim, D. S.; Yang, S. S.; Lee, S. K.; Kwon, T. H.; Lee, S. S., Physical Modeling and Analysis of Microlens Formation Fabricated by a Modified Liga Process. *Journal of Micromechanics and Microengineering* **2003,** *13* (5), 523-531.

39. Lee, B. K.; Kim, D. S.; Kwon, T. H., Replication of Microlens Arrays by Injection Molding. *Microsystem Technologies-Micro-and Nanosystems-Information Storage and Processing Systems* **2004,** *10* (6-7), 531-535.

40. Lee, S. K.; Lee, K. C.; Lee, S. S., A Simple Method for Microlens Fabrication by the Modified Liga Process. *Journal of Micromechanics and Microengineering* **2002,** *12* (3), 334-340.

41. Ford, S. M.; Davies, J.; Kar, B.; Qi, S. D.; McWhorter, S.; Soper, S. A.; Malek, C. K., Micromachining in Plastics Using X-Ray Lithography for the Fabrication of Micro-Electrophoresis Devices. *Journal of Biomechanical Engineering-Transactions of the Asme* **1999,** *121* (1), 13-21.

42. Park, D. S. W.; Hupert, M. L.; Witek, M. A.; You, B. H.; Datta, P.; Guy, J.; Lee, J. B.; Soper, S. A.; Nikitopoulos, D. E.; Murphy, M. C., A Titer Plate-Based Polymer Microfluidic Platform for High Throughput Nucleic Acid Purification. *Biomedical Microdevices* **2008,** *10* (1), 21-33.

43. Soper, S. A.; Ford, S. M.; Qi, S.; McCarley, R. L.; Kelly, K.; Murphy, M. C., Polymeric Microelectromechanical Systems. *Anal Chem* **2000,** *72* (19), 642A-651A.

44. Berlier, J. E.; Rothe, A.; Buller, G.; Bradford, J.; Gray, D. R.; Filanoski, B. J.; Telford, W. G.; Yue, S.; Liu, J. X.; Cheung, C. Y.; Chang, W.; Hirsch, J. D.; Beechem, J. M.; Haugland, R. P., Quantitative Comparison of Long-Wavelength Alexa Fluor Dyes to Cy Dyes: Fluorescence of the Dyes and Their Bioconjugates. *J Histochem Cytochem* **2003,** *51* (12), 1699-1712.

# Appendix: Permissions

AMERICAN CHEMICAL SOCIETY LICENSE
TERMS AND CONDITIONS

Sep 29, 2009

---

This is a License Agreement between Jason Emory ("You") and American Chemical Society ("American Chemical Society") provided by Copyright Clearance Center ("CCC"). The license consists of your order details, the terms and conditions provided by American Chemical Society, and the payment terms and conditions.

All payments must be made in full to CCC. For payment instructions, please see information listed at the bottom of this form.

| | |
|---|---|
| License Number | 2270931328052 |
| License Date | Sep 16, 2009 |
| Licensed content publisher | American Chemical Society |
| Licensed content publication | Analytical Chemistry |
| Licensed content title | Single-Molecule Detection of Specific Nucleic Acid Sequences in Unamplified Genomic DNA |
| Licensed content author | Alonso Castro et al. |
| Licensed content date | Oct 1, 1997 |
| Volume number | 69 |
| Issue number | 19 |
| Type of Use | Thesis/Dissertation |
| Requestor type | Not specified |
| Format | Print and Electronic |
| Portion | Table/Figure/Chart |
| Number of Table/Figure/Charts | 1 |
| Author of this ACS article | No |
| Order reference number | |
| Title of the thesis / dissertation | Single-Molecule Detection of Unique Genome Signatures: Applications in Molecular Diagnostics and Homeland Security |

| | |
|---|---|
| Expected completion date | Dec 2009 |
| Estimated size(pages) | 200 |
| Billing Type | Invoice |
| Billing Address | 2033 Maple Ridge Ave |
| | Baton Rouge, LA 70816 |
| | United States |
| Customer reference info | |
| Total | 0.00 USD |

AMERICAN CHEMICAL SOCIETY LICENSE
TERMS AND CONDITIONS

Sep 29, 2009

---

---

This is a License Agreement between Jason Emory ("You") and American Chemical Society ("American Chemical Society") provided by Copyright Clearance Center ("CCC"). The license consists of your order details, the terms and conditions provided by American Chemical Society, and the payment terms and conditions.

All payments must be made in full to CCC. For payment instructions, please see information listed at the bottom of this form.

| | |
|---|---|
| License Number | 2270930938268 |
| License Date | Sep 16, 2009 |
| Licensed content publisher | American Chemical Society |
| Licensed content publication | Journal of the American Chemical Society |
| Licensed content title | Approaching Real-Time Molecular Diagnostics: Single-Pair Fluorescence Resonance Energy Transfer (spFRET) Detection for the Analysis of Low Abundant Point Mutations in K-ras Oncogenes |
| Licensed content author | Musundi B. Wabuyele et al. |
| Licensed content date | Jun 1, 2003 |
| Volume number | 125 |
| Issue number | 23 |
| Type of Use | Thesis/Dissertation |
| Requestor type | Not specified |
| Format | Print and Electronic |
| Portion | Table/Figure/Chart |
| Number of Table/Figure/Charts | 1 |
| Author of this ACS article | No |
| Order reference number | |
| Title of the thesis / dissertation | Single-Molecule Detection of Unique Genome Signatures: Applications in Molecular Diagnostics and Homeland Security |

| | |
|---|---|
| Expected completion date | Dec 2009 |
| Estimated size(pages) | 200 |
| Billing Type | Invoice |
| Billing Address | 2033 Maple Ridge Ave<br><br>Baton Rouge, LA 70816<br>United States |
| Customer reference info | |
| Total | 0.00 USD |

ACS / RIGHTSLINK TERMS & CONDITIONS
THESIS/DISSERTATION

INTRODUCTION
The publisher for this copyrighted material is the American Chemical Society. By clicking "accept" in connection with completing this licensing transaction, you agree that the following terms and conditions apply to this transaction (along with the Billing and Payment terms and conditions established by Copyright Clearance Center, Inc. ("CCC"), at the time that you opened your Rightslink account and that are available at any time at <http://myaccount.copyright.com>).

LIMITED LICENSE
Publisher hereby grants to you a non-exclusive license to use this material. Licenses are for one-time use only with a maximum distribution equal to the number that you identified in the licensing process; any form of republication must be completed within 60 days from the date hereof (although copies prepared before then may be distributed thereafter).

GEOGRAPHIC RIGHTS: SCOPE
Licenses may be exercised anywhere in the world.

RESERVATION OF RIGHTS
Publisher reserves all rights not specifically granted in the combination of (i) the license details provided by you and accepted in the course of this licensing transaction, (ii) these terms and conditions and (iii) CCC's Billing and Payment terms and conditions.

PORTION RIGHTS STATEMENT: DISCLAIMER
If you seek to reuse a portion from an ACS publication, it is your responsibility to examine each portion as published to determine whether a credit to, or copyright notice of, a third party owner was published adjacent to the item. You may only obtain permission via Rightslink to use material owned by ACS. Permission to use any material published in an ACS publication, journal, or article which is reprinted with permission of a third party must be obtained from the third party owner. ACS disclaims any responsibility for any use you

make of items owned by third parties without their permission.

REVOCATION
The American Chemical Society reserves the right to revoke a license for any reason, including but not limited to advertising and promotional uses of ACS content, third party usage, and incorrect figure source attribution.

LICENSE CONTINGENT ON PAYMENT
While you may exercise the rights licensed immediately upon issuance of the license at the end of the licensing process for the transaction, provided that you have disclosed complete and accurate details of your proposed use, no license is finally effective unless and until full payment is received from you (by CCC) as provided in CCC's Billing and Payment terms and conditions. If full payment is not received on a timely basis, then any license preliminarily granted shall be deemed automatically revoked and shall be void as if never granted. Further, in the event that you breach any of these terms and conditions or any of CCC's Billing and Payment terms and conditions, the license is automatically revoked and shall be void as if never granted. Use of materials as described in a revoked license, as well as any use of the materials beyond the scope of an unrevoked license, may constitute copyright infringement and publisher reserves the right to take any and all action to protect its copyright in the materials.

COPYRIGHT NOTICE: DISCLAIMER
You must include the following copyright and permission notice in connection with any reproduction of the licensed material: "Reprinted (“Adapted” or “in part”) with permission from REFERENCE CITATION. Copyright YEAR American Chemical Society."

WARRANTIES: NONE
Publisher makes no representations or warranties with respect to the licensed material.

INDEMNITY
You hereby indemnify and agree to hold harmless publisher and CCC, and their respective officers, directors, employees and agents, from and against any and all claims arising out of your use of the licensed material other than as specifically authorized pursuant to this license.

NO TRANSFER OF LICENSE
This license is personal to you or your publisher and may not be sublicensed, assigned, or transferred by you to any other person without publisher's written permission.

NO AMENDMENT EXCEPT IN WRITING
This license may not be amended except in a writing signed by both parties (or, in the case of publisher, by CCC on publisher's behalf).

OBJECTION TO CONTRARY TERMS
Publisher hereby objects to any terms contained in any purchase order, acknowledgment, check endorsement or other writing prepared by you, which terms are inconsistent with these

terms and conditions or CCC's Billing and Payment terms and conditions. These terms and conditions, together with CCC's Billing and Payment terms and conditions (which are incorporated herein), comprise the entire agreement between you and publisher (and CCC) concerning this licensing transaction. In the event of any conflict between your obligations established by these terms and conditions and those established by CCC's Billing and Payment terms and conditions, these terms and conditions shall control.

JURISDICTION
This license transaction shall be governed by and construed in accordance with the laws of the District of Columbia. You hereby agree to submit to the jurisdiction of the courts located in the District of Columbia for purposes of resolving any disputes that may arise in connection with this licensing transaction.

THESES/DISSERTATION TERMS
Publishing implications of electronic publication of theses and dissertation material
Students and their mentors should be aware that posting of theses and dissertation material on the Web prior to submission of material from that thesis or dissertation to an ACS journal may affect publication in that journal. Whether Web posting is considered prior publication may be evaluated on a case-by-case basis by the journal's editor. If an ACS journal editor considers Web posting to be "prior publication", the paper will not be accepted for publication in that journal. If you intend to submit your unpublished paper to ACS for publication, check with the appropriate editor prior to posting your manuscript electronically.

If your paper has already been published by ACS and you want to include the text or portions of the text in your thesis/dissertation in print or microfilm formats, please print the ACS copyright credit line on the first page of your article: "Reproduced (or 'Reproduced in part') with permission from [FULL REFERENCE CITATION.] Copyright [YEAR] American Chemical Society." Include appropriate information.

Submission to a Dissertation Distributor: If you plan to submit your thesis to UMI or to another dissertation distributor, you should not include the unpublished ACS paper in your thesis if the thesis will be disseminated electronically, until ACS has published your paper. After publication of the paper by ACS, you may release the entire thesis (not the individual ACS article by itself) for electronic dissemination through the distributor; ACS's copyright credit line should be printed on the first page of the ACS paper.

Use on an Intranet: The inclusion of your ACS unpublished or published manuscript is permitted in your thesis in print and microfilm formats. If ACS has published your paper you may include the manuscript in your thesis on an intranet that is not publicly available. Your ACS article cannot be posted electronically on a publicly available medium (i.e. one that is not password protected), such as but not limited to, electronic archives, Internet, library server, etc. The only material from your paper that can be posted on a public electronic medium is the article abstract, figures, and tables, and you may link to the article's DOI or post the article's author-directed URL link provided by ACS. This paragraph does

not pertain to the dissertation distributor paragraph above.

Other conditions:

v1.1

Gratis licenses (referencing $0 in the Total field) are free. Please retain this printable license for your reference. No payment is required.

If you would like to pay for this license now, please remit this license along with your payment made payable to "COPYRIGHT CLEARANCE CENTER" otherwise you will be invoiced within 30 days of the license date. Payment should be in the form of a check or money order referencing your account number and this license number 2270931328052. If you would prefer to pay for this license by credit card, please go to http://www.copyright.com/creditcard to download our credit card payment authorization form.

Make Payment To:
Copyright Clearance Center
Dept 001
P.O. Box 843006
Boston, MA 02284-3006

If you find copyrighted material related to this license will not be used and wish to cancel, please contact us referencing this license number 2270931328052 and noting the reason for cancellation.

Questions? customercare@copyright.com or +1-877-622-5543 (toll free in the US) or +1-978-646-2777.

NATURE PUBLISHING GROUP LICENSE
TERMS AND CONDITIONS

Sep 29, 2009

---

---

This is a License Agreement between Jason Emory ("You") and Nature Publishing Group ("Nature Publishing Group") provided by Copyright Clearance Center ("CCC"). The license consists of your order details, the terms and conditions provided by Nature Publishing Group, and the payment terms and conditions.

All payments must be made in full to CCC. For payment instructions, please see information listed at the bottom of this form.

| | |
|---|---|
| License Number | 2270951311274 |
| License date | Sep 16, 2009 |
| Licensed content publisher | Nature Publishing Group |
| Licensed content publication | Nature Genetics |
| Licensed content title | Mutation detection and single-molecule counting using isothermal rolling-circle amplification |
| Licensed content author | Paul M. Lizardi, Xiaohua Huang, Zhengrong Zhu, Patricia Bray-Ward, David C. Thomas, David C. Ward |
| Volume number | |
| Issue number | |
| Pages | |
| Year of publication | 1998 |
| Portion used | Figures / tables |
| Requestor type | Student |
| Type of Use | Thesis / Dissertation |
| Billing Type | Invoice |
| Company | Jason Emory |
| Billing Address | 2033 Maple Ridge Ave<br><br>Baton Rouge, LA 70816<br>United States |

Customer reference info

| | |
|---|---|
| Total | 0.00 USD |

NATURE PUBLISHING GROUP LICENSE
TERMS AND CONDITIONS

Sep 29, 2009

---

---

This is a License Agreement between Jason Emory ("You") and Nature Publishing Group ("Nature Publishing Group") provided by Copyright Clearance Center ("CCC"). The license consists of your order details, the terms and conditions provided by Nature Publishing Group, and the payment terms and conditions.

All payments must be made in full to CCC. For payment instructions, please see information listed at the bottom of this form.

| | |
|---|---|
| License Number | 2270951177101 |
| License date | Sep 16, 2009 |
| Licensed content publisher | Nature Publishing Group |
| Licensed content publication | Nature Materials |
| Licensed content title | Single-quantum-dot-based DNA nanosensor |
| Licensed content author | Chun-Yang Zhang , Hsin-Chih Yeh , Marcos T. Kuroki and Tza-Huei Wang |
| Volume number | |
| Issue number | |
| Pages | |
| Year of publication | 2005 |
| Portion used | Figures / tables |
| Requestor type | Student |
| Type of Use | Thesis / Dissertation |
| Billing Type | Invoice |
| Company | Jason Emory |
| Billing Address | 2033 Maple Ridge Ave<br><br>Baton Rouge, LA 70816<br>United States |
| Customer reference info | |

| | |
|---|---|
| Total | 0.00 USD |

NATURE PUBLISHING GROUP LICENSE
TERMS AND CONDITIONS

Sep 29, 2009

---

---

This is a License Agreement between Jason Emory ("You") and Nature Publishing Group ("Nature Publishing Group") provided by Copyright Clearance Center ("CCC"). The license consists of your order details, the terms and conditions provided by Nature Publishing Group, and the payment terms and conditions.

All payments must be made in full to CCC. For payment instructions, please see information listed at the bottom of this form.

| | |
|---|---|
| License Number | 2270950993584 |
| License date | Sep 16, 2009 |
| Licensed content publisher | Nature Publishing Group |
| Licensed content publication | Nature Methods |
| Licensed content title | Digital quantification using amplified single-molecule detection |
| Licensed content author | Jonas Jarvius, Jonas Melin, Jenny Göransson, Johan Stenberg, Simon Fredriksson, Carlos Gonzalez-Rey, Stefan Bertilsson, Mats Nilsson |
| Volume number | |
| Issue number | |
| Pages | |
| Year of publication | 2006 |
| Portion used | Figures / tables |
| Requestor type | Student |
| Type of Use | Thesis / Dissertation |
| Billing Type | Invoice |
| Company | Jason Emory |
| Billing Address | 2033 Maple Ridge Ave<br><br>Baton Rouge, LA 70816<br>United States |

Customer reference info

| | |
|---|---|
| Total | 0.00 USD |

NATURE PUBLISHING GROUP LICENSE
TERMS AND CONDITIONS

Sep 29, 2009

This is a License Agreement between Jason Emory ("You") and Nature Publishing Group ("Nature Publishing Group") provided by Copyright Clearance Center ("CCC"). The license consists of your order details, the terms and conditions provided by Nature Publishing Group, and the payment terms and conditions.

All payments must be made in full to CCC. For payment instructions, please see information listed at the bottom of this form.

| | |
|---|---|
| License Number | 2270950810286 |
| License date | Sep 16, 2009 |
| Licensed content publisher | Nature Publishing Group |
| Licensed content publication | Nature Biotechnology |
| Licensed content title | Molecular Beacons: Probes that Fluoresce upon Hybridization |
| Licensed content author | Sanjay Tyagi, Fred Russell Kramer |
| Volume number | |
| Issue number | |
| Pages | |
| Year of publication | 1996 |
| Portion used | Figures / tables |
| Requestor type | Student |
| Type of Use | Thesis / Dissertation |
| Billing Type | Invoice |
| Company | Jason Emory |
| Billing Address | 2033 Maple Ridge Ave<br><br>Baton Rouge, LA 70816<br>United States |
| Customer reference info | |

Total 0.00 USD

Terms and Conditions for Permissions

Nature Publishing Group hereby grants you a non-exclusive license to reproduce this material for this purpose, and for no other use, subject to the conditions below:

1. NPG warrants that it has, to the best of its knowledge, the rights to license reuse of this material. However, you should ensure that the material you are requesting is original to Nature Publishing Group and does not carry the copyright of another entity (as credited in the published version). If the credit line on any part of the material you have requested indicates that it was reprinted or adapted by NPG with permission from another source, then you should also seek permission from that source to reuse the material.

2. Permission granted free of charge for material in print is also usually granted for any electronic version of that work, provided that the material is incidental to the work as a whole and that the electronic version is essentially equivalent to, or substitutes for, the print version. Where print permission has been granted for a fee, separate permission must be obtained for any additional, electronic re-use (unless, as in the case of a full paper, this has already been accounted for during your initial request in the calculation of a print run). NB: In all cases, web-based use of full-text articles must be authorized separately through the 'Use on a Web Site' option when requesting permission.

3. Permission granted for a first edition does not apply to second and subsequent editions and for editions in other languages (except for signatories to the STM Permissions Guidelines, or where the first edition permission was granted for free).

4. Nature Publishing Group's permission must be acknowledged next to the figure, table or abstract in print. In electronic form, this acknowledgement must be visible at the same time as the figure/table/abstract, and must be hyperlinked to the journal's homepage.
5. The credit line should read:

   Reprinted by permission from Macmillan Publishers Ltd: [JOURNAL NAME] (reference citation), copyright (year of publication)

   For AOP papers, the credit line should read:

   Reprinted by permission from Macmillan Publishers Ltd: [JOURNAL NAME], advance online publication, day month year (doi: 10.1038/sj.[JOURNAL ACRONYM].XXXXX)

6. Adaptations of single figures do not require NPG approval. However, the adaptation should be credited as follows:

Adapted by permission from Macmillan Publishers Ltd: [JOURNAL NAME] (reference citation), copyright (year of publication)

7. Translations of 401 words up to a whole article require NPG approval. Please visit http://www.macmillanmedicalcommunications.com for more information. Translations of up to a 400 words do not require NPG approval. The translation should be credited as follows:

   Translated by permission from Macmillan Publishers Ltd: [JOURNAL NAME] (reference citation), copyright (year of publication).

We are certain that all parties will benefit from this agreement and wish you the best in the use of this material. Thank you.

v1.1

Gratis licenses (referencing $0 in the Total field) are free. Please retain this printable license for your reference. No payment is required.

If you would like to pay for this license now, please remit this license along with your payment made payable to "COPYRIGHT CLEARANCE CENTER" otherwise you will be invoiced within 30 days of the license date. Payment should be in the form of a check or money order referencing your account number and this license number 2270950810286. If you would prefer to pay for this license by credit card, please go to http://www.copyright.com/creditcard to download our credit card payment authorization form.

Make Payment To:
Copyright Clearance Center
Dept 001
P.O. Box 843006
Boston, MA 02284-3006

If you find copyrighted material related to this license will not be used and wish to cancel, please contact us referencing this license number 2270950810286 and noting the reason for cancellation.

Questions? customercare@copyright.com or +1-877-622-5543 (toll free in the US) or +1-978-646-2777.

Dear Mr Emory

The Royal Society of Chemistry hereby grants permission for the use of the material specified below in the work described and in all subsequent editions of the work for distribution throughout the world, in all media including electronic and microfilm. You may use the material in conjunction with computer-based electronic and information retrieval systems, grant permissions for photocopying, reproductions and reprints, translate the material and to publish the translation, and authorize document delivery and abstracting and indexing services. The Royal Society of Chemistry is a signatory to the STM Guidelines on Permissions (available on request).

Please note that if the material specified below or any part of it appears with credit or acknowledgement to a third party then you must also secure permission from that third party before reproducing that material.

Please ensure that the published article carries a credit to The Royal Society of Chemistry in the following format:

[Original citation] – Reproduced by permission of The Royal Society of Chemistry

and that any electronic version of the work includes a hyperlink to the article on the Royal Society of Chemistry website. The recommended form for the hyperlink is http://dx.doi.org/10.1039/DOI suffix, for example in the link http://dx.doi.org/10.1039/b110420a the DOI suffix is 'b110420a'. To find the relevant DOI suffix for the RSC paper in question, go to the Journals section of the website and locate your paper in the list of papers for the volume and issue of your specific journal. You will find the DOI suffix quoted there.

Regards

Gill Cockhead

Contracts & Copyright Executive

Gill Cockhead (Mrs), Contracts & Copyright Executive

Royal Society of Chemistry, Thomas Graham House

Science Park, Milton Road, Cambridge CB4 0WF, UK

Tel +44 (0) 1223 432134, Fax +44 (0) 1223 423623

http://www.rsc.org

-----Original Message-----

From: jemory1@lsu.edu [mailto:jemory1@lsu.edu]

Sent: 16 September 2009 20:53

To: CONTRACTS-COPYRIGHT (shared)

Subject: Permission Request Form: Jason Emory

Name : Jason Emory

Address :

202 Choppin Hall

Baton Rouge LA, 70816

Tel : 225-578-7707

Fax : 225-578-3458

Email : jemory1@lsu.edu

I am preparing the following work for publication:

Article/Chapter Title : Single-Molecule Detection of Unique Genome Signatures: Applications in Molecular Diagnostics and Homeland Securtiy

Journal/Book Title :

Editor/Author(s) : Jason M. Emory

Publisher : Louisiana State University and Agricultural and Mechanical College

I would very much appreciate your permission to use the following material:

Journal/Book Title : Analyst

Editor/Author(s) : zhang, C. Y.; Johnson, L. W.

Volume Number : 131

Year of Publication : 2006

Description of Material : Figure 1

Page(s) : 484-488

Journal/Book Title : Analyst

Editor/Author(s) : Zhang, C. Y.; Chao, S. Y.; Wang, T. H.

Volume Number : 130

Year of Publication : 2005

Description of Material : Figure 1

Page(s) : 483-488

Journal/Book Title : Analyst

Editor/Author(s) : Alonso Castro and Richard T. Okinaka

Volume Number : 125

Year of Publication : 2000

Description of Material : Figure 1

Page(s) : 9-11

Any Additional Comments :

I am completing a doctoral dissertation at Louisiana State University entitled "Single-Molecule Detection of Unique Genome Signatures: Applications in Molecular Diagnostics and Homeland Security." I would like your permission to reprint in my dissertation excerpts from the articles listed above.

DISCLAIMER:

# Vita

Jason M. Emory was born in Manassas, Virginia, to Coy and Cheryl Emory in 1975. He is the youngest of two sons and grew up in Monroe, North Carolina. He attended Parkwood High School and graduated in 1993 as a North Carolina Scholar. Jason went on to attend East Carolina University in Greenville, North Carolina, from fall 1993 to May 1999. He transferred to University of North Carolina at Charlotte in the fall of 1999 and graduated with a Bachelor of Science degree in chemistry with a concentration in biochemistry in 2001.

Jason continued on at UNC Charlotte in the master's program under the direction of Brian Cooper. During this time, his research work involved the implementing of a single-molecule electrophoresis (SME) detection system. In 2004, Jason graduated with his Master of Science in chemistry, his thesis title was Ultrasensitive Detection of Fluorescently Labeled Molecules in Channel Electrophoresis as an Approach to High-Throughput Proteomics. He presented his work at national and regional meeting including SERMACS, HPCE and ACS.

In the fall of 2003, Jason enrolled at Louisiana State University in the doctoral program in the chemistry department. His work was performed under the direction of Professor Steven A. Soper. Jason's doctoral work focused on the development of novel detection platforms to increase sample throughput or provide portable analysis using genetic molecular markers with a ligase detection reaction using single-pair fluorescent resonance energy transfer. His work was presented at several national and international conferences (PITTCON, and μTAS). The degree of Doctor of Philosophy will be conferred at the May 2010 commencement ceremony.